UNIVERSITY OF NAPLES FEDERICO II

POLYTECHNIC AND BASIC SCIENCES SCHOOL

Ph.D. in Chemical Sciences

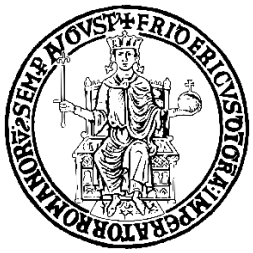

Synthesis and development of nature-inspired molecules with immunomodulant activity

Marcello Mercogliano

Advisors:

Prof. Marina Della Greca (Dept. of Chemical Sciences, Unina)

Dr. Emiliano Manzo (ICB – CNR)

Examiner:

Prof. Antonio Molinaro (Dept. of Chemical Sciences, Unina)

XXXVI CYCLE 2020 – 2023

Coordinator: Prof. Angelina Lombardi

A mia mamma

Index

Abbreviations V

Summary XI

Chapter 1: Introduction

1.1 Marine natural products: the bioactive potential 1

1.1.1 Immunomodulatory activity of marine metabolites 3

1.1.2 Marine-derived glycolipids 4

1.2 The immune system 7

1.2.1 Components of the immune system 7

1.2.2 Innate and adaptive immunity 12

1.2.2.1 Innate immunity 13

1.2.2.2 Adaptive immunity 14

1.2.3 Dendritic cells 14

1.2.4 Glycolipids in immunity 17

1.3 Receptors of the innate immunity 18

1.3.1 C-type lectin receptors (CLRs) 21

1.3.1.1 Dectin-1 22

1.3.2 Triggering receptors expressed on myeloid cells (TREMs) 25

1.3.2.1 TREM2: Activation pathway and ligands 25

1.3.2.2 TREM2 related diseases 28

1.3.2.3 TREM2 in Alzheimer 29

Chapter 2: Results and discussion

2.1 Synthesis and biological activity of sterol derivatives 31

2.1.1 Bioassay screening platform 31

2.1.2 Immunological reporter cell assays and chemical synthesis of sterol derivatives 32
2.1.2.1 Preparation of sulphated sterol derivatives..... 34
2.1.2.2 Synthesis of brominated and acetyl cholesterol 35
2.1.2.3 Synthesis of phosphate cholesterol..... 37
2.1.2.4 Synthesis of β-glyco-cholesterols..... 38
2.1.3 Reporter cells assays of synthetized sterol derivatives 40
2.1.4 Conclusions 43
2.2 Synthesis of more stable Sulfavant A analogues 44
2.2.1 Sulfavant A: a new immunomodulator adjuvant and first synthetic TREM2 ligand..... 44
2.2.2 Synthesis of Sulfavant A derivatives 46
2.2.2.1 Synthesis of Sulf-etherate..... 46
2.2.2.2 TREM2 reporter cell analysis on Sulf-etherate 49
2.2.2.3 Synthesis of Sulf-amidate: different approaches 50
2.2.3 Conclusions 55
2.3 Synthesis of a fluorescent analogue of Sulfavant A..... 56
2.3.1 Synthetic procedure..... 58
2.3.2 Biological assays 64
2.3.3 Exploiting Sulf-BODIPY fluorescence properties in a biological context 65
2.3.3.1 Bioimaging study 66
2.3.3.2 In vivo study on Zebrafish 68
2.3.3.3 In vivo study on mice 70
2.3.4 Conclusions 71
2.4 Docking experiments 72
2.4.1 Docking simulations..... 74
2.4.2 Biological assays 83

2.4.3 Conclusions 85

Chapter 3: Study of the interaction between glycan and galectins by ^{19}F-NMR

3.1 Galectins, glycans and their interactions 87
3.1.1 Galectins 87
3.1.2 Glycans 90
3.1.3 ^{19}F-NMR to study protein-glycan interaction 91
3.2 Aim of the project 94
3.3 Preparation of the fluorinated galectins 94
3.4 Titration experiments 96
3.5 Conclusions and prospects 100

Chapter 4: Conclusions and prospects

Chapter 5: Experimental section

5.1 Synthesis of nature-inspired sterol derivatives 107
5.1.1 Synthesis of sulphated sterol derivatives 107
5.1.2 Synthesis of cholesteryl bromide 109
5.1.3 Synthesis of acetyl cholesterol 110
5.1.4 Synthesis of cholesterol phosphate 111
5.1.5 Synthesis of sulfoquinovosyl cholesterol 112
5.1.6 Dectin 1 reporter assay 118
5.2 Synthesis of potentially more stable Sulfavant A analogues 119
5.2.1 Synthesis of Sulf-etherate 119
5.2.2 TREM2 reporter assay 124
5.2.3 Synthesis of Sulf-amidate 124

5.3 Synthesis of Sulf-BODIPY 133
5.3.1 Synthesis of Me_4BODIPY-undecanoic acid 133
5.3.2 Synthesis of Sulf-BODIPY 135
5.3.3 Biological analysis 140
5.3.3.1 Preparation of dendritic cells 140
5.3.3.2 Cells staining and stimulation 140
5.3.3.3 Real time PCR analysis 141
5.3.3.4 In vitro bioimaging experiments on hDCs 141
5.3.3.5 Animal husbandry, larval exposure and imaging 142
5.3.3.6 Ex vivo fluorecence imaging experiment 142
5.3.3.7 Brains Extraction and analysis via HPLC-UV 143
5.4 Docking experiments 143
5.4.1 System preparation 143
5.4.2 Molecular docking simulation 144
5.4.3 MMGBSA calculations 144
5.4.4 Synthesis of Sulfavant C6 145
5.5 Preparation of fluorinated galectins and ^{19}F-NMR spectra 147
References 148
Appendix 188
Acknowledgements 197

Abbreviations

(AD) = Alzheimer's disease

(ADME) = Absorption, distribution, metabolism and excretion

(AIM2) = Absent in melanoma-2

(ALRs) = (Absent in melanoma-2)-like receptors

(ALS) = Amyotrophic lateral sclerosis

(ANOVA) = Analysis of variance

(APCs) = Antigen-presenting cells

(APOE) = Apolipoprotein E

(ASC) = Apoptosis-associated speck-like protein containing CARD

(BCR) = B cell receptor

(BODIPY) = 4,4-difluoro-4-bora-3a,4a-diaza-*s*-indacene

(calcd) = Calculated

(CARD9) = Caspase Recruitment Domain Family Member 9

(cDCs) = Conventional dendritic cells

(CDR) = Complementary-determining region

(CHOS) = Cholesteryl sulphate

(CLEC7A) = C-type lectin domain family 7

(CLRs) = C-type lectin receptors

(CNS) = Central nervous system

(COX) = Co-crystallized ligand

(CRD) = Carbohydrate recognition domain

(CTLD) = C-terminal leptin-like domain

(DAMPs) = Damage-associated molecular patterns

(DAP) = DNAX-activating protein

(DAPI) = 4',6-diamidin-2-phenylindole

(DBU) = 1,8-diazabiciclo[5.4.0]undec-7-ene

(DCC) = *N,N′*-dicyclohexylcarbodiimide

(DCs) = Dendritic cells

(DGDGs) = Digalactosyl diacylglycerols

(DMAP) = 4-dimethylaminopyridine

(DMEM) = Dulbecco's modified eagle medium

(DMF) = *N,N*-dimethylformamide

(dpf) = Days post-fertilization

(DTT) = Dithiothreitol

(EDTA) = Ethylenediaminetetraacetic acid

(Egr) = Early growth response

(ERK) = Extracellular signal-regulated kinase

(FBS) = Foetal bovine serum

(FITC) = Fluorescein 5-isothiocyanate

(Gal) = Galactose

(GBPs) = Glycan-binding proteins

(GFP) = Green fluorescent protein

(glyphosate) = N-(phosphonomethyl)glycine

(GM-CSF) = Granulocyte macrophagecolony stimulating factor

(GSLs) = Glycosphingolipids

(hDCs) = Human dendritic cells

(HEK) = Human embryonic kidney

(HEK-blue) = Secreted embryonic alkaline phosphatase

(HILIC) = Hydrophilic interaction chromatography columns

(HPLC) = High-Performance Liquid Chromatography

(HRESIMS) = High-resolution electrospray ionisation mass spectrometry

(HSV) = Herpes simplex virus

(IFN) = Interferon

(Ig) = Immunoglobulin

(IL) = Interleukin

(IPTG) = Isopropyl-β-D-1-thiogalactopyranoside

(ITAM) = Immunoreceptor tyrosine-based activation motif

(K_d) = Dissociation constant

(LacNAc) = *N*-acetyllactosamine

(LPS) = Lipopolysaccharide

(LRR) = Leucine-rich repeat

(M9) = Minimal medium

(MGDGs) = Monogalactosyl diacylglycerols

(MHC) = Major histocompatibility complex

(MIF) = Migration inhibitory factor

(MLR) = Mixed lymphocyte reaction

(MMR) = Macrophage mannose receptor

(MoDCs) = Monocyte-derived dendritic cells

(MTBE) = Methyl tert-butyl ether

(NKT) = Natural killer T

(NHD) = Nasu-Hakola disease

(NFAT) = Nuclear factor of activated T-cell

(NF-κB) = Nuclear factor kappa-light-chain-enhancer of activated B cells

(NLRs) = (Nucleotide oligomerization domain)-like receptors

(NMR) = Nuclear magnetic resonance

(NOD) = Nucleotide oligomerization domain

(OVA) = Ovalbumin

(PAMPs) = Pathogen-associated molecular patterns

(PBS) = Phosphate buffered saline

(PCR) = Polymerase chain reaction

(PD) = Parkinson's disease

(pDCs) = Plasmacytoid dendritic cells

(PMSF) = Phenylmethylsulfonyl fluoride

(PS18) = Phosphatidylserine with C18 lipid chains

(Py) = Pyridine

(PYD) = PYRIN-PAAD-DAPIN domain

(PPW) = Protein preparation wizard

(PRRs) = Pattern recognition receptors

(PS18) = Phosphatidylserine with C18 acyl chains

(OPLS) = Optimized potentials for liquid simulations

(rac) = Racemic

(RC6) = Sulf-R with C6 acyl chains

(RIG-I) = Retinoic acid-inducible gene-I

(RLRs) = (Retinoic acid-inducible gene-I)-like receptors

(RNA) = Ribonucleic acid

(SC6) = Sulf-S with C6 acyl chains

(SD) = Standard deviation

(SDS-PAGE) = Sodium dodecyl sulphate - polyAcrylamide gel electrophoresis

(SEAP) = Secreted embryonic alkaline phosphatase

(SEC) = Size exclusion chromatography

(SEF) = Symmetrical electromagnetic field

(SFK) = Tyrosine-protein kinase

(SP) = Standard precision

(SPE) = Solid phase extraction

(SQDGs) = Sulfoquinovosyl diacylglycerols

(SRC) = Non-receptor tyrosine kinase

(Sulf-A) = Sulfavant A

(Sulf-A C6) = Sulfavant A with C6 acyl chains

(Sulf-BODIPY) = Sulfavant A BODIPY

(Sulf-etherate) = Sulfavant A with etherated lipid chains

(Sulf-amidate) = Sulfavant R with amidated lipid chains

(Sulf-R) = Sulfavant R

(Sulf-S) = Sulfavant S

(Syk) = Spleen tyrosine kinase

(TAMs) = Tumour-associated macrophages

(TCR) = T cell receptor

(TEA) = Triethylamine

(TLC) = Thin layer chromatography

(TLRs) = Toll-like receptors

(TMD) = Transmembrane domain

(TMSBr) = Bromotrimethylsilane

(TMSOTf) = Trimethylsilyl trifluoromethanesulfonate

(TREMs) = Triggering receptors expressed on myeloid cells

(TRIS) = Tris(hydroxymethyl)aminomethane hydrochloride

(TYROBP) = Transmembrane immune signaling adaptor

(sTREM2) = Soluble TREM2

(WGA) = Wheat-germ agglutinin

Summary

Discovering substances able to regulate human immune system has long been a crucial research goal. Despite huge scientific progress, the challenge remains unsolved, and we continue to fight daily against incurable diseases. Nature, providing a broad spectrum of compounds with pharmaceutical potential, has historically inspired biomedical and drug formulations. In particular, the marine environment harbours a vast number of metabolites that exhibit an enormous biological and structural diversity, acting as an exceptional framework for drug discovery. The objective of this dissertation is to discover and synthetize novel compounds with immunomodulatory activity, drawing inspiration from natural products of marine origin.

The activation and modulation of the immune response, starts by triggering of specific immune components, such as antigen-presenting cells (APCs) by their receptors. In this regard, dendritic cells (DCs) are the most important and highly effective APC representing a bridge between the innate and adaptive immune systems. A key point in this context is their maturation process, which leads to the production of both co-stimulatory factors and cytokines up to antigen presentation, triggering and regulating innate and adaptive immune response. However, compounds with bioactive potential that can induce DC maturation must first be recognised by specific receptors of innate immune cells, known as pattern recognition receptors (PRRs), which make up the body's initial line of defence. Their interaction with specific ligands leads to the activation and regulation of immunity, with the aim of achieving homeostatic conditions after harmfull antigens elimination. Specifically, trigger cell receptors as Dectin-1 and TREM2, represent the focus of this thesis, for their ability to activate and at same time modulate the innate immune system.

In the laboratories of the Institute of Biomolecular Chemistry (ICB-CNR) in Pozzuoli, a bioimmunoassay-guided screening platform was developed for the isolation and characterization of marine natural compounds with immunomodulatory potential. This protocol led to the identification of cholesteryl sulphate (CHOS) as a new ligand

of the Dectin-1b receptor. On this basis, part of this dissertation focused on the synthesis and purification of several sterol derivatives by implementing minor structural alterations to investigate their interactions with the receptor and identify the key structural components involved in the recognition process.

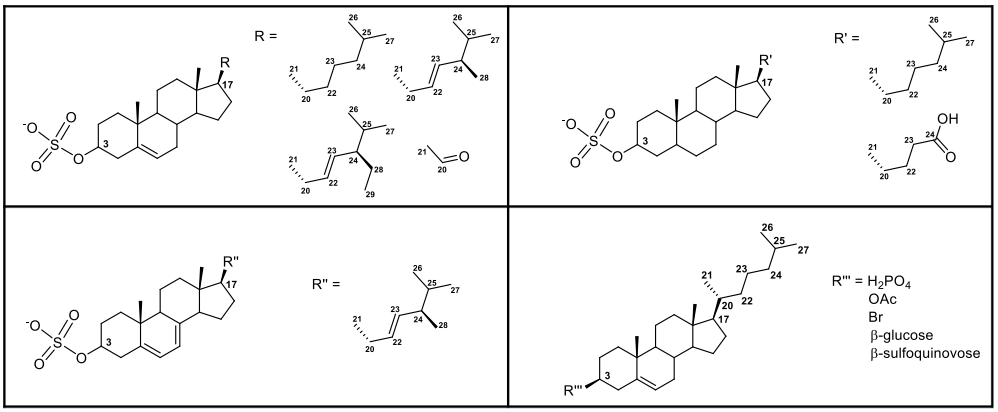

Synthetized sterol derivatives

Receptor screening assays were carried out on the synthetized molecules by performing biological tests on Dectin-1b reporter cells. In human DC biological assays, CHOS induced the expression of the DC co-stimulatory marker CD86. Structure modifications enabled the identification of the chemical factors able to influence receptor affinity.

Glycoglycerolipids represent an interesting group of marine metabolites widely distributed in microalgae. In particular, α-sulfoquinovosyl diacylglycerols (α-SQDGs), sulphur-containing anionic glycolipids, found in marine microalgae and characterized by anti-tumour and immunomodulatory properties, presented a peculiar biological behaviour. In this regard, this thesis had as starting point the study and development of Sulfavant A (Sulf-A), an α-SQDGs-inspired synthetic β-

sulfoquinovosyl diacylglycerol, capable of inducing the activation and maturation of DCs by an unprecedented immune mechanism.

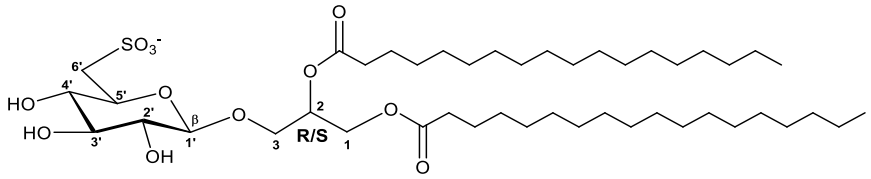

Structure of 1,2-*O*-distearoyl-3-*O*-β-D-sulfoquinovosylglycerol (Sulfavant A)

The biological behaviour of Sulf-A led to the upregulation of the MHC-II complex and co-stimulatory molecules via a TLR-independent mechanism, without the release of conventional cytokines. Moreover, Sulf-A exerted its biological function through the specific binding with TREM2, making it the first synthetic ligand of this receptor. Following pharmacokinetic studies on Sulf-A, a section of this thesis outlined the synthesis of two chemically more stable analogues of Sulf-A: Sulf-etherate and Sulf-amidate. These analogues differed in the way the lipid chains are linked to the glycerol moiety, with ether and amide linkages, respectively.

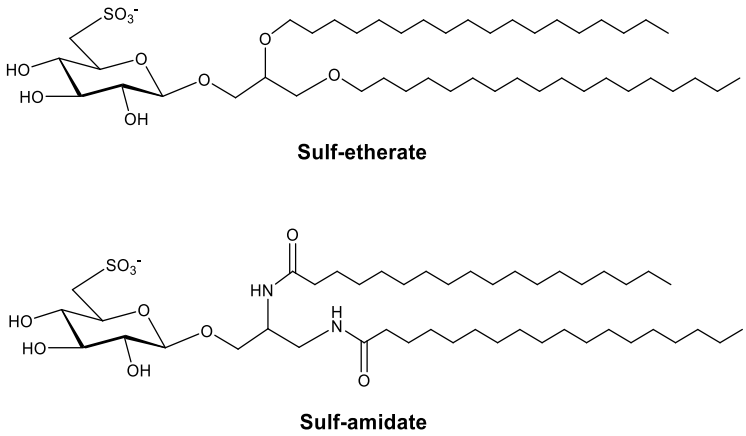

Structure of Sulf-etherate and Sulf-amidate

Since there are currently insufficient information available on how Sulf-A interact with TREM2, structural modifications of these analogues and side-by-side biological assays could help to shed light on the recognition mechanism and the most involved structural determinants. Sulf-etherate was synthesised through the different approach of the acetylated trichloroacetimidate glucose donor and the glycerol acceptor with eighteen carbon atom ether chains, followed by their coupling. The synthesis of Sulf-amidate is ongoing, and the various strategies employed to achieve the final molecule are outlined.

The potential pharmacological development of Sulf-A highlighted the need to better understand the behaviour of this molecule in the biological environment and, for this reason, part of this thesis focused on synthesising and characterising a fluorescent derivative, called Sulf-BODIPY.

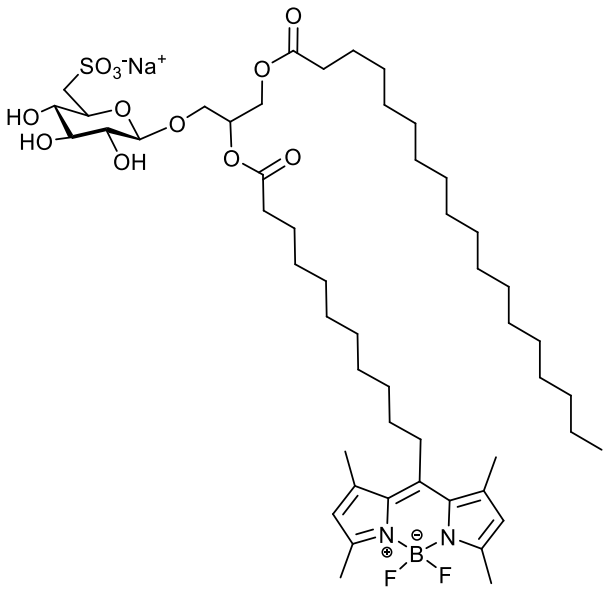

Structure of 1-*O*-stearoyl-2-*O*-Me$_4$BODIPY-undecanoyl-3-*O*-β-D-sulfoquinovosyl-rac-glycerol (Sulf-BODIPY)

The fluorescent tag BODIPY, often used in lipid trafficking studies, was chosen for its good spectroscopic properties and stability. In Sulf-BODIPY, the fluorescent moiety was attached to glycerol via a C-11 spacer. The *in vitro* evaluation of immunomodulatory activity of Sulf-BODIPY on human DCs, comparable to that of Sulf-A, showed that the introduction of the fluorescent tag did not significantly affect the biological activity. This fluorescent compound opened the way to the use of various fluorescence-based techniques and numerous studies aimed at elucidating the mechanism of action and interaction with TREM2, biodistribution and behaviour in the biological environment. Bioimaging and *in vivo* experiments on zebrafish and murine models are described, contributing to knowledge about the biodistribution of Sulfavant A.

Furthermore, molecular docking experiments were conducted to determine which TREM2 part and binding pocket were implicated in the interaction with Sulf-A. Docking data and interaction free energy were calculated for Sulf-A, mycolic acid and phosphatidylserine and their derivatives with C18 and C6 lipid chains. This study allowed the investigation of the amino acid residues most involved in ligand binding and structural ligand functions with the greatest influence. The simulation results were validated by experimental biological assays using TREM2 WT reporter cells.

With the aim of implementing chemical tools to investigate the activation mechanisms of innate immune cells, part of the thesis was carried out at the CIC-BioGUNE Institute in Bilbao studying the binding between galectins and glycans by ^{19}F-NMR. Galectins can affect both innate and adaptive immunity by either enhancing or inhibiting immune and inflammatory responses and regulating intracellular and extracellular pathways. Glycans, widely distributed in all living organisms, are polysaccharides mostly coating all cells. In addition to their important role as structural and energy reserves, glycans have multiple biological functions and their recognition leads to the activation of numerous signalling pathways. The use of ^{19}F-NMR provided a significant tool to investigate the binding interaction by simplified spectra. The process entails ^{19}F-labelling of a widely preserved Trp residue, present in

all galectins, by using an optimised protocol and monitoring the variations in the NMR signals after ligand interaction.

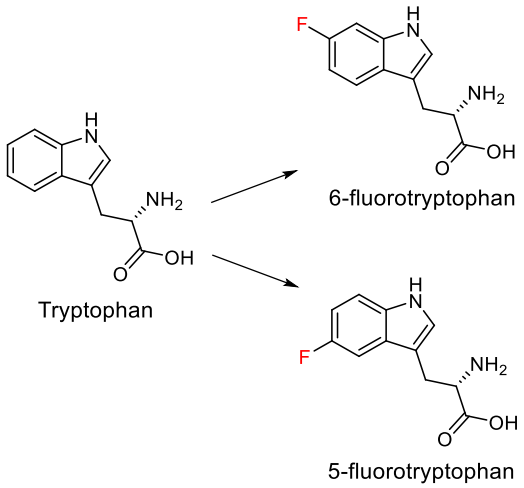

Fluorine-labelled tryptophans at positions 5 and 6

The labelled galectins were subjected to affinity controls using titration experiments to ensure the interaction affinity was maintained without alteration by fluorine presence. Human cells expressing a uniform surface of glycans have been employed to create a quasi-natural interaction environment that, with the advantages of ^{19}F-NMR, has proven to be an excellent approach to unravel the secrets of galectin-glycan interactions.

Chapter 1: Introduction

1.1 Marine natural products: the bioactive potential

Natural products have been a valuable and historical source of therapeutic agents, and since the early 1990s, there has been increasing interest in their development due to the improved methods of separation and purification, spectroscopic techniques, and biological assays. It is common knowledge that natural substances have long been used to treat various diseases since ancient times and continue to serve as the primary basis for developing novel therapeutic agents.

Our planet is covered by more than 70% by water, in which more than three hundred thousand species of marine organisms are classified. These organisms exhibit a high level of biological diversity and environmental adaptability, making them suitable for various pharmacological and biotechnological applications.(1,2) Marine organisms offer an extensive range of metabolites, exhibiting significant biological and structural diversity and serving as privileged scaffolds in drug discovery.(3) In this regard an increasing number of marine compounds, natural or nature-inspired, are commercially available as drugs or are entering clinical trials, attracting the interest of many pharmaceutical companies. Furthermore, every year, the count of marine natural products in the late clinical phase is increasing, along with the potential to discover new active therapeutic agents for currently incurable desease.(4–8) The biomedical potential of these substances is extremely large, considering fields from the inhibition of cellular processes, including apoptosis, angiogenesis, migration and cell adhesion to anti-inflammatory and anti-tumour activity, regulation of immune-mediated diseases and many others.(9–14) Regarding the anti-cancer drugs, marine substances play a dominant role. About 60% of authorized drugs and many more in the preclinical stage are derived from marine sources.(15) According to the National Cancer Institute, only 0.1% of terrestrial samples showed antitumor activity, while approximately 1% of marine samples demonstrated such activity.(16) This fact statistically illustrates the higher promising bioactivity of natural marine products which has grown a lot in recent decades (**Figure 1**).

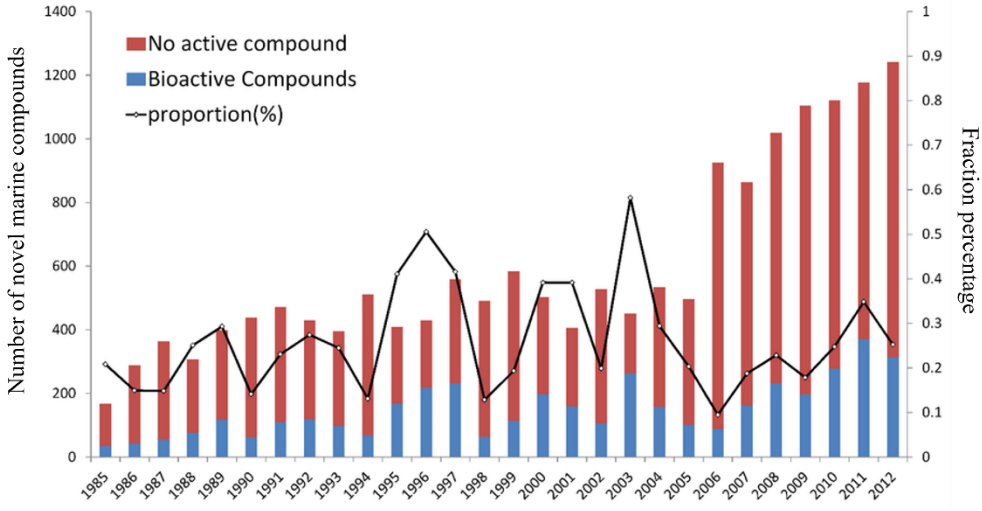

Figure 1: Variation in number of new marine natural products between 1985 and 2012.(17)

According to recent events, an example of the beneficial impact of marine metabolites can be seen in COVID-19, the ongoing disease that has struck our planet for the past three years causing approximately 240,000 deaths. In this regard antiviral marine products acts as potential inhibitors against RNA viruses, promoting recovery from SARS-Co V-2.(18)

In the sea, microalgae are among the oldest organisms able to grow in different types of environments, even the most extreme. The interest in microalgae in last years also relates to their ability to overcome the problem of low production quantities, making them highly favourable for mass cultivation, specifically for industrial purposes.(19) The microalgae-derived molecules, including polysaccharides, lipids, phlorotannins, glycolipids and carotenoids have already showed huge potential in pharmaceutical, cosmetic and nutraceutical applications.(20–23) Studies of marine algae have revealed numerous health-promoting effects including anticoagulant, anticancer, anti-hypolipidemic, anti-hypertensive, antioxidant, antibacterial, and immunomodulatory activities.(24) Several analysis showed how brown algae-derived fucoidans promoted cytokines synthesis activation, exhibiting immunotropic activity and boosting the

immune response.(25) In particular, great interest has been focused on the diatom *Thalassiosira weissflogii* (CCMP 1336) standing out for immune-stimulating properties, such as the production of IL-6, which is relevant in immune regulation, inflammation and oncogenesis.(26) Ahmad et al. reported an extensive collection of marine algal-derived compounds and their therapeutic chemical constituents.(27)

1.1.1 Immunomodulatory activity of marine metabolites

The ability to mediate the immune system response is one of the most intriguing and demanding challenges of recent decades. Immunomodulation enables the modification and regulation of the immune response, and substances with this ability are promising candidates for new medical therapies. Many marine compounds are able to modulate the immune system and cellular functions, controlling inflammation and maintaining immune homeostasis.(28,29) Thanks to ongoing technological advancements, it is feasible to employ an array of techniques to assess the immunomodulatory capacity. Usually, the effects of marine compounds on the most important components of the immune system are analysed by powerful techniques and assays such as ELISA, Western blot, real-time PCR and immunofluorescence.(30–33)

Marine fungi, known for their anti-inflammatory properties, can influence the immune system thanks to the presence of polysaccharides, already highly used for the treatment of immune disease.(34) A noteworthy instance is the α-D-glucan YCP derived from the marine fungi *Phoma herbarum* YS4108, which has demonstrated the ability to control T lymphocytes and dendritic cells functions *in vitro* assays.(35) Sponges are among the most studied marine organisms due to their interesting anti-inflammatory, anticancer and immunomodulatory properties. A recent study reports how *in vivo* tests of crude extracts of the sponge *Haliclona (Soestella)* sp. led to a decrease in immune cells resulting in an immunomodulatory activity, confirmed also by the increase of TNF-alpha level in the plasma.(36) Montuori et al. proposed in 2022 a collection of the most recently discovered marine organisms with

immunomodulatory properties.(37) As shown above, microalgae can be cultivated in significant volumes and are immune to climate variations, which permits extensive product development.(19) Moreover, these organisms are particularly suitable for study of new lead compounds for their adaptivity properties to extreme habitats, that makes them an important source of bioactive components such as lipids, vitamins and pigments. They are also sustainable producers of polysaccharides with biological benefits. For example, β-glucans extracted from the microalga *Phaeodactylum tricornutum* may bind to particular cell receptors and alter the innate immune system.(38) In this regard, in addition to polysaccharides, glycolipids also have demonstrated significant biological functionality and impact on the immune system. These compounds are predominantly found in echinoderms and marine sponges, as well as in macro and microalgae.

1.1.2 Marine-derived glycolipids

Glycolipids are a broad class of natural compounds belonging to the glycosidic derivatives and were first isolated in 1942.(39) The huge variety of structural combinations of glycolipids led to the formation of the different subclasses: glycoglycerolipids; glycosphingolipids (GSLs); phosphoglycolipids; trehalose glycolipids; sophorolipids; rhamnolipids; sugar-linked alcohol lipids; phenolic glycolipids; steryl glycolipids. They are complex amphiphilic glycoconjugates with a basic structure consisting of a mono- or oligosaccharide group attached to a sphingolipid (glycosphingolipids class) or a glycerol group (glycoglycerolipids class) with one or two fatty acids with varying possible degrees of unsaturation (**Figure 2**).

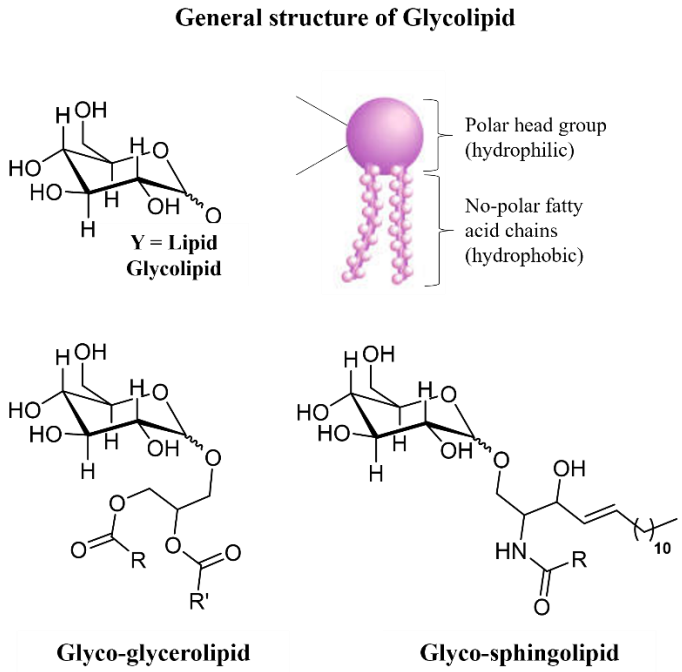

Figure 2: General structure of glycolipids and of the main subclasses glyco-glycerolipids and glyco-sphingolipid.

These molecules are vital constituents of cell membranes present in all living organisms, displaying pivotal and captivating biological characteristics and playing key roles in cellular interactions and signal transduction.(40–42)

Their amphiphilic structure, consisting of a polar sugar moiety linked to a hydrophobic one, imparts significant surfactant properties and partition at the interfaces between liquid phases. Most marine biosurfactants are applied in the environmental field, while their biomedical potential is yet to be fully exploited. The enormous biological and pharmacological potential of these substances has only recently begun to be understood and the scientific community is now constantly in pursuit of marine-sourced glycolipids exhibiting structural diversity for potential therapeutic benefits.

Despite participating in a broad range of biological functions, commercially available glycolipids remain elusive due to the low yields of isolation and purification processes. From this point of view microalgae is a separate topic, as it produces large amounts of glycolipids with anti-inflammatory, anti-fungal, anti-microbial, and anti-tumour properties.(43–47) Sponges are also an important source of glycolipids. Agelasphins, α-galactosylceramides isolated from the sponge *Agelas mauritiana*, and their synthetic analogues, have been shown to have immunostimulatory activity.(48,49) Among them two plakosides (β-galactosylceramides) from *Plakortis simplex*, showed a strong immunosuppressive behaviour.(50) Glycoglycerolipids are the most abundant glycolipids in nature and can be found in bacteria, plants and animals. Their general structure consists in a sugar group, mono-, di- or poly-saccharide, linked to a 1,2-diacyl-*sn*-glycerol moiety by glycosidic linkage with α or β anomeric configurations. Biological activity and behaviour can vary depending on the position, length and unsaturation degree of the acyl chains on the glycerol, on structure of sugar moiety and anomeric configurations.(51) Depending on these structural variables, they can also present different applications in the biological field and could be generally distinguished as follows: monogalactosyl diacylglycerols (MGDGs); digalactosyl diacylglycerols (DGDGs); sulfoglycoglycerolipids.(51) In the family of sulfoglycoglycerolipids, α-sulfoquinovosyl diacylglycerols (α-SQDGs), often found in marine algae, are a particularly relevant group of sulphur-containing anionic glycolipids, highlighting antitumour and immunomodulatory properties. Examples are glycolipids extracted from *Gracilaria verrucosa*, *Chondria crassicaulis*, *Porphyridium purpureum*, and *Ulvella lens*.(52–55) Moreover, it has been reported that a fraction rich in α-SQDGs from marine organisms was active against human herpes simplex virus (HSV) infection with a strong antiviral activity against HSV-1 and HSV-2.(56–58) The immunomodulatory potential of α-SQDGs has been already widely discussed in the literature although their mechanism is not fully understood. *In vitro* and *in vivo* assays have reported that synthetic SQDG analogues regulate the human mixed lymphocyte reaction (MLR), but also prime human DCs through a TLR2/TLR4 independent mechanism, inducing DCs maturation with

upregulation of MHC II molecules and co-stimulatory proteins (CD83, CD86), as well as modulation of pro-inflammatory cytokines (IL-12 and IFN-γ).(59,60)

1.2 The immune system

The pressure exerted by natural selection is constant and inexhaustible and because of this, humans have always had to fight throughout their lives with a multitude of pathogenic microorganisms. As Covid-19 has taught us, new infectious diseases have the same potential to shape future human history as those of the past. To understand how to address these troubles, we need to understand how our immune system works and how to maximize its potential. The diverse responses of the immune system are based on the selective expression of specific gene families. Indeed, cells 'read' their environment through receptors and then change the way they use the genes encoded by their DNA, activating or deactivating them. The immune system should be able to discriminate between 'self' and 'non-self' and between harmless non-self and dangerous non-self. Most of the research to date has focused on understanding how to achieve the first goal, as it has been shown that the immune system is able to classify and remember the structure of individual molecules.

1.2.1 Components of the immune system

The immune system comprises specialised organs, cells, structures, tissues and biological processes, cooperating to combat infection, cell damage and illnesses and dedicated to safeguarding the organism against foreign invaders, thereby preserving its integrity (**Figure 3**). In order to make the most of its potential to remedy or solve health problems that have always plagued mankind, it's necessary to know more about the essential components of this system and their functions.

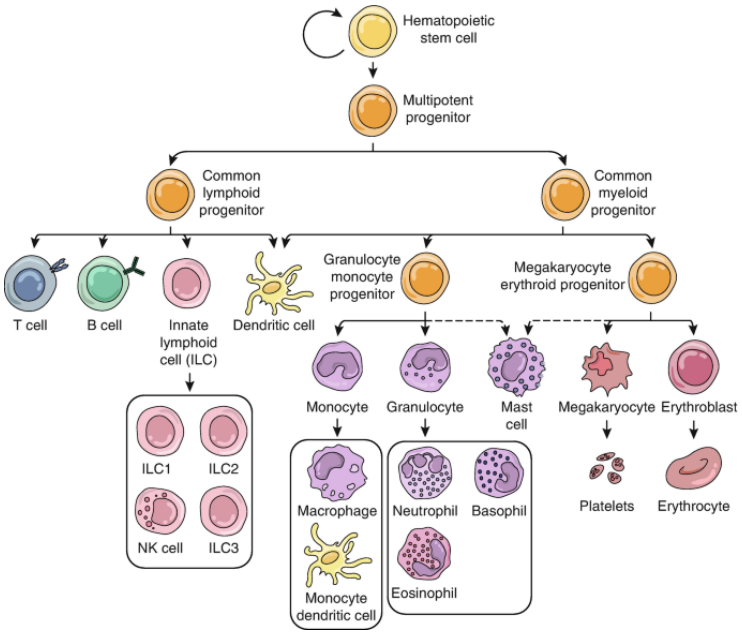

Figure 3: Main types of immune system cells.

The principal components of the immune system in an organism are: bone marrow, thymus, spleen, white blood cells, antibodies, major histocompatibility complex (MHC), cytokines, complement system and lymphatic system. Thymus filters and controls the contents of the blood producing white blood cells, T-lymphocytes. The bone marrow is where all the body's blood cells originate, including T and B lymphocytes. (61) While B lymphocytes mature in the bone marrow, T lymphocytes migrate to the thymus. (62) The thymus is active only until puberty, afterward it gradually deteriorates and is replaced by fat and connective tissue. This is where the T cells multiply and differentiate. As the T and B lymphocytes mature, they migrate to the lymph nodes and spleen, where they remain until the immune system is compromised.(63)

There are three main types of T cells: helpers, regulatory, and cytotoxic.(64) T-helper express CD4 molecules on their surface and serve as the main source of cytokines. The T-dependent immune response can be categorised into subgroups of varying

clinical relevance, mainly cell Th1 and humoral Th2. For example, a Th1 response is predominant in tuberculoid leprosy, and a Th2 response dominates in lepromatous leprosy.(65,66) Th1 response could lead to a distinctive autoimmune disorder, such as type 1 diabetes and multiple sclerosis, while a Th2 response could promote IgE production and development of allergic disorders.(67–70) Another T-response is represented by Th17 cells that may contribute to other autoimmune disorders such as psoriasis and rheumatoid arthritis.(71,72)

About 5-15% of the lymphocytes in the blood are B cells. Their main function is to develop into plasma cells, able to produce and secrete antibodies. During B cell development, the genes that encode for immunoglobulins (IGs) undergo rearrangement, resulting in the ability to identify an extensive range of distinct antigens.(73) After passing through the differentiation stages of early B cells, those that interact with the autoimmune antigen are eliminated from the immature B cell population by inactivation or apoptosis, so that the immune system does not recognise them as foreign.(74) The cells that are not eliminated further develop into mature native B cells and are transferred from the bone marrow to the peripheral lymphoid organs, where they can encounter antigens. The immune response to antigens involves two main phases: the primary and secondary immune responses. The primary response leads to the transformation into lymphoblasts, which then differentiate into memory cells capable of countering the same antigen in the future, albeit with limited protective immunity. (75) The secondary reaction is triggered by subsequent antigen exposure and leads to maturation of plasma cells that produce antibodies, eventually released into the bloodstream and tissues.

Lymphocytes also include cells known as natural killer T (NKT) cells, which have a function similar to that of T cells, but without receptor rearrangements. Activated NKT cells secrete IL-4 and interferon-γ. They may help and regulate immune responses and can have non-specific cytotoxic activity against virus-infected cells and cancer cells.(76)

The major histocompatibility complex (MHC) represents one of the most complex gene sets in the human genome. The primary role of MHC molecules is to bind to antigens, facilitating subsequent recognition by T cells. We can distinguish three classes of these molecules: class I, class II and class III.(77) Class I MHC molecules are able to bind peptides from cytosolic proteins and are found on almost all cells.(78,79) Class II molecules are found in antigen-presenting cells such as dendritic cells and bind antigens from extracellular proteins.(80) Class III molecules functions in the immune response remain unclear.

Dendritic cells, monocytes, macrophages and B cells constitutively express class II MHC molecules and therefore act as so-called professional antigenic presenting cells (APCs). Dendritic cells are found in tissues throughout the body. Skin dendritic cells (distinct from follicular dendritic cells) work as sentinel APCs, taking up antigen and moving to the lymph nodes where they can encounter and activate T cells. They have receptors for the crystallisable fragment (Fc) region of immunoglobulin (Ig) G, as well as for complement. These receptors enable them to bind immune complexes and subsequently exhibit them to B cells within the germinal centres of secondary lymphoid organs.(81,82)

Monocytes are the precursors of tissue macrophages. Monocytes are circulating blood cells, constituting approximately 10% of peripheral leukocytes in humans and roughly 4% in mice and are composed of numerous subclasses with varied size, shape, and gene profiles. At sites of infection, T cells become active, produce cytokines, such as interferon-gamma (IFN-gamma), which lead to the generation of macrophage migration inhibitory factor (MIF), fundamental to innate immunity. MIF promotes the pro-inflammatory functions of host immune cells and is implicated in the pathogenesis of sepsis and autoimmunity.(83,84)

Macrophages are activated by cytokines like IFNγ, interleukin (IL)-4, IL-13 and various microbial components (e.g. lipopolysaccharides). Activated macrophages kill intracellular organisms and secrete cytokines.(85)

Granulocytes are a type of leukocyte that contain granules of enzymes in their cytoplasm. Neutrophils, basophils and eosinophils are all types of granulocytes. Neutrophils are considered the first responders of the innate immune system and circulate with macrophages in the blood, looking for potential problems.(86) Both cells can phagocytose bacteria and interact with other immune cells.

Cytokines are proteins that affect cell interaction and communication.(87,88) They differentiate into:

- Lymphokines, produced by lymphocytes;
- Monokines, produced by monocytes;
- Chemokines, with chemotactic activity;
- Interleukins (IL), produced by a leukocyte.

Cytokines can also be divided into pro-inflammatory and anti-inflammatory groups. The former are responsibleof inflammatory response, while the latter can regulate it. This category includes Interferons (IFNs), which are signalling proteins able to influence viral replication by protecting cells from infection.(89) They regulate antigen presentation by increasing the expression of MHC antigens.

Antibodies, also known as immunoglobulins, identify antigens located on the surface of microbes that flag them as foreign, with the objective of destroying them. There are five main classes of antibodies, according to their structure and their activity: IgG, IgM, IgA, IgD, and IgE.(90)

The spleen is the largest secondary lymphoid organ in our body and acts as a filter, removing microbes and eliminating old or damaged red blood cells. It also facilitates interactions between antigen-presenting cells and lymphocytes.(91)

The complement system is one of the most critical connections between innate and adaptive immunity. It consists of proteins that, when activated at the site of infection, trigger a cascade of inflammatory responses. In practice, the activation of a few

proteins undergoes significant amplification due to succeeding enzymatic reactions, resulting in a rapid and more robust response.(92)

The lymphatic system is a network of delicate tubes that run throughout the body. Its fundamental roles include regulating fluid balance, responding to bacterial threats, fighting cancerous cells, neutralising toxic cellular waste, and absorbing dietary fats from the intestines.(93,94)

1.2.2 Innate and adaptive immunity

Since the science of immunology was born, the most prominent dichotomy has been between adaptive immunity (‘acquired immunity’) and innate immunity (‘natural immunity’). Innate immune system is the first line of defence against pathogens while the adaptive one acts as a second line of defence. Innate immune responses are not specific as those of the adaptive system which can also protect against a re-exposure to the same pathogen. These two systems provide unceasing protection to our body precisely through their mutually beneficial nature: the innate response is fast but lack of specificity (this can sometimes lead to normal tissues damages); the adaptive response is accurate but takes several days to develop (**Figure 4**).(95)

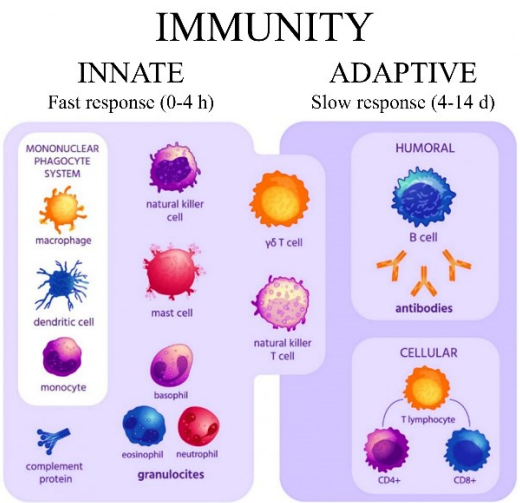

Figure 4: Innate and adaptive immune system cell types.

1.2.2.1 Innate immunity

Innate immunity is an ancient system of microbial recognition, working with a fixed number of germ-line-encoded receptors which recognise selective structural components of microorganisms and viruses. A distinctive feature of innate responses is that they remain unchanged regardless of the frequency of antigens encountered and therefore they lack immunological memory. It is now widely accepted that the innate immune system cascade plays a key role in the development, training and shaping of adaptive effector mechanisms.(96)

A key point in the immune system role is the ability to distinguish between what we call infectious non-self and its opposite, which is largely determined by genome-encoded receptors and the development of lymphocytes. During their life cycle, pathogens generate several conserved molecules that are not present in the internal eukaryotic environment. Some species of microbes contain similar molecular patterns recognisable as infectious non-self entities called pathogen-associated molecular patterns (PAMPs).(97) They are recognised by the PRRs (Pattern Recognition Receptors), specific receptors expressed on the cell surface of some phagocytic cells not undergoing rearrangement.(98)

Their primary roles involve phagocytosis, the activation of pro-inflammatory signalling pathways, the activation of complement and coagulation cascades, and the induction of apoptosis. Over the years, an increasing number of family members with diverse functions have been uncovered.(99) Sometimes, these cells can resolve infections independently, while in other cases, they require support from the adaptive system. In these cases, the innate immune system can direct the adaptive one by providing information about pathogen's nature via the expression of costimulatory molecules, such as CD80 and CD86, present on the surface of antigen-presenting cells (APCs), among which stand out the dendritic cells (DCs).(100,101)

1.2.2.2 Adaptive immunity

Adaptive immunity is a more sophisticated defence system based on a specific response triggered by antigens. The hallmarks of the adaptive system are recognition specificity and memory, which is the capacity to remember the immune response towards a particular pathogen.(102) The first response is amplified by a cascade of events involving all the cells of the immune system. The higher complexity of this system compared to the innate one is demonstrated, for instance, by the development of customised antibodies after antigen recognition and processing, improving future responses.

The evolution of the adaptive immune system has resulted in a broad recognition repertoire for both self and non-self antigens. Antigen-presenting cells (APCs) collaborate closely with T and B lymphocytes to produce selective immunological effectors against the pathogen dictated by an ever-growing immunological memory with the goal of achieving host immune homeostasis.(103) The functioning of the adaptive system consists of a first phase of antigen processing by macrophages and dendritic cells and a second phase of presentation to T- and B-lymphocytes that ensure its recognition by specific receptors (TCR and BCR). Lymphocytes, originating in the lymphatic system, interact with specific receptors created by gene segments assembled in a large number of possible combinations. Antigen binding to these receptors results in activation, proliferation and differentiation into effector cells through a process of clonal selection which typically occurs within the specialised environment of lymphoid tissue. Secondly, the response of activated T-cells leaving the lymphoid tissue and heading for the site of interest, or the release of antibodies from activated B-cells, subsequently occurs.

1.2.3 Dendritic cells

Steinman and Cohn first identified DCs in mouse spleens due to morphological features that differentiated them from macrophages.(104) Subsequent identification

relied on specific markers and biological functions, including the capacity to travel to lymphoid organs to trigger T lymphocytes.(105–107) The discovery of DCs, together with the later identification of pattern recognition receptors (PRRs), has made them a key point in the perpetual conversation between innate and adaptive immunity.(108) Decades of research have now demonstrated the importance of DCs in initiating adaptive immune responses and their ability to influence the outcome of immune activation.

They are a heterogeneous population of cells located at the interface between innate and adaptive immunity.(109) DCs can be divided into two main groups: plasmacytoid DCs (pDCs) and conventional DCs (cDCs) (**Figure 5**). cDCs are involved in the production of proinflammatory cytokines for the early immune response while pDCs are involved in the production of type I interferons (IFNs) and immune suppression in the immature state.(110,111)

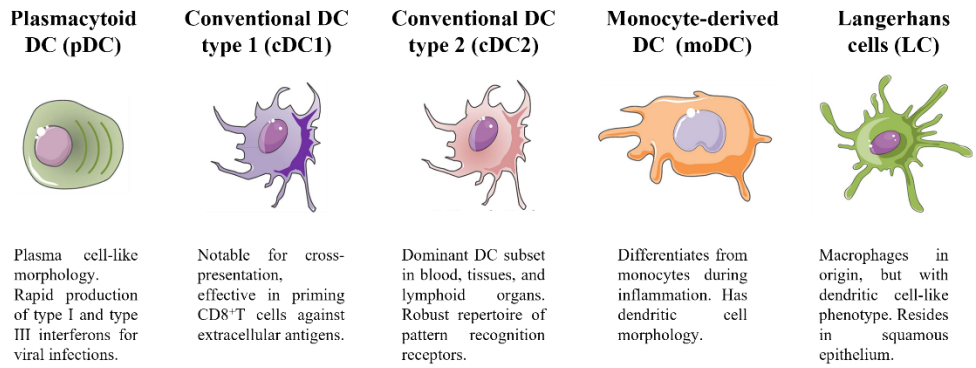

Figure 5: Subclasses of dendritic cells.

Initially, DCs are called immature and sample the peripheral tissue environment through the activities of endocytosis and macropinocytosis. During their life cycle, a crucial event is the process of maturation, which occurs when DCs recognize a pathogen. This prompts the degradation of the pathogen into peptides that stimulate

the production of co-stimulatory agents. The expression of the MHC class II complex increase, leading to the migration to the lymph node and ultimately to the activation of naive T cells that are specific to the antigen and will differentiate into pro- or anti-inflammatory subgroups.(109,112–114) The differences between mature and immature DCs are numerous, spanning from cytokine generation to co-stimulatory factor expression to the presentation of antigens (**Figure 6**).

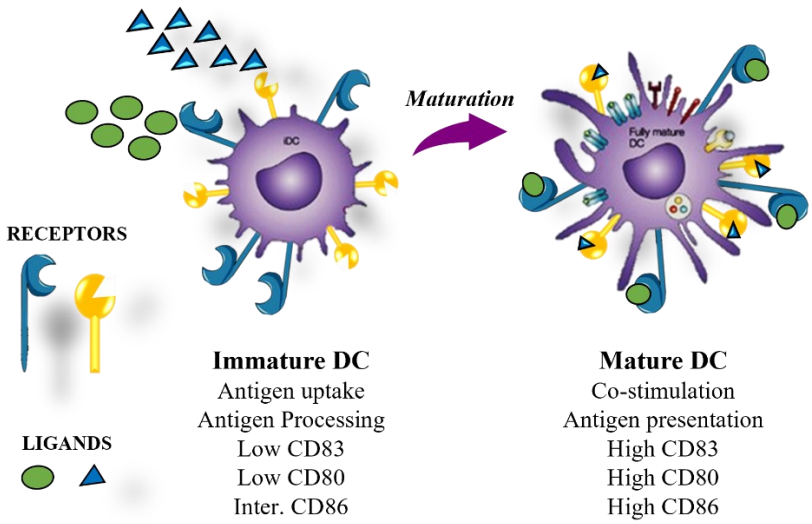

Figure 6: Differences between immature and mature DCs.

The maturation process of DCs can change according to different environmental and endogenous stimuli, influencing lymphocyte activities and generated compounds.(115–117) Subsequent to the maturation process, the synthesis of cytokines (e.g., IL-12 and IL-10) chemokines (which attract phagocytes, lymphocytes, and naive T cells to the maturation site) and interferons that enhance innate and adaptive resistance begins.(118–121) Mature cells upregulate the expression of receptors for phagocytosis and endocytosis and increase the production of costimulatory molecules such as CD40, CD80, CD86, and various members of the TNF receptor family that undergo different morphological alterations.(122)

The DC maturation process can be tracked by the expression of phenotypic markers, useful to estimate the immunomodulatory properties of compounds. This technique is currently viewed as a valuable approach for discovering new immunomodulatory agents. Since DCs play a critical role in controlling immunity, they are a sensible target for clinical scenarios related to T cells.(123–127)

1.2.4 Glycolipids in immunity

In addition to their role in human metabolism, lipids also play important roles in the immune system, performing functions ranging from signalling inflammation to mediating intracellular signals and activating cell receptors. In addition, lipids can act as antigens and regulate immunity by activating T cells, being involved in many immunological response mechanisms.(128) Several reviews have already highlighted the effects and capabilities of glycolipids within the immune system.(129,130)

For example, glycolipids can target TLRs receptors, resulting in activation of the immune response. One of the most significant examples is lipid A, which potently stimulates host defence systems by activating TLR4.(131,132)

Another protein family, crucial in immune activation is represented by CD1 proteins, displaying structural homology with MHC class I molecules, but with the peculiarity to present lipid-based antigens to T cells.(133) As a result of the localisation of different isoforms in subcellular compartments, they allow APCs to present a variety of glycolipid antigens that are targeted by different pathways once inside the cell.(134) Thanks to the semi-invariant TCR, NKT cells recognise glycolipids presented in the context of the CD1d molecule.(135–137) The ability to alter the function of NKT lymphocytes in different contexts using different ligands may make them potential immunomodulatory agents.

Recently, the ability of these substances to induce immunomodulatory activity has been demonstrated by the ability of a synthetic β-sulfoquinovosyldiacylglycerol to induce unconventional DC maturation leading to an up-regulation of MHC complex

and co-stimulatory molecules without release of conventional cytokines.(59,138) Glycolipids are promising as novel immunomodulatory agents and their pharmacological potential supports the ongoing efforts of scientific research in this field.

1.3 Receptors of the innate immunity

Receptors of the innate immune system are the body's first line of defence in the early stages of infection. A better understanding of their function and their downstream effects can potentially lead to improvements in the immune response, as well as ways to improve vaccines action and prevent autoimmunity. While bridging between innate and adaptive immunity, they may have non-specific anti-infection, anti-tumour and other immunoprotective effects upon the recognition of pathogenic microorganisms. The recognition is mediated by several receptors among which stand out the pattern recognition receptors (PRRs), which interact with pathogen-associated molecular patterns (PAMPs), such as microbial nucleic acids, lipoproteins and carbohydrates and damage-associated molecular patterns (DAMPs) (**Figure 7**).(139–141)

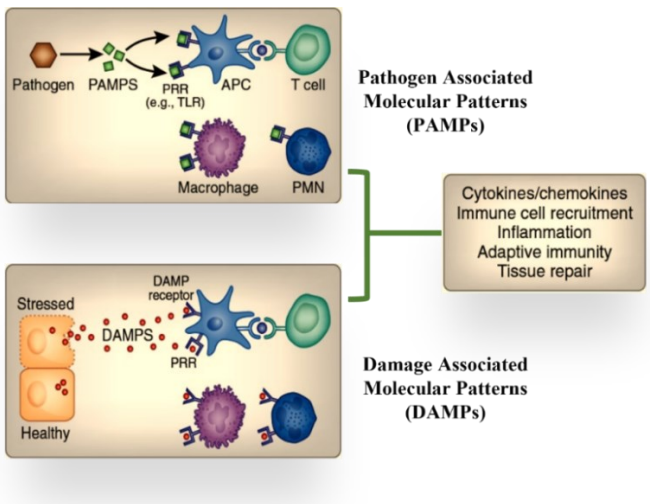

Figure 7: PAMPs and DAMPs recognition.

The recognition of PAMPs and DAMPs leads to the activation of the antimicrobial and inflammatory response by APCs and the subsequent intervention of adaptive immunity for the ultimate elimination of pathogens.(142) Binding of PRRs has two primary outcomes: firstly, it creates a danger signal to cells, which initiates a signalling cascade aimed at directing the body's defence; secondly, it induces selected cells' competency to present antigens to T lymphocytes. The stimulation of PRRs induces the maturation of APCs, as dendritic cells (DCs), and stabilises molecules on the surface of the histocompatibility complex (MHC), inducing antigen presentation. This process activates co-stimulatory molecules, which determine T-cell proliferation and differentiation.(143–145) During this event, a cascade of signals is generated and processes of phagocytosis, respiratory burst and release of cytokines and chemokines begin. PRRs activation by natural or artificial ligands and their regulation are fundamental for the immune response shaping.

They are mainly classified into the following families: Toll-like receptors (TLRs), nucleotide oligomerization domain (NOD)-like receptors (NLRs), retinoic acid-inducible gene-I (RIG-I)-like receptors (RLRs), C-type lectin receptors (CLRs), and absent in melanoma-2 (AIM2)-like receptors (ALRs) (**Figure 8**).(146)

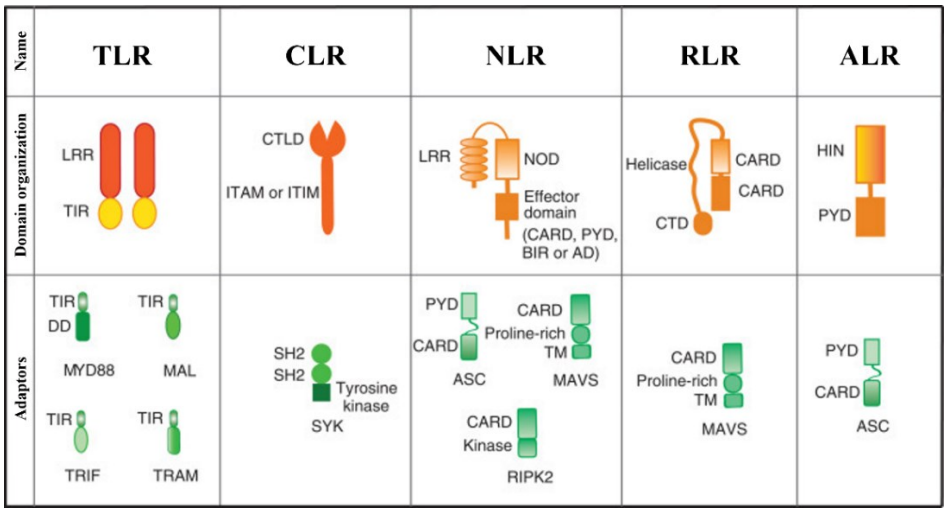

Figure 8: Main subclasses of pattern recognition receptors (PRRs).(147)

Toll-like receptors (TLRs) are membrane-bound PRRs that can recognise conserved structures of PAMPs and initiate signalling responses. Although there are some variations among different TLRs in their molecular pattern recognition, their overall structure is quite conserved. All TLRs contain an extracellular leucine-rich repeat (LRR) domain that is responsible for binding to the ligand. The LRR domain is linked to a transmembrane domain and an intracellular domain from which signal transduction begins. TLR signalling begins when specific adapters, such as MyD88, trigger the activation of associated kinases and subsequent downstream factors.(148,149)

NLRs are cytoplasmic receptors that recognise PAMPs from internalised microbial components.(150) They are intracellular PRRs consisting of three domains that are independently involved in nucleotide binding, ligand recognition and protein recognition. The most prominent members of the NOD subfamily are NOD1 and NOD2 that mediate the recognition of specific bacterial components. In general, these proteins have a regulatory function in inflammatory responses and also appear to act as cytosolic sensors for the induction of apoptosis.(151–153)

RLRs are intracellular PRRs that, together with TLR7 and TLR9, recognise viral nucleic acids and mount an antiviral immune response.(154,155) This is supported by the fact that RIG-I induces the expression of a reporter gene in the IFN-β promoter region.(156–158)

ALRs have the ability to recognise intracellular DNA. The C-terminal domain can identify and bind double-stranded DNA, while the N-terminal PYD domain binds to the apoptosis-associated speck-like protein (ASC) PYD domain. This induces the production of inflammasome and the release of specific interleukins. Additionally, ALRs regulate apoptosis in tumour initiation and development contexts.(159–161)

1.3.1 C-type lectin receptors (CLRs)

The class of C-type lectins is the most studied after the TLR class, and scientific interest on them has increased critically in recent years. They comprise over 1000 proteins, categorised into 17 groups based on their roles and structures.(162)

They are mostly expressed on antigen-presenting cells such as macrophages and DCs and are considered phagocytic PRRs. They recognise PAMPs (usually carbohydrates expressed on the surface of microorganisms) and place pathogens in cytoplasmic vesicles for direct digestion.(163,164) Carbohydrate recognition is enabled by a spherical carbohydrate recognition domain (CRD).(165–167) The interaction of CLRs with ligands and subsequent signalling (mostly via spleen tyrosine kinase) regulates homeostasis and immunity.(168) In addition, CLRs are able to cross-talk with other PRRs, specifically TLRs, to enhance or down-regulate inflammatory responses and promote immunogenic 'fine-tuning' necessary to avoid harmful or autoimmune responses.(142)

In general, CLRs can be divided into transmembrane and secretory receptors.(165,169,170) The collagen lectin family is the most prominent group of secretory receptors.(171) Based on their structure, transmembrane receptors can be classified as either type I or type II.(172) DEC-205 and the macrophage mannose receptor (MMR) are both examples of type I transmembrane proteins containing multiple CRDs. In contrast, type II transmembrane CLRs have a single CRD domain and include Dectin-1, Dectin-2, Mincle, DC-SIGN and DNGR-1.(173)

Dectin-1 and Dectin-2 are the most studied CLRs and are mainly involved in the recognition of fungi.(174,175) Dectin-1 has been one of the cellular effectors that has been targeted with small molecules in this thesis, thus a deeper discussion of its features is reported in the following section. Dectin-2 recognises mainly α-mannans on the cell wall of fungi, but also lipoglycans of various bacterial species. However, the research community remains unaware of the recognition mechanism.(176–179)

1.3.1.1 Dectin-1

Dendritic cell-associated C-type lectin-1 (Dectin-1) is primarily expressed on myeloid cells such as monocytes, macrophages, DCs and neutrophils, but has also been detected on B cells, certain T-cell subsets and epithelial cells.(180,181) Dectin-1 is a type II membrane glycoprotein consisting of a C-terminal leptin-like domain (CTLD) separated from the cell membrane by a short STALK region, a transmembrane domain (TMD) and an intracellular domain containing an immunoreceptor tyrosine-based activation motif (ITAM) domain (**Figure 9**).

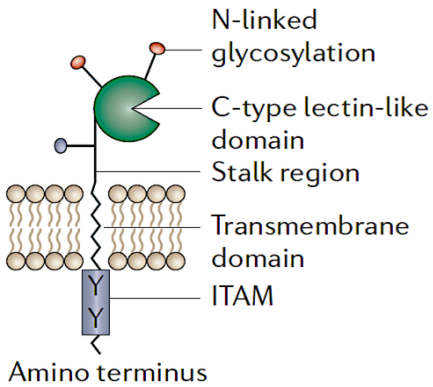

Figure 9: Dectin-1 structure.(182)

Dectin-1 is a 28 kDa transmembrane protein composed of 244 amino acids and six cysteine residues. In contrast to many other C-type lectin receptors, it lacks cysteine residues in the stalk region required for dimerization. The receptor should therefore behave as a monomer but, recent reports suggest a still unknown mechanism involving the bridge of two Dectin-1 monomers before the interaction with Tyrosine-protein kinase (Syk).(183,184)

The protein is encoded by member A of the C-type lectin domain family 7 (CLEC7A), a gene consisting of six exons and five introns. The exons determine the structure of

dectin-1, while the intron-exon boundaries contain donor-acceptor sites that lead to alternative splicing and the subsequent generation of different Dectin isoforms. Eight structurally different isoforms from A to H can be generated. Isoform A is considered to be the major isoform with full-length structure from the C′ to the N′ terminus. Isoform B has all the structural features of isoform A except for the stalk region. Isoforms C and D exhibit alterations in the CRD region, isoforms E and F have no stem and no transmembrane region, and isoforms G and H have some insertions in the CRD and transmembrane regions.(185)

Glycosylation is an important post-translational modification of proteins that is key to the immune system and the regulation of biological activity, so much that abnormalities in this mechanism are usually associated with the onset of malignancy.(186,187) Therefore, the identification of receptors, as Dectin-1, that bind glycans is of primary importance for the treatment of human infectious and autoimmune diseases. Dectin-1 recognises in fact β-(1,3) and (1,6) glucans, polysaccharides commonly found on the cell walls of pathogens including fungi and some bacteria.(188,189) Dectin-1 recognition differs depending on the structure of the glucans, including polymer length and side chain branching. Dectin-1 is crucial in antifungal immunity as it detects multiple fungal species including pathogens such as *Candida albicans*, *Aspergillus fumigatus*, *Coccidioides immitis*, *Pneumocystis carinii* and *Cryptococcus*.(190–198) Several additional endogenous ligands, such as galactosylated immunoglobulins and galectins, are known to bind to this receptor.(199).

Ligand recognition by Dectin-1 can trigger and regulate numerous cellular responses, including phagocytosis, autophagy, DC maturation and the production of cytokines and chemokines.(200) Dectin-1 is able to determine the development of adaptive immune responses by stimulating both Th1 and Th17 responses. While Th1 responses are important for the control of systemic infections by intracellular pathogens, Th17 responses are essential for controlling mucosal fungal infections.(201,202) Furthermore, this receptor is also involved in allergy, promoting humoral responses via Th22 through the regulation of IL-22 and IL-33, which are crucial in the

modulation of these diseases, (203) as well as in the control of autoimmune diseases such as arthritis and ulcerative colitis and neuroimmune diseases.(204,205)

Dectin-1 mediates intracellular signalling via hem-ITAM, a modified ITAM containing a single tyrosine residue in its intracellular tail that is phosphorylated by the SRC family of SFK protein tyrosine kinases.(206) This phosphorylation subsequently results in the recruitment and activation of spleen protein tyrosine kinase (Syk), which triggers additional downstream signalling pathways. This Syk-mediated signalling involves the caspase recruitment domain (CARD9) and activation of NF-κB, responsible for the production of cytokines and chemokines, via a Card9/Bcl10/Malt1 complex.(184,207–209) Dectin-1 also controls a Syk-independent signalling pathway via a serine-threonine kinase (Raf-1), which combines with the Syk-dependent signalling pathway at the site of nuclear factor-kappa (NF-κB) stimulation.(210,211) Dectin-1 also causes nuclear factor-activated T-cell (NFAT) activation in dendritic cells (DCs) and macrophages, which leads to the regulation of early growth response (Egr) family transcription factors and cyclooxygenase-2 (**Figure 10**).(207)

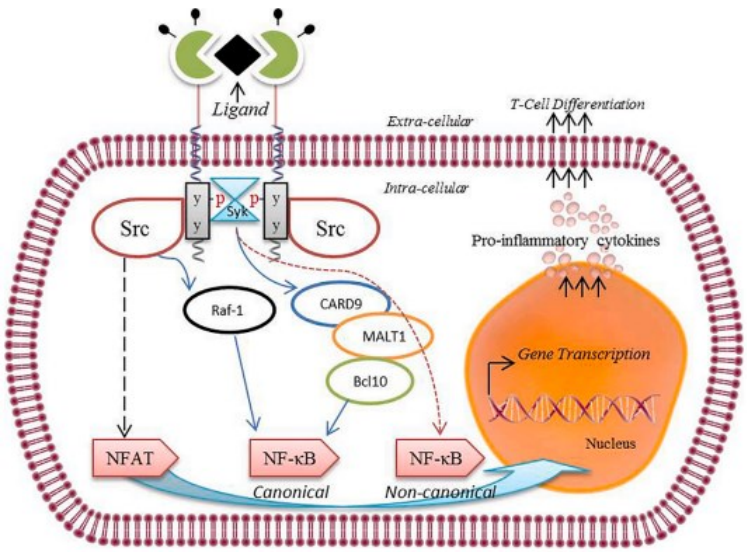

Figure 10: Dectin-1 mediated intracellular signaling after ligand binding.(185)

The discovery of new ligands for this receptor would constitute a crucial advance in the modulation of its downstream effects and thus the regulation of immune system intervention.

1.3.2 Triggering receptors expressed on myeloid cells (TREMs)

Triggering Receptors Expressed on Myeloid Cells (TREMs) are a family of receptors whose main role is to modulate the responses of the myeloid cells on which they are expressed. Their functions may be either positive or negative and is often linked to neurodegenerative disorders. These receptors belong to the immunoglobulin superfamily and have a single extracellular immunoglobulin V-type domain followed by a short stalk (19-172 a.a.) leading to a single transmembrane helix and terminates with a cytosolic tail (195-230 a.a.) lacking signalling motifs.(212) In addition to the membrane-bound form, soluble ectodomains can be generated by alternative splicing or proteolytic processing.(213,214) Human and mouse TREMs are encoded by gene clusters on human chromosome 6p21.1 and mouse chromosome 17C, respectively. The human cluster includes NCR2, TREM1, TREML4, TREML2, TREM2 and TREML1. The mouse cluster includes TREM5, TREM4, TREM1, TREM3, TREML4, TREML2, TREML6 and TREM2.(215) TREM1 was the first TREM to be identified and shows upregulation in response to LPS.(216) Its activation by unknown ligands leads to an enhanced immune response that can be effective against pathogens, but sometimes harmful to the host too.(217,218)

1.3.2.1 TREM2: Activation pathway and ligands

Human TREM2 is a polypeptide chain consisting of 230 amino acids first identified in human DCs and in a mouse macrophage cell line.(219,220) TREM2 macrophages mainly include microglia in the central nervous system, osteoclasts in bone, but also subsets in liver, intestine, skin and tumours. A co-crystallised structure of TREM2

with a synthetic analogue of phosphatidylserine showed that TREM2 arranges as three-dimensional trimers of dimers with a binding site at the interface of each dimer (**Figure 11**).(221)

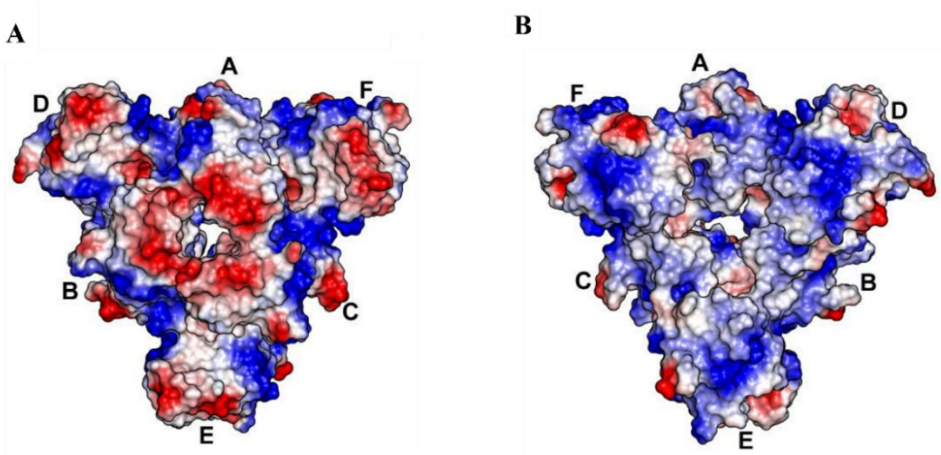

Figure 11: A Electrostatic surface diagram of trimeric packing of six WT TREM2 molecules with inner trimer oriented in a forward-facing manner and exterior neighbouring molecules toward the posterior. **B** Electrostatic surface diagram of trimeric packing of six WT TREM2 molecules with exterior neighbouring molecules oriented in a forward-facing manner and inner trimer toward the posterior.(221)

Although the TREM2 functions and mechanisms are still under investigation, it works through the 12 kDa DNAX-activating protein (DAP12) that is encoded by TYROBP and includes ITAM-like motifs.(222) Upon activation, phosphorylation of ITAM tyrosines by SRC kinases allows docking of the protein tyrosine kinase SYK, which stimulates downstream signalling (**Figure 12**).(223,224) In addition, DAP12 signalling overlaps with that of TLRs receptors, such as extracellular signal-regulated kinase (ERK) resulting in a dense and complex network of cellular responses to external stimuli.(225,226)

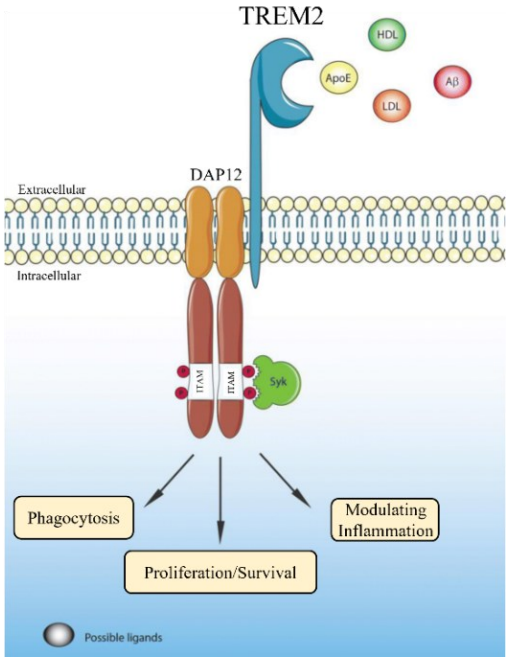

Figure 12: TREM2 ligands, signalling and functions. Ligands binding induces the association of TREM2 to DAP12 through an electrostatic interaction generating tyrosine phosphorylation of DAP12 within its ITAMS by Src family kinases.(227)

The importance of finding the ligands of this receptor and understanding the mechanism of binding is particularly relevant given its close association with inflammatory, autoimmune and neurodegenerative diseases. Although the binding mechanism is still unclear, TREM2 can recognise phospholipids, glycolipids, sulphatides and lipoproteins, as well as the apolipoprotein E (APOE).(138,228–231) Moreover, it has been demonstrated that TREM-2 downregulates DC and macrophage function in presence of TLR ligands derived from bacteria and viruses such as LPS.(232) TREM-2 binds extensively to Gram-positive and Gram-negative bacteria through the action of anionic bacterial products or other anionic carbohydrates, as occurs in the recognition of astrocytoma cell lines.(233) This suggests that TREM-2 recognition by pathogens is also mediated by surface-expressed charged carbohydrates.

1.3.2.2 TREM2 related diseases

TREM2 and its mutations were initially associated with Nasu-Hakola disease (NHD), a rare condition resulting in multiple issues throughout adolescence, followed by early dementia and eventually premature death.(234–236) Patients with NHD presented DAP12 or TREM2 loss-of-function variants. Multiple studies have established the crucial role of TREM2 in osteoclasts and microglia. Manipulation of TREM2 expression affects the expression of chemokine receptors, phagocytosis, transcription of inflammatory cytokines, and phagocytosis of apoptotic cells.(237) However, these *in vitro* findings are not always validated by *in vivo* experiments, and the rationale for this remains unclear.

TREM2 also appears to play an important role in cancer: thousands of tumours from the Cancer Genome Atlas and the Genotype Tissue-Expression Project have been shown to express this receptor.(238) It is highly expressed in Tumour-associated Macrophages (TAMs) in both human and mouse tumours. Blocking it with a monoclonal antibody has been shown to limit tumour growth and enhance the cytotoxic CD8+ anti-tumour T-cell response.(239) TREM2 has also been extensively studied in human breast cancer, renal cell carcinoma and ductal adenocarcinoma of the pancreas and has shown immunomodulatory activity.(240–245) Considering both the high expression of TREM2 on microglia and the involvement of microglia activity in myelin remodelling in the central nervous system, TREM2 also has potential in the treatment of demyelinating diseases. Indeed, TREM2 has been shown to bind to myelin lipids, phagocytose them and transmit intracellular signals.(246,247) Other neurodegenerative diseases associated with TREM2 variants include Alzheimer's disease, Parkinson's disease, amyotrophic lateral sclerosis (ALS) and frontotemporal dementia.(248–252)

1.3.2.3 TREM2 in Alzheimer

One of the neuropathologies most closely associated to TREM2 is Alzheimer's disease (AD), a common disease of the elderly worldwide. In fact, attention to this receptor has intensified in the last decade because mutant forms of TREM2 increase the risk of developing AD.(253–256) Indeed, TREM2 has been shown to recognize and favour microglial phagocytosis of the neurotoxic β-amyloid peptides (Aβ) that form the amyloid plaques typical of Alzheimer's disease.(257–259) Studies in mouse models of Aβ accumulation and AD patients have shown that the hypofunctional TREM2-R47H variant (where Hystidine replaces Arginine at position 47) impairs the ability of microglia to encapsulate Aβ plaques, thereby facilitating AD progression.(260,261) In particular, the TREM2-R47H and TREM2-R62H (where Hystidine replaces Arginine at position 62) variants had reduced ability to bind possible ligands, presumably due to significant structural changes triggered by the mutations.(228–230,262,263) Kober and colleagues explained how specific point mutations in TREM2 resulted in various neurodegenerative disorders via two distinct loss-of-function mechanisms. These mechanisms were verified in a separate paper via *in silico* investigations.(264,265) TREM2 is essential for the microglial response to Aβ, as the TREM2-DAP12-SYK complex supports protein synthesis and the energy cost required for microglia to react to Aβ accumulation.(223,266) Some studies have shown that an anti-TREM2 agonist antibody can penetrate the blood-brain barrier and activate microglia in mouse models of AD.(267–269) The first clinical trial evaluating the efficacy and safety of an anti-TREM2 antibody in slowing the progression of AD is currently underway (NCT04592874, ClinicalTrials.gov).(270) It is likely that subsequent studies in this field will focus on identifying novel generations of TREM2 agonists and antagonists, with the potential to impact ligand binding or the cellular adaptors DAP12 and DAP10.

Chapter 2: Results and discussion

2.1 Synthesis and biological activity of sterol derivatives

2.1.1 Bioassay screening platform

In the laboratories of the Institute of Biomolecular Chemistry (ICB-CNR) in Pozzuoli, an immunoassay-guided screening platform has been developed for the extraction and purification of natural compounds of marine origin to search for new molecules with immunomodulatory activity.(271) The experimental procedure was based on phenotypic assays to select chemicals from a panel of growth factor-dependent immature mouse dendritic cells (D1). Parallel experiments were conducted in both TREM2 and Dectin-1b reporter cells, expressing the specific receptors. Following positive tests on D1, further tests on human monocyte-derived dendritic cells (MoDCs) were conducted. An example of this approach was the bioassay-guided fractionation and purification of biologically active compounds from the marine diatom *Thalassiosira weissflogii* (CCMP-1336), able to induce DCs maturation.(272) Several immunomodulatory compounds have been isolated and characterised from this diatom, including a promising fraction containing α-SQDG.

Briefly, the experimental procedure consists of diluting the methanol extracts obtained from the wet diatom pellet in water and loading them on a poly(styrene-divinylbenzene) (HR-X) support (reversed phase support), following a method called solid phase extraction (SPE).(26,273) The major components of the mixture are eluted to obtain several fractions of different polarity, which are biologically tested. The immunoactive fractions are then purified by a second fractionation step by HILIC column (normal phase support) and the test-positive fractions are then purified by HPLC. Finally, the pure molecules are characterised and assayed (**Figure 13**).

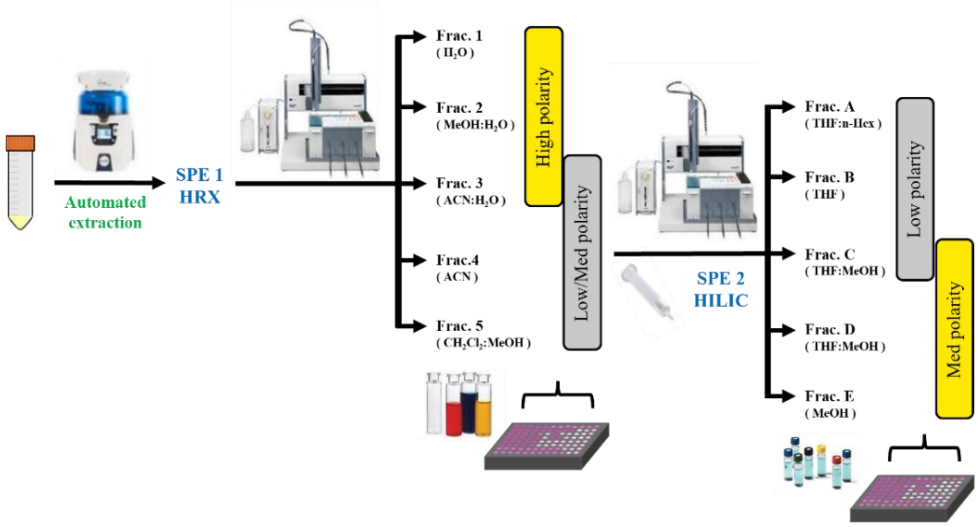

Figure 13: Immunoassay-guided screening platform for the extraction and purification of natural compounds of marine origin.(26)

2.1.2 Immunological reporter cell assays and chemical synthesis of sterol derivatives

The protocol mentioned above performed on microalga *Skeletonema marinoi* extracts, led to the identification of cholesterol sulphate (CHOS), already evaluated for the peculiar ability to induce apoptosis in protists.(274) CHOS was analysed at different concentrations and showed the ability to induce human DC maturation and activate Dectin-1b reporter cells, using Zymosan (known Dectin-1b ligand) as positive control.(275) This is the first example of a small molecule able to bind Dectin-1, chemically different from β-1,3 glucans. These results were confirmed even by analysis on a synthetic cholesterol sulphate prepared by our literature procedure.(276)

The analysis performed showed that the Dectin-1b receptor, when activated by CHOS, induced DC maturation with no effect on cytokine release but a decrease of IL-10 and IL-6. Interesting activity of this molecule was evident in the modulation of inflammatory response in DC by performing co-stimulation experiments with CHOS

(1 and 10 μg/mL) together with LPS (5 ng/mL). Changes were observed in the expression of the inflammatory IL-12p40 subunit (found in both pro-inflammatory interleukin IL-12 and IL-23), by cytofluorimetry and real-time PCR. CD86 expression doubles in the presence of LPS compared to unstimulated cells but decreases in a dose-dependent manner in presence of cholesterol sulphate with a significant suppression of pro-inflammatory gene expression, compared to the up-regulation induced by single treatment with LPS.

It is well known that cholesterol sulphate is also recognized as stimulating ligand of macrophage inducible C-type lectin receptor (Mincle), a receptor expressed on myeloid cells including macrophages and DCs and able to sense mycobacteria, pathogenic fungi and DAMPS, resulting in the production of inflammatory cytokines.(277) These interactions can determine synergistic or antagonistic effects, crucial for a general immunogenic regulatory mechanism.(201,202) The immune system, in fact, involves innumerable responses, signaling pathways interactions and simultaneous effector mechanisms and the ability to fine tune and balance this immunological apparatus is vital to provide an appropriate and self-limiting outcome. Binding assays on reporter cells excluded the recognition of cholesterol sulphate by TLR2 and TLR4, deeply involved in the cross-talk interactions with CLRs.

The ability of CHOS to bind both receptors was evident in no inflammatory effects occurred with cholesterol sulphate after DC maturation, possibly due to the Mincle and Dectin-1 antagonistic interactions, corroborating the deep cross-talk between the two receptors. Both Dectin1 and Mincle have been associated with a pro-inflammatory response, hence, the dual axis of Mincle/Dectin-1b was shown to provide an immune-regulatory response.(278)

The biological properties of cholesterol sulphate, related to the ability to bind both Mincle and Dectin-1, lie in its structure. Therefore, synthetic preparation of sterol-based sulphate derivatives, potentially able to interact only with Dectin-1, represents a crucial step for the assessment of immunomodulatory activity and possible pharmacological applications linked to the functions of this receptor, pivotal for

immune response modulation. The synthesis of several analogues with different chemical structure variants was crucial to define the structural determinants affecting biological activity and to optimize their immunomodulatory properties.

2.1.2.1 Preparation of sulphated sterol derivatives

Starting from the cholesteryl sulphate, several analogues have been synthesized introducing small structural changes, not only aimed at optimizing their activity but also investigating the structural determinants involved in the interaction with the receptor. The structural regions most affected by the modifications were those at the 3- and 17-position groups of the steroid core as these should be the most exposed sites to the first interaction with the receptor. As native cholesterol did not bind, unlike CHOS, a range of derivatives was synthesised maintaining the sulphate group in position 3 and modifying the residual structure. For this purpose, inspired by the work of Huang and colleagues, the generalised 3-*O*-steroid sulphation on sterol analogues was used (**Scheme 1**).(279) Triethylamine sulfur trioxide complex (Et_3N-SO_3) as electrophilic reagent offered conspicuous advantages for the preparation of a wide variety of sulphated compounds, as persulphation, low degradation, and feasibility in the work-up.(280) Moreover, the solvent used in the reaction was the anhydrous *N,N*-dimethylformamide (DMF), where all the different sterols were soluble, resulting in an homogeneous reaction mixture and very fast reaction rate.

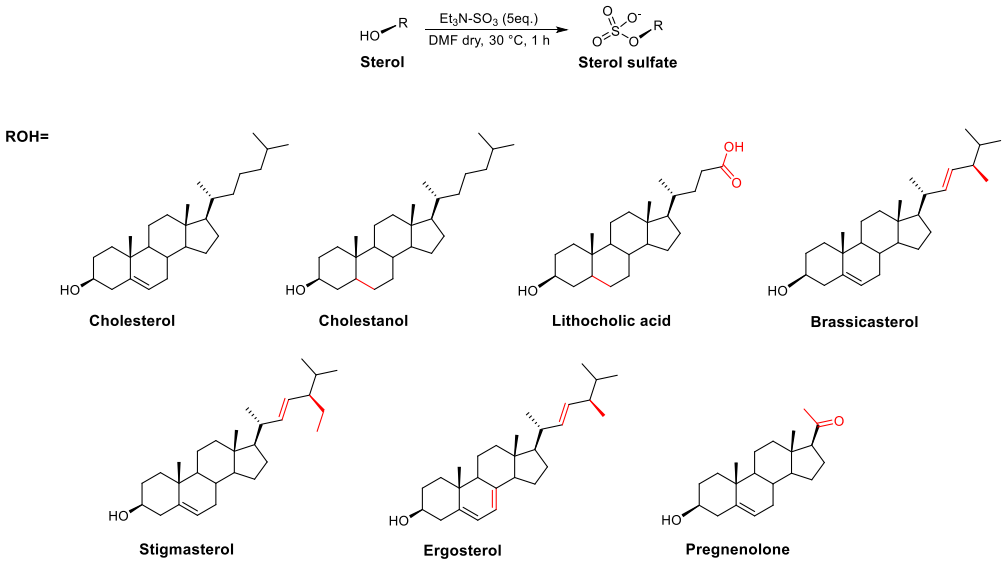

Scheme 1: General sulphation reaction for the synthesis of sulphated sterol derivatives (the structural modifications from cholesterol are highlighted in red).

2.1.2.2 Synthesis of brominated and acetyl cholesterol

With the aim to evaluate the weight of the sulphate group on the immunoactivity and in the receptor recognition process, not-sulphated sterol analogues were prepared. Attention was initially focused on alo- and ester-derivatives. First, 3-β-bromo cholesterol was prepared. In detail, in order to preserve the sterol carbon 3 stereochemistry, a two-step reaction procedure was employed. The first step involved the introduction on position 3 of a leaving methanesulphonate group for the bromine substitution. The reaction was carried out in presence of triethylamine (TEA) as base and under anhydrous conditions to give compound **1** (**Scheme 2**).

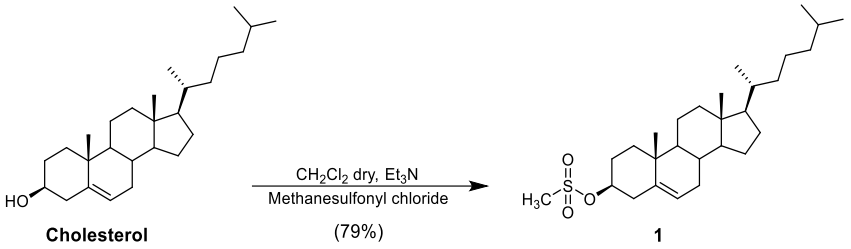

Scheme 2: Synthesis of methanesulphonyl cholesterol.

The second step consisted in a nucleophilic substitution on compound **1** by bromide, in presence of boron trifluoride diethyl etherate (BF_3OEt_2) as Lewis acid promoter and bromotrimethylsilane (TMSBr), to give compound **2** (**Scheme 3**). The non-classical carbocation formation allows to get retention of cholesterol C-3 β-configuration.(281)

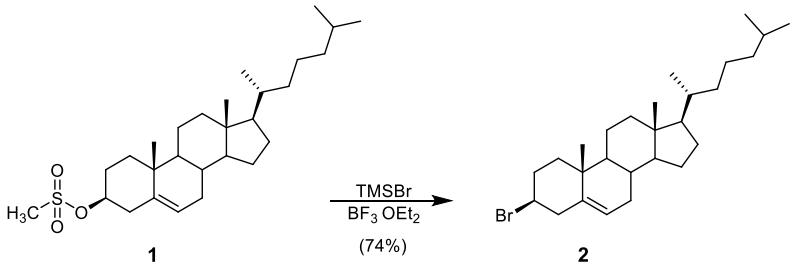

Scheme 3: Synthesis of cholesterol bromide.

The ester derivative, 3-β-*O*-acetyl cholesterol, was prepared by simple acetylation reaction under nucleophilic catalysis conditions, using anhydrous pyridine (Py) as solvent/catalyst and acetic anhydride (Ac_2O) as acetylating agent (**Scheme 4**).

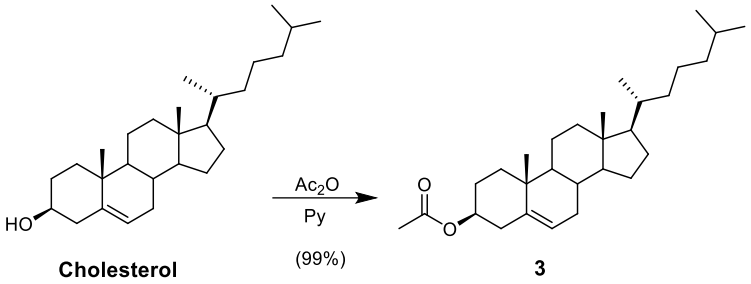

Scheme 4: Synthesis of acetyl cholesterol.

2.1.2.3 Synthesis of phosphate cholesterol

To also investigate the impact of the anionic charged group in position 3, another derivative was prepared, the 3-β-*O*-phosphate cholesterol. In this case a phosphorylation reaction of the sterol hydroxyl group was provided by a phosphorylating agent [phosphorus (III)], used in literature.(282) The chemical basis of this reaction is the oxidation of phosphorylating phosphites by carbon tetrahalides in presence of alcohol.(282) Trimethyl phosphite was used as phosphorylating agent because of the good stability due to the *O*-methyl groups. The reaction was solvent dependent giving best yields when performed in pyridine. In detail, in presence of tetrabromomethane (CBr_4), the trimethyl phosphite $P(OMe)_3$ reacted with the hydroxyl group of cholesterol to give compound **4** (**Scheme 5**). The main aspect of this reaction is the iterative exchange reaction between the tetralkoxyphosphonium salt and a new ROH. Although most of the alkyl nucleophilic groups used to protect the phosphate can be cleaved by a nucleophilic agent, the choice of CH_3 as protecting groups was particularly suitable due to their stability and low cost.(282). Methyls deprotection was subsequently carried out under anhydrous conditions using trimethylsilylbromide.(283)

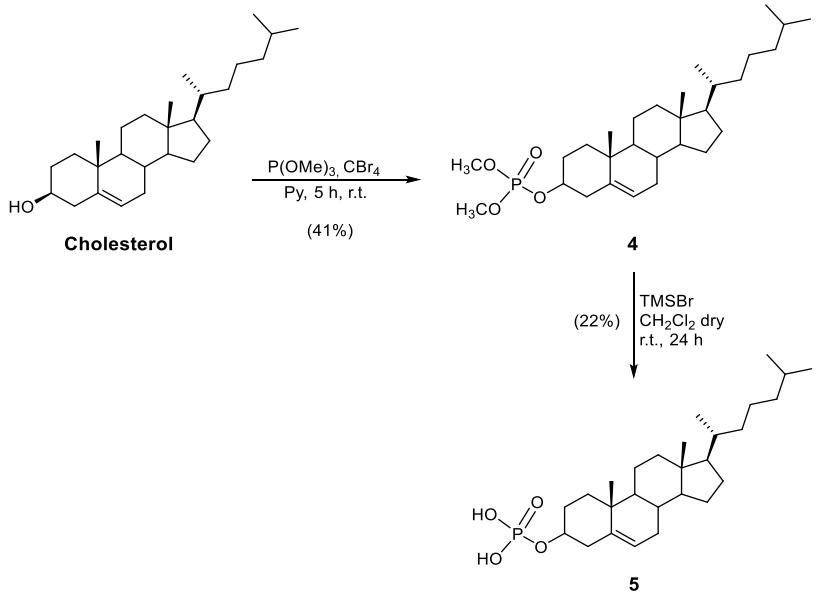

Scheme 5: Synthesis of phosphate cholesterol.

2.1.2.4 Synthesis of β-glyco-cholesterols

Substitution on sterol hydroxyl by a neutral or charged glycosides, led to the obtainment of β-glycocholesterols, a new class of promising immunomodulators, given the enormous potential of sugar structures in triggering and modulating an immunological response. These molecules combine the structural characteristics of immunomodulant glyco- and sterol derivatives. Considering the peculiar immunological activity of a nature inspired β-6'-sulfoquinovosyldistearoyl glycerol (Sulfavant A), a sulfoquinovose fragment was linked to cholesterol on carbon 3 by a β-configuration glycosidic bond.(138) The synthetic strategy to obtain the β-6'-sulfoquinovosyl-cholesterol was inspired by Manzo et al. procedure for the synthesis of Sulfavant A (**Scheme 6**).(59) In detail the synthetic approach started with the acetylation of D-glucose and selective deacetylation at the anomeric position with benzylamine ($BnNH_2$) and further derivatization to the trichloroacetimidate intermediate (compound **8**) using 1,8-diazabiciclo[5.4.0]undec-7-ene (DBU) as catalyst. Using trichloroacetimidate as leaving group and boron trifluoride diethyl

etherate (BF_3OEt_2) as Lewis acid, it was possible to couple the cholesterol to get the intermediate **9** preserving the β configuration thanks to the anchimeric assistance of the nearby acetate. The glucosyl cholesterol (compound **10**) was achieved by deprotection of the acyl groups by Zemplén reaction.(284) With the aim of inserting the sulphonic group at position 6', tritylation and acetylation of the sugar led to compound **12**. Position 6' was deprotected with chlorotrimethylsilane and sodium iodide and protected again with a tosylate group to have a better leaving group (compound **14**).(285) After the insertion of the thioacetate group, the sulfonic function was obtained at position 6' through oxidation using ammonium heptamolybdate, with no impact on the double bond, which is susceptible to some oxidation conditions. The sulfoquinovosyl cholesterol **17** was obtained by Zemplén deacetylation.

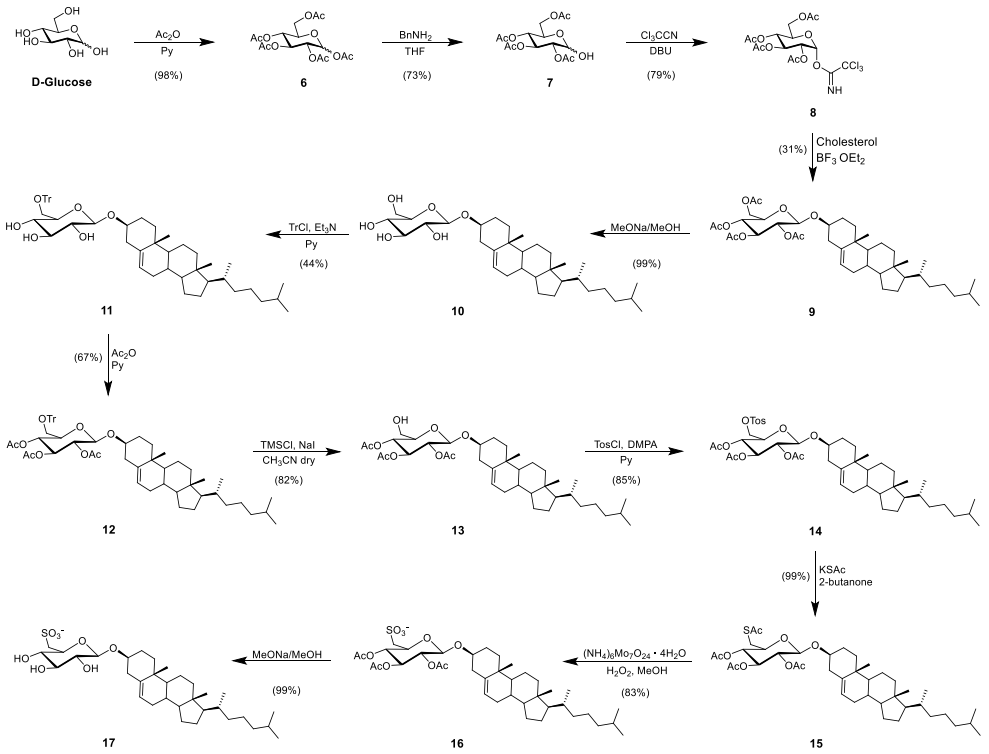

Scheme 6: Synthetis of β-D-6'-sulfoquinovosyl-cholesterol.

2.1.3 Reporter cells assays of synthetized sterol derivatives

Receptor screening assays were performed with Dectin-1b reporter cells on all synthesised sterol derivatives, with the aim to identify potential new ligands for the Dectin-1b receptor and define chemical structural determinants crucial for the interaction with the protein. In the reporter cell line used, Dectin-1b was associated with a signalling pathway involving Nf-kB and the transcription of alkaline phosphatase (SEAP), a reporter protein secreted into the extracellular medium after ligand binding in a manner proportional to the strength of the interaction. First of all, the synthetic cholesterol sulphate was tested on Dectin-1b reporter cells using Zymosan as reference showing affinity for the receptor (**Figure 14**).

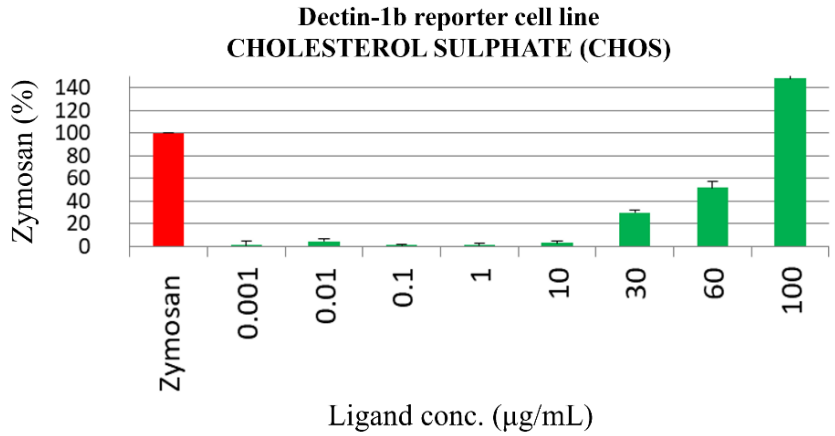

Figure 14: Reporter cell assay of cholesterol sulphate using Zymosan as reference.

Subsequently, all the other synthetised molecules (**Figure 15)** were assayed on Dectin-1b reporter cells in the range 1 ng - 60 µg/mL using CHOS at a concentration of 60 µg/mL as a reference.

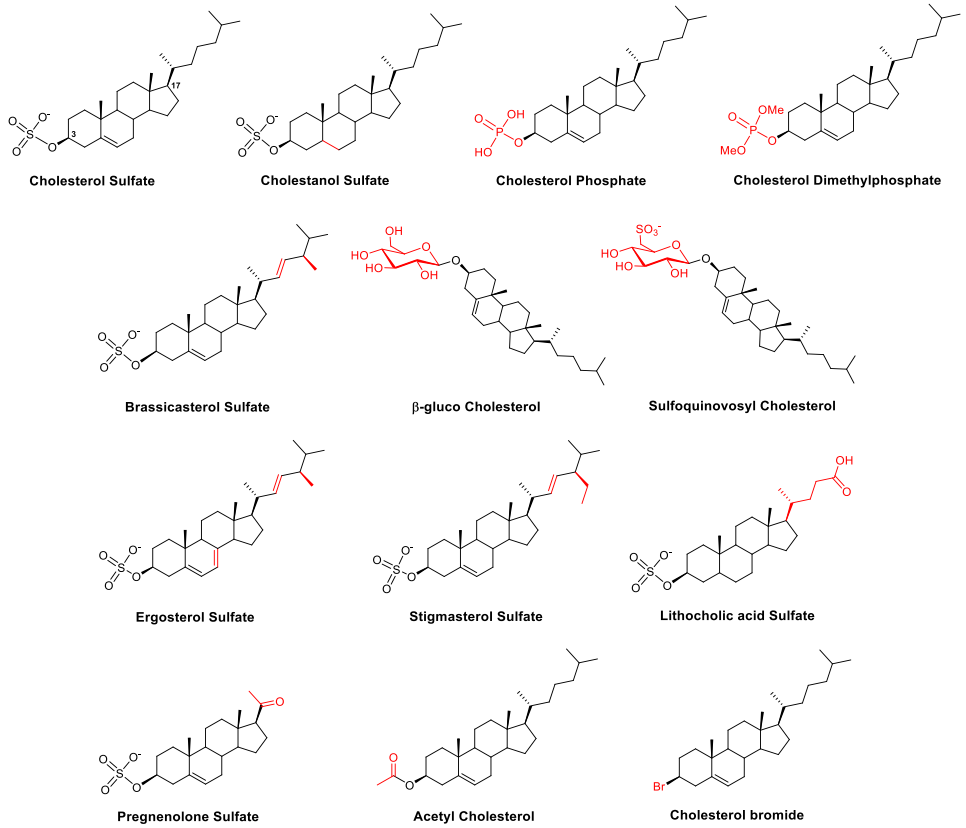

Figure 15: Sterol derivatives tested as potential Dectin-1b ligand (the structural motifs different from cholesterol are highlighted in red).

Data showed that sterol derivatives with modified C17 side chain ste were not active, suggesting that the side chain play a key role in the receptor recognition. Another key modification of the structure was the substitution of the group on carbon 3, as only the simulataneous presence of negative charge and a sulphur atom allowed binding of the receptor. In fact, the biological assays allowed the identification of only two compounds, besides CHOS, able to interact with Dectin-1b: sulfoquinovosyl cholesterol and cholestanol sulphate (**Figure 16**).

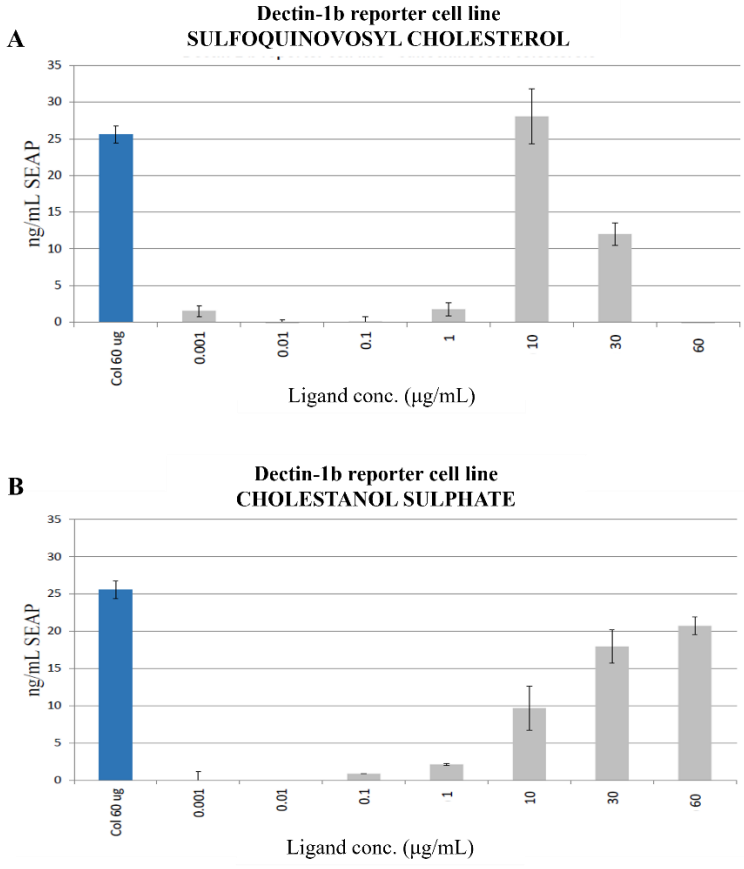

Figure 16: A Reporter cell assay on sulfoquinovosyl cholesterol; **B** Reporter cell assay on cholestanol sulphate. All the molecules were tested on Dectin-1b reporter cells in the range 1 ng - 60 µg/mL using cholesterol sulfphate as reference.

From the evaluation of the biological results, the following considerations can be made:

- A negative charge on the group in position 3 can promote the recognition of the cellular target.
- A sulfur-containing negative charged group on carbon 3 can promote the recognition of the cellular target.

- Changes in the cholesterol C17-side chain could lead to loss of ability to bind the receptor.

2.1.4 Conclusions

Dectin-1 is a highly promising receptor for immune response modulation, whose potential remains largely unexplored. It can induce NF-kB activation through two independent signalling mechanisms, as well as NFAT triggering. Modulation of pathways like NF-kB and NFAT through different signalling mechanisms is a key target for the regulation of the immune response in infection and inflammatory disease. (211)

In this section, the preparation of sterol derivatives as potential new ligands for Dectin-1 was presented. Starting from the characterization of cholesterol sulphate as a novel ligand of Dectin-1, a range of sterol analogues, presenting modifications mainly on positions 3 and 17, was synthesised and assessed for the ability to bind Dectin-1. Preliminary biological assays using a Dectin-1b reporter cell line suggested that some structural elements, are important in receptor recognition.(271) All derivatives in which the side chain on C17 has been modified from the original cholesterol structure, showed a loss of activity towards the receptor, suggesting that this structural part is particularly involved in recognition. The change in position 3 would also appear to influence binding. A number of derivatives with very different functional groups at this position was synthesised and biologically tested. The only derivatives that maintained affinity towards Dectin-1 were those where an oxidised negative charged sulphur atom was present, giving this element a fundamental role. Future studies will focus on the identification and characterisation of other possible sterol-based ligands of Dectin-1, with the aim of developing new therapeutic strategies for the treatment of inflammatory diseases and for the development of antifungal and anticancer therapies.

2.2 Synthesis of more stable Sulfavant A analogues

2.2.1 Sulfavant A: a new immunomodulator adjuvant and first synthetic TREM2 ligand

Sulfavant A originated from a chemical optimisation process of natural α-D-sulfoquinovosyl-diacylglycerols (α-SQDG), immunomodulatory compounds characterised by a sulphonic group at the 6'-carbon of quinovose linked to a diacylglycerol residue. As reported, Sulf-A stimulated dendritic cell maturation by an unprecedented TLR-independent homeostatogenic mechanism and was effective as a vaccine adjuvant in an experimental anti-melanoma vaccine model, resulting in delayed and reduced tumour growth.(59) The Sulf-A-induced maturation of DCs with homeostatic and regulatory functions was specifically mediated by TREM2 and probably controlled by NFAT transcription factors. The antibodies secretion induced by Sulf-A in *in vivo* mice immunisation experiment against ovalbumine antigen, confirmed molecule's potential to activate the immune system.(59)

Flow cytometry technique was used to measure parameters indicative of the maturation of DCs, following treatment with Sulf-A. In this regard *in vitro* biological assays led to a modification of the expression of costimulatory molecules CD86 and CD83, and the MHC class II HLA-DR. In this context, it is noteworthy that the phenotypic marker CD83, which is exclusive for a full DC maturation, is not detectable in other antigen-presenting cells (APCs) that do not trigger naïve T cells and is therefore a reliable biological factor. $CD83^{+}$ DCs have important implications against several diseases such as malaria, tuberculosis and cancer, and for the improvement of vaccine adjuvants activity.(286,287)

After treatment of DCs with SULF A, the expression levels of the markers CD86 and and CD83 increased in a dose-dependent manner. Sulfavant A also did not induce production of pro-inflammatory cytokines.(59,138,288)

As the DC immunological response is often mediated by TLR2 and TLR4 receptors, further assays were performed to investigate the action mechanism responsible for the

immunomodulatory activity of Sulf-A. Tests on HEK293 cells co-transfected to express TLR-2 or TLR-4 and the alkaline phosphatase reporter gene, using Pam2CSK4 (PAM) (TLR2 agonist) and LPS (TLR4 agonist) as positive controls, were performed. The Sulf-A mechanism of action was found to be TLR-independent, as no effect on TLR activation was observed under the same conditions that led to maturation of DCs.(59)

This recent discovery justified the interest in studying this product and its analogues for the treatment of diseases related to TREM-2 dysfunction, such as chronic and neurodegenerative diseases.(212,289–291)

During preclinical development of Sulfavant A, pharmacokinetics analyses were carried out for the evaluation of biodistribution of the molecule in murine models. We noted a gradual metabolization of the molecule in the first hours after intraperitoneal administration. In order to increase the permanence of the molecules in the body and development of new methods for the oral administration of this drug as well, two more chemically stable derivatives of Sulf-A were synthesised. The new two molecules, named Sulf-etherate and Sulf-amidate, mantain the same structure of Sulf-A but replacing the ester functions by ether or amide groups respectively (**Figure 17**).

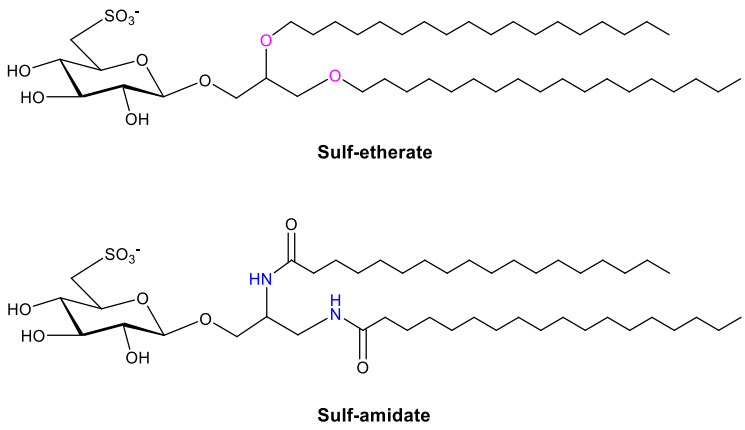

Figure 17: Structures of Sulf-etherate and Sulf-amidate.

2.2.2 Synthesis of Sulfavant A derivatives

2.2.2.1 Synthesis of Sulf-etherate

The synthetic strategy used for the preparation of Sulf-etherate proceeded by coupling of two building blocks: the peracetylated trichloroacetimidate glucose donor (Compound **8**) and the glycerol acceptor with C18 ether chains (**building block 2**) (**Scheme 7**).

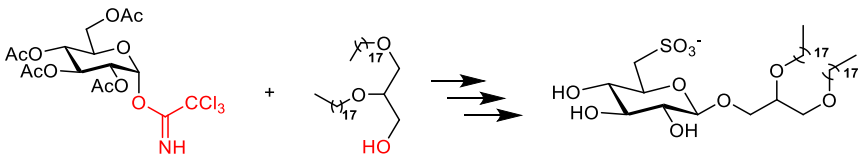

Scheme 7: Coupling of peracetylated trichloroacetimidate glucose donor with **building block 2** to get Sulf-etherate.

The preparation of compound **8** was already described in **Scheme 6**. For the preparation of **building block 2**, an 1,2-*O*-isopropylidene-protected glycerol was used (**Scheme 8**). The free primary hydroxyl was protected with a benzyl group by benzyl bromide and sodium hydride treatment. The subsequent isopropylidene removal was performed in one hour at room temperature with Dowex H^+, an acidic resin with various 'green' advantages such as non-toxicity, low cost, easy separation and reusability. The obtained diol was then coupled with stearyl bromide, using tetrabutylammonium iodide (TBAI) as catalyst, able to transform the alkyl bromide in the more reactive alkyl iodide. The alkyl bromide was previously obtained by $LiAlH_4$-induced reduction of stearic acid followed by Appel reaction to substitute the hydroxyl group with a bromine using triphenylphosphine and tetrabromomethane.(292) Finally, the benzyl group was removed by hydrogenolysis with hydrogen in presence of Pd/C (10%) to give **building block 2**.

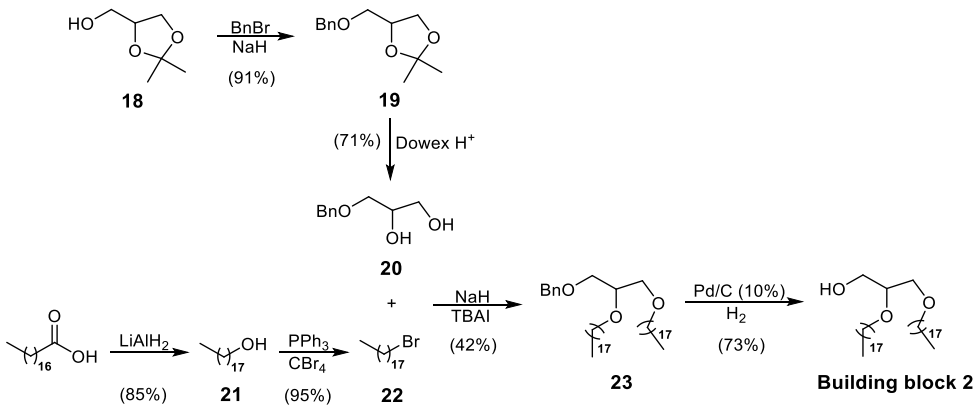

Scheme 8: Synthesis of **building block 2**.

The coupling between the two synthetized building blocks occurred via a Schmidt glycosidation, to give β-glucosyl derivative **24** (**Scheme 9**). Schmidt glycosylation is currently one of the most popular methods of glycosylation, involving a Lewis acid as catalyst, in this case BF_3.(293) Despite the fact that certain precautions must be taken regarding the reaction conditions to obtain the desired product, such as low temperature and an anhydrous environment, this reaction has become popular because of the mildly acidic coupling conditions and the possibility of modifying the α/β selectivity by using different glycosyl donors and coupling reagents. Compound **24** was then deprotected by Zemplén deacetylation with sodium methoxide in methanol. The 6'-position of the sugar was selectively functionalized with iodine using of triphenylphosphine, molecular iodine and 2,6-lutidine following the Traboni et al. procedure and then completely acetylated with acetic anhydride in pyridine to get compound **27**.(294)

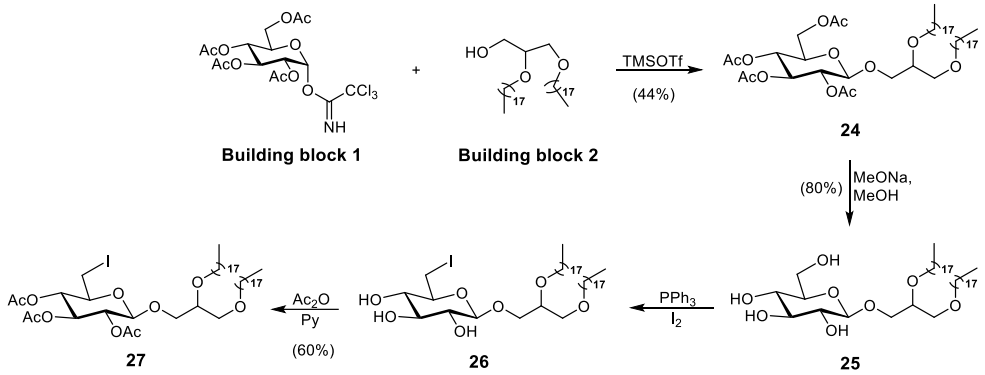

Scheme 9: Glycosilation and 6' derivatization.

The presence of iodine in the 6' position allows a wide range of easy derivatizations. In our case, we were able to introduce a thioacetate group by adding potassium thioacetate (**Scheme 10**). Oxidation of the thioacetic group with hydrogen peroxide in acetic acid led to the obtainment of a sulfonic group in position 6' (compound **29**). Finally, deprotection of the sugar with further Zemplén deacetylation yielded the Sulf-etherate.

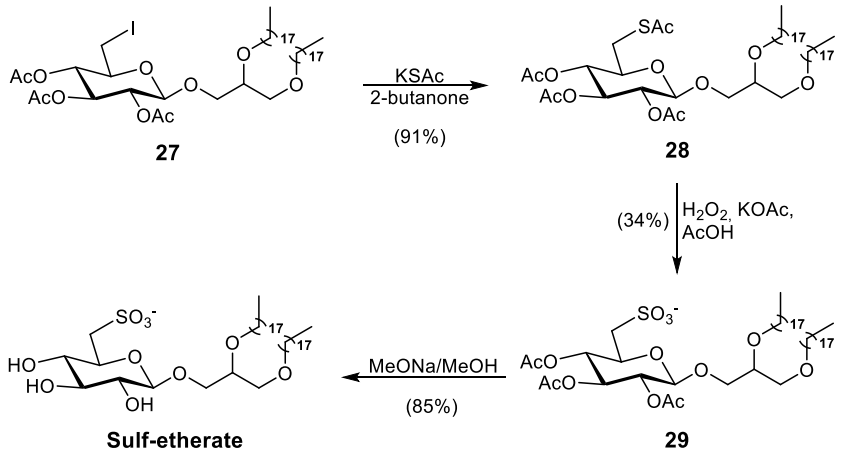

Scheme 10: Last reaction steps for the synthesis of Sulf-etherate.

2.2.2.2 TREM2 reporter cell analysis on Sulf-etherate

The affinity of Sulf-etherate towards TREM2 WT receptor was tested by analysis on reporter cells (**Figure 18**). In this regard, a consolidated TREM2-reporter cell line transducing receptor engagement by synthesis of GFP, was used.(295) GFP, a protein expressed by the jellyfish *Aequorea victoria*, has become a widely used tool in molecular biology. Its size, spectroscopic and fluorescence properties make it particularly suitable for this type of study, and a reliable marker of gene expression in individual eukaryotic cells when fluorescence is measured by flow cytometry.(296,297) When exposed to radiation of a specific wavelength, GFP emits bright green light, although specific modifications can now produce radiations at different wavelengths.

Human TREM2 was transfected in reporter cells expressing GFP under the control of NFAT, such that Ca^{2+} mobilization turns on GFP expression when TREM2 is engaged. Reporter activation and the subsequent GFP expression, were assessed after overnight incubation by flow cytometry. Sulf-eterate showed a dose-dependent response in the range from 0.1 ng/mL to 600 µg/mL showing an affinity towards TREM2 comparable to Sulf-A.

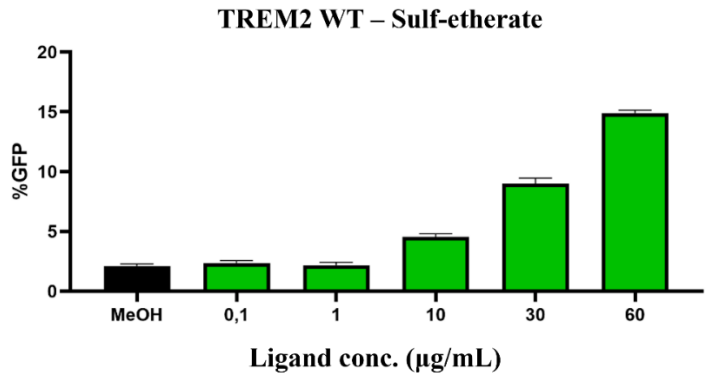

Figure 18: Dose-dependent response of human TREM2-reporter cells on Sulf-etherate using MeOH as control.

2.2.2.3 Synthesis of Sulf-amidate: different approaches

The synthesis of the amidated derivative has proved to be very problematic due to the known difficulties in the preparation of synthetic derivatives comprising two vicinal amide functions. Despite these difficulties and the various attempts through the design of different synthetic strategies that could favor the achievement of this goal, it was almost possible to arrive to the final product. All the different strategies undertaken for this synthesis are described below, together with the difficulties encountered.

In the first strategy, allyl alcohol was used as starting reagent and was brominated through the bromine addition. Replacement of bromine with sodium azide, by SN2 substitution, led to the diazide product. Due to their acute toxicity and explosiveness, sodium azide and compound **31** were handled with special caution and appropriate safety equipment. Sodium azide was added inside the extraction hood using a plastic spatula, avoiding contact with metal surfaces to prevent the formation of heavy metal azides, which are highly shock-sensitive explosives. The stereospecific coupling reaction in anhydrous condition with the previously prepared peracetylated glucose, gave the β-glucoside derivative **32** (**Scheme 11**).

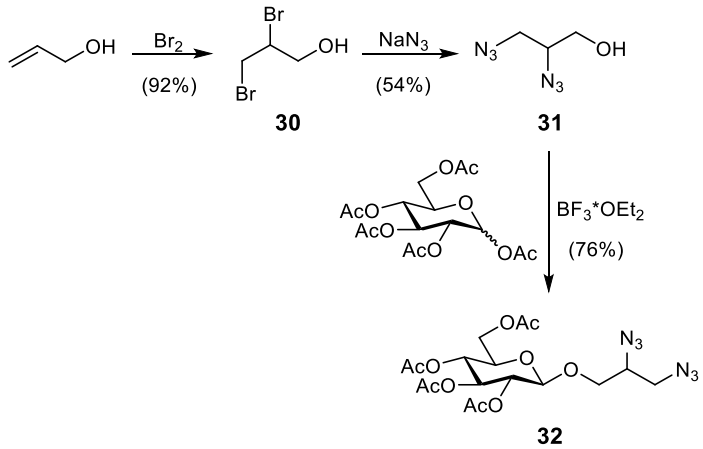

Scheme 11: Synthesis of β-glucosyl-rac-glycerol di-azide.

The azides were reduced to amines by a palladium-catalysed transfer hydrogen and then two stearic acid chains were condensed to the glycerol moiety making amide bonds (**Scheme 12**). Nucleophilic attack by the amine groups was facilitated by the *in-situ* conversion of stearic acid into acyl chloride using thionyl chloride ($SOCl_2$). The *N*-stearoyl derivative **34** was deprotected with sodium methoxide in methanol following the Zemplén method to get compound **35**. With the aim to introduce sulphonic function in position 6', the hydroxyl group was protected with a trityl group, a well-known sugar protecting group which, due to its size, can only derivatize primary position 6'. Unfortunately, the trityl derivatization presented unexpected very scarce yields, despite the use of different experimental conditions involving reaction temperature and solvents modification along with reagents ratio and amount change. This was likely due to the interference of the *N*-acyl groups during the trityl insertion.

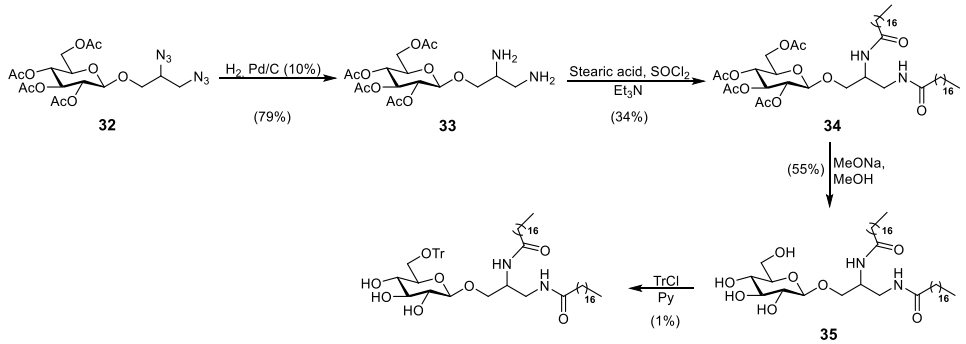

Scheme 12: First approach for the synthesis of Sulf-amidate.

In a second approach efforts were made to introduce sulfonic function in position 6' of the sugar before adding lipid chains via amide bonds (**Scheme 13**). Intermediate **32** was deacetylated and selectively tritylated at position 6'. After sugar acetylation, selective deprotection of the trityl group with sodium iodide and trimethylsilyl chloride afforded compound **39**. A tosyl leaving group was introduced at the 6' position and then replaced by a thioacetyl function thanks to an 80 °C reaction with

potassium acetate. The last step was the reduction of the azides by catalytic hydrogenation with palladium on carbon, but unfortunately the reaction product was strongly retained by the metal catalyst. Attempts to release it under mild and acidic conditions only resulted in its degradation.

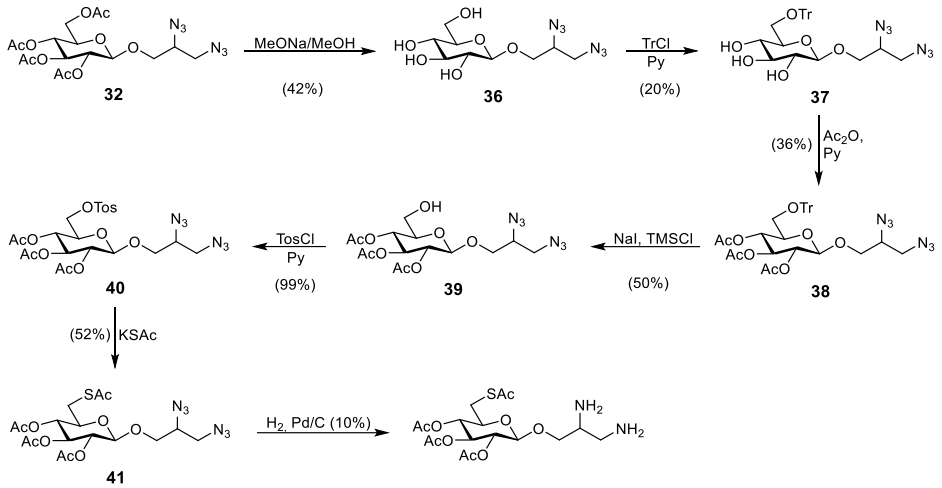

Scheme 13: Second approach for the synthesis of Sulf-amidate.

With the aim to overcome the problems encountered so far, a new chemical strategy has been designed, including the synthesis of a 6'-thioacetate glycosidic donor (**building block A**) and of the aglycone (1,2-*N*-distearoyl glycerol) (**building block B**) before their subsequent coupling (**Scheme 14**).

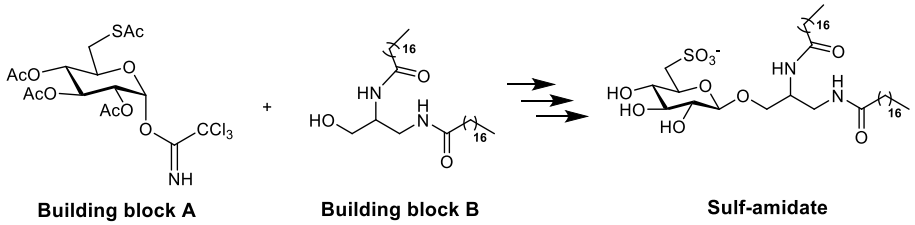

Scheme 14: Building block strategy for the synthesis of Sulf-amidate.

To prepare **building block A** (**Scheme 15**), the anomeric position of D-glucose was selectively protected by a methyl group with acid chloride in methanol and the position 6' was selectively iodised and replaced by a thioacetate group by Traboni et al. procedure described previously (**Scheme 9**), obtaining compound **45** (**Scheme 15**).(294) Subsequent treatment with acetic anhydride in acetic acid in presence of a strong acid catalyst as H_2SO_4, replaced the methoxyl- with acetyl group that was finally selectively removed with benzylamine. The final step consisted in the formation of the donor trichloroacetimidate using trichloroacetonitrile and DBU as catalyst under anhydrous conditions.

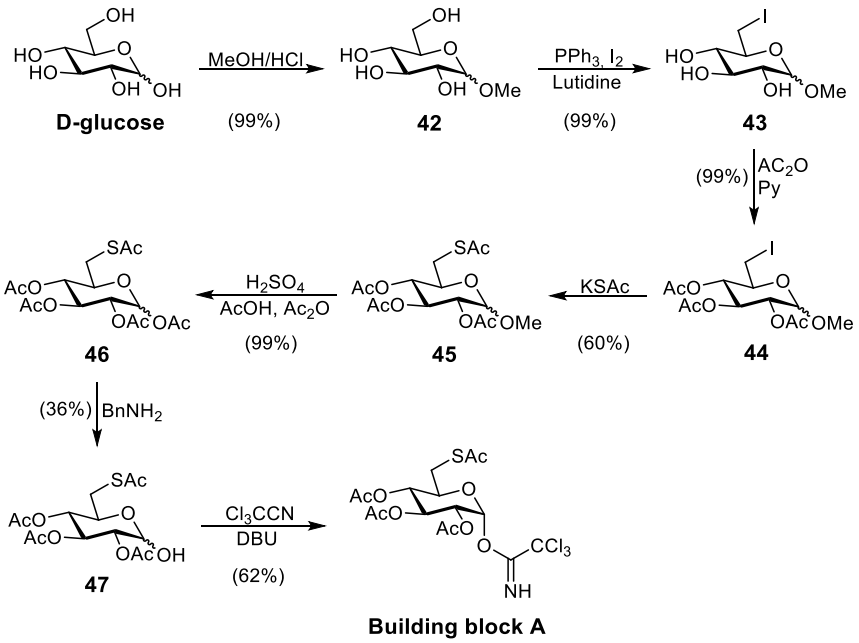

Scheme 15: Synthesis of 6'-thioacetate glycosidic donor (**building block A**).

For the preparation of **building block B,** reduction of compound **31**, by Staudinger's reaction, gave the diamine **48** (**Scheme 16**).(298) This reaction was possible by a mild method in which phosphine and azide were first treated to form the phosphine imide, which was then hydrolysed to form a phosphinoxide and an amine. Compound **48** was

filtered in water and lyophilised. The subsequent reaction involved condensation of **48** in pyridine at 60 °C with stearic anhydride, previously obtained by stearic acid dehydration, forming the *N*-stearoyl derivative **50**. Zemplén reaction was carried out at 65 °C to deprotect only the hydroxyl group and obtain **building block B**.

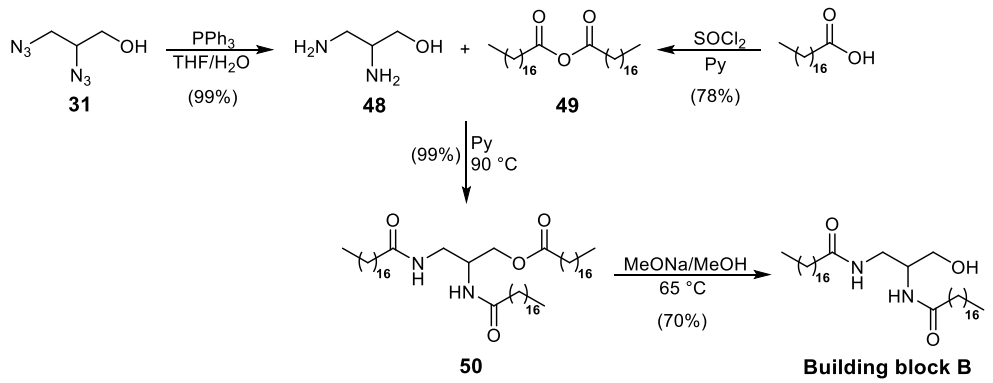

Scheme 16: Synthetic strategy for the preparation of 1,2-*N*-distearoyl glycerol (**building block B**).

The product was finely purified by size exclusion chromatography (SEC) to prepare it for coupling with the sugar, ensuring that there was no residual stearic acid which could compete in this reaction. The coupling between **building block A** and **B** was then carried out using two different methods: the first with trimethylsilyltriflate and the second with boron trifluoride etherate as catalysts, both under strictly anhydrous conditions (**Scheme 17**).

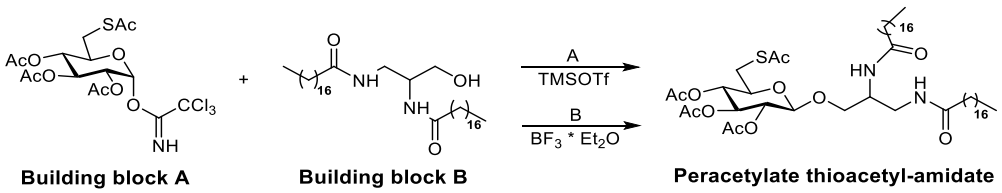

Scheme 17: Two different glycosylation reactions to get peracetylated thioacetyl-amidate.

Unfortunately, both reactions resulted in a very little amount of product, probably due to the particularly unarmed aglycone providing a low nucleophilic hydroxyl group and partially quenching the Lewis acid catalyst. It was possible to characterize the product by mass spectrometry but not by NMR and the amount was not enough to continue the synthesis.

2.2.3 Conclusions

In the frame of preclinical Sulfavant A development, pharmacokinetic studies led on murine model showed that the molecule presented a few hours residence time in the body after intraperitoneal administration. In order to increase the permanence and to develop new methods of administration of this drug, two more chemically stable derivatives of Sulf-A were designed. In this regard, attention was focused on the synthesis of the two Sulf-A analogues, Sulf-etherate and Sulf-amidate, with lipid chains attached to the glycerol moiety by ether and amide bonds respectively. The resulting structural changes, compared to the progenitor Sulfavant A, could not only favor greater stability of the molecules in physiological environment, but also provide information about the effect of these modifications on the interactions with TREM2, driving in this way the preparation of further potent derivatives.

Due to the different binding between the lipid and glyceridic part, the synthetic approach used for Sulf-A was not applicable. For Sulf-etherate derivative, a new strategy was therefore developed involving the combination of two building blocks, the acetylated trichloroacetimidate glucose donor (**building block A**) and the glycerol acceptor containing C18 ether chains (**building block B**). Sulf-etherate was tested on TREM2 reporter cells and showed interesting binding affinity towards this receptor. The current progress in the synthesis of Sulf-amidate has been reported including various approaches with the relative difficulties encountered. In a first approach, the lipid chains were bound to the already sugar-bound portion of glycerol, but the hydroxyl at the 6' position could not be modified. In contrast, in the second approach, thioacetate group was efficiently introduced at position 6’ of the sugar, but the

insertion of the lipid chains was impeded due to the product's strong retention by the catalyst after the eterogeneous hydrogenolysis. In the last approach, the two building blocks were prepared separately, the first with the thioacetate trichloroacetimidate donor and the second with the aglycone with pre-bound lipid chains to the glycerol via amide bonds. However, the glycosylation reaction was unsuccessful due to the unfavourable properties of the aglycone. Currently, the problem that hindered the second approach has been solved. Indeed, the hydrogenation of the azides was no longer carried out with a palladium catalyst but with triphenylphosphine in THF at 90 °C. This recently led to the obtainment of the next intermediate from which the synthesis can be resumed.

2.3 Synthesis of a fluorescent analogue of Sulfavant A

Before Sulfavants, no synthetic TREM2 ligands have been reported and functional aspects of TREM2 transduction signalling are still not totally explored. Therefore, crucial steps for the pharmacological development of this class of immunomodulators are further studies of the in-depth biological mechanism, disclosure and subcellular localisation of cellular targets and *in vivo* ADME (absorption, distribution, metabolism and excretion). Hence, we decided to design a fluorescent analogue of Sulf-A introducing a suitable fluorescent tag (**Figure 19**). It is clear that having a molecule with both immunomodulatory and fluorescent activity can be a huge step forward.

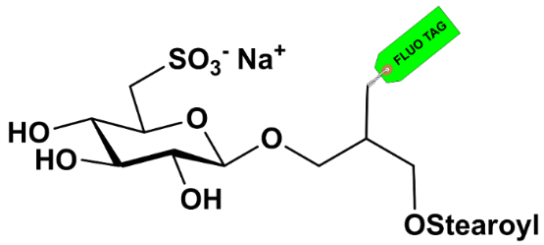

Figure 19: Sulf-A with an acyl chain replaced by a fluorescent tag.

The use of fluorescence had, and still has, a huge impact on biological and biomedical research, since it enables not only to visualize normal physiological processes with high temporal and spatial resolution, but also to detect multiple signals, to track molecules *in vivo*, to have elucidations on the interaction with the cellular target, and to shed light on many pathobiological processes underpinning disease states.(299–305) Fluorescent labelling is extensively employed across numerous fields, particularly for in-depth analyses of proteins and nucleic acids. However, it remains relatively underdeveloped concerning glycolipids, potentially due to their structural and synthetic complexity.(306) However, recent years have seen an increase in the development of glycolipids coupled to fluorescent probes.(307,308) For example, 4,4-difluoro-4-bora-3a,4a-diaza-*s*-indacene (BODIPY) has already been used to label sphingolipids for metabolism and trafficking studies in animal cells without any significant change in biological properties.(309,310)

The selection of an appropriate fluorescent probe to link to the β-SQDG represents a critical challenge for the use of this technique on this class of molecules. Although there are numerous potential fluorescent probes available, the BODIPY dyes, consisting of a dipyrrin framework with a BF_2 core, have garnered interest because of their suitable properties: high absorption and fluorescence quantum yield, good photo- and chemical-stability, high solubility and resistance to self-aggregation (**Figure 20**).(311–318)

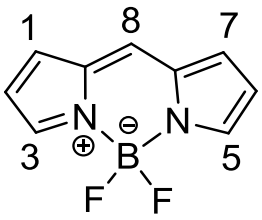

Figure 20: BODIPY core structure.

Several studies reported how low molecular weight molecules of BODIPY with a hydrophobic character can easily penetrate the lipid layers of cell membranes by interacting with the hydrophobic parts of proteins.(319,320) In particular, substitutions on *meso* position of the rings (*i.e.*, 8-position-substituent) can significantly affect the overall structure.(321) The membrane penetration can be improved by introducing an additional hydrophobic moiety, such as an alkyl chain. Furthermore, the presence of reactive groups that may be present on the meso chain can be a key point for the formation of new covalent bonds with biologically active compounds.

For this reason, a feasible and versatile synthesis of Me_4-BODIPY derivative of Sulfavant A has been designed, in order to develop a general synthetic strategy for the preparationof fluorescent analogues of this class of immunomodulators. The obtained fluorescent compound, named Sulf-BODIPY, exhibited equivalent *in vitro* activity to that of Sulf-A and has been utilised in bio-imaging experiments in the presence of hDCs, as well as in *in vivo* experiments on both Zebrafish and mice (**Sections 2.3.3.2** and **2.3.3.3**).

2.3.1 Synthetic procedure

For the preparation of the Sulf-BODIPY, the synthetic strategy concerned the coupling between the Me_4-BODIPY core and the glycerol portion of a 1-*O*-mono-stearoyl Sulf-A, through an alkyl chain spacer long enough to structurally simulate a stearic acid residue. Therefore, the two building blocks were prepared separately: the first containing the fluorescent probe bound to an acyl chain of 11 carbon atoms; the second consisting of the 1-*O*-monostearoyl derivative of Sulf-A (**Figure 21**).

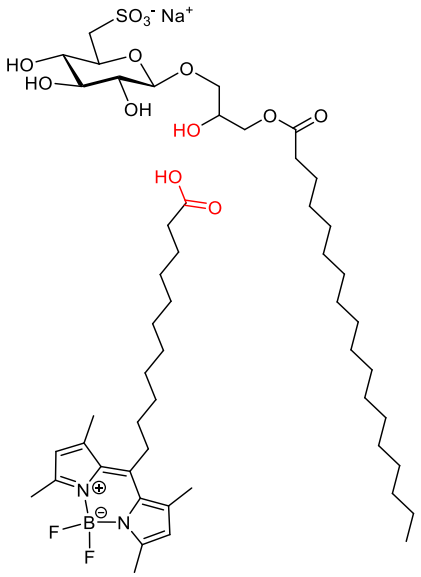

Figure 21: Syntones used in the synthesis of Sulf-BODIPY.

For the preparation of the acyl chain containing the fluorescent tag, we started from dodecanedioic acid (**Scheme 18**). First of all, dodecandioic acid was protected with two methyl groups to make ester functions, using hydrogen chloride in methanol solution. Then it was deprotected at only one end with mild basic hydrolysis conditions and subsequently transformed into the corresponding acyl chloride **53** by thionyl chloride in methanol, increasing in this way the susceptibility to a nucleophilic attack. The formation of the BODIPY core was inspired by the procedure of Boldyrev and Molotkovsky.(322) The first step involved the acylation of 2,4-dimethylpyrrole by the previously prepared acyl chloride, followed by the condensation with another pyrrolic unit to generate a symmetrical dipyrinium salt. The second step involved deprotonation of the salt with a base and fluoroboration with BF_3OEt_2.(323) Chelation with boron difluoride (BF_2) limited the rotational freedom of the molecule and enabled the conversion of a non-fluorescent compound into a fluorophore.(324) The presence of two methyls at positions 2 and 4 favored the substitution at pyrrole position 8 (meso), being the only site for the attachment of the acyl chain. Finally, demethylation

with potassium hydroxide gave the fluorescent acyl chain ready to be coupled to the monostearoyl Sulf-A derivative**.**

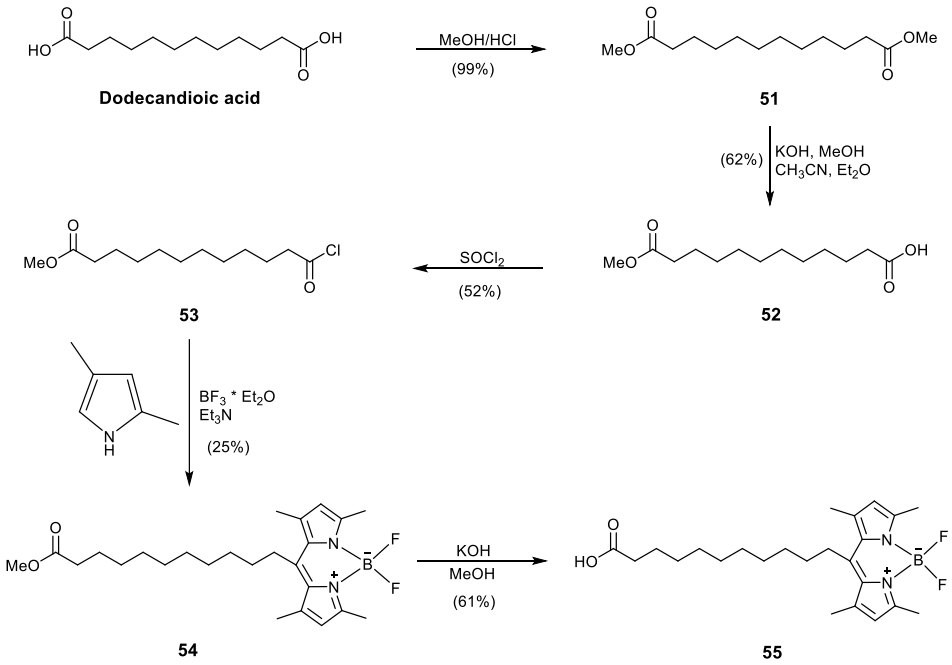

Scheme 18: Synthetic strategy for the preparation of the fluorescent tag.

For the preparation of the monostearoyl Sulf-A derivative, the synthetic strategy was inspired by the Sulfavant A preparation strategy (**Scheme 19**).(325) After the complete acetylation of D-glucose, the selective deprotection of the anomeric position with benzylamine and further derivatization with trichloroacetimidate, compound **8** was obtained. This product was coupled with isopropyliden glycerol acceptor using BF_3OEt_2 in an inert environment and paying particular attention to the reaction temperature (-10 °C) in order to avoid the formation of by-products such as ortho-ester or alpha-glycosidic derivative. The β-glucosyl **56** was obtained thanks to the neighbouring group participation of the acetate in position 2' of the trichloroacetimidate derivative. The subsequent Zemplén deacetylation led to the key

intermediate **57**, versatile building block potentially useful for the preparation of a wide range of neutral and charged glycoglycerolipids (**Figure 22**).

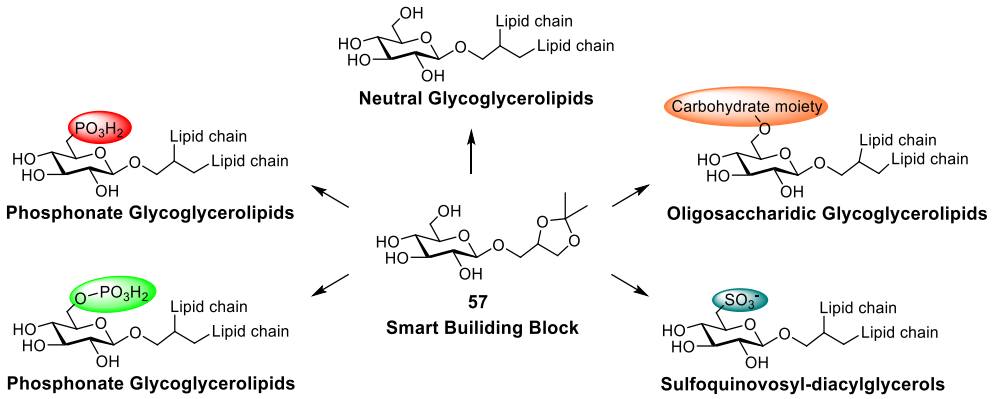

Figure 22: Putative use of compound **57** for the access to biologically active glycoglycerolipids**.**(325)

This product was directly functionalized through a cheap and versatile procedure using a combination of triphenylphosphine, iodine and 2,6-lutidine that allowed to obtain the selective iodination on carbon 6' in mild solvent–free conditions (**Scheme 19**).(294) Compound **58** was acetylated *in situ* leading to intermediate **59**.(294,326) Addition of potassium thioacetate resulted in the very fast generation of thioacetate **60** in high yields.(294) The isopropylidene residue was then selectively removed under soft acidic conditions using zinc nitrate as mild Lewis acid to get **61**.

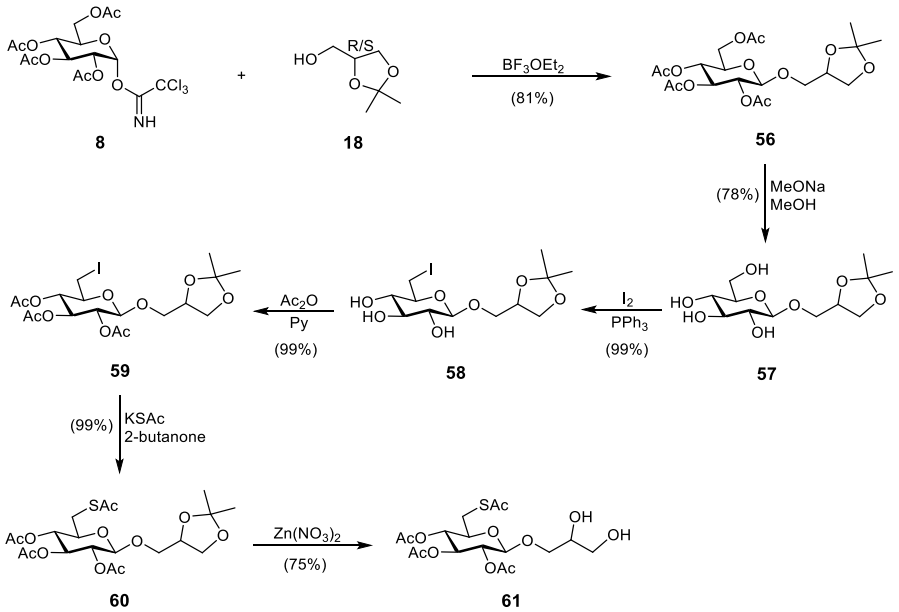

Scheme 19: Glycosylation reaction and 6' derivatization.

At this point, a single stearic acid chain was linked on the primary hydroxyl group of the glycerol residue thanks to a strict control of the equivalents of reagents and of the temperature (4 °C) (**Scheme 20**).

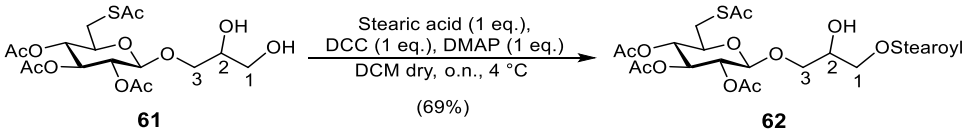

Scheme 20: Single-chain stearic acid condensation under controlled conditions.

In fact, it is possible to selectively insert the acyl chain only on the primary OH by playing on the different reactivity of the exposed hydroxyl groups. This can be achieved by keeping the temperature low and using a small amount of stearic acid. In

this way, the procedure allowed step-wise introduction of different acyl residues at C-1 and C-2 of glycerol, permitting the control of fatty acid regiospecificity.(327)

Due to the instability of Me_4BODIPY-undecanoyl under the conditions used for the oxidation reaction of the 6' sugar group, an alternative method had to be found to avoid the replacement of the fluorides by hydroxyl groups. As illustrated in **Scheme 21**, the oxidative reaction, to get the sulfonic function in position 6', was carried out with hydrogen peroxide (40%) before the introduction of the fluorescent probe. After the oxidation, another DCC-based condensation with the acyl chain containing the fluorescent tag, led to the fluorescent product **6**.

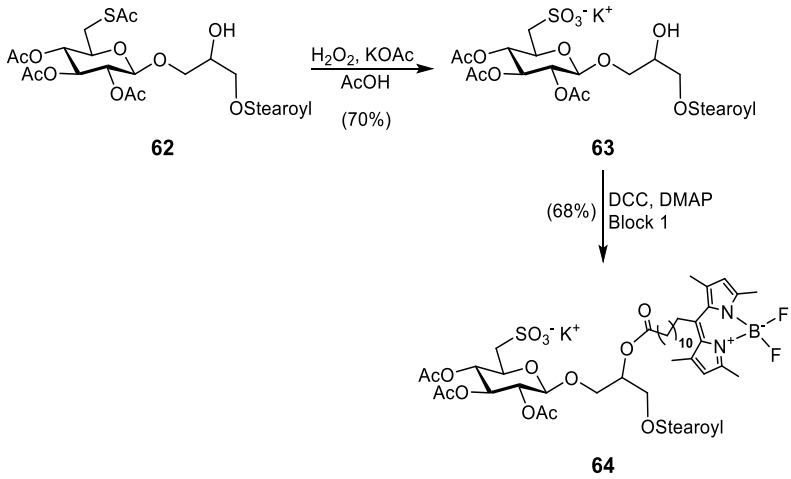

Scheme 21: Oxidation and introduction of the fluorescent tag.

Finally, the compound was deacetylated using hydrazine in a mixture of ethanol and water (85:15) to produce Sulf-BODIPY (**Scheme 22**).(328,329)

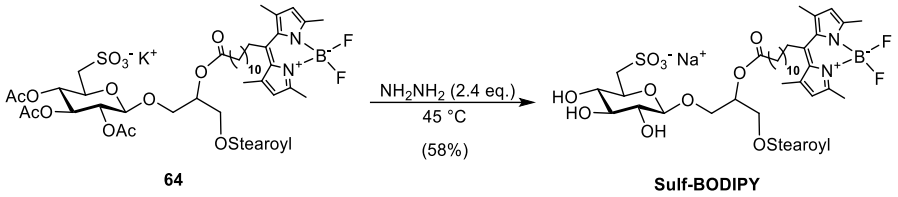

Scheme 22: Hydrazinolysis to get Sulf-BODIPY.

Harsh conditions (2-4 equivalents of hydrazine monohydrate, reaction time of 4-6 hours, and temperature range of 40-80 °C) are commonly described in the literature for the use of hydrazine monohydrate. While these conditions lead to the breakage of all the acyl groups of the molecule, it was possible to deacetylate the sugar preserving lipid chains by using fewer hydrazine equivalents, controlled reaction times, and temperature of 45 °C. Furthermore, by carrying out the reaction in ethanol/water, it was reasonable to consider that the hydrazine molecules may not have easy access to ester bonds committed in the hydrophobic layer of the long lipid chains.(329)

This strategy is particularly versatile and opens the way for the preparation of other fluorescent BODIPY β-sulfoquinovosylacylglycerol analogues.

2.3.2 Biological assays

As previously anticipated, Sulf-A was able to induce the maturation of moDCs *in vitro* in the concentration range 10 nM - 10 μM through the upregulation of phenotypic markers such as CD86 and CD83 and the gene expression, without secretion, of specified inflammatory cytokines (IL-12p40, IFNγ). Considering that the introduction of a new structural component, such as the fluorescent probe, could lead to an alteration in the biological response, the immunomodulatory effect of Sulf-BODIPY was evaluated. In this regard, the fluorescent derivative stimulated the upregulation of the phenotypic markers CD83 and CD86 and HLA-DR in a dose-dependent manner

in the range between 10 nM and 10 μM with a maximum activity at 10 μM (**Figure 23**).

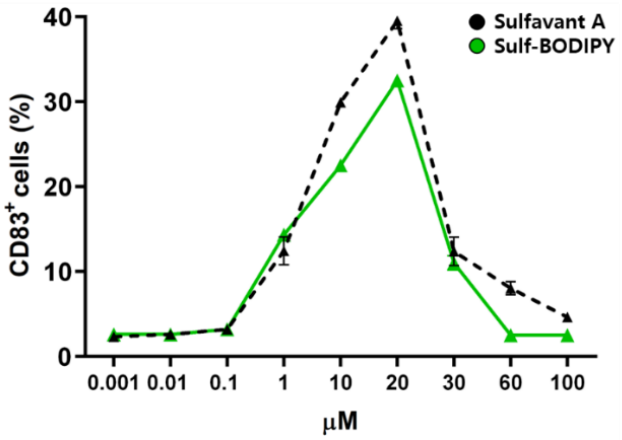

Figure 23: Percentage expression of the phenotypic marker $CD83^+$ as a function of ligand concentration. Sulfavant A and Sulf-BODIPY appear to have comparable ability to induce dendritic cell maturation *in vitro*.

Based on these results, it was clear that the biological response to the fluorescent molecule was comparable to that of Sulfavant A, demonstrating that the biological behaviour was preserved despite the introduction of the fluorescent tag.

2.3.3 Exploiting Sulf-BODIPY fluorescence properties in a biological context

In recent years, advances in instrument design and synthetic fluorescent probes have increased the use of fluorescence imaging in biomedical research. These advances in fluorescence-based techniques have enabled the precise real-time study of protein and small ligand dynamics within complex cellular contexts.(330) Bioimaging is a relatively new technique that integrates anatomical structure with functional data, like

electric and magnetic fields, to provide information on structure and positioning. With this technique, images at cellular level can be obtained, providing information about the whole body, organs and tissues. Bioimaging is a non-invasive approach that can aid in disease management and understanding, as well as in problem identification in the clinical field. In our study, Sulf-BODIPY localisation within the cellular environment was visualised, thus providing additional insight into the biological mechanism. Employed by researchers, *in vivo* fluorescence imaging is a potent method for studying live events.(331–334) The understanding of animal immune systems comparable to those of humans has been frequently employed to quantitatively screen diseases, diagnose, and monitor post-treatment progress. This information could advance the pharmacological development of Sulfavant A.

2.3.3.1 Bioimaging study

In view of the pharmacological interest and a preclinical development of Sulf-A, it is of paramount importance to understand the behaviour and fate of this molecule in *in vitro* and *in vivo* biological environment. In this regard, real-time observation of the cellular and subcellular distribution of the molecule with *in vivo* assays result as key elements to further study and understand the potential of this compound.

With this aim, a live cell imaging experiment was performed with Sulf-BODIPY in the presence of hDC (**Figure 24**). The experiment showed the formation of fluorescent aggregates in the cytoplasm due to rapid cellular internalisation of the fluorescent molecule.

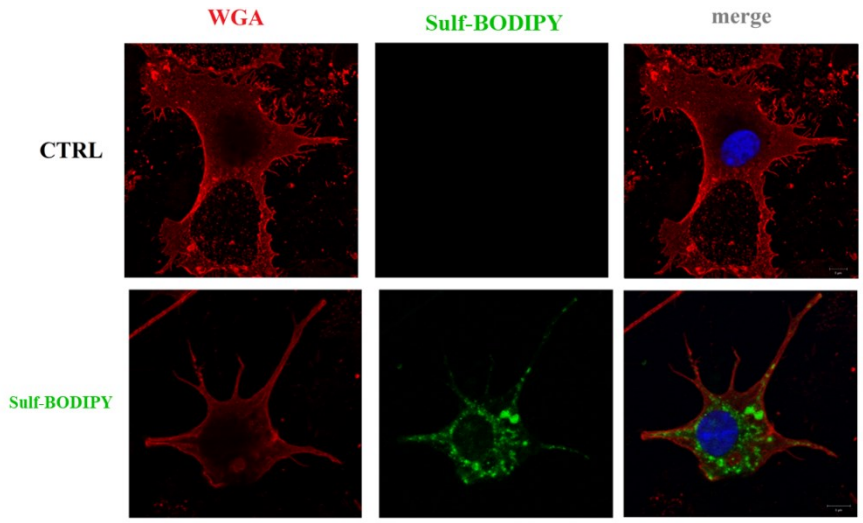

Figure 24: Confocal microscopy images showing the formation of green fluorescent aggregates in the cytoplasm of human dendritic cells stained with DAPI (blue), Sulf-BODIPY (green) and WGA (red).

The plasma membrane was stained with wheat-germ agglutinin (WGA), while the nucleus was stained with 4',6-diamidin-2-phenylindole (DAPI), a fluorescent organic dye often used to identify the nucleus, and no nuclear invasion was observed. The cellular internalisation of the fluorescent probe opens several questions about the TREM2 interaction, its metabolism and the possibility of phagocytosis of the TREM2-binding ligand.

The biological response induced by TREM2 is closely linked to the cellular distribution of the protein, but the precise mechanism by which TREM2 recognises the ligand and diffuses into intracellular compartments remains undefined. The formation of these fluorescent aggregates could be explained by internalisation of the receptor after binding. Moreover, after ligand recognition, TREM2 ectodomain could be cleaved by various enzymes to secrete a soluble protein form (sTREM2) into the extracellular space as a signalling molecule.(335,336) For these reasons, the formation of fluorescent cytoplasmic pools raises questions about the origin and fate of TREM2 before and after ligand-induced activation. Having this fluorescent molecule could

therefore help to answer and explain some information about the distribution and functions of TREM2.

2.3.3.2 In vivo study on Zebrafish

Preclinical development is a key objective for new lead compounds such as Sulfavants, and studies of biodistribution and *in vivo* ADME in animal models, by Sulf-BODIPY, could facilitate reliable analysis and future progress of these molecules. In this regard, experiments were conducted in zebrafish, a non-mammalian vertebrate model particularly suitable for preliminary *in vivo* studies of potential drugs. Zebrafish larvae at 3 days post-fertilisation were exposed to 8 µg/mL of Sulf-BODIPY for 24 hours and then subjected to imaging to detect the bio-localisation of the fluorescent molecule. Importantly, the concentration of the compound did not alter growth or induce mortality in the animals, confirming the non-toxic nature of this molecule. Fluorescence was observed in specific tissues of the digestive system and especially in the yolk sac, intestinal lumen and pancreas (**Figure 25**).

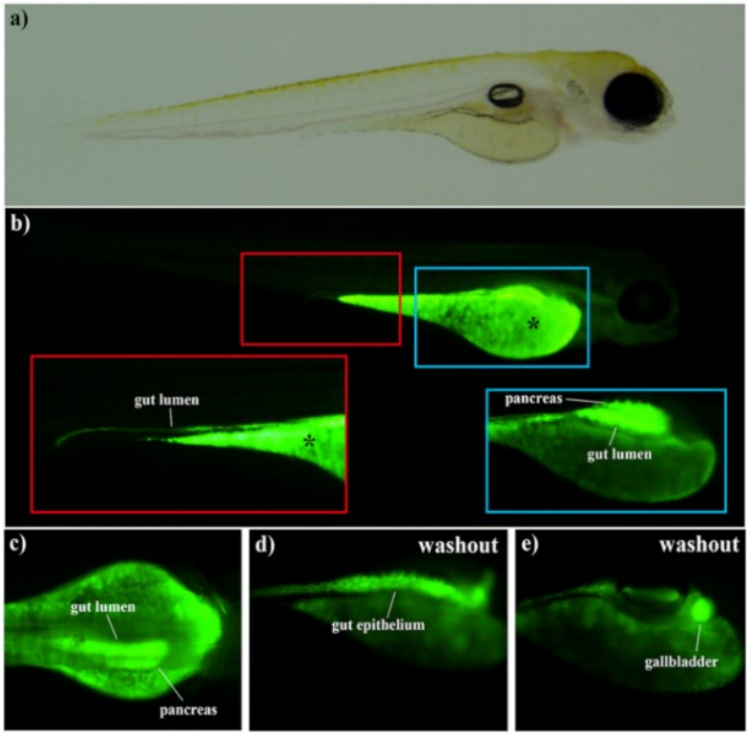

Figure 25: Bioaccumulation of Sulf-BODIPY in zebrafish larvae. **a**) Conventionally-raised 4 dpf zebrafish larvae under a bright field microscope. **b-c**) 24 h 8 µg/mL Sulf-BODIPY-treated 4 dpf larvae showed accumulation in yolk sac, gut lumen and pancreas. Sulf-BODIPY was detected in gut epithelium and gall bladder after 24 h washout in 5 dpf larvae.

After 24 hours of washout, Sulf-BODIPY fluorescence decreased in the yolk sac, but was still detectable in the intestinal lumen and pancreas, and appeared in the intestinal epithelium and gallbladder, showing an accumulation over time in these two areas. The absence of toxicity and the exceptional stability of fluorescence in the zebrafish model demonstrated the reliability of this molecule for application in more complex living systems. Considering the therapeutic potential of targeting TREM2 in the tumour microenvironment, the bio-visualisation and permanence of TREM2 in the digestive organs was particularly attractive for the development of the zebrafish model for the study of various diseases such as digestive tract tumours.(337–339) From here

it will be possible to approach in vivo anti-cancer experiments in more complex tumour models to evaluate the effects of Sulfavants.

2.3.3.3 In vivo study on mice

Given the importance of TREM2 in microglia, in the central nervous system (CNS) and in general in the neurodegenerative diseases progression, the ability of a molecule to interact or block the recognition site of this receptor may have important implications in many neuropathologies, such as Alzheimer's, Parkinson's and multiple sclerosis. A key requirement for TREM2-interacting molecules such as Sulfavants is the ability of these molecules to cross the blood-brain barrier to reach the target. To this end, *in vivo* experiments on murine model were carried out to check if Sulf-BODIPY was able to diffuse into the brains of mice. Fluorescence imaging showed a significant accumulation of the molecule in the brains compared to untreated control mice, confirming the ability of molecule to enter in the CNS (**Figure 26**).

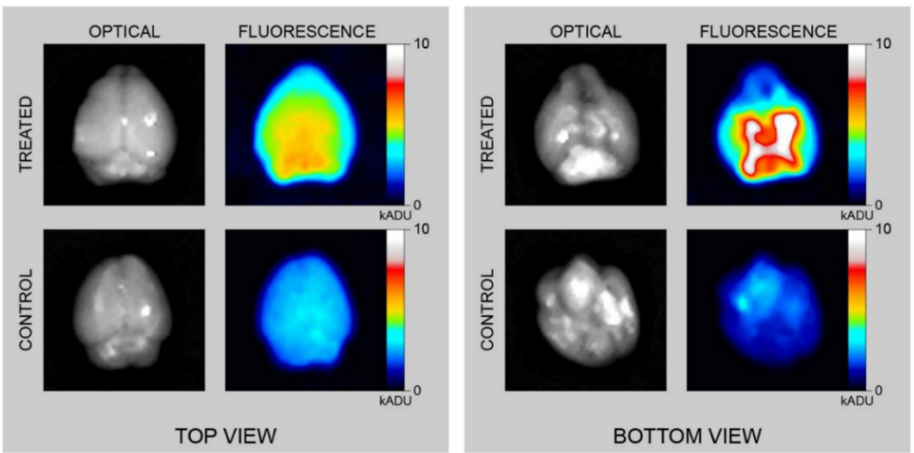

Figure 26: Ex vivo fluorescent imaging showing the ability of Sulf-BODIPY to cross the blood-brain barrier and accumulate in the brains of treated mice.

To further confirm the data, the brains were subjected to homogenisation, extraction and HPLC-UV analysis, which confirmed the presence of the entire Sulf-BODIPY molecule in the treated brains. This additional property of the molecule opened the way to further therapeutic applications in the field of neuropathology.

2.3.4 Conclusions

Sulfavants are a recently developed group of molecular adjuvants that use the β-sulfoquinovoside glycerol backbone to interact with the TREM2 receptor, resulting in the modulation of the immune response. A synthetic strategy has been developed for the preparation of a fluorescent analogue, Sulf-BODIPY, whose main steps are the glycosylation of the trichloroacetimidate glucose donor with the acceptor (rac)-1,2-*O*-isopropylidene glycerol and the introduction of the undecanoyl moiety Me_4-BODIPY after the oxidation of the 6'-carbon of the sugar to the sulphonic function. This synthesis may open the way to the preparation of other fluorescent derivatives of this family of immunomodulators and help the comprehension of the complex biological mechanisms of Sulfavants. It was demonstrated that the compound retained its biological activity regarding the up-regulation of phenotypic markers of DCs maturation, despite the introduction of the fluorescent tag. Molecular imaging techniques allowed the visualisation of Sulf-BODIPY inside the cell, leading to several hypotheses about the mechanism of receptor function. *In vivo* experiments were performed on zebrafish getting information on its localization and distribution in view of Sulfavants pharmacological development. Considering the potential of TREM2 engagement in ensuring the CNS health, the ability of the Sulf-BODIPY to cross the blood-brain barrier of mice was crucial for the applicability in neurodegenerative diseases.

2.4 Docking experiments

In addition to interact with some pathogen-associated molecular patterns such as lipopolysaccharides and mycolic acid derivatives, TREM2 is able to bind "eat me" signals such as phospholipids, sulphatides and lipoproteins, which are particularly abundant in the brain.(228–230,263,340,341) A close association between neuropathologies and dysfunctions imputable to missense mutations in TREM2 has been the clearest evidence of the crucial role of this protein in the CNS. In particular, a recurrent variant leading to the substitution of arginine by histidine at position 47 (R47H) seems to be a constant in Alzheimer's (AD) and Parkinson's (PD) diseases.(254,342) This mutation alters binding with potential ligands, making TREM2 less efficient in providing microglia-mediated protection of neuronal tissue.(228,264) In this regard TREM2 Ig- domain has three complementary-determining region loops (CDR1 to CDR3) contributing to ligand binding, but only the CDR2 loop, probably due to its positively charged patch, addresses crucial interactions with *bona fide* ligand and undergoes a significant conformational change in the TREM2-R47H mutant form.(265,343) In addition, the R47H mutation was also associated with increased levels of hyperphosphorylated tau protein around amyloid plaques, with subsequent exacerbation of Alzheimer's disease.(344) Based on this evidences, independent studies indicated that TREM2 activation may be crucial for the prevention and treatment of neurodegenerative processes and that the search for agonist ligands is a key to the development of new treatments for neuropathologies. As said before, TREM-2-mediated Sulfavant A activity defined a homeostasis-determining process, supporting a potential mechanism of fine-tuning in several physiological or pathological contexts, including inflammation, immune disorders and cancer. The evaluation of the structural characteristics of the ligand-binding domain appears to be a crucial step in the study and development of further potential agonist molecules capable of triggering TREM2 functions. Furthermore, given that different putative ligands can mediate numerous functions of TREM2, it is important to understand at a molecular level how this protein manages to interact with them.(345)

A first three-dimensional characterisation of TREM2 by X-ray crystallographic analysis by Kober and coworkers highlighted the presence of a polar pocket and a long and narrow hydrophobic portion on the surface of the extracellular immunoglobulin domain, corresponding to the putative regions interacting with the polar head and acyl chains of phospholipids, respectively.(264) Following this work, Sudom et al isolated and characterised a co-crystal of the protein with a synthetic molecule (1,2-dihexanoyl-sn-glycero-3-phospho-L-serine) structurally similar to the putative ligand phosphatidylserine, in which TREM2 is organised in trimers of dimers with a ligand pocket at each dimer interface (**Figure 27**).(221)

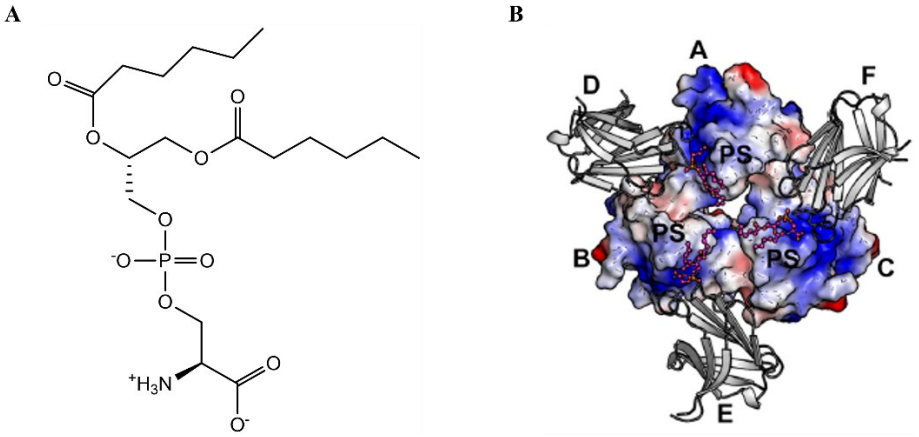

Figure 27: A Structure of 1,2-dihexanoyl-sn-glycero-3-phospho-L-serine (COX); **B** WT TREM2 structure co-cristallyzed with COX (fuchsia sticks), including inner trimer (electrostatic surface) and outer TREM2 protomers of higher-order complex (gray cartoon).(221)

The identification of this pocket as well as information about its structure could rationalize the high TREM2 binding promiscuity and pave the way for the rational design of possible functional agonists. In the next paragraph, the ability of this pocket to interact with recognised small ligands was evaluated through parallel docking and reporter cell assays.

2.4.1 Docking simulations

Following the identification of Sulfavant A as the first synthetic ligand of TREM2, molecular docking simulations were carried out to get insights into the ligand binding mode. Considering only the extracellular domain of the protein, the first step was to look for pocket or region of the protein with which our molecule could have stable interactions.

From literature studies emerged two different binding pockets for the small anionic putative TREM2 ligands, sphingosine-1-phosphate by Xue and phosphatidylserine C6 analogue by Sudom respectively.(221,346) Although the model of Xue and co-workers predicted an aspartic acid 104 (D104) as crucial residue for the interaction with the sphingosine phosphate group, Sudom et al model, based on the isolation and characterization of dimer TREM2-phosphatidylserine C6 analogue co-crystal, highlighted a quite distant binding pocket. The co-crystallized structure highlighted a binding region at the interface between two protein chains, within a larger structure formed by trimers of dimers. Furthermore, the binding pocket is located near the region affected by the large conformational change due to the substitution of arginine by histidine in the mutated form R47H. As a first step, docking simulations were performed on the two epimers Sulfavant R and Sulfavant S (Sulf-R and Sulf-S), of which Sulf-A is a mixture.

A preliminary study was conducted to investigate the preferred region for Sulfavants binding. The best Sulfavants poses were those involving the amino acid residues of the pocket identified by Sudom. These data can be considered reasonable also taking into account the structural similarity between Sulfavants and COX. For these reasons, this model was chosen as starting point and a more detailed investigation on this interaction area was performed using the X-ray data of the TREM2 WT dimer complex (6B8O).

Representative parameters in these studies were the Docking Score, used to predict the binding affinity between ligand and target, the MMGBSA, for the evaluation of the free energy of binding of small ligands to biological macromolecules, and the

MMGBSA ligand efficiency, the free energy index normalised to the number atoms, useful to compare molecules with different sizes.(347)

Figure 28 shows the obtained top-scored MMGBSA poses obtained for Sulf-R and Sulf-S using a shape constrain on the cognate ligand. Both the epimers are predicted to establish interactions within the considered pocket, reproducing the binding mode experimentally observed for the COX, orienting its polar portion into the lower part of the cavity with the 6' sulphonic group in the pocket bottom, in correspondence of a positive amino acid nest, and the hydrophobic portion outside, resting on the protein surface.

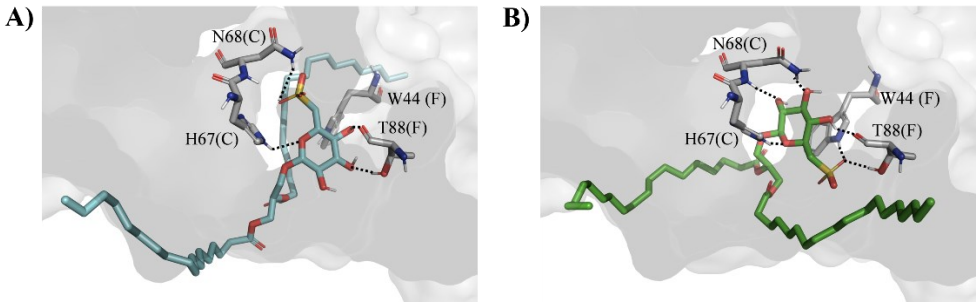

Figure 28: Top MMGBSA scored poses returned by docking simulations of **A)** Sulf-R and **B)** Sulf-S performed using a shape constraint on the COX. Ligands and important residues are rendered as sticks, whereas the protein is represented as a surface. H-bonds are represented by dotted black lines and only polar hydrogen atoms are shown.

Interactions took place between two TREM2 chains (in this study C and F) and were strengthened by several contacts with residues of both chains. In detail, the polar head of both epimers, engaged H-bond interactions with H67(C), N68(C), W44(F), and T88(F). This was also confirmed by the obtained docking scores, MM-GBSA scores and normalized MMGBSA scores (i.e., MMGBSA ligand efficiency) reported in **Table 1**, showing that the simulation results did not appear to be much affected by the

glyceridic configuration and the affinity of Sulfavants for the receptor was higher than the cognate ligand.

Ligand	*Docking score (kcal/mol)*	*MMGBSA score (kcal/mol)*	*MMGBSA ligand efficiency*
COX	-3,04	-38,78	-1,32
Sulf-R	-5,76	-124,17	-2,14
Sulf-S	-5.47	-117.25	-2.02

Table 1: Top Docking scores and MMGBSA energy values of Sulf-R and -S returned by docking simulations performed using a shape constraint on the cognate ligand.

Most of the computed binding energy was due to the Coulomb contribution (electrostatic complementarity), as evidenced by the corresponding values, which were -17.71 kcal/mol for COX and -90 kcal/mol for Sulf-R/S. This was likely caused by the interactions between the pocket and the polar head of the ligands. No specific interactions were observed for the lipid moiety, oriented towards the hydrophobic protein surface, consistently with not reliable and variable electron density data reported by Sudom et al.(221) On this basis, additional simulations were performed imposing a conformational constraint only on the polar part of the COX, based on the SMART string [O-]C(=O)C([N+]([H])([H])[H])COP([O-])(=O)OC (see the experimental section for methodological details). Therefore, complete flexibility for the lipid moiety was allowed while limiting the conformational sampling of the polar head. **Figure 29** illustrates the top-scoring MMGBSA poses obtained using the SMART constraint.

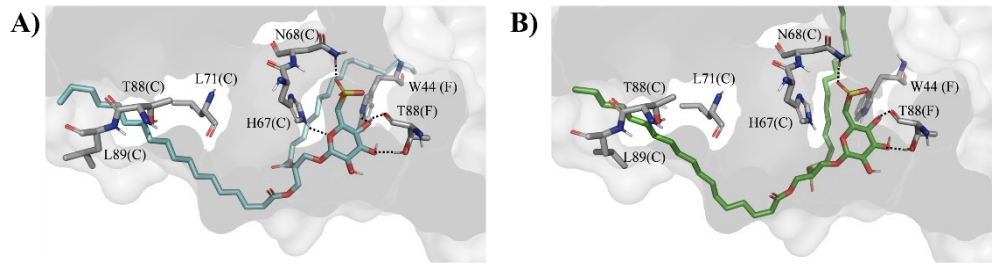

Figure 29: A-B) Top MMGBSA scored poses returned by docking simulations on **A)** Sulf-R and **B)** Sulf-S performed using a SMART constraint on the cognate ligand. Ligands and important residues are rendered as sticks, whereas the protein is represented as a surface. H-bonds are represented by dotted black lines and only polar hydrogen atoms are shown.

As before, the polar head of both epimers adopted the same orientation within the binding pocket preserving the same H-bond interactions, while the poses suggested that the lipidic moieties, when unconstrained, could adopt a wide range of different conformations and orientations. Indeed, for both epimers one lipidic tail seems to fit into a hydrophobic pocket and interact via Van der Waals forces with L71(C), T88(C), and L89(C). Finally, the increased MMGBSA and normalized MMGBSA scores further support the effectiveness of using the SMART constraint approach (**Table 2**).

Ligand	***Docking score (kcal/mol)***	***MMGBSA score (kcal/mol)***	***MMGBSA ligand efficiency***
Sulf-R	-4,57	-136,22	-2,35
Sulf-S	-5.36	-139.73	-2.41

Table 2: Top Docking scores and MMGBSA energy values returned by docking simulations performed using a SMART constraint on the cognate ligand (see the section materials and methods for methodological details).

Encouraged by these preliminary results and since the polar part of the Sulfavants appeared to play a crucial role in molecular recognition, an analogue of Sulf-A with a reduced six carbons hydrophobic moiety (same length as COX) was synthetized (**Scheme 23**). Compound **61** was prepared starting from D-glucose following the synthetic strategy for the preparation of Sulf-A by Ziaco et al.(325) The acyl chains were added via a DCC-mediated condensation with hexanoic acid, while the sulfonic function in position 6', was inserted by hydrogen peroxide (40%) to get compound **66**. Finally, hydrazinolysis under controlled conditions, led to Sulf-A C6 by selective sugar deacetylation.

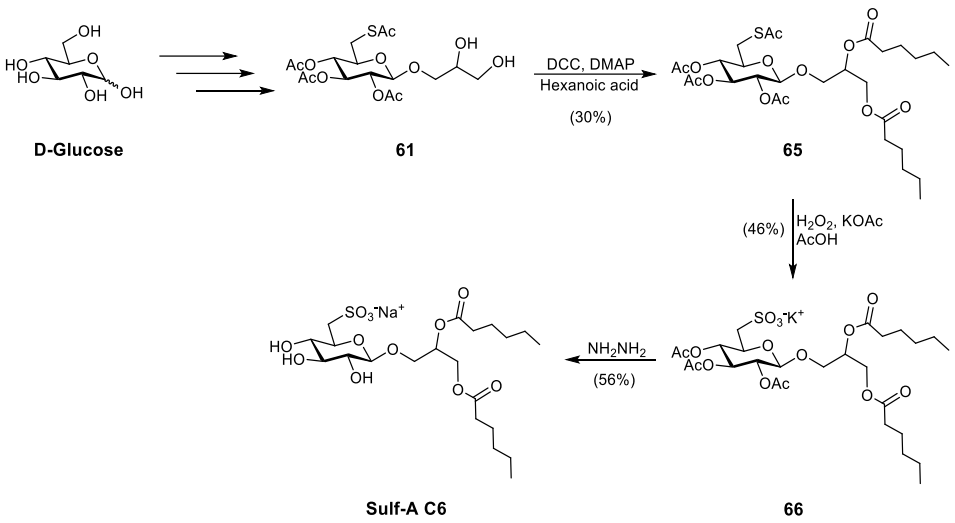

Scheme 23 Synthesis of Sulf-A C6.

The same docking protocol was followed to perform molecular docking simulations on Sulf-A variants with hexanoyl tails, named RC6 and SC6 (**Figure 30**).

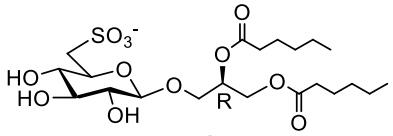

RC6

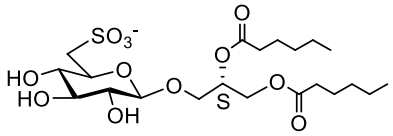

SC6

Figure 30: Structures of RC6 and SC6.

Again, the polar part of the molecules well fit into the pocket, having the same binding mode, and form H-bond interactions with H66(C), N67(C), and T88(F) (**Figures 31**).

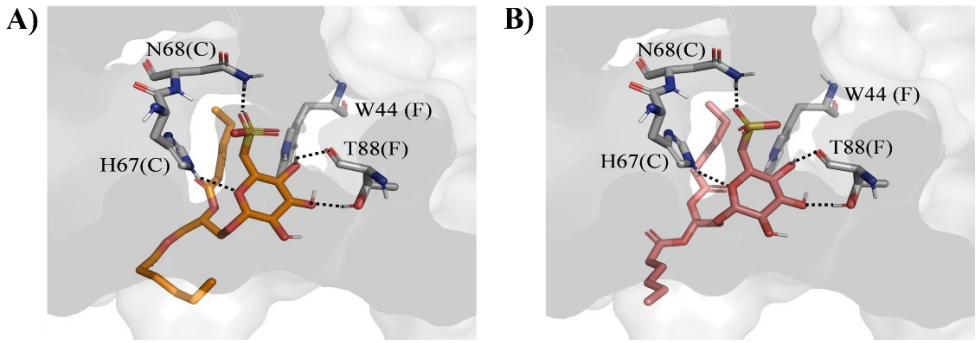

Figure 31: **A-B)** Top MMGBSA scored poses returned by docking simulations on **A)** RC6 and **B)** SC6 performed using a SMART constraint on the cognate ligand. Ligands and important residues are rendered as sticks, whereas the protein is represented as a surface. H-bonds are represented by dotted black lines and only polar hydrogen atoms are shown.

It was predicted that the lipid moiety established van der Waals interactions with some amino acids of the hydrophobic protein surface in the CDR1 loop (W70, L71, L72,

S73, F74). Remarkably, the normalized MMGBSA scores indicated that RC6 and SC6 had better scores than COX, suggesting higher affinity for TREM-2 (**Table 3**).

Ligand	*Docking score (kcal/mol)*	*MMGBSA score (kcal/mol)*	*MMGBSA ligand efficiency*
RC6	-2.00	-71.81	-2.12
SC6	-1.96	-70.00	-2.09

Table 3: Top Docking scores and MMGBSA energy values returned by docking simulations on RC6 and SC6 performed using a SMART constraint on the cognate ligand (see the section materials and methods for methodological details).

To further evaluate the influence of different length lipid chain on model reliability and to have a better comparison against Sulfavants, docking simulations were performed on phosphatidylserine with C18 lipid chains (PS18), more similar to natural derivatives used in the biological assays (**Figure 32**).

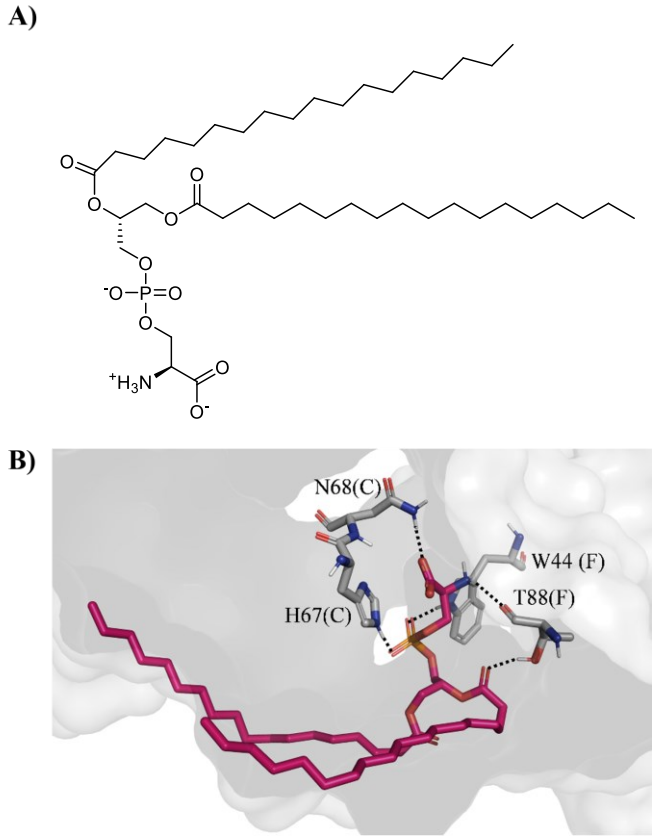

Figure 32: A) 2D structure of PS18; **B)** Top MMGBSA scored pose returned by docking simulations on PS18 performed using a SMART constraint on the cognate ligand. Ligand and important residues are rendered as sticks, whereas the protein is represented as a surface. H-bonds are represented by dotted black lines and only polar hydrogen atoms are shown.

As expected, the predicted binding mode was similar to COX, with the polar head establishing H-bond interactions with H67(C), N68(C), W44(F), and T88(F). Moreover, PS18 showed a similar electrostatic complementarity to COX, as demonstrated by the values of -20.40 kcal/mol and -17.71 kcal/mol respectively. The energy values obtained were better than those of COX but slightly worse than Sulf-R and Sulf-S, in agreement with the biological data. **Table 4** resumes the docking scores, MM-GBSA scores and normalized MMGBSA scores obtained from the docking simulation performed.

Ligand	*Docking score (kcal/mol)*	*MMGBSA score (kcal/mol)*	*MMGBSA ligand efficiency*
PS18	-4.72	-105.21	-1.95
AM6	-5.44	-134.23	-3.20
AM18	-1.87	-69.59	-3.87

Table 4: Top Docking scores and MMGBSA energy values returned by docking simulations performed on PS18, AM6 and AM18 using a SMART constraint on the cognate ligand (see the section materials and methods for methodological details).

Mycolic acid, another putative ligand of TREM2, was also considered in this docking study, although it could not be included in the simulation programme due to its long lipid chains (~C60) and the excessive rotamers number.(348) Analogues with six (AM6) and eighteen (AM18) carbon atoms chains were evaluated, with the aim to have a direct comparison with the molecules previously analysed. **Figure 33** shows the top-scoring MMGBSA poses of AM18 and AM6, obtained using the SMART constraint on the COX. As previously seen for the other molecules, the polar part of the compound fit well into the pocket interacting with S40 and N68. The calculated scores (**Table 4**) were better than those of the other compounds. Remarkably, despite their smaller polar part compared to Sulfavant A, both AM18 and AM6 exhibited a computed binding energy primarily driven by Coulomb contribution (~-80 kcal/mol). This suggested that the electrostatic attraction between the compounds and the polar pocket residues contributed significantly to their binding affinity, thanks to the strong tendency of acid and alcohol groups to interact with the protein dimer residues.

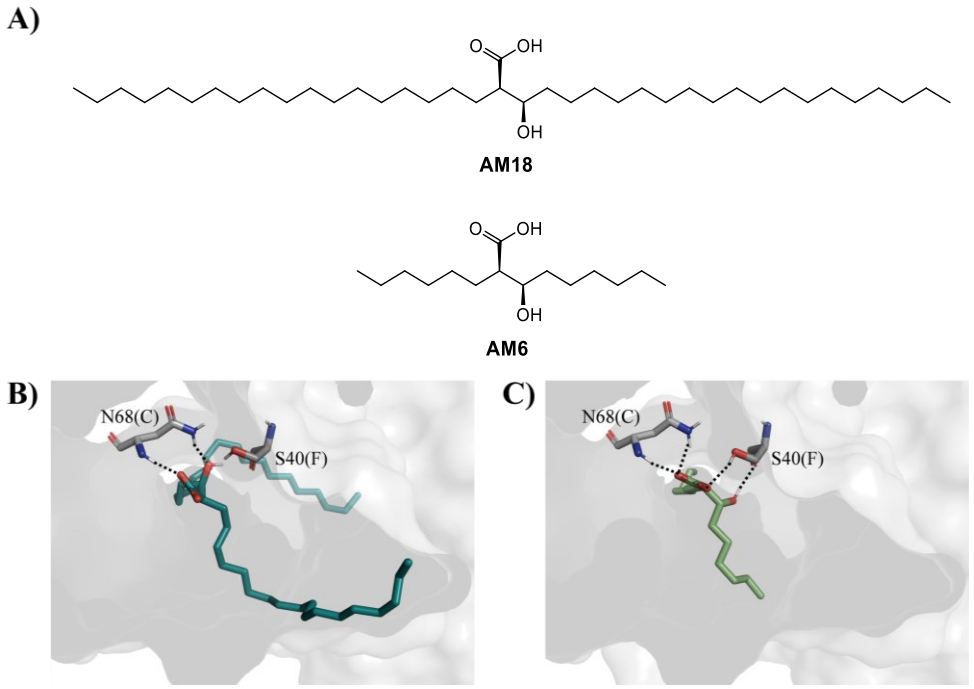

Figure 33: **A)** 2D structure of AM18 and AM6; **B-C)** Top MM-GBSA scored poses returned by docking simulations on **B)** AM18 and **C)** AM6 performed using a SMART constraint on the COX. Ligands and important residues are rendered as sticks, whereas the protein is represented as a surface. H-bonds are represented by dotted black lines.

The consistency and alignment of results obtained from both docking simulations and biological data suggest the reliability of the simulation model proposed. Furthermore, the identified binding pocket appears to be suitable for characterizing the interaction between TREM2 and small anionic ligands.

2.4.2 Biological assays

Parallel biological experiments were performed on Sulf-A, mycolic acid and natural phosphatidylserine, using an established TREM2 reporter cell line that responds through GFP synthesis. This represented a tool to define the experimental molecular affinities with the protein.(349) The different ligands were separately incubated and

receptor activation was measured as GFP^+-expressing cells by flow cytometry. The response was dose-dependent in the range of 0.1 to 60 μg/mL (**Figure 34**).

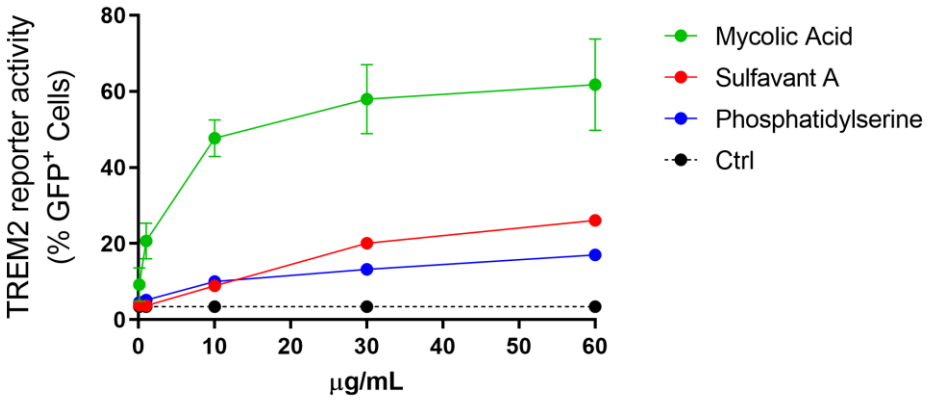

Figure 34: Dose-dependent response of human TREM2-reporter cells to mycolic acid, Sulfavant A and phosphatidylserine. The black curve indicates the reporter cells treated only with vehicle (MeOH).

The trend and the intensity of the curves agreed with the docking data, highlighting a greater affinity of Sulfavant A and C6 derivatives than phosphatidylserine. The parallelism and coherence of the results from biological and computational approaches proved the consistency of the proposed model and the possibility of proposing this binding pocket as suitable for the description of the interaction of TREM2 with small anionic ligands. Although the docking model appeared only partially suitable for studying the interactions of the ligand hydrophobic part, the polar one seems to fit particularly well, making this method potentially suitable for a more in-depth study of biological optimization and design of further small anionic molecules as new potential TREM2 ligands.

2.4.3 Conclusions

By means of molecular docking simulations, a more comprehensive exploration of the interaction mechanisms between Sulfavants and TREM2 WT was performed. Starting from the X-ray structure published by Sudom and co-workers, displaying the TREM2 WT protein co-crystallised with a synthetic phosphatidylserine analogue, a combined biological and molecular docking approach was undertaken. The obtained docking poses reproduced the binding mode of the TREM2-phosphatidylserine C6 analogue co-crystal (COX), according to which TREM2 molecular recognition is the result of specific interactions involving the ligand polar portion while not much can be predicted regarding the hydrophobic moiety. Reporter cell assays showed that Sulfavant A has a higher receptor affinity than phosphatidylserine consistently with the obtained docking data. These results could represent a starting point to design new small molecules able to bind TREM2, deeply involved in numerous neurodegenerative diseases.

Chapter 3: Study of the interaction between glycan and galectins by ^{19}F-NMR

3.1 Galectins, glycans and their interactions

3.1.1 Galectins

Mammals express several glycan-binding proteins (GBPs). Among them, galectins were the first family of GBPs to be associated with immunoregulatory activity.(350,351) These proteins belong to the lectin family and have multiple functions in the regulation of the immune system.(352–354) More than 16 galectins have been identified in vertebrates and are classified according to their structure. They fall into three subgroups: prototypic galectins, which consist of two non-covalently linked identical subunits; chimaera-type galectins, where there is one carbohydrate recognition domain (CRD) and a long non-lectin domain (including only galectin-3); and tandem repeat galectins, which contain at least two different CRDs separated by a small linker of variable length within the same polypeptide (**Figure 35**).(355–357)

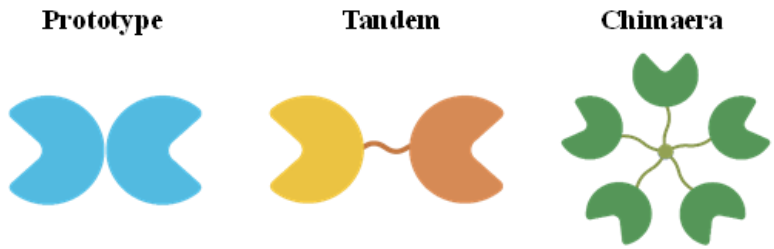

Figure 35: General structure of the three main classes of galectins.

Galectins share conserved sequence motifs in the CRD that confer affinity preferentially to galactose-containing glycans present on a broad range of glycoconjugates.(358) In addition, specific side-interactions with adjacent sites enhance the interaction that mainly takes place in the central part of the binding pocket. This gives each galectin a high specificity for larger saccharides and the opportunity to use them for specific interaction study techniques. Galectins are synthesised in the cytosol and then released from the cell by a mechanism that

bypasses the endoplasmic reticulum and the Golgi.(359,360) They can then interact with glycoconjugates and modulate cell signalling and survival. Except for galectin-3, which has a splicing form containing a transmembrane domain, galectins are soluble proteins.(361)

T-cell studies were the first to demonstrate the regulatory activity of galectins in immunity, in particular their ability to modulate the development and contraction processes of an immune response. For example, it has been shown that galectins are able to interact with a number of glycoproteins involved in T-cell activation by inducing receptor and membrane changes.(362–364) In addition, galectins can modulate APCs by inducing T-cell differentiation.(365) Specifically, several investigations have focused on galectin-1, which is involved in the process of T-cell contraction and ultimately apoptosis. However, *in vitro* studies have suggested that other galectins may also have immunosuppressive properties.(366–370) As with T cells, B cell responses can also be regulated, for instance by galectin-9, which can increase plasma cell IgA production, or by galectin-3, which plays a negative role in B cell differentiation.(371,372) Thus, galectins can act on different aspects of innate and adaptive immunity, either enhancing or suppressing immune and inflammatory responses, as extensively discussed in a recent review of the biological functions of galectins by Liu and Stowell.(373) Galectins can regulate several intracellular (to be further investigated) and extracellular pathways in different types of innate immune cells such as macrophages (**Figure 36**).

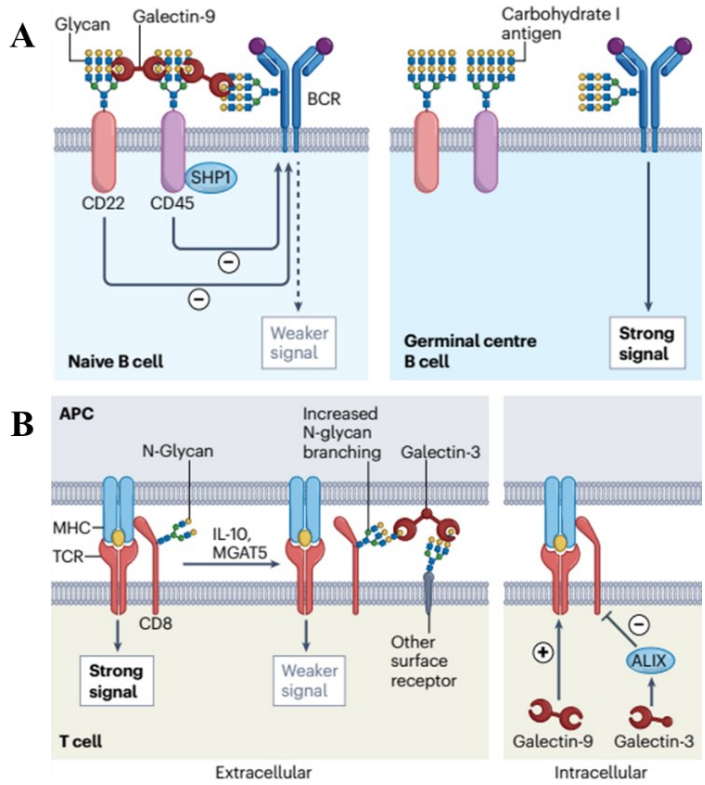

Figure 36: **A** B cells activation by galectin-9; **B** T cells activation by galectin-3.(373)

Two *in vivo* galectin-3 knockout studies showed that it plays a role in suppressing cytokines such as IL-10 and IL-23 in dendritic cells.(374,375) Additionally, galectin-3 and galectin-9 knockdown experiments in microglia suggested a potential influence on actin dynamics, resulting in reduced phagocytosis.(376,377) Some studies also found that galectin-3 is implicated in neurodegenerative diseases, such as PD and Huntington's disease, where galectin-3 deletion reduced microglial activation and inflammation.(378–380) Alternatively, galectins can also directly attack pathogens and contribute to the host's defence against bacteria, parasites, fungi and viruses. The current wealth of new information promises a future scenario in which individual members of the galectin family or their ligands will be used as potent anti-inflammatory mediators and selective modulators of the immune response. The binding of galectins to glycans and the existence of crucial receptors on the cell

surface enables their primary functions. However, their functions have mainly been studied in vitro. Therefore, additional information is required through experiments with human cells or *in vivo* studies.

3.1.2 Glycans

Glycans, along with nucleic acids, proteins and lipids, are one of the four primary categories of macromolecules found in living systems and consist of individual monosaccharide units linked together. The key to their diversity lies in the ability of individual monosaccharide residues to bind in different ways. Indeed, each monosaccharide may exist in furan or pyran form, with its anomeric orientation being either alpha or beta, and each monosaccharide can bind through its anomeric position to any of the hydroxyl groups of another monomer. Glycans can be N-, O- or C-linked to proteins via specific amino acid residues. In N-glycosylation, the reducing end of an oligosaccharide binds to the amide nitrogen of a protein asparagine (Asn) residue. O-glycosylation takes place upon binding to the hydroxyl groups of serine or threonine, and less frequently to tyrosine or hydroxylysine (**Figure 37**).(381,382)

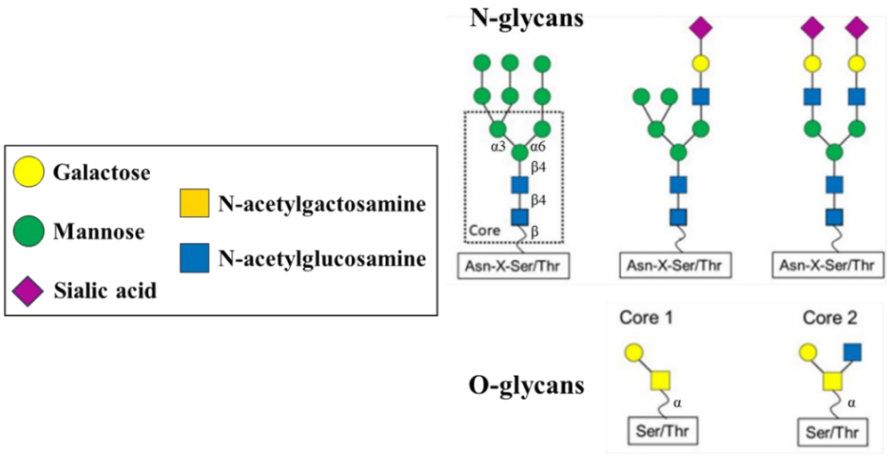

Figure 37: N- and O-glycans with their core structures.(382)

For a long time, it was accepted that glycans had only structural or energy reserve functions, but it is now recognised that they are heavily involved in communication between cells of all biological kingdoms. Glycans are found in almost all living cells and play a fundamental role in cell-cell interactions by providing numerous functions in molecular recognition, immunity, and inflammation. It is therefore unsurprising that there are many examples of infectious agents recognising such glycans with high specificity and expressing glycans on their own surface to modulate their antigenicity.(383) Their roles differed depending on the tissue, developmental stage and environmental context. To date, the biological functions covered by glycans are known to be highly diverse, ranging from structural and modulatory roles to intrinsic and extrinsic recognition, alteration of cell signalling and regulation of immunity.(384) In the context of this thesis, the ability to be specifically recognised by galectins and the study of their interaction has been the main focus.

3.1.3 ^{19}F-NMR to study protein-glycan interaction

NMR is currently the most extensively employed method for studying carbohydrates, revealing their conformational and structural properties and their interactions with receptors.(385) The breadth and accuracy of NMR make it a suitable technique for unravelling the interactions and dynamics of glycans. Carbohydrate-specific recognition of glycans is at the centre of key events of biological and biomedical interest.(386) As mentioned above, most of these interactions involve lectins, and in particular the interaction with galectins has significant biological implications.(373,387–389). The interaction involves the synergistic combination of intermolecular hydrogen bonding via a key Histidine, interacting with the axial 4-OH hydroxyl of the canonical β-Galactose (Gal) moiety, electrostatic interactions, and CH-π stacking interactions between the less polar face of the galactose ring and highly conserved tryptophan residue present in all galectins (**Figure 38**). The CH-π stacking interaction between sugar and tryptophan is of fundamental importance in the stabilisation of glycan/lectin complexes.(390–394) Theoretical and experimental

studies have shown that the dispersive component is the major factor in the CH-π interaction, overshadowing the contribution of the electrostatic factor. The selectivity and specificity of the molecular recognition process was largely determined by the aromatic rings within the receptors. These aromatic elements could play a crucial role in hindering the binding of some sugar epimers. This was achieved by steric factors, where the arrangement of the aromatic rings hindered interactions with specific sugars. In addition, the aromatic rings created environments that were unfavourable for axial hydroxyl groups, adding another layer to the selectivity of the molecular recognition process.

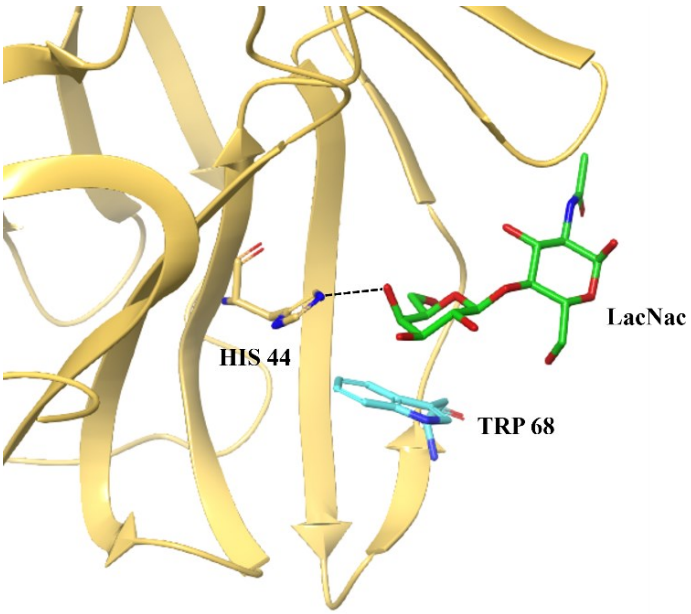

Figure 38: Histidine interacting with the axial 4-OH hydroxyl of the β-Galactose moiety and CH-π stacking interaction between Galectin-1 (1W6P) and LacNAc.

It is noteworthy that in this case, the electrostatic factor plays a minor role and strict orientation of partners is not required due to their dynamic nature. Solvation effects

are also important, especially when highly polar charged species or groups are involved.(394)

NMR has been widely used to study protein-glycan interactions using both receptor- and ligand-based methods.(395,396) One of the most used methods is to ^{15}N-label the protein and specifically assign all ^{1}H ,^{15}N signals, being a time consuming and relatively expensive process. An alternative may be to label the tryptophan rings with a fluorine atom and follow the interaction process with fluorine NMR. Fluorinated sugars have been extensively employed in both chemistry and biology.(397) Recently, it has been shown that chemical modifications of the Trp rings including this type of labelling do not affect the affinity towards neutral sugars.(398) For example, the interaction of different F-W-containing versions of two human galectins (galectin-3 and galectin-8) were not particularly affected by the presence of fluorine, while the use of ^{19}F-NMR spectroscopy allowed to detect interaction features between these lectins and its ligands, and has been satisfactorily employed with other systems.(398) Indeed, despite the complexity of the environment, the generated spectra are very simple to analyse. Moreover, the slow exchange chemical shift time scale is extremely useful to discriminate binding processes and to distinguish independent recognition events that take place at two different binding sites within the same lectin.(399) For example, the T_2-filtered relaxation properties of ^{19}F, exploiting the enhanced R_2 relaxation rate intrinsic to the bound state, allowed the study of a library of 2-deoxy-2-trifluoroacetamido-α-mannoside analogues of Langerin and the visualisation of secondary binding pockets close to the canonical calcium binding site.(400) The use of ^{19}F-NMR to monitor the interaction between glycans and labelled galectins proved to be very efficient and was employed in this study (**Section 3.4**). Of course, in order to investigate the sugar binding, a key tryptophan moiety must be involved and be subsequently labelled before being inserted into the protein according to a specific protocol. Taking into account these considerations, the examination of ^{19}F-W binding may represent an advantageous approach to examine the selective or competitive binding of various glycans by lectins.

3.2 Aim of the project

Given the importance of the interaction between proteins and glycans described in the previous sections, and as one of the aims of this thesis was to study molecules able to regulate the immune response, the galectin-glycan interaction was investigated using fluorine NMR. This study specifically focused on:

- Labelling the tryptophans of different types of galectins to study them with fluorine NMR.
- To check whether there are significant changes in affinity against a known ligand after the labelling process.
- Study the behaviour of galectins in a cellular context simulating the natural environment.
- Observe and analyse the behaviour of galectins while they are competing against each other in the same environment.

3.3 Preparation of the fluorinated galectins

Different fluorinated galectins were prepared, placing the fluorine in different positions of the tryptophan, in order to obtain more information both on the best position for labelling and on the behaviour of each protein. A plasmid with a specific antibiotic resistance was introduced into Escherichia coli cultures (BL21) to express the protein of interest. They were then transformed and grown in a minimal medium (M9). The labelling process was achieved by the addition of glyphosate and exogenous addition of aromatic amino acids. Glyphosate was used to block the pathway of tryptophan production and, unfortunately, the other aromatics were suppressed as well. Thus, tyrosine and phenylalanine were added manually at staggered times and then the marked tryptophan was added last (the only source of W available to the protein during folding process). Finally, protein production was induced by isopropyl β-D-1-thio-galactopyranoside (IPTG). IPTG is an allolactose mimic, a metabolite of lactose, which induces transcription of the lac operon. After

binding, it allosterically releases the tetrameric repressor from the lac operon, allowing transcription of genes in the lac operon. The labelled galectins were then purified either by AKTA and SEC or by an affinity column with agarose resin. In particular, the following fluorinated galectins were obtained: Galectin-3 CRD 5FW and 6FW; Galectin-8 5FW C-terminal, and N-terminal; Galectin-7 CRD 5FW; Galectin-1 5FW (**Figure 39**).

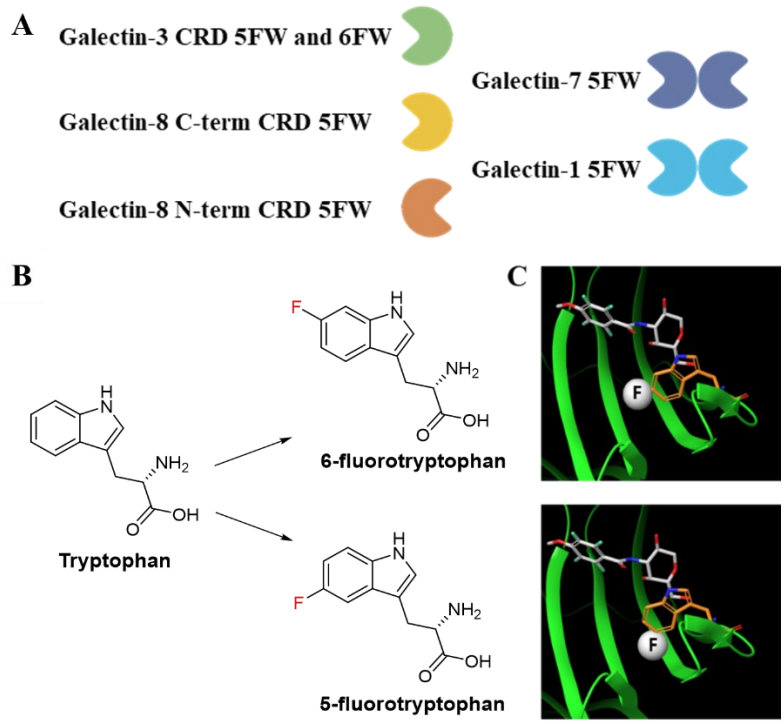

Figure 39: **A** List of successfully labelled galectins; **B** Schematic representation of the labelled tryptophans with a fluorine atom at position 6 and 5; **C** Schematic 3D view of the CH-π stacking interactions provided by 5FW and 6FW with a simple Gal-containing ligand.

Attempts were made to obtain galectin-4 and galectin-9 5FW, but the introduction of fluorine did not allow the correct refold of the protein.

3.4 Titration experiments

The presence of ^{19}F-labelled proteins was verified by ^{1}H and ^{19}F-NMR methods. To verify that the inclusion of fluorine did not lead to changes in the interaction affinity of galectins, a titration experiment was performed using galectin-3 CRD 5FW and α-2,3-sialyllactosamine as ligand. In this type of experiment, the protein is mixed in the NMR tube with a known ligand. The concentration of the ligand is gradually increased, NMR spectra are recorded, and changes in the signal relative to the labelled tryptophan are monitored by ^{19}F-NMR. As the concentration of the ligand is increased, the signal due to the labelled tryptophan of the free protein should decrease, while that of the bound protein should increase. This is indeed what was observed herein: by gradually increasing the concentration of the ligand from 0.5 to 10 equivalents, it was possible to see the onset of a new signal at a lower chemical shift relative to the bound protein while the signal from the free protein quickly vanished (**Figure 40**).

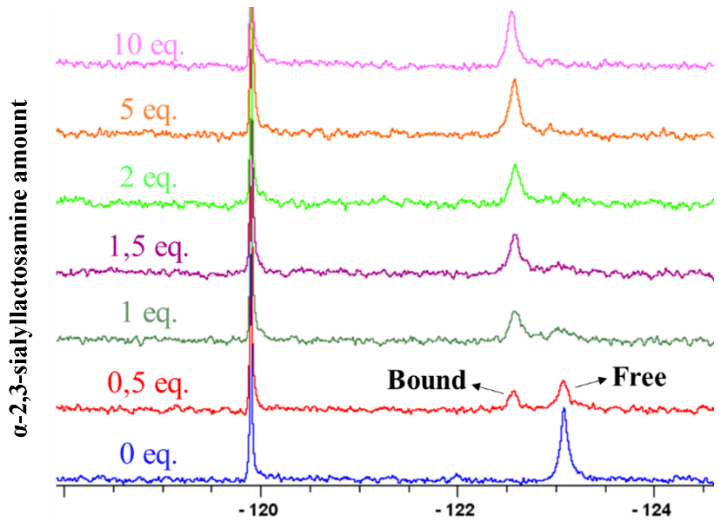

Figure 40: Titration experiment using galectin-3 CRD 5FW 75 μM and α-2,3-sialyllactosamine as ligand.

By plotting the percentage of bound protein as a function of ligand concentration and fitting the results using the Hill equation, it was possible to get a curve from which the K_d was estimated (**Figure 41**).

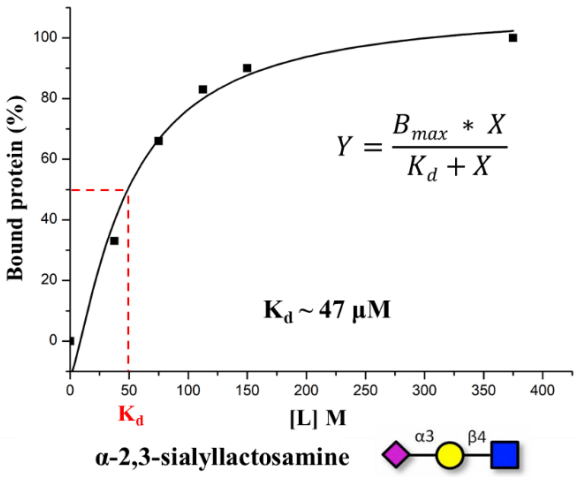

Figure 41: Percentage of galectin-3 5FW bound as a function of the concentration of α-2,3-sialylactosamine. Hill's equation was used to fit the titration points, where B_{max} represents the maximum number of binding sites in the same units as the Y-axis, X represents the ligand concentration, and Y represents the specific binding.

This equation describes the equilibrium binding of a ligand to a receptor, as a function of increasing ligand concentration. When the protein is half saturated with the ligand, the concentration of the ligand is equal to K_d. It is the equilibrium dissociation constant, expressed in the same units as the x-axis: concentration. Therefore, when the ligand concentration is equal to K_d, half of the binding sites are occupied at equilibrium. The value obtained was about 47 μM, basically identical to that obtained from the same titration method for the unlabelled protein. Thus, the fluorine at

position 5 of the key tryptophan ring did not cause any significant change in the affinity.

In a cellular context, however, galectins bind glycans on glycoproteins and glycolipids associated to other cellular components, including the cell surface. Due to the difficulty and complexity of characterising the natural cellular environment, there is currently no detailed understanding of the binding specificities of galectins in the cellular context. Due to the great advantages of ^{19}F-NMR, it was hypothesized that it could be possible to obtain some information on galectin-glycan interaction using glycan-expressing cells, simulating an environment similar to the natural one. Thus, titration experiments were carried out by placing galectin-3 CRD 5FW and mammalian HEK293F cells, which have a homogeneously glycosylated surface, in the NMR tube. Again, the concentration of the ligand, and thus of the cells, was gradually increased and a ^{19}F-NMR was spectrum recorded at each step (**Figure 42**).

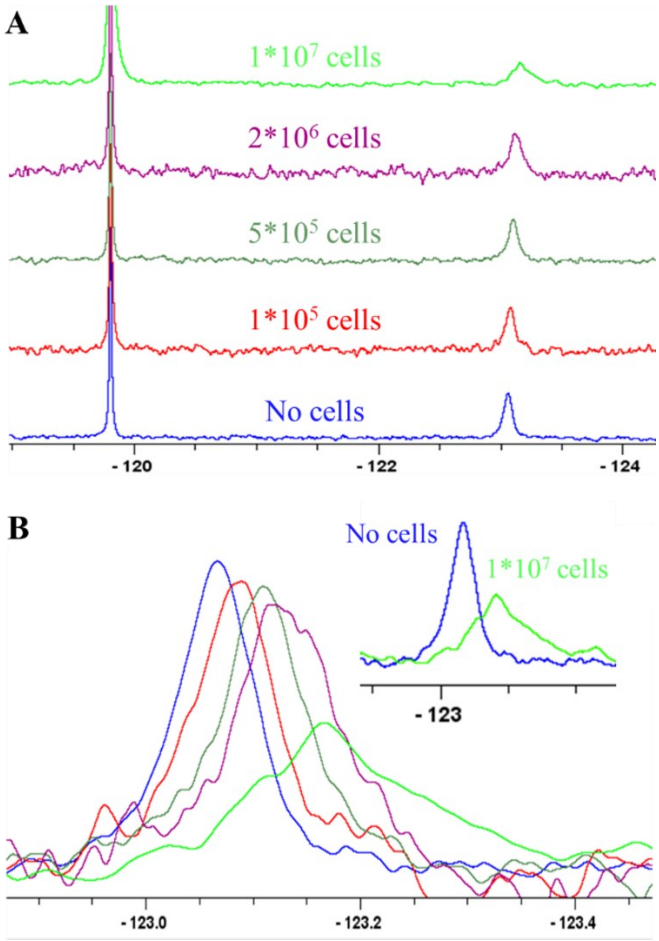

Figure 42: **A** Titration experiment using galectin-3 CRD 5FW and HEK293F cells with a homogeneous glycosylated surface; **B** Spectra superposition and zoom on the comparison between the experiment without cells and with ten million cells.

In the first experiment, 0.1 million cells were used, but no particular changes were observed. In the second experiment, 0.5 million cells were used and in the third, 2 million cells were used, but again no changes were observed save a small chemical shift. In the last experiment, 10 million cells were used: in this case, a signal shift of about 0.1 ppm and a broadening effect were observed, which could indicate the interaction of the components involved. Nevertheless, since the density of the solution also increases with the number of cells, density-related distortion effects could also

take place, making wider the NMR signals. Thus, these initial experiments need to be further assessed. As next step, titration experiments will be carried out with non-glycosylated cells or cells treated with enzymes to prevent glycosylation. This can help to understand whether the changes in the NMR signal are due to a real interaction or just to a change in the environment. The possibility to study the behaviour of galectins and glycans in an environment so close to the real world could answer many unsolved questions.

3.5 Conclusions and prospects

During my time at CIC bioGUNE in Bilbao, I have been able to deepen my knowledge in the field of biomolecules that influence the immune system, following the same thread of my project. Indeed, in addition to the interactions of glycolipids and sterol derivatives in the biological field, the recognition and activation of galectins and glycans display important effects on immune regulation and cellular homeostasis. Moreover, I was also able to deepen my knowledge of advanced NMR techniques, which can be applied in a wide range of fields and are outstanding for characterising molecules and studying protein-ligand interactions.

Several galectins were prepared labelling the tryptophan with a fluorine atom and then purified. The retention of the interaction affinity was checked by titration experiments with a known ligand comparing the K_d. In order to have the interacting environment as close as possible to the natural one, titration experiments were performed with mammalian cells expressing glycans, and a clear change in signal relative to fluorinated tryptophan was observed using 10 million cells. In the future, other galectins labelled in other positions of the tryptophan ring will be prepared and their behaviour in the presence of mammalian cells will be tested. In addition, competition experiments between several galectins could be interesting to obtain information on the specificity and priority of the interaction. Finally, the use of engineered cells could be an important part of this study. The development of stable genetic engineering strategies led to the chance to eliminate specific glycosyltransferases responsible for

the main glycosylation biosynthetic pathways. This has allowed to create cell libraries with an almost homogeneous set of glycans on the surface of glycosylated molecules.(401,402) The study of the interaction with this cell types could lead to the discovery of the determinants involved in galectin binding in a physiological context.

Chapter 4: Conclusions and prospects

The aim of this PhD thesis was the study of nature-inspired synthetic molecules with immunomodulatory properties. Specifically, the focus was on glycoglycerolipid molecules able to stimulate specific immune system receptors and modulate their response. Several compounds with distinct molecular scaffolds were assessed. Results were obtained using and combining multiple techniques including synthesis, mass spectrometry, nuclear magnetic resonance and molecular docking.

A section of this dissertation was devoted to the preparation of several sterol derivatives as potential new ligands of the cellular receptor Dectin-1, key target for the regulation of the immune response in infections and inflammatory diseases. Following the identification of cholesterol sulphate as a Dectin-1 ligand, an investigation was carried out to determine the most crucial structural chemical determinants responsible for receptor recognition. Modifications were mostly on the side chain on C17 and on the group in position 3, but also in some cases in the steroid core. Preliminary biological assays, using Dectin-1b reporter cell lines, suggested that most of the modifications caused a decrease in receptor binding affinity. In detail, modification in position 17 of cholesterol produced a decrease of affinity; the functional groups inserted on carbon 3 had very different features, and the screening of the synthetized products on reporter cells showed how the presence of a charged sulfur-containing function favored receptor recognition. These findings, alongside future tests on biological activity, could provide helpful insights into this receptor's workings, paving the way to treatments of inflammatory diseases, contributing to development of antifungal and anticancer therapies.

Another important innate receptor, focus of this thesis, was TREM2, widely present on many innate immune cells but mainly expressed on microglia within the central nervous system. The discovery of its ligands and the elucidation of its mechanism of interaction are crucial given its close association with inflammatory, autoimmune and neurodegenerative diseases. Sulfavant A, a sulpholipid inspired by chemical optimisation of natural α-D-sulfoquinovosyl-diacylglycerols (α-SQDG), was proved to have immunomodulatory properties such as the ability to stimulate the maturation of dendritic cells by a TLR-independent mechanism. In the ICB-CNR laboratories

where this thesis was carried out, Sulfavant A was recognised as the first synthetic ligand of TREM2. During preclinical studies and preliminar pharmacokinetic analysis, showing a Sulfavant A metabolization in the first hours after administration, one of the goals of this thesis was to synthesise two chemically more stable Sulfavant A analogues: Sulf-etherate and Sulf-amidate, with lipid chains linked to the glycerol moiety by ether and amide bonds respectively. In the case of Sulf-amidate, the synthesis of the final product is still ongoing, but three different approaches have been presented along with their difficulties and problems, giving crucial information on the best way to complete their chemical preparation in progress. For what concern the synthesis of Sulf-etherate, it resulted from the coupling of two building blocks: the acetylated trichloroacetimidate glucose donor and the glycerol acceptor containing eighteen-carbon ether chains. After glycosylation, the derivatisation of the group in position 6' of the sugar to obtain a sulphonic group finally led to the final product. The affinity of Sulf-etherate towards TREM2 WT receptor was tested by analysis on TREM2 reporter cells via indirect expression of GFP, showing a good affinity for this receptor.

The advances in fluorescence-based techniques have enabled the precise real-time study of protein and small ligand dynamics within complex cellular contexts. The possible pharmacological development of Sulfavant A highlighted the need for a better understanding of its behaviour in a biological context. Therefore, a synthetic strategy has been developed for the preparation of a fluorescent analogue named Sulf-BODIPY, whose main steps were the glycosylation of the trichloroacetimidate glucose donor with the acceptor rac-1,2-*O*-isopropylidene glycerol and the introduction of the undecanoyl moiety Me_4-BODIPY after the oxidation of the 6'-carbon of the sugar to the sulphonic function. As Sulfavant A, the fluorescent compound was able to activate and stimulate the maturation of dendritic cells despite the introduction of the fluorescent tag, as demonstrated by the up-regulation of the phenotypic marker CD83. Molecular imaging techniques enabled *in vitro* visualisation of Sulf-BODIPY within cells and *in vivo* analysis in zebrafish and mice models provided critical information on the localisation and possible distribution of Sulfavants in biological environments.

The synthetic procedure's versatility and the advantages of a molecule that is both immunomodulatory and fluorescent could be an essential tool for chemical biology studies and pharmacological progress.

Another section of this PhD thesis regarded the study of the interaction between Sulfavant A and TREM2 WT protein by molecular docking simulations. Starting from the X-ray structure published by Sudom and co-workers displaying the TREM2 WT protein co-crystallised with a synthetic phosphatidylserine analogue (COX), a combined biological and molecular docking approach was employed. Sulfavant A fit well in the pocket and followed the same binding mode of COX. The molecule's polar head was identified as the crucial structural component in these predictions, and its negative charge fits snugly into a nest of positively charged amino acids. Reporter cell assays showed that Sulfavant A has a stronger receptor affinity than phosphatidylserine consistently with the obtained docking data. An analogue of Sulfavant A with C6 lipid chains was synthesised to better compare with COX and used in simulation and biological assays. The obtained results could represent a starting point for the design of new small molecules able to bind TREM2.

In the CIC bioGUNE research institute in Bilbao, the study of the interaction between galectins and glycans has been carried out exploiting the advantages of ^{19}F-NMR. Several galectins were prepared, labelled with fluorine and purified. Titration experiments were performed to check the affinity preservation and the behaviour of these proteins with real mammalian cells. In the future, galectin competition experiments and the use of engineered cells could provide important information on the behaviour of these molecules in a physiological environment.

Starting with the synthesis of new nature-inspired molecules with promising immunomodulatory activity, along with performing parallel computational simulations and biological analysis, the goal of this PhD work was to offer a thorough body of knowledge in the field of glycolipids and immunomodulation, paving the way for future pharmacological applications in the treatment of immune dysregulation-based diseases.

Chapter 5: Experimental section

General experimental procedure

1D- and 2D-NMR spectra were recorded on a Bruker Avance-400 (400.13 MHz) and on a Bruker DRX-600 equipped with a TXI CryoProbe in $CDCl_3$ and CD_3OD (δ values are referred to $CHCl_3$ and CH_3OH at 7.26 and 3.34 ppm respectively). ESI-MS was conducted on a Micromass Q-TOF micro. HR-MS spectra were acquired using a Q-Exactive Hybrid Quadrupole-Orbitrap mass spectrometer (Thermo Scientific). TLC plates (Kieselgel 60 F254) and silica gel powder (Kieselgel 60, 0.063-0.200 mm) were from Merck. All the reagents were purchased from Sigma-Aldrich and used without any further purification. All the synthetic intermediates were characterized by NMR spectroscopy. For Dectin-1 reporter cell bioassays, HEK-Blue™ hDectin-1b Cells (SEAP Reporter 293 cells) were employed.

5.1 Synthesis of nature-inspired sterol derivatives

5.1.1 Synthesis of sulphated sterol derivatives

General sulphation procedure: The sterol derivative (2 mg, 0.005 mmol) was dissolved in anhydrous *N,N*-dimethylformamide (0.2 mL) and 5 eq. of triethylamine sulfur trioxide complex (4.71 mg, 0.025 mmol) was added. The reaction was kept for 1 hour at 30 °C under argon atmosphere. The product was purified by reversed-phase HPLC on a Phenomenex analytical RP18 column using a methanol/water gradient as eluent at a flow rate of 1 ml/min.

Cholesterol sulphate ((3S,8S,9S,10R,13R,14S,17R)-10,13-dimethyl-17-[(R)-6-methylheptan-2-yl]-2,3,4,7,8,9,10,11,12,13,14,15,16,17-tetradecahydro-1H-cyclopenta[a]phenanthren-3-yl sulphate) was obtained with the general sulphation procedure in quantitative yield. **^{1}H-NMR (600 MHz, $CDCl_3/CD_3OD$):** δ 5.38 (1H, m, H-6), 4.22 (1H, m, H-3), 2.55 (1H, m, H_a-4), 2.38 (1H, m, H_b-4), 2.11-1.07 (26H, overlapped, aliphatic methylenes), 1.02 (3H, s, H-19), 0.93 (3H, m, H-21), 0.87 (6H,

m, H-26, H-27), 0.70 (3H, s, H-18). HRESIMS *m/z* 488.2976 $[M + Na]^+$ (calcd for $C_{27}H_{45}O_4SNa$, 488.2936).

Stigmasterol sulphate ((3S,8S,9S,10R,13R,14S,17R)-17-[(2R,5R,E)-5-ethyl-6-methylhept-3-en-2-yl]-10,13-dimethyl-2,3,4,7,8,9,10,11,12,13,14,15,16,17-tetradecahydro-1H-cyclopenta[a]phenanthren-3-yl sulphate) was obtained with the general sulphation procedure in quantitative yield. **^{1}H-NMR (600 MHz, $CDCl_3/CD_3OD$):** δ 5.39 (1H, m, H-6), 5.17 (1H, dd, J = 8.56, 15.12 Hz, H-23), 5.04 (1H, dd, J = 8.56, 15.12 Hz, H-22), 4.20 (1H, m, H-3), 2.56 (1H, m, H_a-4), 2.37 (1H, m, H_b-4), 2.12-1.05 (23H, overlapped,), 1.04 (3H, s, H-19), 1.03 (3H, s, H-21), 0.88-0.81 (9H, overlapped, H-26, H-27, H-29). HRESIMS *m/z* 514.3093 $[M + Na]^+$ (calcd for $C_{29}H_{47}O_4SNa$, 514.3093).

Cholestanol sulphate ((3S,5S,8R,9S,10S,13R,14S,17R)-10,13-dimethyl-17-[(R)-6-methylheptan-2-yl]-hexadecahydro-1H-cyclopenta[a]phenanthren-3-yl sulphate) was obtained with the general sulphation procedure in quantitative yield. **^{1}H-NMR (600 MHz, $CDCl_3/CD_3OD$):** δ 4.29 (1H, m, H-3), 2.06-0.97 (31H, overlapped, aliphatic methylenes), 0.91 (3H, m, H-21), 0.87 (6H, m, H-26, H-27), 0.82 (3H, s, H-19), 0.66 (3H, s, H-18). HRESIMS *m/z* 490.3122 $[M + Na]^+$ (calcd for $C_{27}H_{47}O_4SNa$, 490.3093).

Brassicasterol sulphate ((3S,8S,9S,10R,13R,14S,17R)-17-[(2R,5R,E)-5,6-dimethylhept-3-en-2-yl]-10,13-dimethyl-2,3,4,7,8,9,10,11,12,13,14,15,16,17-tetradecahydro-1H-cyclopenta[a]phenanthren-3-yl sulphate) was obtained with the general sulphation procedure in quantitative yield. **^{1}H-NMR (600 MHz, $CDCl_3/CD_3OD$):** δ 5.37 (1H, m, H-6), 5.19 (2H, m, H-22, H-23), 4.21 (1H, m, H-3), 2.55 (1H, m, H_a-4), 2.37 (1H, m, H_b-4), 2.13-1.05 (21H, overlapped, aliphatic methylenes), 1.03-1.00 (6H, m, H-21, H-19), 0.92 (3H, m, H-28), 0.83 (6H, bt, J = 6.75, H-26, H-27), 0.70 (3H, s, H-18). HRESIMS *m/z* 500.2910 $[M + Na]^+$ (calcd for $C_{28}H_{45}O_4SNa$, 500.2936).

Lithocholic acid sulphate ((3S,5S,8R,9S,10S,13R,14S,17R)-17-[(R)-4-carboxybutan-2-yl]-10,13-dimethylhexadecahydro-1H-

cyclopenta[a]phenanthren-3-yl sulphate) was obtained with the general sulphation procedure in quantitative yield. **^{1}H-NMR (600 MHz, $CDCl_3/CD_3OD$):** δ 4.30 (1H, m, H-3), 2.36-1.03 (28H, overlapped, aliphatic methylenes), 1.00-0.96 (6H, overlapped, H-19, H-21), 0.72 (3H, s, H-18). HRESIMS *m/z* 476.2325 $[M + Na]^+$ (calcd for $C_{24}H_{37}O_6SNa$, 476.2209).

Pregnenolone sulphate ((3S,8S,9S,10R,13S,14S,17S)-17-acetyl-10,13-dimethyl-2,3,4,7,8,9,10,11,12,13,14,15,16,17-tetradecahydro-1H-cyclopenta[a]phenanthren-3-yl sulfate) was obtained with the general sulphation procedure in quantitative yield. **^{1}H-NMR (600 MHz, $CDCl_3/CD_3OD$):** δ 5.38 (1H, m, H-6), 4.21 (1H, m, H-3), 2.64-2.53 (2H, overlapped, H_a-4, H-17), 2.37 (1H, m, H_b-4), 2.15 (3H, bs, H-21), 2.17-1.09 (18H, overlapped, aliphatic methylenes), 1.05 (3H, s, H-19), 0.64 (3H, s, H-18). HRESIMS *m/z* 418.1792 $[M + Na]^+$ (calcd for $C_{21}H_{31}O_5SNa$, 418.1790).

Ergosterol sulphate ((3S,9S,10R,13R,14R,17R)-17-[(2R,5R,E)-5,6-dimethylhept-3-en-2-yl]-10,13-dimethyl-2,3,4,9,10,11,12,13,14,15,16,17-dodecahydro-1H-cyclopenta[a]phenanthren-3-yl sulphate) was obtained with the general sulphation procedure in quantitative yield. **^{1}H-NMR (600 MHz, $CDCl_3/CD_3OD$):** δ 5.56 (1H, m, H-6), 5.37 (1H, m, H-7), 5.21 (2H, m, H-22, H-23), 4.31 (1H, m, H-3), 2.72 (1H, m, H_a-4), 2.42 (1H, m, H_b-4), 2.17-1.24 (18H, overlapped, aliphatic methylenes), 1.04 (3H, m, H-21), 0.95 (3H, bs, H-19), 0.93 (3H, d, H-28), 0.86-0.82 (6H, overlapped, H-26, H-27), 0.64 (3H, s, H-18). HRESIMS *m/z* 498.2799 $[M + Na]^+$ (calcd for $C_{28}H_{43}O_4SNa$, 498.2780).

5.1.2 Synthesis of cholesteryl bromide

Compound 1 ((3S,8S,9S,10R,13R,14S,17R)-10,13-dimethyl-17-[(R)-6-methylheptan-2-yl]-2,3,4,7,8,9,10,11,12,13,14,15,16,17-tetradecahydro-1H-cyclopenta[a]phenanthren-3-yl methanesulfonate): cholesterol (200 mg, 0.52 mmol) was dissolved in anhydrous dichloromethane (2 mL), the solution cooled to 0

°C and 1.5 eq. of triethylamine (0.11 mL, 0.77 mmol) and 1.05 eq. of methanesulfonyl chloride (0.043 mL, 0.55 mmol) were added dropwise. After 30 minutes the reaction was brought to room temperature and left overnight. After evaporation of solvent, the dry crude product was dissolved in dichloromethane and methanol was added. The mixture was cooled to -20 °C to promote the crystallization and then filtered under vacuum, to obtain compound **1** (190 mg, 0.41 mmol, 79 %). **^{1}H-NMR (600 MHz, $CDCl_3$/CD_3OD):** δ 5.41 (1H, m, H-6), 4.50 (1H, m, H-3), 3.00 (3H, s, CH_3 mesyl group), 2.55-2.44 (2H, overlapped, H-4), 2.04-1.03 (26H, overlapped, aliphatic methylenes), 1.01 (3H, s, H-19), 0.90 (3H, m, H-21), 0.85 (6H, m, H-26, H-27), 0.67 (3H, s, H-18). HRESIMS *m/z* 487.3223 $[M + Na]^+$ (calcd for $C_{28}H_{48}O_3Na$, 487.3217).

Compound 2 ((3S,8S,9S,10R,13R,14S,17R)-3-bromo-10,13-dimethyl-17-[(R)-6-methylheptan-2-yl]-2,3,4,7,8,9,10,11,12,13,14,15,16,17-tetradecahydro-1H-cyclopenta[a]phenanthrene): compound **1** (92 mg, 0.19 mmol) was dissolved in anhydrous dichloromethane (2 mL). 2 eq. of boron trifluoride diethyl etherate (0.049 mL, 0.40 mmol) and 1.1 eq. of bromotrimethylsilane (0.029 mL, 0.22 mmol) were added to the solution. The solution was left 1 h and then subjected to double extraction: the first one with dichloromethane and baking soda, the second one with dichloromethane and water. The organic phase has been purified by silica gel chromatography in hexane getting the desired compound **2** (63.5 mg, 0.14 mmol, 74 %). **^{1}H-NMR (600 MHz, $CDCl_3$):** δ 5.36 (1H, m, H-6), 3.92 (1H, m, H-3), 2.74 (1H, m, H_a-4), 2.58 (1H, m, H_b-4), 2.21-1.06 (26H, overlapped, aliphatic methylenes), 1.03 (3H, s, H-19), 0.91 (3H, m, H-21), 0.86 (6H, overlapped, H-26, H-27), 0.67 (3H, s, H-18). HRESIMS *m/z* 471.2623 $[M + Na]^+$ (calcd for $C_{27}H_{45}BrNa$, 471.2597).

5.1.3 Synthesis of acetyl cholesterol

Compound 3 (1-{(3S,8S,9S,10R,13R,14S,17R)-10,13-dimethyl-17-[(R)-6-methylheptan-2-yl]-2,3,4,7,8,9,10,11,12,13,14,15,16,17-tetradecahydro-1H-cyclopenta[a]phenanthren-3-yl}propan-2-one): cholesterol (13 mg, 0.034 mmol) was dissolved in anhydrous pyridine (0.5 mL) and acetic anhydride (0.25 mL) was

added. The reaction proceeded at room temperature overnight was stopped after control by TLC. The dry reaction crude was purified by direct-phase HPLC, on a Phenomenex analytical column (silica), using a UV detector. Hexane/isopropanol gradient was chosen as eluent system at flow rate of 1 ml/min. Compound **3** was obtained in quantitative yield. **^{1}H-NMR (600 MHz, $CDCl_3$):** δ 5.38 (1H, m, H-6), 4.60 (1H, m, H-3), 2.31 (2H, m, H-4), 2.03 (3H, s, CH_3 acetyl group), 2.01-1.03 (26H, overlapped, aliphatic methylenes), 1.01 (3H, s, H-19), 0.91 (3H, m, H-21), 0.86 (6H, overlapped, H-26, H-27), 0.67 (3H, s, H-18). HRESIMS *m/z* 451.3611 $[M + Na]^+$ (calcd for $C_{29}H_{48}O_2Na$, 451.3547).

5.1.4 Synthesis of cholesterol phosphate

Compound 4 ((3S,8S,9S,10R,13R,14S,17R)-10,13-dimethyl-17-[(R)-6-methylheptan-2-yl]-2,3,4,7,8,9,10,11,12,13,14,15,16,17-tetradecahydro-1H-cyclopenta[a]phenanthren-3-yl dimethyl phosphate): cholesterol (113 mg, 0.29 mmol) was dissolved in anhydrous pyridine (0.3 mL) and 1.1 eq. of tetrabromomethane (106 mg, 0.32 mmol) were added. After cooled the mixture to 0 °C, 1.3 eq. of trimethyl phosphite (0.044 mL, 0.38 mmol) were added dropwise. The reaction proceeded at room temperature for 5 h and was stopped after control by TLC. The mixture was evaporated under nitrogen and then purified by silica gel chromatography using a petroleum ether/diethyl ether gradient (8:2 to 2:8 v/v). The product obtained was further purified by reversed-phase HPLC, on a Phenomenex semipreparative column (RP-18), using a UV detector and methanol as eluent system at a flow rate of 3 ml/min., to give the compound **4** (57 mg, 0.12 mmol, 41 %). **^{1}H-NMR (600 MHz, $CDCl_3$):** δ 5.34 (1H, m, H-6), 4.16 (1H, m, H-3), 3.71 (6H, dd, J = 11.18, J = 1.90 Hz, 2 CH_3 phosphate group), 2.39 (2H, m, H-4), 1.99-1.00 (26H, overlapped, aliphatic methylenes), 0.97 (3H, s, H-19), 0.87 (3H, m, H-21), 0.82 (6H, overlapped, H-26, H-27), 0.63 (3H, s, H-18). HRESIMS *m/z* 517.3476 $[M + Na]^+$ (calcd for $C_{29}H_{51}O_4PNa$, 517.3418).

Compound 5 ((3S,8S,9S,10R,13R,14S,17R)-10,13-dimethyl-17-[(R)-6-methylheptan-2-yl]-2,3,4,7,8,9,10,11,12,13,14,15,16,17-tetradecahydro-1H-cyclopenta[a]phenanthren-3-yl dihydrogen phosphate): compound **4** (58 mg, 0.12 mmol) was dissolved in anhydrous dichloromethane (2 mL) and 3 eq. of bromotrimethylsilane (0.046 mL, 0.035 mmol) were added dropwise under argon atmosphere at 0 °C. The reaction was allowed to proceed at room temperature for 24 h and was stopped after control by TLC. The mixture was evaporated and then ethanol (2 mL) was added leaving the solution stirring for 2 h. The mixture was evaporated again and purified by silica gel chromatography using methanol as eluent. The product was further purified by reversed-phase HPLC, on a Phenomenex semipreparative column (RP-18), using a UV detector and methanol as eluent system at a flow rate of 3 ml/min., to give the compound **5** (1 mg, 0.002 mmol, 22 %). **^{1}H-NMR (600 MHz, $CDCl_3/CD_3OD$):** δ 5.38 (1H, m, H-6), 4.07 (1H, m, H-3), 2.42 (2H, m, H-4), 2.05-1.06 (26H, overlapped, aliphatic methylenes), 1.02 (3H, s, H-19), 0.93 (3H, m, H-21), 0.87 (6H, overlapped, H-26, H-27), 0.69 (3H, s, H-18). HRESIMS *m/z* 517.3476 $[M + Na]^+$ (calcd for $C_{29}H_{51}O_4PNa$, 517.3418).

5.1.5 Synthesis of sulfoquinovosyl cholesterol

Compound 6 (Peracetylated-D-glucose) (325)**:** D-glucose (2.00 g, 0.011 mol) was dissolved in anhydrous pyridine (26 mL) and acetic anhydride (10 mL) was added. The reaction mixture was left stirring for 3 h at 25 ºC. After an extraction with water and chloroform, the organic phase was dried with anhydrous sodium sulphate, filtered and then evaporated under reduced pressure. Finally, it was purified by silica gel chromatography using a gradient of light petroleum ether/diethyl ether (9:1 to 3:2 v/v) to give compound **6** (4.20 g, 10.77 mmol, 98 %). **^{1}H-NMR (600 MHz, $CDCl_3$):** δ 6.32 (1H, d, J = 3.3 Hz, H-1 α-form), 5.71 (1H, d, J = 8.18 Hz, H-1 β-form), 5.46 (1H, dd, J = 9.7 Hz, J = 9.7 Hz, H-4), 5.12 (1H, m, H-3), 5.11 (1H, m, H-2), 4.28 (1H, dd, J = 6.37 Hz, J = 11.1 Hz, H_a-6), 4.11 (1H, dd, J = 6.7 Hz, J = 11.1 Hz, H_b-6), 3.85

(1H, m, H-5), 2.17-2.00 (15H, 5 OAc). HRESIMS *m/z* 413.1065 $[M + Na]^+$ (calcd for $C_{16}H_{22}O_{11}Na$, 413.1060).

Compound 7 (2',3',4',6'-*O*-tetraacetyl-D-glucose) (325)**:** compound **6** (4.20 g, 0.011 mol) was dissolved in tetrahydrofuran (40 mL) and 1.5 eq. of benzylamine (1.8 mL, 16.5 mmol) were added. The reaction mixture was stirred overnight at 25 ºC and after portioning between water and chloroform, the organic phase was evaporated under reduced pressure and purified by silica gel chromatography using a gradient of light petroleum ether/diethyl ether (9:1 to 3:7 v/v) to give compound **7** (2.78 g, 7.97 mmol, 73 %). **^{1}H-NMR (600 MHz, $CDCl_3$):** δ 5.52 (1H, t, J = 9.6 Hz, H-3), 5.45 (1H, d, J = 3.5 Hz, H-1), 5.09 (1H, t, J = 9.3 Hz, H-4), 4.90 (1H, dd, J = 3.5 Hz, J = 9.6 Hz, H-2), 4.35−4.20 (2H, m, H-6), 4.15−4.05 (1H, m, H-5), 2.05 (3H, s, OAc), 2.00 (3H, s, OAc), 1.95 (3H, s, OAc), 1.90 (3H, s, OAc). HRESIMS *m/z* 371.0980 $[M + Na]^+$ (calcd for $C_{14}H_{20}O_{10}Na$, 371.0954).

Compound 8 (1'-*O*-trichloroacetimidate-2',3',4',6'-*O*-tetraacetyl-D-glucose) (325)**:** compound **7** (2.78 g, 0.008 mol) was dissolved in a mixture of anhydrous dichloromethane (24 mL) and trichloroacetonitrile (8.0 mL). 0.2 eq. of 1,8-diazabicycle[5.4.0]undec-7-ene (0.25 mL, 1.68 mmol) was added and the reaction mixture was stirred for 2 h at 0 °C on activated 4 Å molecular sieves. After filtration on celite and evaporation under reduced pressure, the mixture was purified by silica gel chromatography using a gradient of petroleum ether/diethyl ether (9:1 to 7:3 v/v) to give compound **8** (3.12 g, 6.35 mmol, 79 %). **^{1}H-NMR (600 MHz, $CDCl_3$):** δ 6.56 (1H, d, J = 3.8 Hz, H-1), 5.57 (1H, dd, J = 9.2 Hz, J = 9.2 Hz, H-4), 5.18-5.14 (1H, overlapped, H-2, H-3), 4.28 (1H, m, H-5), 4.26 (1H, m, H_a-6), 4.13 (1H, m, H_b-6), 2.09-2.01 (12H, 4 OAc). HRESIMS *m/z* 514.0059 $[M + Na]^+$ (calcd for $C_{16}H_{20}Cl_3O_{10}Na$, 514.0050).

Compound 9 ((3S,8S,9S,10R,13R,14S,17R)-3-*O*-β-[(2',3',4',6'-*O*-tetraacetyl)-D-glucose]-10,13-dimethyl-17-[(R)-6-methylheptan-2-yl]-2,3,4,7,8,9,10,11,12,13,14,15,16,17-tetradecahydro-1H-cyclopenta[a]phenanthrene): compound **8** (64 mg, 0.13 mmol) was dissolved in

anhydrous dichloromethane (1.5 mL) and 1.2 eq. of cholesterol (60 mg, 0.16 mmol) were added to the solution. The reaction was kept for 3 h at -20 °C with activated 4 Å molecular sieves. 0.2 eq. of boron trifluoride diethyl etherate (0.0032 mL, 0.02 mmol) were added twice and the reaction proceeded over night at -10 °C. After addition of triethylamine (4 µL), the solution was filtered on celite and evaporated under reduced pressure and then purified on the silica gel chromatography using a gradient of petroleum ether/diethyl ether (95:5 to 1:1 v/v) to give compound **9** (28.9 mg, 0.04 mmol, 31 %). **^{1}H-NMR (600 MHz, $CDCl_3$):** δ 5.34 (1H, m, H-6), 5.19 (1H, t, J = 9.60 Hz, H-3'), 5.06 (1H, bt, J = 9.60 Hz, H-4'), 4.94 (1H, bt, J = 9.93 Hz, H-2'), 4.58 (1H, d, J = 7.95 Hz, H-1'), 4.24 (1H, dd, J = 4.81, J = 12.20 Hz, H_a-6'), 4.09 (1H, dd, J = 2.52, J = 12.20 Hz, H_b-6'), 3.67 (1H, m, H-5'), 3.47 (1H, m, H-3), 2.22 (2H, m, H-4), 2.11-2.01 (12H, overlapped, 4 OAc), 1.97-0.99 (26H, overlapped, aliphatic methylenes), 0.96 (3H, s, H-19), 0.90 (3H, s, H-21), 0.85 (6H, m, H-26, H-27), 0.66 (3H, s, H-18). HRESIMS *m/z* 739.4398 $[M + Na]^+$ (calcd for $C_{41}H_{64}O_{10}Na$, 739.4392).

Compound 10 ((3S,8S,9S,10R,13R,14S,17R)-3-*O*-β-D-glucose-10,13-dimethyl-17-[(R)-6-methylheptan-2-yl]-2,3,4,7,8,9,10,11,12,13,14,15,16,17-tetradecahydro-1H-cyclopenta[a]phenanthrene): compound **9** (28.9 mg, 0.04 mmol,) was submitted to Zemplén reaction, in CH_3OH/CH_3ONa 0.5 M (2 mL) for 2 h at room temperature. The solution was evaporated under reduced pressure and purified by silica gel chromatography using a chloroform/methanol (1:0 to 7:3 v/v) gradient. Then it was further purified by reversed-phase HPLC, on a Phenomenex analytical column (Phenyl-Hexyl), using a UV detector and methanol as eluent system at a flow rate of 1 ml/min., to give compound **10** in quantitative yield. **^{1}H-NMR (600 MHz, CD_3OD):** δ 5.37 (1H, m, H-6), 4.40 (1H, d, J = 7.79 Hz, H-1'), 3.84 (2H, m, H_a-6'), 3.74-3.57 (5H, overlapped, H-2', H-3', H-4', H_b-6', H-3), 3.28 (1H, m, H-5'), 2.42 (1H, m, H_a-4), 2.28 (1H, m, H_b-4), 2.05-1.05 (26H, overlapped, aliphatic methylenes), 1.02 (3H, s, H-19), 0.93 (3H, s, H-21), 0.87 (6H, m, H-26, H-27), 0.70 (3H, s, H-18). HRESIMS *m/z* 571.3918 $[M + Na]^+$ (calcd for $C_{33}H_{56}O_6Na$, 571.3970).

Compound 11 ((3S,8S,9S,10R,13R,14S,17R)-3-*O*-β-[(6'-*O*-trityl)-D-glucose]-10,13-dimethyl-17-[(R)-6-methylheptan-2-yl]-2,3,4,7,8,9,10,11,12,13,14,15,16,17-

tetradecahydro-1H-cyclopenta[a]phenanthrene): β-glucosyl-cholesterol (**10**) (158 mg, 0.288 mmol) was dissolved in anhydrous pyridine (1.5 mL). 2 eq. of triphenylmethyl chloride (161 mg, 0.57 mmol) and 3 eq. of triethylamine (126 µL, 0.09 mmol) were added to the solution. The mixture reaction was stirred for 72 h at 60 °C and stopped after control by TLC. After evaporation, the mixture was purified by silica gel chromatography using a gradient of petroleum ether/dichloromethane (1:1 to 2:8 v/v) and subsequent dichloromethane/methanol (1:0 to 9:1 v/v) gradient to give compound **11** (100 mg, 0.126 mmol, 44 %). **^{1}H-NMR (600 MHz, $CDCl_3$):** δ 7.48-7.21 (15H, overlapped, trityl portion), 5.37 (1H, m, H-6), 4.42 (1H, d, J = 7.70 Hz, H-1'), 3.64 (1H, m, H-3), 3.55-3.37 (5H, overlapped, H-2', H-3', H-4', H-6'), 3.34 (1H, m, H-5'), 2.40 (1H, m, H_a-4), 2.31 (1H, m, H_b-4), 2.11-1.05 (26H, overlapped, aliphatic methylenes), 1.02 (3H, s, H-19), 0.95 (3H, s, H-21), 0.89 (6H, m, H-26, H-27), 0.70 (3H, s, H-18). HRESIMS *m/z* 813.5082 $[M + Na]^+$ (calcd for $C_{52}H_{70}O_6Na$, 813.5070).

Compound 12 ((3S,8S,9S,10R,13R,14S,17R)-3-*O*-β-[(2',3',4'-*O*-triacety-6'-*O*- β-trityl)-D-glucose]-10,13-dimethyl-17-[(R)-6-methylheptan-2-yl]-2,3,4,7,8,9,10,11,12,13,14,15,16,17-tetradecahydro-1H-cyclopenta[a]phenanthrene): compound **11** (100 mg, 0.13 mmol) was dissolved in anhydrous pyridine (2 mL) and acetic anhydride (1 mL) was added. The reaction proceeded at room temperature overnight and was stopped after control by TLC. The mixture was evaporated and compound **12** (80 mg, 0.087 mmol, 67 %) was obtained. **^{1}H-NMR (600 MHz, $CDCl_3$):** δ 7.52-7.22 (15H, overlapped, trityl portion), 5.40 (1H, m, H-6), 5.18-5.15 (2H, overlapped, H-3', H-4'), 5.05 (1H, bt, J = 7.82 Hz, H-2'), 4.63 (1H, d, J = 7.88 Hz, H-1'), 3.62-3.53 (2H, overlapped, H-5', H-3), 3.23 (1H, dd, J = 1.70, J = 10.29 Hz, H_a-6'), 3.10 (1H, dd, J = 4.86, J = 10.23 Hz, H_b-6'), 2.30 (2H, m, H-4), 2.08 (3H, s, OAc), 2.01 (3H, s, OAc), 1.75 (3H, s, OAc), 1.94-1.07 (26H, overlapped, aliphatic methylenes), 1.05 (3H, s, H-19), 0.95 (3H, s, H-21), 0.89 (6H, m, H-26, H-27), 0.71 (3H, s, H-18). HRESIMS *m/z* 939.5392 $[M + Na]^+$ (calcd for $C_{58}H_{76}O_9Na$, 939.5382).

Compound 13 ((3S,8S,9S,10R,13R,14S,17R)-3-*O*-β-[(2',3',4'-*O*-triacetyl)-D-glucose]-10,13-dimethyl-17-[(R)-6-methylheptan-2-yl]-2,3,4,7,8,9,10,11,12,13,14,15,16,17-tetradecahydro-1H-cyclopenta[a]phenanthrene): compound **12** (80 mg, 0.087 mmol) was dissolved in anhydrous acetonitrile (3.5 mL). 3 eq. of chlorotrimethylsilane (0.033 mL, 0.26 mmol) and 3 eq. of sodium iodide (39 mg, 0.26 mmol) were added. The reaction proceeded at 0 °C for 3 h and was stopped after control by TLC. The solution was subjected to extraction between ethyl ether and water. The organic phase was purified by silica gel chromatography using a gradient of petroleum ether/dichloromethane (3:7 to 1:9 v/v) and subsequent dichloromethane/methanol (1:0 to 95:5 v/v) gradient to give compound **13** (48 mg, 0.071 mmol, 82 %). **^{1}H-NMR (600 MHz, $CDCl_3$):** δ 5.34 (1H, m, H-6), 5.22 (1H, t, J = 9.46, H-3'), 5.00 (1H, t, J = 9.46, H-4'), 4.91 (1H, bt, J = 7.83 Hz, H-2'), 4.61 (1H, d, J = 7.98 Hz, H-1'), 3.69 (1H, dd, J = 2.24, J = 12.59, H_a-6'), 3.58 (1H, dd, J = 5.13, J = 12.59, H_b-6'), 3.52-3.46 (2H, overlapped, H-5', H-3), 2.25 (1H, m, H_a-4), 2.16 (1H, m, H_b-4), 2.03 (6H, bs, 2 OAc), 1.99 (3H, s, OAc), 2.09-1.01 (26H, overlapped, aliphatic methylenes), 0.97 (3H, s, H-19), 0.90 (3H, s, H-21), 0.85 (6H, m, H-26, H-27), 0.65 (3H, s, H-18). HRESIMS *m/z* 697.4299 $[M + Na]^+$ (calcd for $C_{39}H_{62}O_9Na$, 697.4287).

Compound 14 ((3S,8S,9S,10R,13R,14S,17R)-3-*O*-β-[(2',3',4'-*O*-triacety-6'-*O*-β-tosyl)-D-glucose]-10,13-dimethyl-17-[(R)-6-methylheptan-2-yl]-2,3,4,7,8,9,10,11,12,13,14,15,16,17-tetradecahydro-1H-cyclopenta[a]phenanthrene): compound **13** (48 mg, 0.071 mmol) was dissolved in anhydrous pyridine (1 mL). 3 eq. of *p*-toluenesulfonyl chloride (40.6 mg, 0.21 mmol) and 1.2 eq. of 4-*N,N-d*imethylaminopyridine (10.4 mg, 0.085 mmol) were added. The reaction proceeded overnight at room temperature and was stopped after control by TLC. After evaporation, the mixture was purified by silica gel chromatography using a gradient of petroleum ether/dichloromethane (1:1 to 2:8 v/v) and subsequent dichloromethane/methanol (1:0 to 95:5 v/v) gradient to give compound **14** (50 mg, 0.06 mmol, 85 %). **^{1}H-NMR (600 MHz, $CDCl_3$):** δ 7.76 (2H, d, J = 7.75 Hz, H_a aromatic), 7.33 (2H, d, J = 7.75 Hz, H_b aromatic), 5.35 (1H, m, H-6), 5.16 (1H, bt, J

= 9.49, H-3'), 4.86 (2H, overlapped, H-2', H-4'), 4.53 (1H, d, *J* = 7.91 Hz, H-1'), 4.06 (2H, m, H-6'), 3.73 (1H, m, H-5'), 3.42 (1H, m, H-3), 2.44 (3H, s, CH_3 tosyl group), 2.23-2.08 (2H, m, H-4), 2.01 (3H, bs, OAc), 1.99 (3H, bs, OAc), 1.97 (3H, s, OAc), 1.85-1.00 (26H, overlapped, aliphatic methylenes), 0.97 (3H, s, H-19), 0.91 (3H, s, H-21), 0.86 (6H, m, H-26, H-27), 0.67 (3H, s, H-18). HRESIMS *m/z* 851.4403 $[M + Na]^+$ (calcd for $C_{46}H_{68}O_{11}SNa$, 851.4375).

Compound 15 ((3S,8S,9S,10R,13R,14S,17R)-3-*O*-β-[(2',3',4'-*O*-triacety-6'-*O*-β-thioacetyl)-D-glucose]-10,13-dimethyl-17-[(R)-6-methylheptan-2-yl]-2,3,4,7,8,9,10,11,12,13,14,15,16,17-tetradecahydro-1H-cyclopenta[a]phenanthrene): compound **14** (50 mg, 0.06 mmol) was dissolved in 2-butanone (5 mL) and 5 eq. of potassium thioacetate (34.3 mg, 0.30 mmol) were added. The reaction mixture was stirred at 80 °C for 2 hours and then the solvent was evaporated at reduced pressure. The resulting material was purified by silica gel chromatography using a gradient of petroleum ether/dichloromethane (1:1 to 3:7 v/v) and subsequent dichloromethane/methanol (1:0 to 99:1 v/v) gradient to give compound **15** in quantitative yield (42.3 mg, 0.058 mmol). **^{1}H-NMR (600 MHz, $CDCl_3$):** δ 5.34 (1H, m, H-6), 5.16 (1H, t, *J* = 9.53, H-3'), 4.96-4.89 (2H, overlapped, H-2', H-4'), 4.53 (1H, d, *J* = 7.94 Hz, H-1'), 3.56 (1H, m, H-5'), 3.44 (1H, m, H-3), 3.22 (1H, dd, *J* = 2.80, *J* = 14.15, H_a-6'), 3.00 (1H, dd, *J* = 7.42, *J* = 14.15, H_b-6'), 2.33 (3H, s, SAc), 2.19 (2H, m, H-4), 2.06 (3H, bs, OAc), 2.02 (3H, bs, OAc), 1.98 (3H, s, OAc), 1.97-1.02 (26H, overlapped, aliphatic methylenes), 0.97 (3H, s, H-19), 0.90 (3H, s, H-21), 0.85 (6H, m, H-26, H-27), 0.66 (3H, s, H-18). HRESIMS *m/z* 755.4204 $[M + Na]^+$ (calcd for $C_{41}H_{64}O_9SNa$, 755.4154).

Compound 16 ((3S,8S,9S,10R,13R,14S,17R)-3-*O*-β-[(2',3',4'-*O*-triacetyl)-D-sulfoquinovosyl)]-10,13-dimethyl-17-[(R)-6-methylheptan-2-yl]-2,3,4,7,8,9,10,11,12,13,14,15,16,17-tetradecahydro-1H-cyclopenta[a]phenanthrene): compound **15** (9 mg, 0.012 mmol) was dissolved in methanol (1.7 mL) together with hydrogen peroxide 30 % (0.16 mL) and 5 eq. of ammonium heptamolybdate tetrahydrate (6.98 mg, 0.06 mmol). The reaction mixture was stirred for 48 h at room temperature and stopped after control by TLC. The

solution was subjected to extraction between dichloromethane and water to get compound **16** (7.5 mg, 0.01 mmol, 83 %). **^{1}H-NMR (600 MHz, $CDCl_3$):** δ 5.36 (1H, m, H-6), 5.23 (1H, t, J = 9.31, H-3'), 4.92-4.87 (2H, overlapped, H-2', H-4'), 4.72 (1H, d, J = 8.02 Hz, H-1'), 4.08 (1H, m, H-5'), 3.60 (1H, m, H-3), 3.04 (2H, m, H-6'), 2.29 (2H, m, H-4), 2.06 (6H, bs, 2 OAc), 1.99 (3H, bs, OAc), 1.97-1.00 (26H, overlapped, aliphatic methylenes), 0.99 (3H, s, H-19), 0.93 (3H, s, H-21), 0.87 (6H, m, H-26, H-27), 0.69 (3H, s, H-18). HRESIMS *m/z* 737.3952 $[M-H]^-$ (calcd for $C_{39}H_{61}O_{11}S$, 737.3940).

Compound 17 ((3S,8S,9S,10R,13R,14S,17R)-3-*O*-β-D-sulfoquinovosyl-10,13-dimethyl-17-[(R)-6-methylheptan-2-yl]-2,3,4,7,8,9,10,11,12,13,14,15,16,17-tetradecahydro-1H-cyclopenta[a]phenanthrene): compound **16** (5 mg, 0.01 mmol) was submitted to a Zemplén reaction in CH_3OH/CH_3ONa 0.25 M (1 mL). The product was purified by silica gel chromatography using a gradient of dichloromethane/methanol (95:5 to 7:3 v/v) and then by reversed-phase HPLC, on a Phenomenex semi preparative column (Phenyl-Hexyl), using a UV detector and a methanol/water gradient as eluent system at a flow rate of 4 ml/min. to give the final β-6'-sulfoquinovosyl-cholesterol (**17**) in quantitative yield. **^{1}H-NMR (600 MHz, $CDCl_3/CD_3OD$):** 5.39 (1H, m, H-6), 4.43 (1H, d, J = 7.73 Hz, H-1'), 3.75 (1H, m, H-5'), 3.66 (1H, m, H-3), 3.40-3.37 (2H, overlapped, H-3', H_a-6'), 3.17 (1H, m, H-4'), 3.11 (1H, t, J = 9.38, H-2'), 2.97 (1H, dd, J = 8.23, J = 14.35 H_b-6'), 2.44 (1H, m, H_a-4), 2.27 (1H, m, H_b-4), 2.11-1.09 (26H, overlapped, aliphatic methylenes), 1.05 (3H, s, H-19), 0.98 (3H, s, H-21), 0.91 (6H, m, H-26, H-27), 0.75 (3H, s, H-18). HRESIMS *m/z* 611.3688 $[M-H]^-$ (calcd for $C_{33}H_{55}O_8S$, 611.3623).

5.1.6 Dectin 1 reporter assay

The Dectin-1b reporter cell line used is derived from embryonic cells that have been engineered to express a secreted alkaline phosphatase (SEAP) in response to Dectin-1 ligand stimulation. The reporter lines have a half-life of 12-15 propagations (P_0 - P_{15}). During P_0 the cells grow in culture medium consisting of Dulbecco's Modified

Eagle Medium (DMEM), 10% foetal bovine serum (FBS), 1% penicillin (50 μg/mL) 1% streptomycin (5 ng/mL). Starting from P_1, Puromycin 1 μg/mL and HEK-Blue CLR Selection antibiotics were added to the complete DMEM medium. HEK-Blue™ hDectin-1b Cells (SEAP reporter cells) (Invivogen, San Diego, CA, USA) were plated in 96-well plates at 4 × 105 cells/well in 0.2 mL/well of HEK-Blue™ medium (Invivogen, San Diego, CA, USA) and incubated overnight. MeOH was used as solvent to dissolve compounds and by performing the coating of the plate with 0.05 mL of solution of lipids at indicated concentration. Each compound was tested in the concentration range 1 ng/mL-60 μg/mL. Reporter cells activity was assessed after overnight incubation as quantification of secreted alkaline phosphatase (SEAP) released in the medium by reading the optical density (OD) at 655 nm. Zymosan was used as positive control under the same conditions at concentration of 100 μg/mL according to manufacturer's instructions. Quantitative data (ng/mL) were obtained by a standard curve for the SEAP protein.

5.2 Synthesis of potentially more stable Sulfavant A analogues

5.2.1 Synthesis of Sulf-etherate

Compound 19 (1,2-*O*-isopropylidene-3-*O*-benzyl-rac-glycerol): sodium hydride (0.353 g, 14.7 mmol) was portion-wise added to (*S*)-(+)-1,2-isopropylideneglycerol (**18**) (0.9 g, 6.85 mmol) dissolved in THF (11 mL) and after 30 min of stirring, benzyl bromide (1.27 g, 7.5 mmol) was added. After stirring for 20 h at 60 °C the mixture was purified by silica gel chromatography using a hexane/diethyl ether (9:1 v/v) gradient to give compound **19** (1.38 g, 6.2 mmol, 91 %). **^{1}H-NMR (400 MHz, $CDCl_3$):** δ 7.35-7.32 (5H, overlapped, aromatic group), 4.578 (2H, bs, CH_2 benzyl group), 4.30 (1H, m, H-2), 4.06 (1H, m, H_a-3), 3.74 (1H, m, H_b-3), 3.56 (1H, m, H_a-1), 3.47 (1H, m, H_b-1), 1.42 (3H, s, CH_3 isopropylidene), 1.36 (3H, s, CH_3 isopropylidene). HRESIMS *m/z* 245.1178 $[M + Na]^+$ (calcd for $C_{13}H_{18}O_3Na$, 245.1154).

Compound 20 (3-*O*-benzyl-rac-glycerol): compound **19** (1.38 g, 6.2 mmol) was dissolved in methanol/water 95:5 (10 mL) and Dowex H^+ (10 g) was added. After 1.5 h of stirring the mixture was filtered and evaporated. The mixture was purified by silica gel chromatography using a chloroform/methanol (9:1 v/v) gradient to give compound **20** (0.801 g, 4.4 mmol, 71 %). **^{1}H-NMR (400 MHz, $CDCl_3$):** δ 7.29-7.17 (5H, overlapped, aromatic group), 4.55 (2H, bs, CH_2 benzyl group), 3.84 (1H, m, H-2), 3.63 (1H, m, H_a-3), 3.59-3.49 (3H, overlapped, H_b-3, H_a-1, H_b-1). HRESIMS *m/z* 155.0704 $[M + Na]^+$ (calcd for $C_6H_{12}O_3Na$, 155.0684).

Compound 21 (1-Hexadecanol): stearic acid (3.6 g, 28 mmol) was dissolved in anhydrous diethyl ether (20 mL) and lithium aluminum hydride (6.38 g, 168 mmol) was added at 0 °C. After stirring at room temperature overnight the hydride excess was destroyed by hydrochloride acid 1 M and the mixture was stirred for 30 min and portioned between water and diethyl ether. The organic phase was then evaporated under reduced pressure to get compound **21** (5.8 g, 24 mmol, 85 %). **^{1}H-NMR (400 MHz, $CDCl_3$):** δ 3.63 (2H, t, J = 6.65 Hz, CH_2 α), 1.56 (2H, m, CH_2 β), 1.46-1.16 (30H, m, aliphatic methylenes), 0.86 (3H, t, J = 6.9 Hz, CH_3). HRESIMS *m/z* 293.2831 $[M + Na]^+$ (calcd for $C_{18}H_{38}ONa$, 293.2820).

Compound 22 (1-Bromohexadecane): compound **21** (1.58 g, 5.85 mmol) along with carbon tetrabromide (4.32 g, 13 mmol) were dissolved in dry diethyl ether (40 ml). Triphenylphosphine (3.40 g, 13 mmol) was added portion-wise observing the formation of a white precipitate. After one hour of stirring, the resulting suspension was filtered to separate insoluble triphenylphosphinoxide. The mixture was concentrated under vacuum and purified by silica gel chromatography using hexane/diethyl ether (95:5 v/v) gradient to give compound **22** (1.84 g, 5.56 mmol, 95%). **^{1}H-NMR (400 MHz, $CDCl_3$):** δ 3.40 (2H, t, J = 6.84 Hz, CH_2 α), 1.85 (2H, m, CH_2 β), 1.34-1.24 (30H, m, aliphatic methylenes), 0.88 (3H, t, J = 7.0 Hz, CH_3). HRESIMS *m/z* 355.1988 $[M + Na]^+$ (calcd for $C_{18}H_{37}BrNa$, 355.1976).

Compound 23 (1-*O*-benzyl-2,3-*O*-stearyl-rac-glycerol): sodium hydride (0.634 g, 26.4 mmol) was added portion-wise at 0 °C to compound **20** (0.801 g, 6.07 mmol)

dissolved in anhydrous DMF (7 mL) and the temperature was increased to 25 °C. Subsequently, TBAI (100 mg, 0.27 mmol) was added along with 1-hexadecanyl bromide (4.00 g, 13.1 mmol). After 40 h of stirring at room temperature the mixture was evaporated and purified by silica gel chromatography using a light petroleum ether/diethyl ether (1:0 to 0:1 v/v) gradient to give **23** (1.17 g, 1.85 mmol, 42 %). **^{1}H-NMR (400 MHz, $CDCl_3$):** δ 7.38-7.25 (5H, overlapped, aromatic group), 4.58 (2H, bs, CH_2 benzyl group), 3.63-3.47 (5H, overlapped, H_a-1, H_b-1, H_a-3, H_b-3, H-2), 3.43 (4H, t, J = 6.65 Hz, 2 CH_2 α), 1.57 (4H, m, 2 CH_2 β), 4.29 (1H, m, H-5'), 1.35-1.24 (60H, overlapped, aliphatic methylenes), 0.89 (6H, *t*, J = 6.9 Hz, 2 CH_3). HRESIMS *m/z* 709.6469 $[M + Na]^+$ (calcd for $C_{46}H_{86}O_3Na$, 709.6475).

Building block 2 (1,2-*O*-stearyl-rac-glycerol): compound **23** (1.17 g, 1.85 mmol) was dissolved in THF/MeOH 1:1 (15 mL) and Pd-C (10%) (200 mg) was added. After stirring overnight at room temperature, the mixture was filtered, evaporated and purified by silica gel chromatography using a light petroleum ether/ethyl acetate (1:0 to 25:1) gradient to give **building block 2** (733 mg, 1.35 mmol, 73 %). **^{1}H-NMR (400 MHz, $CDCl_3$):** δ 3.69 (1H, m, H-2), 3.66-3.40 (4H, overlapped, H_a-1, H_b-1, H_a-3, H_b-3,), 3.43 (4H, t, J = 6.60 Hz, 2 CH_2 α), 1.55 (4H, m, 2 CH_2 β), 1.30-1.23 (60H, overlapped, aliphatic methylenes), 0.86 (6H, t, J = 6.9 Hz, 2 CH_3). HRESIMS *m/z* 619.6046 $[M + Na]^+$ (calcd for $C_{39}H_{80}O_3Na$, 619.6005).

Compound 24 (1,2-*O*-distearyl-3-*O*-β-[(2',3',4',6'-*O*-tetracetyl)-D-glucosyl]-rac-glycerol): compound **23** (810 mg, 1.5 mmol) was dissolved in anhydrous dichloromethane (8 mL) with 4 Å molecular sieves and the solution was stirred for 1 h under argon. Compound **8** (740 mg, 1.5 mmol) dissolved in anhydrous dichloromethane (6 mL), was added to the previous solution cooled at 0 °C. Trimethylsyliltrifluoromethanesulfonate (333 mg, 1.5 mmol) was added dropwise and the mixture was stirred overnight at 0 °C. After neutralization with pyridine (0.09 mL), the mixture was purified by silica gel chromatography using chloroform to get compound **24** (587 mg, 0.68 mmol, 44 %) as pale-yellow oil. **^{1}H-NMR (400 MHz, $CDCl_3$):** δ 5.17 (1H, bt, J = 9.49 Hz, H-3'), 5.07 (1H, bt, J = 9.49 Hz, H-4'), 4.97 (1H, m, H-2'), 4.58 and 4.55 (1H, d, J = 7.84 Hz, H-1' R and H-1' S epimer), 4.26 (1H,

m, H_a-6'), 4.12 (1H, m, H_b-6'), 3.86 (1H, dd, *J* = 4.69, 10.36 Hz, H_a-3), 3.68 (1H, m, H-5'), 3.61 (1H, dd, *J* = 5.6, 10.36 Hz, H_b-3), 3.58-3.36 (7H, overlapped, 2 CH_2 α, H-2, H-1), 2.12-1.99 (12H, overlapped, 4 OAc), 1.65-1.55 (4H, overlapped, 2 CH_2 β), 1.34-1.19 (60H, overlapped, aliphatic methylenes), 0.87 (6H, t, *J* = 6.70 Hz , 2 CH_3). HRESIMS *m/z* 949.6987 $[M + Na]^+$ (calcd for $C_{53}H_{98}O_{12}Na$, 949.6956).

Compound 25 (1,2-O-distearyl-3-O-β-D-glucosyl-rac-glycerol): compound **24** (458 mg, 0.53 mmol) was dissolved in methanolic solution (15 mL) of MeONa (0.2 M). The mixture was stirred for 3 h, evaporated and purified by silica gel chromatography using a gradient of petroleum ether/chloroform (1:1 to 2:8 v/v) and subsequent chloroform/methanol (1:0 to 95:5 v/v) gradient to give compound **25** (299 mg, 0.42 mmol, 80 %). **^{1}H-NMR (400 MHz, $CDCl_3$):** *δ* 4.33 (1H, d, *J* = 7.05 Hz, H-1'), 3.93 (1H, m, H_a-3), 3.84 (2H, m, H-6'), 3.68-3.36 (11H, overlapped, H_b-3, H-1, H-2', H-3', H-4',H-2, 2 CH_2 α), 3.32 (1H, m, H-5'), 1.56 (4H, overlapped, 2 CH_2 β), 1.38-1.19 (60H, overlapped, aliphatic methylenes), 0.88 (6H, t, *J* = 6.70 Hz, 2 CH_3). HRESIMS *m/z* 781.6546 $[M + Na]^+$ (calcd for $C_{45}H_{90}O_8Na$, 781.6533).

Compound 26 and 27 (1,2-*O*-distearyl-3-*O*-β-[(2',3',4'-*O*-triacetyl-6'-iodo)-D-glucosyl]-rac-glycerol): 1.5 eq. of iodine (50 mg, 0.20 mmol) were added to a mixture of compound **25** (100 mg, 0.13 mmol) and 1,5 eq. of triphenylphosphine (51 mg, 0.19 mmol) in 2,6-dimethylpyridine (0.5 mL, 2.6 mmol). The mixture was stirred for 2 h at 80 °C and subsequently acetylated by the addition of pyridine (2 mL) and acetic anhydride (1 mL). The reaction mixture was stirred at room temperature overnight. After evaporation of the solvent under a stream of nitrogen, the mixture was purified by silica gel chromatography using a gradient of petroleum ether/diethyl ether (1:0 to 7:3 v/v) to give compound **27** (70 mg, 0.08 mmol, 60 %) as a yellowish oil. **^{1}H NMR (400 MHz, $CDCl_3$):** *δ* 5.16 (1H, bt, *J* = 9.60 Hz, H-3′), 4.98-4.91 (2H, overlapped, H-2', H-4'), 4.59 (1H, d, *J* = 7.90 Hz, H-1'), 3.84 (1H, dd, *J* = 5.1, *J* = 10.6 Hz, H_a-3), 3.63-3.34 (9H, overlapped, H-5', H_b-3, H-1, H-2, 2 CH_2 α), 3.26 (1H, dd, *J* = 2.4 Hz, *J* = 14.3 Hz, H_a-6'), 3.14 (1H, t, *J* = 7.1 Hz, *J* = 10.6 Hz, H_b-6'), 2.09-2.01 (9H, overlapped, 3 OAc), 1.55 (4H, m, 2 CH_2 β), 1.34-1.22 (60H, overlapped,

aliphatic methylenes), 0.92-0.84 (6H, overlapped, 2 CH_3). HRESIMS *m/z* 1017.5874[M + Na]$^+$ (calcd for $C_{51}H_{95}IO_{10}Na$, 1017.5868).

Compound 28 (1,2-*O*-distearyl-3-*O*-β-[(2',3',4'-*O*-triacetyl-6'-thioacetyl)-D-glucosyl]-rac-glycerol): compound **27** (77 mg, 0.077 mmol) was dissolved in 2-butanone (8 mL) and potassium thioacetate (58 mg, 0.51 mmol) was added. The reaction mixture was stirred at 80 °C for 2.5 h and after evaporation under reduced pressure, the mixture was purified by silica gel chromatography using a light petroleum ether/diethyl ether gradient (98:2 to 85:15 v/v) to give compound **28** (66 mg, 0.70 mmol, 91 %) as a colourless oil. **^{1}H-NMR (400 MHz, $CDCl_3$):** δ 5.16 (1H, t, *J* = 9.15 Hz, H-3'), 4.99-4.91 (2H, overlapped, H-2', H-4'), 4.52 (1H, d, *J* = 7.9 Hz, H-1'), 3.84 (1H, dd, *J* = 4.56, 10.46 Hz, H_a-3), 3.65-3.36 (7H, overlapped, H-5', H_b-3, H-2, H-1, 2 CH_2 α), 3.25 (1H, dd, *J* = 2.41 Hz, *J* = 14.03 Hz, H_a-6'), 3.05 (1H, dd, *J* = 6.94 Hz, *J* = 14.03 Hz, H_b-6'), 2.33 (3H, s, SAc), 2.09-1.97 (9H, overlapped, OAc), 1.60 - 1.50 (4H, overlapped, 2 CH_2 β), 1.32-1.26 (60H, overlapped, aliphatic methylenes), 0.92-0.84 (6H, overlapped, 2 CH_3). HRESIMS *m/z* 965.6742 [M + Na]$^+$ (calcd for $C_{53}H_{98}SO_{11}Na$, 965.6728).

Compound 29 (1,2-*O*-distearyl-3-*O*-β-[(2',3',4'-*O*-triacetyl)-D-sulfoquinovosyl]-rac-glycerol): compound **28** (66 mg, 0.70 mmol) was dissolved in a mixture of potassium acetate (160 mg), aq. H_2O_2 (0.6 mL) (34% w/v) and acetic acid (10 mL). The reaction mixture was stirred overnight at 40 °C and after evaporation under a stream of nitrogen, it was purified by silica gel chromatography using a gradient of chloroform/methanol (1:0 to 95:5 v/v) to give compound **29** (24 mg, 0.024 mmol, 34 %) as a colourless oil. **^{1}H-NMR (400 MHz, $CDCl_3$):** δ 5.19 (1H, bt, *J* = 8.88 Hz, H-3'), 4.95-4.84 (2H, overlapped, H-2', H-4'), 4.62 (1H, d, *J* = 7.91 Hz, H-1'), 4.05 (1H, m, H-5'), 3.91 (1H, m, H_a-3), 3.66-3.29 (8H, overlapped, H_b-3, H-2, H-1, 2 CH_2 α), 3.02 (2H, overlapped, H-6'), 2.04-1.95 (9H, overlapped, OAc), 1.52 (4H, overlapped, 2 CH_2 β), 1.32-1.20 (60H, overlapped, aliphatic methylenes), 0.84 (6H, bt, *J* = 6.74 Hz, 2 CH_3). HRESIMS *m/z* 947.6476 [M-H]$^-$ (calcd for $C_{51}H_{95}SO_{13}$, 947.6498).

Sulf-etherate (1,2-O-distearyl-3-O-β-D-sulfoquinovosyl-rac-glycerol): compound **29** (24 mg, 0.024 mmol) was dissolved in methanolic solution (2 mL) of MeONa (0.2 M). The mixture was stirred for 1 h, evaporated and purified by silica gel chromatography using a chloroform/methanol (1:0 to 85:15 v/v) gradient to give Sulf-etherate (16 mg, 0.02 mmol, 85 %). **^{1}H-NMR (400 MHz, $CDCl_3$/CD_3OD 1:1):** δ 4.29 (1H, d, J = 7.98 Hz, H-1'), 3.97 (1H, dd, J = 5.4 Hz, J = 11.0 Hz, H_a-3), 3.75 (1H, overlapped, H-5'), 3.70-3.42 (8H, overlapped, H_b-3, H-2, H-1, 2 CH_2 α, H-3', H-4') 3.36 (1H, overlapped, H_a-6'), 3.27 (1H, overlapped, H-2'), 3.07 (1H, dd, J = 7.3 Hz, J = 13.9 Hz, H_b-6'), 1.57 (4H, m, 2 CH_2 β), 1.37-1.23 (60H, overlapped, aliphatic methylenes), 0.88 (6H, bt, J = 6.80 Hz, 2 CH_3). HRESIMS *m/z* 821.6223 $[M-H]^-$ (calcd for $C_{45}H_{88}SO_{10}$, 821.6181).

5.2.2 TREM2 reporter assay

2B4 GFP-NFAT reporter T cells stably transfected with human TREM2 cDNAs were provided by Prof. Marco Colonna from Washington University in St. Louis. For the binding assay cells (2 × 105 cells/well) were plated in flat 96-well plate in 0.2 mL/well of RPMI medium and incubated overnight. MeOH was used as solvent to dissolve compounds and by performing the coating of the plate with 0.05 mL of solution of lipids at indicated concentration. Reporter cells activity was assessed after overnight incubation as percentage of GFP^+ cells subtracted from background (vehicle controls) measured by flow cytometry. Data were acquired by BD C6 ACCURI instruments (BD Bioscience, Frankin Lake, NJ, USA).

5.2.3 Synthesis of Sulf-amidate

Compound 30 (2,3-Dibromopropanol) (410)**:** Allyl alcohol (1 g, 4.6 mmol) was dissolved in dichloromethane (13 mL) and the solution kept at -40 °C. 1 eq. of Br_2 (1 mL, 9.2 mmol) was added dropwise and the solution was allowed to reach the room

temperature. After one night the reaction was quenched with an aqueous solution of $Na_2S_2O_3$ (12 mL) until the solution became pale-yellow. The solution was subjected to extraction between dichloromethane and a sodium chloride solution, filtered and dried at reduced pressure to give compound **30** (3.77 g, 15.8 mmol, 92 %). **^{1}H-NMR (400 MHz, $CDCl_3$):** δ 4.36 (1H, m, H-2), 4.02 (2H, bd, J = 4.18 Hz, H-3), 3.86 (2H, m, H-1). HRESIMS *m/z* 238.8680 $[M + Na]^+$ (calcd for $C_3H_6Br_2ONa$, 238.8683).

Compound 31 (2,3-Diazidopropanol) (410)**:** compound **30** (3.77 g, 15.8 mmol) was dissolved in dry dimethylformamide (53 mL) and 3 eq. of sodium azide (6.16 g, 95 mmol) were added in two times. The reaction was set at 70 °C and left for 24 h under argon atmosphere. The solution was subjected to extraction between ethyl acetate and distilled water, filtered and dried at reduced pressure to give compound **31** (1.40 g, 8.5 mmol, 54 %). **^{1}H-NMR (600 MHz, $CDCl_3$):** δ 3.76 (1H, dd, J = 4.69 and 11.36 Hz, H_a-3), 3.69 (1H, dd, J = 5.86, 11.36 Hz, H_b-3), 3.64 (1H, m, H-2), 3.49 (1H, dd, J = 4.69, 12.79 Hz, H_a-1), 3.42 (1H, dd, J = 6.88, 12.79 Hz, H_b-1). HRESIMS *m/z* 165.0524 $[M + Na]^+$ (calcd for $C_3H_6N_6ONa$, 165.0501).

Compound 32 (1-*O*-β-[(2',3',4',6'-*O*-tetracetyl)-D-glucosyl]-2,3-diazido-rac-propanol): compound **31** (700 mg, 4.93 mmol) was dissolved in dry dichloromethane (14 mL) with 4 Å molecular sieves and peracetylated glucose (1.27 g, 3.2 mmol) was added. The reaction was set to 0 °C and 1.5 eq. of BF_3Et_2O (0.9 mL, 7.4 mmol) diluted in DCM dry (2 mL) was added dropwise. The solution was kept 1 h at 0 °C and overnight at 4 °C. The reaction was quenched with triethylamine (0.41 mL, 2.93 mmol) and extracted with DCM/H_2O 1:1. The organic phase was filtered and dried at reduced pressure to give compound **32** (1.83 g, 3.7 mmol, 76 %). **^{1}H-NMR (400 MHz, $CDCl_3$):** δ 5.20 (1H, t, J = 9.54 Hz, H-3'), 5.09 (1H, m, H-4'), 5.02 (1H, m, H-2'), 4.56 and 4.58 (1H, 2d, J = 7.97 Hz, H-1', C2 R and C2 S epimer), 4.25 (1H, m, H_a-6'), 4.15 (1H, m, H_b-6'), 3.97 (1H, m, H_a-3), 3.75 (1H, m, H-2), 3.72 and 3.70 (1H, 2 m, H-5', C2 R and C2 S epimer), 3.64 (1H, m, H_b-3), 3.40 (1H, m, Ha-1), 3.31 (1H, m, H_b-1), 2.10-2.00 (12H, overlapped, 4 OAc). HRESIMS *m/z* 495.1456 $[M + Na]^+$ (calcd for $C_{17}H_{24}N_6O_{10}Na$, 495.1452).

Compound 33 (1-*O*-β-[(2',3',4',6'-*O*-tetracetyl)-D-glucosyl]-2,3-rac-diaminopropanol): compound **32** (55 mg, 0.12 mmol) was dissolved in methanol (1.5 mL) and a catalytical amount of Pd/C (10 %) was added. The reaction was kept under a steam of hydrogen at room temperature overnight. A drop of HCl (12 M) was added to the solution and the mixture was filtered on a double paper filter and dried at reduced pressure to give compound **33** (42 mg, 0.095 mmol, 79 %). **^{1}H-NMR (400 MHz, $CDCl_3$):** δ 5.29 and 5.28 (1H, 2t, overlapped, J = 9.48 Hz, H-3', C2 R and C2 S epimer), 5.07 and 5.06 (1H, 2t, overlapped, J = 9.78 Hz, H-4', C2 R and C2 S epimer), 4.98 (1H, overlapped, H-2', C2 R and C2 S epimer), 4.89 and 4.88 (1H, 2d, overlapped, J = 8.02 Hz, H-1', C2 R and C2 S epimer), 4.27 (2H, m, H_b-6'), 4.10 (2H, m, H_b-3), 4.00 and 3.98 (1H, 2m, H-5', C2 R and C2 S epimer), 3.88 and 3.82 (1H, 2m, H-2, C2 R and C2 S epimer), 3.33 (2H, m, H_b-1, C2 R and C2 S epimer), 2.07-1.95 (12H, overlapped, 4 OAc). HRESIMS *m/z* 443.1640 $[M + Na]^+$ (calcd for $C_{17}H_{28}N_2O_{10}Na$, 443.1642).

Compound 34 (1-*O*-β-[(2',3',4',6'-*O*-tetracetyl)-D-glucosyl]-2,3-*N*-distearoyl-rac-diaminopropanol): compound **33** (40 mg, 0.13 mmol) was dissolved in dry dichloromethane (2 mL). 3 eq. of triethylamine (0.12 mL, 0.78 mmol)and 1.2 eq. of stearic acid (88.7 mg, 0.31 mmol) were added. Then 1.5 eq. of thionyl chloride (0.03 mL, 0.39 mmol) were added. The reaction was left 2 h at room temperature. After solvent evaporation under a stream of nitrogen, it was purified by silica gel chromatography using a gradient of petroleum ether/chloroform (1:1 to 0:1 v/v) and chloroform/methanol (1:0 to 9:1 v/v) to give compound **34** (15 mg, 0.015 mmol, 34 %). **^{1}H-NMR (400 MHz, $CDCl_3$):** δ 6.76 and 6.56 (1H, 2d, J = 6.74 Hz, CHN<u>H</u>, C2 R and C2 S epimer), 6.31 and 6.23 (1H, m, CH_2N<u>H</u>, C2 R and C2 S epimer), 5.20 (1H, m, H-3'), 5.06 (1H, m, H-4'), 4.96 (1H, m, H-2'), 4.52 (1H, 2d, overlapped, J = 7.98 Hz, H-1'), 4.23 (1H, m, H-6'), 4.11 and 4.04 (1H, 2m, H-2, C2 R and C2 S epimer), 3.87 (1H, dd, J = 10.48 and 4.25 Hz, H-3a), 3.72 (1H, m, H-5'), 3.57 (1H, m, H_b-3), 3.48 (1H, m, H_a-1), 3.32 (1H, m, H_b-1), 2.33 (2H, t, J = 7.54 Hz, CH_2 α), 2.16 (2H, m, CH_2 α), 2.10-1.96 (12H, overlapped, 4 OAc), 1.59 (4H, m, 2CH_2 β), 1.26

(56H, bs, aliphatic methylenes), 0.88 (6H, t, J = 6.50 Hz, $2CH_3$). HRESIMS *m/z* 975.6865 $[M + Na]^+$ (calcd for $C_{53}H_{96}N_2O_{12}Na$, 975.6861).

Compound 35 (1-*O*-β-D-glucosyl-2,3-*N*-distearoyl-rac-diaminopropanol): compound **34** (15 mg, 0.015 mmol) was dissolved in methanolic solution (1 mL) of MeONa (0.2 M). The mixture was stirred for 1 h, evaporated and purified by silica gel chromatography using a chloroform/methanol (1:0 to 9:1 v/v) gradient to give compound **35** (6.7 mg, 0.008 mmol, 55 %). **^{1}H-NMR (400 MHz, CD_3OD):** δ 4.23 (1H, d, J = 7.70 Hz, H-1'), 4.08 and 4.00 (1H, 2m, H-2, C2 R and C2 S epimer), 3.93 (1H, dd, J = 10.12 and 3.80 Hz, Ha-3), 3.85 (1H, m, H_a-6'), 3.72 (1H, m, H_b-3), 3.46 (1H, m, H_a-1), 3.44-3.23 (5H, overlapped, H-2', H-3', H-4', H-5', H_b-1), 2.25 (2H, t, J = 7.37 Hz, CH_2 α), 2.16 (2H, m, CH_2 α), 1.58 (4H, m, $2CH_2$ β), 1.25 (56H, bs, aliphatic methylenes), 0.86 (6H, t, J = 6.50 Hz, 2 CH_3). HRESIMS *m/z* 807.6440 $[M + Na]^+$ (calcd for $C_{45}H_{88}N_2O_8Na$, 807.6438).

Compound 36 (1-*O*-β-D-glucosyl-2,3-diazido-rac-propanol): compound **32** (136 mg, 0.29 mmol) was dissolved in methanolic solution (2.5 mL) of MeONa (0.2 M). The mixture was stirred for 2 h at room temperature, evaporated and purified by silica gel chromatography using a chloroform/methanol (1:0 to 8:2 v/v) gradient to give compound **36** (40 mg, 0.13 mmol, 42 %). **^{1}H-NMR (400 MHz, CD_3OD):** δ 4.32 (1H, bt, J = 6.74 Hz, H-1'), 3.99 (1H, m, H_a-3), 3.92-3.86 (2H, overlapped, H_a-6', H-2), 3.74-3.67 (2H, overlapped, H_b-6', H_b-3), 3.59 (1H, m, H_a-1), 3.45 (1H, m, H_b-1), 3.38 (1H, m, H-3'), 3.30 (2H, overlapped, H-4', H-5'), 3.23 (1H, m, H-2'). HRESIMS *m/z* 327.1032 $[M + Na]^+$ (calcd for $C_9H_{16}O_6N_6Na$, 327.1029).

Compound 37 (1-*O*-β-[(6'-*O*-trityl)-D-glucosyl]-2,3-diazido-rac-propanol): compound **36** (126 mg, 0.41 mmol) was dissolved in pyridine (3.1 mL) and 1 eq. of triethylamine (0.058 mL, 0.41 mmol) was added. The reaction was set to 60 °C and 2 eq. of triphenylmethyl chloride (231 mg, 0.82 mmol) were added in three times. The reaction was stopped after 48 h and the solvent evaporated under a stream of nitrogen. The product was purified by silica gel chromatography using a gradient of petroleum ether/chloroform (1:1 to 0:1 v/v) and subsequently a gradient of chloroform/methanol

(1:0 to 9:1 v/v) to give compound **37** (45 mg, 0.082 mmol, 20 %).**^{1}H-NMR (400 MHz, CD_3OD):** δ 7.50-7.25 (15H, overlapped, trityl group), 4.32 (1H, bt, J = 6.87 Hz, H-1'), 4.04 (1H, dd, J = 4.49, 10.72, H_a-3), 3.88 (1H, overlapped, H-2), 3.77 (1H, m, H_b-3), 3.64-3.56 (1H, m, H_a-1), 3.52 (1H, m, H_a-6'), 3.48 (1H, overlapped, H_b-1), 3.38 (1H, dd, J = 6.42, 12.83, H-3'), 3.27 (1H, m, H-2'), 3.13 (2H, overlapped, H-4', H-5'), 2.77 (1H, m, H-6'b). HRESIMS *m/z* 569.2133 $[M + Na]^+$ (calcd for $C_{28}H_{30}O_6N_6Na$, 569.2125).

Compound 38 (1-*O*-β-[(2',3',4'-*O*-triacetyl-6'-*O*-trityl)-D-glucosyl]-2,3-diazido-rac-propanol): compound **37** (45 mg, 0.16 mmol) was dissolved in pyridine (4 mL) and 1.5 mL di acetic anhydride were added. The reaction was kept overnight at room temperature, evaporated under nitrogen and purified by silica gel chromatography using a petroleum ether/diethyl ether gradient (9:1 to 6:4 v/v) to give compound **38** (39 mg, 0.058 mmol, 36 %). **^{1}H-NMR (400 MHz, $CDCl_3$):** δ 7.45-7.21 (15H, overlapped, trityl group), 5.21-5.13 (2H, overlapped, H-4', H-3'), 5.06 (1H, bq, J = 9.08 Hz, H-2') 4.58 and 4.56 (1H, 2d, J = 7.71 Hz, H-1', C2 R and C2 S epimer), 4.05 (1H, m, H_a-3), 3.75-3.68 (2H, overlapped, H_b-3, H-2), 3.57 (1H, m, H-5'), 3.44 (1H, m, H_b-1), 3.33 (1H, dd, J = 6.41 and 12.83 Hz, H_a-1), 3.28 (1H, bd, J = 10.58, H_a-6'), 3.10 (1H, m, H_b-6'), 2.09 (3H, s, AcO), 2.05 (3H, s, AcO), 1.99 (3H, s, AcO). HRESIMS *m/z* 695.2446 $[M + Na]^+$ (calcd for $C_{34}H_{36}O_8N_6Na$, 695.2441).

Compound 39 (1-*O*-β-[(2',3',4'-*O*-triacetyl)-D-glucosyl]-2,3-diazido-rac-propanol): compound **38** (39 mg, 0.058 mmol) was dissolved in anhydrous acetonitrile (0.61 mL) and 3 eq. of sodium iodide (27.5 mg, 0.18 mmol) were added. The reaction was set at 0 °C and 3 eq. of trimethylsilyl chloride (0.023 mL, 0.174 mmol) were added. The mixture was left overnight and then extracted with dichloromethane and an aqueous solution of $Na_2S_2O_3$. The product was purified by silica gel chromatography using a petroleum ether/diethyl ether gradient (8:2 to 0:1 v/v) to give compound **39** (12.4 mg, 0.028 mmol, 50 %). **^{1}H-NMR (400 MHz, $CDCl_3$):** δ 5.25 (1H, t, J = 9.26 Hz, H-3'), 5.07-4.95 (2H, overlapped, H-4', H-2'), 4.60 (1H, bt, J = 7.41 Hz, H-1', C2 R and C2 S epimer), 4.01 (1H, m, H_a-3), 3.77 and 3.74 (1H, 2m, H-2, C2 R and C2 S epimer), 3.72-3.58 (2H, overlapped, H_a-6', H_b-3),

3.53 (1H, m, H-5'), 3.41 (1H, m, H_a-1), 3.32 (1H, m, H_b-1), 3.10 (1H, bdd, J = 5.10 and 12.67 Hz, H_b-6'), 2.05 (6H, bs, AcO), 2.01 (3H, s, OAc). HRESIMS *m/z* 453.1341 $[M + Na]^+$ (calcd for $C_{15}H_{22}N_6O_9Na$, 453.1346).

Compound 40 (1-*O*-β-[(2',3',4'-*O*-triacetyl-6'-*O*-tosyl)-D-glucosyl]-2,3-diazido-rac-propanol): compound **39** (12.4 mg, 0.028 mmol) was dissolved in pyridine (0.77 mL), 10 eq. of 4-toluenesulfonyl chloride (56.1 mg, 0.28 mmol) and a catalytic amount of 4-dimethylaminopiridine were added. The reaction was left overnight at room temperature and evaporated under nitrogen. The product was purified by silica gel chromatography using a petroleum ether/diethyl ether gradient (7:3 to 0:1 v/v) to give compound **40** in quantitative yield (12.5 mg, 0.027 mmol). **^{1}H-NMR (400 MHz, $CDCl_3$):** δ 7.78 (2H, d, J = 8.10 Hz, H_a tosyl group), 7.36 (2H, d, J = 8.10 Hz, H_b tosyl group), 5.18 (1H, t, J = 8.85 Hz, H-3'), 4.96-4.89 (2H, overlapped, H-4', H-2'), 4.53 (1H, t, J = 7.92 Hz, H-1', C2 R and C2 S epimer), 4.09 (1H, m, H-6'), 3.92 (2H, dd, J = 4.23 Hz, J = 9.94 Hz, H_b-3), 3.78, (1H, m, H-5'), 3.62 (1H, m, H-2), 3.38 (2H, bdd, J = 5.10 Hz, J = 12.67 Hz, H_b-1), 2.45 (3H, s, CH_3 tosyl group), 2.03 (3H, s, AcO), 2.00 (3H, s, AcO), 1.98 (3H, s, AcO). HRESIMS *m/z* 481.1118 $[M + Na]^+$ (calcd for $C_{16}H_{22}N_6O_8SNa$, 481.1118).

Compound 41 (1-*O*-β-[(2',3',4'-*O*-triacetyl-6'-*O*-thioacetyl)-D-glucosyl]-2,3-diazido-rac-propanol): compound **40** (12.5 mg, 0.027 mmol) was dissolved in 2-butanone (1.3 mL) and 6 eq. of potassium thioacetate (18.5 mg, 0.16 mmol) were added. The reaction was kept 2 h at 80 °C and then evaporated under nitrogen. The product was purified by silica gel chromatography using a petroleum ether/diethyl ether gradient (8:2 to 1:1 v/v) to give compound **41** (6.8 mg, 0.014 mmol, 52 %). **^{1}H-NMR (400 MHz, $CDCl_3$):** δ 5.16 (1H, t, J = 9.39 Hz, H-3'), 4.99-4.92 (2H, overlapped, H-4', H-2'), 4.52 (1H, t, J = 7.96 Hz, H-1', C2 R and C2 S epimer), 3.93 (2H, m, H-3), 3.68-3.58 (2H, overlapped, H-5', H-2), 3.39 (2H, m, H-1), 3.26 (1H, dd, J = 2.30 and 14.38 Hz, H_a-6'), 3.03 (1H, dd, J = 6.90, J = 14.38 Hz, H_b-6'), 2.33 (3H, s, SAc), 2.06 (3H, s, AcO), 2.02 (3H, s, AcO), 1.98 (3H, s, AcO). HRESIMS *m/z* 511.1225 $[M + Na]^+$ (calcd for $C_{17}H_{24}N_6O_9SNa$, 511.1223).

Compound 42 (1'-*O*-methyl-glucose): D-glucose (2.01 g, 11.1 mmol) was dissolved in a 1.25 M methanolic solution of hydrogen chloride (15 mL) and the solution was left stirring at 50 °C overnight. The product was purified by silica gel chromatography using a chloroform/methanol (9:1 v/v) gradient to give compound **42** in quantitative yield (2.38 g, 12.3 mmol). **^{1}H-NMR (400 MHz, CD_3OD):** δ 4.70 (1H, d, J = 3.33 Hz, H-1'α), 4.20 (1H, d, J = 7.77 Hz, H-1'β), 3.87 (1H, dd, J = 12.09 Hz, J = 24.07 Hz, H_a-6'), 3.67-3.73 (1H, dd, J = 5.26 Hz, J = 11.56 Hz, H_b-6'), 3.64 (1H, m, H5'), 3.56 (3H, s, methyl-α), 3.43 (3H, s, methyl-β), 3.40-3.28 (2H, overlapped, H-3', H-4'), 3.22 (1H, t, J = 8.41, H-2'). HRESIMS *m/z* 217.0690 $[M + Na]^+$ (calcd for $C_7H_{14}O_2Na$, 217.0688).

Compound 43 and 44 (1'-*O*-methyl-2',3',4'-*O*-triacetyl-6'-iodo-D-glucose): compound **42** (2.38 g, 12.3 mmol) was dissolved in anhydrous lutidine (15.5 mL). 1.2 eq. of triphenylphosphine (3.8 g, 14.7 mmol) and 1.2 eq. of I_2 (3.65 g, 14.7 mmol) were rapidly added and the solution was left 2.5 h at 80 °C. After TLC control the mixture was diluted in pyridine (5 mL) and acetic anhydride (5 mL) were added, leaving the reaction going overnight. The product was evaporated under nitrogen and then purified by silica gel chromatography using a petroleum ether/diethyl ether gradient (9:1 to 4:6 v/v) to give compound **44** in quantitative yield (6.5 mg, 15.1 mmol). **^{1}H-NMR (400 MHz, $CDCl_3$):** δ 5.46 (1H, t, J = 9.8 Hz, H-3), 4.99-4.83 (2H, overlapped, H-2, H-4), 4.45 (1H, d, J = 7.96, H-1), 3.79 (1H, m, H-5), 3.48 (3H, s, MeO), 3.30 (1H, dd, J = 10.8 Hz, J = 2.56 Hz, H_a-6), 3.15 (1H, dd, J = 10.8 and 8.57 Hz, H_b-6), 2.10-1.99 (9H, overlapped, 3 AcO). HRESIMS *m/z* 453.0026 $[M + Na]^+$ (calcd for $C_{13}H1_9IO_8Na$, 453.0022).

Compound 45 (1'-*O*-methyl-2',3',4'-*O*-triacetyl-6'-thioacetyl-D-glucose): compound **44** (6.5 g, 15.1 mmol) was dissolved in 2-butanone (20 mL) and 6 eq. of potassium thioacetate (10.3 mg, 90.6 mmol) were added. The reaction was kept 2.5 h at 80 °C and then evaporated under nitrogen. The product was purified by silica gel chromatography using a petroleum ether/diethyl ether gradient (1:0 to 1:1 v/v) to give compound **45** (3.4 g, 9.04 mmol, 60 %). **^{1}H-NMR (400 MHz, $CDCl_3$):** δ 5.43 (1H, t, J = 9.75, H-3), 5.00-4.88 (2H, overlapped, H-2, H-4), 4.38 (1H, d, J = 7.96, H-1), 3.91

(1H, m, H-5), 3.48 (3H, s, MeO), 3.30 (1H, dd, J = 14.13 Hz, J = 2.83 Hz, H_a-6), 3.06 (1H, dd, J = 14.13 and 6.09 Hz, H_b-6), 2.34 (3H, s, AcS), 2.10-1.99 (9H, overlapped, 3 AcO). HRESIMS *m/z* 401.0879 $[M + Na]^+$ (calcd for $C_{15}H_{22}O_9SNa$, 401.0882).

Compound 46 (1',2',3',4'-*O*-tetracetyl-6'-thioacetyl-D-glucose): compound **45** (751 mg, 1.99 mmol) was dissolved in a mixture of acetic acid (35 mL) and acetic anhydride (35 mL). The solution was placed under stirring in an ice bath and 96 % sulfuric acid (0.75 mL) was added dropwise in 30 min. The reaction mixture was allowed to reach the room temperature and was kept for 20 h. Ice water (50 mL) was added and the mixture was extracted using ice water and dichloromethane and then sodium bicarbonate and dichloromethane to give compound **46** in quantitative yield (872 mg, 2.15 mmol) as a colourless oil. **^{1}H-NMR (400 MHz, $CDCl_3$):** δ 6.13 (1H, d, J = 3.66 Hz, H-1), 5.30 (1H, t, J = 9.87 Hz, H-3), 4.94-4.87 (2H, overlapped, H-2, H-4), 4.00, 1H, m, H-5), 3.05 (2H, m, H-6), 2.22 (3H, s, AcS), 2.11-2.02 (9H, overlapped, 3 AcO). HRESIMS *m/z* 429.0833 $[M + Na]^+$ (calcd for $C_{16}H_{22}O_{10}SNa$, 429.0831).

Compound 47 (2',3',4'-*O*-triacetyl-6'-thioacetyl-D-glucose): compound **46** (1.25 g, 3.08 mmol) was dissolved in tetrahydrofuran (10 mL) and 1.5 eq. of benzylamine (0.54 mL, 4.62 mmol) was added. The reaction mixture was stirred overnight at 25 ºC and evaporated under nitrogen and purified by silica gel chromatography using a gradient of light petroleum ether/diethyl ether (8:2 to 1:1 v/v) to give compound **47** (410 mg, 1.13 mmol, 36 %). **^{1}H-NMR (400 MHz, $CDCl_3$):** δ 5.47 (1H, t, J = 9.72 Hz, H-3), 5.38 (1H, d, J = 3.54 Hz, H-1α), 4.94 (1H, t, J = 9.72 Hz, H-4), 4.83 (1H, m, H-2), 4.69 (1H, d, J = 7.95 Hz, H-1β), 4.23 (1H, m, H-5), 3.14 (2H, m, H-6), 2.31 (3H, s, AcS), 2.06-1.98 (9H, overlapped, AcO). HRESIMS *m/z* 387.0725 $[M + Na]^+$ (calcd for $C_{14}H_{20}O_9SNa$, 387.0726).

Building block A (1'-*O*-trichloroacetimidate-2',3',4'-*O*-triacetyl-6'-thioacetyl-D-glucose): compound **47** (168 mg, 0.46 mmol) was dissolved in anhydrous dichloromethane (2 mL). 5 eq. of trichloroacetonitrile (0.23 mL, 2.3 mmol) and 0.2 eq. of 1,8-diazabicycle[5.4.0]undec-7-ene (0.014 mL, 0.094 mmol) were added. The

reaction mixture was stirred for 2 h at 0 °C on activated 4 Å molecular sieves. After evaporation under reduced pressure, the mixture was purified by silica gel chromatography using a gradient of petroleum ether/diethyl ether (9:1 to 6:4 v/v) to give **building block A** (144 mg, 0.28 mmol, 62 %). **^{1}H-NMR (400 MHz, $CDCl_3$):** δ 8.67 (1H, s, NH), 6.50 (1H, d, J = 3.66 Hz, H-1), 5.51 (1H, t, J = 9.71 Hz, H-3), 5.10-5.02 (2H, overlapped, H-2, H-4), 4.20 (1H, m, H-5), 3.17 (2H, m, H-6), 2.30 (3H, s, AcS), 2.08 (3H, s, AcO), 2.00 (3H, s, AcO), 1.99 (3H, s, AcO). HRESIMS *m/z* 529.9820 $[M + Na]^+$ (calcd for $C_{16}H_{20}Cl_3NO_9SNa$, 529.9822).

Compound 48 (2,3-Diaminopropanol): compound **31** (500 mg, 3.52 mmol) was dissolved in a mixture of tetrahydrofuran and water 4:1 v/v (20 mL) and triphenylphosphine (1.8 g, 6.87 mmol). The reaction mixture was left overnight at 80 °C. The mixture was diluted with water and then evaporated under reduced pressure. The product was filtered with water to give compound **48** in quantitative yield (338 mg, 3.76 mmol). Compound **48** was lyophilized and used without any further purification. HRESIMS *m/z* 113.0698 $[M + Na]^+$ (calcd for $C_3H_{10}N_2ONa$, 113.0691).

Compound 49 (Stearic anhydride): Stearic acid (6 g, 21.1 mmol) was dissolved in pyridine (1.7 mL) and diethyl ether (165 mL). The reaction was set at -10 °C and 0.5 eq. of thionyl chloride (0.755 mL, 10.41 mmol) were added. The mixture was allowed to proceed at room temperature for 2 h and then filtered on double paper filter with cold diethyl ether. The solvent was evaporated under reduced pressure to give compound **49** (4.5 g, 8.18 mmol, 78 %). **^{1}H-NMR (400 MHz, $CDCl_3$):** δ 2.23 (4H, t, J = 7.37 Hz, 2 $CH_2\alpha$), 1.62 (4H, m, 2 $CH_2\beta$), 1.27 (56H, bs, aliphatic methylenes), 0.88 (6H, t, J = 6.89 Hz, 2 CH_3). HRESIMS *m/z* 573.5221 $[M + Na]^+$ (calcd for $C_{36}H_{70}O_3Na$, 573.5223).

Compound 50 (1-*O*-stearoyl-2,3-*N*-stearoyl-rac-diaminopropanol): Compound **48** (45 mg, 0.05 mmol) was dissolved in pyridine (5 mL) and compound **49** (2.14 g, 3.9 mmol) was added. The reaction was left overnight at 45 °C and evaporated under nitrogen. The product was purified using a petroleum ether/diethyl ether gradient (9:1 to 0:1 v/v) and then a chloroform/methanol gradient (1:0 to 7:3 v/v) to give compound

50 in quantitative yield (86 mg, 0.097 mmol). **^{1}H-NMR (400 MHz, $CDCl_3$):** δ 6.65 (1H, bd, J = 7.13 Hz CHNH), 6.50 (1H, m, CH_2NH), 4.20-4.09 (3H, overlapped, H-2, H-1), 3.37 (2H, m, H-3), 2.32(2H, t, J = 7.38 Hz, CH_2 α acyl), 2.17 (4H, m, 2 CH_2 α amides), 1.62 (6H, m, 3 CH_2β), 1.24 (84H, bs, aliphatic methylenes), 0.86 (9H, m, 3 CH_3). HRESIMS *m/z* 911.8519 $[M + Na]^+$ (calcd for $C_{57}H_{112}N_2O_4Na$, 911.8520).

Building block B (2,3-*N*-stearoyl-rac-diaminopropanol): compound **50** (31 mg, 0.035 mmol) was dissolved in methanolic solution (2.8 mL) of MeONa (0.2 M). The mixture was stirred 48 h at 55 °C, evaporated under nitrogen and purified by silica gel chromatography using a petroleum ether/dichloromethane gradient (1:0 to 0:1 v/v) and then a dichloromethane/methanol gradient (1:0 to 7:3 v/v) to give **building block B** (14.8 mg, 0.024 mmol, 70 %). **^{1}H-NMR (400 MHz, $CDCl_3$):** δ 3.84 (1H, m, H-2), 3.62 (1H, m, H_a-1), 3.53-3.46 (2H, overlapped, H-1, H_a-3), 3.23 (1H, dd, J = 5.83 and 13.87 Hz, H_b-3), 2.19 (4H, m, , 2CH_2 α amides), 1.62 (4H, m, 2 CH_2 β), 1.25 (56H, bs, aliphatic methylenes), 0.88 (9H, bt, J = 7.07 Hz, 3 CH_3). HRESIMS *m/z* 645.5913 $[M + Na]^+$ (calcd for $C_{39}H_{78}N_2O_3Na$, 645.5910).

5.3 Synthesis of Sulf-BODIPY

5.3.1 Synthesis of Me_4BODIPY-undecanoic acid

Compound 51 (Dimethyl dodecanedioate): dodecanedioic acid (6 g, 26 mmol) was dissolved in CH_3OH/HCl (0.5 M) (40 mL). The reaction mixture was stirred for 2 h at 25 ºC and then the solvent was evaporated under reduced pressure to obtain compound **51** in quantitative yield (6.7 g, 26 mmol). **^{1}H-NMR (400 MHz, $CDCl_3$):** δ 3.62 (6H, s, OCH_3), 2.27 (4H, overlapped, CH_2 α), 1.57 (4H, overlapped, CH_2 β), 1.26 (12H, overlapped, aliphatic methylenes). HRESIMS m/z: 281.1765 $[M + Na]^+$ (calcd for $C_{14}H_{26}O_4Na$, 281.1724).

Compound 52 (12-Methoxy-12-oxododecanoic acid): compound **51** (6.7 g, 26 mmol) was dissolved in a mixture of acetonitrile and diethyl ether 1:1 v/v (44 mL) and then KOH (1.6 g, 0.028 mol) and methanol (6 mL) were added at 0 ºC. The

reaction mixture was stirred for 50 h at 4 ºC and then extracted with distilled water and diethyl ether. The aqueous phase was extracted again with ethyl acetate. The solvent was evaporated under reduced pressure to obtain compound **52** (3.87 g, 16 mmol, 62 %). **^{1}H-NMR (400 MHz, $CDCl_3$):** δ 3.67 (3H, s, OCH_3), 2.32 (2H, m, CH_2 α to COOMe), 2.30 (2H, m, CH_2 α), 1.62 (4H, overlapped, CH_2 β), 1.30 (12H, overlapped, aliphatic methylenes). HRESIMS m/z: 267.1432 $[M + Na]^+$ (calcd for $C_{14}H_{26}O_3Na$, 267.1567).

Compound 53 (Methyl-12-chloro-12-oxododecanoate): compound **52** (3.87 g, 16 mmol) was dissolved in anhydrous dichloromethane and 1.5 eq. of thionyl chloride (1.74 mL, 24 mmol) were added. The reaction mixture was stirred at 50 ºC for 16 h and then evaporated under reduced pressure to obtain compound **53** (2.17 g, 8.5 mmol, 52 %). **^{1}H-NMR (400 MHz, $CDCl_3$):** δ 3.65 (3H, s, OCH_3), 2.87 (2H, t, J = 7.1 Hz, CH_2 α), 2.29 (2H, t, J = 6.9 Hz, CH_2 α to COOMe), 1.69 (2H, m, CH_2 β), 1.51 (2H, m, CH_2 β to COOMe), 1.31 (12H, overlapped, aliphatic methylenes). HRESIMS m/z: 285.1276 $[M + Na]^+$ (calcd for $C_{14}H_{25}ClO_2Na$, 285.1228).

Compound 54 (Methyl-11-(Me_4-BODIPY)-undecanoate): compound **53** (2,17 g, 8.5 mmol) was dissolved in anhydrous dichloromethane and 2 eq. of 2,4-dimethylpyrrol (1.6 g, 17 mmol) previously dissolved in dry dichloromethane (16 mL) were added slowly at 25 ºC. The reaction mixture was stirred under reflux condition (50 ºC) for 4 h; successively *N*-hexane (100 mL) was added and then the solvent was evaporated under reduced pressure. The oily product was dissolved in anhydrous dichloromethane (40 mL) and 2 eq. of triethylamine (2.37 mL, 17 mmol) were added. After stirring for 15 min, 4 eq. of boron trifluoride etherate (4.20 mL, 34 mmol) were added twice. The reaction mixture was stirred for 2 h at 24 ºC and the crude product was extracted with an aqueous solution of $NaHCO_3$ and dichloromethane. The organic phase was dried at reduced pressure and purified by silica gel chromatography using a gradient of petroleum ether/chloroform (8:2 to 0:1 v/v) to give compound **54** (0.8 g, 1.80 mmol, 25 %). **^{1}H-NMR (400 MHz, $CDCl_3$):** δ 6.08 (2H, s, methynes), 3.70 (3H, s, OCH_3), 2.96 (2H, m, Me_4BODIPY CH_2 meso), 2.55 (6H, s, BODIPY methyls), 2.43 (6H, s, BODIPY methyls), 2.32 (2H, t, J =7.0 Hz, CH_2 α), 1.62 (2H, m, CH_2 β), 1.32

(14H, overlapped, aliphatic methylenes). HRESIMS *m/z* 446.2945 $[M-H]^-$ (calcd for $C_{25}H_{37}BF_2N_2O_2$, 446.2916).

Compound 55 (Me_4-BODIPY-undecanoic acid): compound **54** (0.8 g, 1.80 mmol) was dissolved in methanol (13 mL) and 4 eq. of KOH 3 M (404 mg, 7.20 mmol) in distilled water (1.8 mL) were added. The reaction mixture was stirred for 24 h at 40 ° C and then acidified to pH 2 adding HCl 1 M. After extraction with ethyl acetate, the organic phase was dried at reduced pressure and purified by silica gel chromatography using a gradient of petroleum ether/diethyl ether (8:2 to 0:1 v/v) to give compound **55 (**0.46 g, 1.1 mmol, 61 %). **^{1}H-NMR (400 MHz, $CDCl_3$):** δ 6.07 (2H, s, methynes), 2.93 (2H, m, Me_4BODIPY CH_2 meso), 2.51 (6H, s, BODIPY methyls), 2.41 (6H, s, BODIPY methyls), 2.34 (2H, t, J = 7.4 Hz, CH_2 α), 1.56 (2H, m, CH_2 β), 1.36-1.44 (14H, overlapped, aliphatic methylenes). HRESIMS *m/z* 432.2791 $[M-H]^-$ (calcd for $C_{24}H_{35}BF_2N_2O_2$, 432.2760).

5.3.2 Synthesis of Sulf-BODIPY

Compound 56 (1,2-*O*-isopropyliden-3-*O*-β-[(2',3',4',6'-*O*-tetracetyl)-D-glucosyl]-rac-glycerol): compound **8** (46.4 g, 94.2 mmol) was dissolved in anhydrous dichloromethane (100 mL) and 1.3 eq. of glycerol acetonide (16.5 g, 125 mmol) were added. The reaction mixture was kept under an argon atmosphere on activated 4 Å molecular sieves at -20 °C and subsequently 0.2 eq. of boron trifluoride etherate (2.87 mL, 23.2 mmol) was divided into two different portions. The first one (1.89 mL, 15 mmol) was added dropwise and stirring was maintained for 3 h. After a second addition of boron trifluoride etherate (0.98 mL, 0.008 mol), the temperature was increased to -10 °C and the reaction mixture was stirred overnight. After neutralization with triethylamine (2.0 mL, 14.3 mmol), the mixture was evaporated under reduced pressure and purified by silica gel chromatography using a gradient of petroleum ether/diethyl ether (8:2 to 1:1 v/v) to give compound **56** (35.5 g, 77 mmol, 81 %) as a white foam. **^{1}H-NMR (400 MHz, $CDCl_3$):** δ 5.13 (1H, bt, J = 9.4 Hz, H-3'), 4.99 (1H, bt, J = 9.8 Hz, H-4'), 4.89 (1H, bt, J = 8.4 Hz, H-2'), 4.53 (1H, d, J = 7.8 Hz, H-

1'), 4.18−3.95 (3H, overlapped, H_b-1, H-2') 3.72−3.51 (5H, overlapped, H-6', H-5', H-3), 2.00 (3H, s, OAc), 1.97 (3H, s, OAc), 1.94 (3H, s, OAc), 1.92 (3H, s, OAc), 1.35 (3H, s, CH_3), 1.30 (3H, s, CH_3). HRESIMS m/z: 485.1635 $[M + Na]^+$ (calcd for $C_{20}H_{30}O_{12}Na$, 485.1629).

Compound 57 (1,2-*O*-isopropyliden-3-*O*-β-D-glucosyl-rac-glycerol) (325)**:** compound **56** (35.5 g, 77 mmol) was dissolved in 0.5 M methanolic solution of CH_3ONa (100 mL). After 2 h of stirring at room temperature, it was possible to get compound **57** (17.7 g, 60.2 mmol, 78 %) as a colourless oil. **^{1}H-NMR (400 MHz, CD_3OD):** δ 4.36 (1H, m, H-2), 4.32 (1H, d, J = 7.6 Hz, H-1'), 4.10 (1H, dd, J = 6.6, 12.6 Hz, H_b-3), 3.93 (1H, dd, J = 5.4, 10.2 Hz, H_a-1), 3.89 (1H, bd, J = 11.0 Hz, H_a-6') 3.81 (1H, m, H_a-3), 3.70−3.65 (2H, overlapped, H_b-6', H_b-1), 3.39−3.30 (3H, overlapped, H-5', H-4', H-3'), 3.22 (1H, bt, J = 8.0 Hz, H-2'), 1.42 (3H, s, CH_3), 1.36 (3H, s, CH_3). HRESIMS m/z: 317.1241, $[M + Na]^+$ (calcd for $C_{12}H_{22}O_8Na$), 317.1207).

Compound 58 and 59 (1,2-*O*-isopropyliden-3-*O*-β-[(2',3',4'-*O*-triacetyl-6'-iodo)-D-glucosyl]-rac-glycerol) (325)**:** iodine (22.9 g, 90.2 mmol) was added to a mixture of compound **57** (17.7 g, 60.2 mmol) and triphenylphosphine (23.6 g, 90 mmol) in 2,6-dimethylpyridine (36.8 g, 317 mmol). The mixture was stirred for 6 h at 80 °C and, subsequently, acetylated by the addition of pyridine (19.0 mL) and acetic anhydride (19.0 mL). The reaction mixture was stirred at room temperature overnight. After evaporation of the solvent under a stream of nitrogen, the mixture was purified by silica gel chromatography using a gradient of petroleum ether/diethyl ether (9:1 to 1:1 v/v) to give compound **59** in quantitative yield (31.8 g, 60 mmol) as a yellowish oil. **^{1}H-NMR (400 MHz, $CDCl_3$):** δ 5.20 (1H, m, H-3'), 5.00 (1H, bt, J = 9.0 Hz, H-2'), 4.90 (1H, bt, J = 9.35 Hz, H-4'), 4.64 (1H, d, J = 7.80 Hz, H-1'), 4.30 (1H, m, H-2), 4.05 (2H, overlapped, H_a-3, H_b-3), 3.85 (1H, dd, J = 5.9, 11.0 Hz, H_a-1), 3.70 (1H, m, H_b-1, H_b -1), 3.53 (1H, m, H-5'), 3.30 (1H, bd, J = 11.0 Hz, H_a-6'), 3.18 (1H, bd, J = 10.9 Hz, H_b-6'), 2.05 (3H, s, OAc), 2.02 (3H, s, OAc), 2.00 (3H, s, OAc), 1.40 (3H, s, CH_3), 1.34 (3H, s, CH_3). HRESIMS m/z: 553.0583, $[M + Na]^+$ (calcd for $C_{18}H_{27}IO_{10}Na$, 553.0541).

Compound 60 (1,2-*O*-isopropyliden-3-*O*-β-[(2',3',4'-*O*-triacetyl-6'-thioacetyl)-D-glucosyl]-rac-glycerol) (325)**:** compound **59** (31.8 g, 60 mmol) was dissolved in 2-butanone (100 mL) and 5 eq. of potassium thioacetate (34 g, 298 mmol) was added to it. The reaction mixture was stirred at 80 °C for 2 h and then the solvent was evaporated under reduced pressure. The residue was purified by silica gel chromatography using a gradient of petroleum ether/diethyl ether (9:1 to 1:1 v/v) to give compound **60** in quantitative yield (28.7 g, 60 mmol) as a yellowish oil. **^{1}H-NMR (400 MHz, $CDCl_3$):** δ 5.18 (1H, m, H-3'), 5.00 (2H, overlapped, H-2', H-4'), 4.55 (1H, d, J = 7.98 Hz, H-1'), 4.24 (1H, m, H-2), 4.03 (2H, overlapped, H_a-3, H_b-3), 3.77−3.68 (2H, overlapped, H_a-1, H_b-1), 3.63 (1H, m, H-5'), 3.25 (1H, bd, J = 12.0 Hz, H_a-6'), 3.05 (1H, bd, J = 10.9 Hz, H_b-6'), 2.34 (3H, s, SAc), 2.09 (3H, s, OAc), 2.04 (3H, s, OAc), 2.00 (3H, s, OAc), 1.41 (3H, s, CH_3), 1.34 (3H, s, CH_3). HRESIMS m/z: 501.1463, $[M + Na]^+$ (calcd for $C_{20}H_{30}NaO_{11}S$, 501.1401).

Compound 61 (3-*O*-β-[(2',3',4'-*O*-triacetyl-6'-thioacetyl)-D-glucosyl]-rac-glycerol) (325)**:** compound **60** (28.7 g, 60 mmol) was dissolved in acetonitrile (200 mL) and 5.0 eq. of zinc nitrate hexahydrate (89.2 g, 300 mmol) were added. The reaction mixture was stirred and heated at 50 °C for 6 h. After evaporation of the organic solvent under reduced pressure, the mixture was diluted with dichloromethane (200 mL) and treated with 1 M $NaHCO_3$ (200 mL). The organic layer was dried over anhydrous Na_2SO_4, filtered, and concentrated to give compound **61** (19.7 g, 45 mmol, 75 %) as a yellowish foam. **^{1}H-NMR (400 MHz, $CDCl_3$):** δ 5.18 (1H, bt, J = 9.51 Hz, H-3'), 4.99 (2H, overlapped, H-2', H-4'), 4.52 (1H, d, J = 8.01 Hz, H-1'), 3.84 (3H, overlapped, H-5', H_a-3, H_b-3), 3.67−3.60 (3H, overlapped, H_a-1, H_b-1, H-2), 3.26 (1H, bd, H_a-6'), 3.03 (1H, bd, H_b-6'), 2.35 (3H, s, SAc), 2.10 (3H, s, OAc), 2.05 (3H, s, OAc), 2.00 (3H, s, OAc). HRESIMS m/z: 461.1097, $[M + Na]^+$ (calcd for $C_{17}H_{26}NaO_{11}S$, 461.1088).

Compound 62 (1-*O*-stearoyl-3-*O*-β-[(2',3',4'-tri-*O*-acetyl-6'-thioacetyl)-D-glucosyl]-rac-glycerol): compound **61** (240 mg, 0.57 mmol) was dissolved in anhydrous dichloromethane (11 mL) prior to addition at 0 °C of 1 eq. of stearic acid (161 mg, 0.57 mmol), 1 eq. of DCC (118 mg, 0.57 mol) and 1 eq. of DMAP (68 mg,

0.57 mmol). The reaction mixture was stirred overnight at 4 °C. After evaporation under reduced pressure, the mixture was purified by silica gel chromatography using a gradient of petroleum ether/chloroform (1:1 to 0:1 v/v) to give **compound 62** (269 mg, 0.39 mmol, 69 %). **^{1}H-NMR (400 MHz, $CDCl_3$):** δ 5.18 (1H, t, J = 8.99 Hz, H-3'), 5.00-4.92 (2H, overlapped, H-2', H-4'), 4.50-4.49 (1H for each of the two epimers, d, J = 7.9 Hz, H-1'), 4.17-3.96 (2H, overlapped, H-3), 3.98 (1H, m, H-2), 3.86-3.80 (1H for each of the two epimers, dd, J = 3.9 Hz, J = 10.7 Hz and J = 5.5 Hz, J = 10.5 Hz, H_a-1), 3.66-3.60 (2H for each of the two epimers, overlapped, H_b-1, H-5'), 3.23 (1H, dd, J = 3.1 and 14.5 Hz, H-6'a), 3.04 (1H, dd, J = 6.27 Hz, J = 13.71 Hz, H_b-6'), 2.34 (3H, s, SAc), 2.36-2.26 (2H, m, CH_2 α), 2.08 (3H, s, OAc), 2.04 (3H, bs, OAc), 2.00 (3H, s, OAc), 1.65-1.55 (2H, m, CH_2 β), 1.36-1.18 (28H, overlapped, aliphatic methylenes), 0.87 (3H, t, J = 7.12 Hz, CH_3). HRESIMS *m/z* 727.3710 $[M+Na]^+$ (calcd for $C_{35}H_{60}O_{12}NaS$, 727.3703).

Compound 63 (1-*O*-stearoyl-3-*O*-β-[(2',3',4'-tri-*O*-acetyl)-D-sulfoquinovosyl]-rac-glycerol): compound **62** (269 mg, 0.39 mol) was dissolved in potassium acetate (540 mg, 5.5 mmol), 34% (w/v) H_2O_2 (0.57 mL) and acetic acid (2 mL). The reaction mixture was stirred for 16 h at 40 °C. After evaporation under a stream of nitrogen, the oily residue was purified by silica gel chromatography using a gradient of chloroform/methanol (1:0 to 8:2 v/v) to give compound **63** (190 mg, 0.27 mmol, 70 %). **^{1}H-NMR (400 MHz, $CDCl_3$/CD_3OD 1/1):** δ 5.23 (1H, t, 9.6 Hz, H-3'), 5.01-4.92 (2H, overlapped, H-2', H-4'), 4.70-4.67 (1H for each of the two epimers, d, J = 7.48 Hz, H-1'), 4.13-4.05 (2H, overlapped, H-3), 4.01 (1H, m, H-2), 3.89 (1H, dd, J = 3.8 Hz, J = 11.1 Hz, H_a-1), 3.81 (1H, dd, J = 6.1 Hz, J = 11.1 Hz, H_b-1), 3.76 (1H, m, H-5'), 3.10-3.01 (2H, overlapped, H-6'), 2.32 (2H, m, CH_2 α), 2.09 (3H, s, OAc), 2.06 (3H, bs, OAc), 1.99 (3H, s, OAc), 1.64-1.53 (2H, m, CH_2 β), 1.35-1.20 (28H, overlapped, aliphatic methylenes), 0.88 (3H, t, J = 7.49 Hz, CH_3). HRESIMS *m/z* 709.3461 $[M-H]^-$ (calcd for $C_{33}H_{57}O_{14}S$, 709.3469).

Compound 64 (1-*O*-stearoyl-2-*O*-Me$_4$BODIPY-undecanoyl-3-*O*-β-[(2',3',4'-tri-*O*-acetyl)-D-sulfoquinovosyl]-rac-glycerol): compound **63** (190 mg, 0.27 mmol) was dissolved in anhydrous dichloromethane (12 mL) prior to addition of 1.6 eq. of

BODIPY-undecanoic acid (**55**) (185 g, 0.43 mmol), 3 eq. of DCC (167 mg, 0.81 mmol) and 2 eq. of DMAP (64 mg, 0.54 mmol). The reaction mixture was stirred for 16 h at 40 °C. After evaporation under reduced pressure, the mixture was purified by silica gel chromatography using a gradient of chloroform/methanol (1:0 to 9:1 v/v) to give compound **64** (161 mg, 0.18 mmol, 68 %). **^{1}H-NMR (400 MHz, $CDCl_3$):** δ 6.03 (2H, s, Me_4BODIPY methynes), 5.27-5.12 (2H, overlapped, H-2, H-3'), 5.00-4.93 (2H, overlapped, H-2', H-4'), 4.60 (1H, bd, 7.70 Hz, H-1'), 4.29 (1H, dd, J = 11.36, J = 22.73 Hz, H_a-1), 4.18-3.90 (3H, overlapped, H_b-1, H-3), 3.73 (1H, m, H-5'), 3.12 (2H, overlapped, H-6'), 2.91 (2H, m, Me_4BODIPY CH_2 *meso*), 2.49 (6H, bs, Me_4BODIPY methyls), 2.40 (6H, bs, Me_4BODIPY methyls), 2.31-2.22 (4H, m, CH_2 α), 2.04-1.93 (9H, s, 3 OAc), 1.67-1.51 (4H, m, CH_2 β), 1.37-1.18 (42H, overlapped, aliphatic methylenes), 0.86 (3H, bt, J = 7.10 Hz, CH_3). HRESIMS *m/z* 1123.6114 $[M-H]^-$ (calcd for $C_{57}H_{90}BF_2N_2O_{15}S$, 1123.6123).

Sulf-BODIPY (1-*O*-stearoyl-2-*O*-Me_4BODIPY-undecanoyl-3-*O*-β-D-sulfoquinovosyl-rac-glycerol): compound **64** (161 mg, 0.18 mmol) was dissolved in aq. ethanol (85%) (40 mL) and 2.4 eq. of hydrazine monohydrate (0.06 mL, 1.3 mmol) were added. The reaction mixture was stirred for 16 h at 45 °C. After evaporation under a stream of nitrogen, the mixture was purified by silica gel chromatography using a gradient of chloroform/methanol (1:0 to 8:2 v/v) to give Sulf-BODIPY (77 mg, 0.1 mmol, 58 %). **^{1}H-NMR (400 MHz, $CDCl_3$/CD_3OD 1/1):** δ 6.06 (2H, s, Me_4BODIPY methynes), 5.28 (m, 1H, H-2), 4.44 and 4.39 (1H for each of the two epimers, dd, J = 3.15 Hz, J = 12.06 Hz, H_a-1), 4.32-4.30 (1H for each of the two epimers, d, J = 7.8 Hz, H-1'), 4.24 and 4.16 (1H for each of the two epimers, dd, J = 6.7 Hz, J = 12.06 Hz, H_b-1), 4.05 (1H, m, H_a-3), 3.78-3.70 (2H, overlapped, H_b-3, H-5'), 3.40 (1H, m, H_a-6'), 3.24 (2H, overlapped, H-2', H-4'), 3.09 (1H, m, H_b-6'), 2.95 (2H, m, Me_4BODIPY CH_2 *meso*), 2.45 (6H, bs, Me_4BODIPY CH_3), 2.40 (6H, bs, Me_4BODIPY CH_3), 2.32-2.24 (4H, overlapped, CH_2 α), 1.67-1.58 (4H, overlapped, CH_2 β), 1.40-1.16 (42H, overlapped, aliphatic metylenes), 0.84 (3H, bt, J = 6.91 Hz, CH_3). HRESIMS *m/z* 997.5800 $[M-H]^-$ (calcd for $C_{51}H_{84}BF_2N_2O_{12}S$, 997.5806).

5.3.3 Biological analysis

5.3.3.1 Preparation of dendritic cells

For each assay human peripheral blood mononuclear cells were isolated from two healthy donors by routine Ficoll density gradient centrifugation. Monocytes were purified from human peripheral blood mononuclear cells using MACS CD14 microbeads (Miltenyi Biotech, Auburn, CA, USA) according to the manufacturer's recommendation. Purity was checked by staining with a FITC-conjugated anti-CD14 antibody (Milteny Biotech, Auburn, CA, USA) and FACS analysis and was routinely found to be greater than 98%. Immature DCs were obtained by incubating monocytes at $1 \cdot 10^6$/ml in RPMI 1640 medium supplemented with 10% fetal calf serum, 1% L-glutamine 2 mM, 1% penicillin and streptomycin, human IL-4 (5 ng/ml) and human GM-CSF (100 ng/ml) for five days.

5.3.3.2 Cells staining and stimulation

After five days in culture, surface staining was performed on monocyte-derived dendritic cells (moDCs) for flow cytometry analysis by using the following conjugated mAbs from (Miltenyi Biotech, Auburn, CA, USA: HLA-DR APC, CD86 APC, CD83 PE, and propidium iodide for the estimation of the cell vitality. All samples were analyzed by flow-cytometer on LSRFortessa™ X-20 cell analyzer (BD Bioscience, Frankin Lake, NJ, USA) according to standard protocol. moDCs were then incubated with natural and synthetic compounds in 12-wells. Stimulation with Pam2CSK4 1 μg/ml (Invivogen, San Diego, CA, USA) was used as positive control. Cells untreated were used as control. After 24 h, expression of all surface markers was estimated again by fluorochrome-conjugated antibodies.

5.3.3.3 Real time PCR analysis

Total RNA was isolated using Trizol Reagent, according to the manufacturer's protocol. RNA quantity and purity were measured with a NanoDrop 2000 spectrophotometer (Thermo Scientific,Waltham, MA, USA). Sample purity was checked by A260/A280 ratios between 1.80 and 2.00. Extracted RNAs from all preparations were in this range. Cytokines mRNA expression was measured by quantitative Real Time-PCR. Results are expressed as means ± SD. All data were analyzed by one way ANOVA followed by the Tukey test for multiple comparison test. A p-value less than 0.05 was considered as statistically significant. All analyses were performed using the GraphPad Prism 6.00 for Windows software (GraphPad Software, San Diego California, USA).

5.3.3.4 In vitro bioimaging experiments on hDCs

hDCs, MUTZ-3 and CCD-33Co cells grown on 24-mm coverslips and were incubated with 100 ng/mL of Sulf-BODIPY for 3 h were fixed with 4% paraformaldehyde for 15 min and washed once in 1× PBS. Cells were then treated with a 10 mg/mL of $NaBH_4$ solution as reported by Clancy[24] to remove the green autofluorescence, permeabilized and blocked in Blocking buffer (1× PBS, 0.5% BSA, 0.05% saponin, 50 mM NH_4Cl, 0.02% NaN_3) for 30 min at room temperature, followed by 1 h incubation with 1 μg/ml of biotinylated wheat germ agglutinin (WGA) lectin. Subsequently, coverslips were washed with 1× PBS and incubated with streptavidin-Alexa549 diluited 1:5000 in Blocking buffer for 20 min at room temperature, stained with DAPI 5 min, washed again and mounted on glass microscopic slides with Mowiol.[16] Immunofluorescence samples were examined under confocal laser microscope (Zeiss LSM 700 confocal microscope systems; Carl Zeiss, Gottingen, Germany) using a 63 × oil-immersion objective (1.4 NA) Optical confocal sections were taken at 1 Airy unit.

5.3.3.5 Animal husbandry, larval exposure and imaging

Adult zebrafish (Casper strain) were maintained on a 14-h light/10-h dark lighting cycle at 28 °C, according to standard protocols (http:// ZFIN.org) and considering the international guidelines specified by the EU Animal Protection Directive 2010/63/EU. Only early life stage zebrafish were used in experiments and no specific additional project authorisation was required. Zebrafish eggs were obtained from natural spawning. Fertilised eggs were selected within the 2- to 8-cell stage and incubated in E3 medium (5 mM NaCl, 0.17 mM KCl, 0.33 mM $CaCl_2$, 0.33 mM $MgSO_4$, 1 × 10–5% Methylene-blue) at 28.5°C. Fresh E3 medium were replaced daily and coagulated or developmentally abnormal embryos were removed. The exposure concentration (8 µg/mL Sulf-BODIPY) originated from an initial dose-response curve, using Sulf-BODIPY molecule, representing a no-effect concentration for mortality. The exposure with Sulf-BODIPY started after hatching, at 3 days post-fertilization (dpf), as the chorion can represent a physical barrier, until 4 dpf. After 24 hours of 8 µg/mL Sulf-BODIPY exposure, zebrafish larvae were anaesthetised in tricaine (MS222, Sigma Aldrich) and then imaged from lateral and dorsal view using a Leica M205 FA fluorescence stereomicroscope equipped with a digital camera (DFC450). Accumulation of Sulf-BODIPY was detected using the green fluorescence laser filter. Bright-field images were analysed for developmental abnormalities (presence or absence of swim bladder development) as well as body alteration (larval length). Experiments were obtained in three replicates, with larvae from separate breeding events (N = 10 larvae per replicate).

5.3.3.6 Ex vivo fluorecence imaging experiment

Sulf-BODIPY (0.5 mg/200 µl PBS) was administered intravenously to C57BL/6 mice at the age of 6 months. Ex vivo brain fluorescence imaging 3 h after injection was performed on a PerkinElmer IVIS Imaging System 200 using a 465 nm excitation filter and a 520 nm emission filter with a 4 s exposure.

5.3.3.7 Brains extraction and analysis via HPLC-UV

Both brains (treated and control) were homogenized using Precellys - Bertini. Subsequently, by lipid extraction with MTBE/MeOH/H_2O, the organic phase enriched with lipids was recovered and subjected to silica gel purification using $CHCl_3$, ACN/MeOH 9:1 and MeOH and obtaining the three fractions (A-C). The fractions were analyzed via HPLC-UV on a Jasco LC-2000 Plus HPLC Series using a Photodiode Array Detector MD-2018. Chromatographic separations were achieved on HPLC Luna 5u C18 (2) 100 Å, LC Column 250 X 4.6 mm (Phenomenex, Italy), at 28 °C by a gradient elution of 0.32 mM ammonium hydroxide solution (0.005%), adjusted to pH 8.0 by acetic acid, and methanol (MeOH). The flow rate was 1.0 mL/min, choosing a λ=500nm as absorption wavelength, equivalent to that of the selected fluorescent tag (BODIPY). The B fraction of the treated brain confirmed the presence of Sulf-BODIPY by comparing the retention time with that of the synthetic Sulf-BODIPY used as a standard.

5.4 Docking experiments

5.4.1 System preparation

The structure of the TREM2 WT protein and specifically the section of the extracellular ligand-binding domain co-crystallized with the Phosphatidylserine (1,2-dihexanoyl-sn-glycero-3-phospho-L-serine) (PS) was used for molecular docking simulations (6B8O, 2.2 Å resolution, released in 2018).(221) This pdb file was optimized and prepared for the docking simulations using the Protein Preparation Wizard (PPW) tool (Schrödinger Release 2022-4: Protein Preparation Wizard; Epik, Schrödinger, LLC, New York, NY, 2022). Such a tool allows for adding missing hydrogen atoms, reconstructing incomplete side chains, assigning the ionization states at physiological pH, setting the orientation of any misoriented groups, removing water molecules, and optimizing the hydrogen bond network. Finally, a force field-based minimization (OPLS-4) was performed. We generate a cubic grid having an inner box

of dimensions 12 Å × 12 Å × 12 Å and an outer box of dimensions 30 Å × 30 Å × 30 Å centring on the centroid of the cognate ligand. The investigated ligands were subjected to ligand preparation using the LigPrep tool, available in Schrodinger Suite 2022-4. LigPrep generates all the tautomers and ionization states at a pH value of 7.0 ± 2.0 and the 3D structures with the correct chirality (Schrödinger Release 2022-4: LigPrep, Schrödinger, LLC, New York, NY, 2022).

5.4.2 Molecular docking simulation

Simulations were performed using the Standard Precision (SP) and the default force field OPLS_2005. The number of generated poses per ligand in the initial phase of docking was increased from 5000 (default setting) to 50000 along with the number of those kept for energy minimization from 400 (default setting) to 4000, to properly explore the conformational space of the ligands during the simulations. During the simulation, the receptor protein was fixed, while full conformational flexibility of the ligands was allowed. Using this protocol, two distinct rounds of docking were performed for each ligand. In the initial round, a shape constraint was applied using the entire co-crystallized PS ligand with a tolerance of 3 Å. For the second round, a SMART constraint (tolerance of 3 Å) was implemented, selecting only the atoms that constitute the polar portion of PS (up to the CH_2 after the glycosidic linkage). In all cases, for each compound, 5 poses were generated as docking result. The protocol was validated by docking the co-crystallized ligand PS, obtaining the highest RMSD = 1.27 Å.

5.4.3 MMGBSA calculations

All ten complexes obtained from the docking experiments for each ligand were subjected to a post-docking minimization using the MM-GBSA method, setting a movement flexibility of 5 Å for amino acid residues.(347) Default dielectric constants,

the OPLS_2005 force field and the VSGB solvation model were used. Outputs were ranked according to the Prime MM-GBSA ΔG (Bind) calculated as follows:

MM-GBSA ΔGbind = complex − ligand – receptor

where complex is the energy contribution calculated from the optimized ligand–receptor complex, and ligand and receptor are the energy contributions calculated from the optimized free ligand and free receptor, respectively. In addition, the MM-GBSA ligand efficiency was computed as the ratio between the MM-GBSA score and the number of heavy atoms. This was done, in order to compare the potential affinities of ligands with different molecular sizes.

5.4.4 Synthesis of Sulfavant C6

Compound 65 (1,2-*O*-hexanoyl-3-*O*-β-[(2',3',4'-tri-*O*-acetyl-6'-thioacetyl)-D-glucosyl]-rac-glycerol): compound **61** (220 mg, 0.50 mmol) was dissolved in anhydrous dichloromethane (4 mL), followed by the addition of 1.5 eq. of DCC (310 mg, 1.51 mmol), 1.5 eq. of DMAP (184 mg, 1.51 mmol), and 1.3 eq. of hexanoic acid (151 mg, 1.31 mmol). The reaction mixture was stirred 48 h at 40 °C and after evaporation under reduced pressure, the mixture was purified by silica gel chromatography using a gradient of petroleum ether/diethyl ether (9:1 to 6:4 v/v) to give compound **65** (94 mg, 0.15 mmol, 30 %) as a colourless oil. **^{1}H-NMR (400 MHz, $CDCl_3$):** δ 5.20−5.141 (2H, m, H-2, H-3'), 4.96−4.89 (2H, m, H-2', H- 4'), 4.47 (1H, d, J = 8.0 Hz, H-1'), 4.28 (1H, dd, J = 4.1, 11.8 Hz, H_a-1), 4.09 (1H, dd, J = 5.7 Hz, J = 11.8 Hz, H_b-1), 3.91 (1H, dd, J = 4.5 Hz, J = 11.1 Hz, H_a-3), 3.65 (1H, dd, J = 5.4, 11.1 Hz, H_b-3), 3.62 (1H, m, H-5'), 3.25 (1H, bd, J = 11.4 Hz, H_a-6'), 3.06 (1H, dd, J = 2.4 Hz, J = 11.4 Hz, H_b-6'), 2.35 (3H, s, SAc), 2.33−2.25 (4H, m, CH_2 α), 2.13−1.99 (9H, s, 3 OAc), 1.65−1.55 (4H, m, CH_2 β), 1.36−1.23 (8H, overlapped, aliphatic methylenes), 0.93−0.85 (6H, overlapped, 2 CH_3). HRESIMS m/z: 657.2565 $[M + Na]^+$ (calcd for $C_{29}H_{46}O_{13}NaS$, 657.2557).

Compound 66 (1,2-*O*-hexanoyl-3-*O*-β-[(2',3',4'-tri-*O*-acetyl)-D-sulfoquinovosyl]-rac-glycerol): compound **65** (94 mg, 0.14 mmol) was dissolved in acetic acid (1 mL) and potassium acetate (0,16 mg, 0.002 mmol) and 30% (w/v) H_2O_2 (0.32 mL, 0.014 mmol) were added. The reaction mixture was stirred overnight at 40 °C. After evaporation, the oily residue was purified by silica gel chromatography using a gradient of chloroform/methanol (99:1 to 8:2 v/v) to give compound **66** (42 mg, 0.065 mmol, 46%, potassium salt) as a colourless oil. **^{1}H-NMR (400 MHz, $CDCl_3$):** δ 5.25-5.15 (2H, m, H-2, H-3'), 5.00−4.80 (2H, m, H-2', H-4'), 4.62 (1H, d, 7.3 Hz, H-1'), 4.31 (1H, bd, J = 11.1 Hz, H_a-1), 4.15−3.90 (3H, overlapped, H_b-1, H_a-3, H_b-3), 3.71 (1H, m, H-5'), 3.20 (2H, overlapped, H-6'), 2.33-2.28 (4H, m, CH_2 α), 2.06−1.98 (9H, s, 3 OAc), 1.64−1.55 (4H, m, CH_2 β), 1.34−1.22 (8H, overlapped, aliphatic methylenes), 0.91−0.88 (6H, overlapped, 2 CH_3). HRESIMS m/z: 639.2337, $[M-H]^-$ (calcd for $C_{27}H_{43}O_{15}S$, 639.2328).

Sulf-A C6 (1,2-*O*-hexanoyl-3-*O*-β-D-sulfoquinovosyl-rac-glycerol): compound **66** (20 mg, 0.032 mmol) was dissolved in aq. ethanol (85%) (1.5 mL), 2.4 eq. of hydrazine monohydrate (11.53 mg, 0.23 mmol) were added dropwise, and the reaction mixture was stirred for 24 h at 44 °C. The excess hydrazine was quenched with benzaldehyde (70.2 mL, 0.69 mmol) and the mixture was stirred for 15 min at room temperature. After evaporation, the crude mixture was then purified by silica gel chromatography using a gradient of chloroform/methanol (98:2 to 8:2 v/v) to give **Sulf-A C6** (9 mg, 0.017 mmol, 56 %) as a white solid. **^{1}H-NMR (400 MHz, $CDCl_3$/CD_3OD 1/1):** δ 5.29 (1H, m, H-2), 4.42 (1H, m, H_a-1), 4.34 and 4.31 (each for 1H, d, 7.8 Hz, H-1' R and S), 4.27-4.16 (1H, m, H_b-1), 4.05 (1H, m, H_b-1), 3.79−3.71 (2H, m, H_b-3, H-5'), 3.42 (1H, m, H-3'), 3.38 (1H, m, H_a-6'), 3.34 (1H, m, H-2'), 3.24 (1H, m, H-4'), 3.07 (1H, m, H_b-6'), 2.38−2.29 (4H, overlapped, CH_2 α), 1.68−1.58 (4H, overlapped, CH_2 β), 1.43−1.29 (8H, overlapped, aliphatic methylenes), 0.94 (6H, overlapped, 2 CH_3). HRESIMS m/z: 513.2015, $[M-H]^-$ (calcd for $C_{21}H_{37}O_{12}S$, 513.2011).

5.5 Preparation of fluorinated galectins and ^{19}F-NMR spectra

N-(phosphonomethyl)glycine (glyphosate), 5-fluoro-DLtryptophan were purchase from Sigma-Aldrich and 6-fluoro-DLtryptophan from Acros Organics. The sequence encoding for the galectins was inserted into a pET21a expression vector (Thermo Fisher) and the final plasmid was designed and synthetized by Gene Script Biotech. The plasmids were used to transform by heat shock method using *E. coli* BL21 (DE3) cells.(403,404)The incorporation of fluorinated tryptophan to the galectins was achieved following a published protocol based on the addition of glyphosate and exogenous aromatic amino acids. Once the transformation was performed, a selected colony was incubated with 5 ml of LB fresh media for 5h. The saturated culture was added in M9 medium and grown overnight. Next, a culture was started in M9 media at an OD600 of 0.1 and grown up to OD600 0.4. At that point, glyphosate (N-(phosphonomethyl)-glycine) (1 g/L) that was first dissolved in 1M sodium hydroxide, phenylalanine (60 mg/L) and tyrosine (60 mg/L) were added to the culture.(405) After one hour the fluorinated tryptophan analogue (120 mg/L) was added, and protein production was induced with 1 mM isopropyl β-D-1-thio-galactopyranoside (IPTG) and the culture continued to grow for 3 h at 37ºC. All proteins were extracted following the same protocol. The cultures were centrifuged and proteins were purified by lactose affinity (α-lactose-agarose resin (Sigma-Aldrich)) or AKTA and then size exclusion chromatography (SEC) .(406–408) The column used for the SEC is the Superdex 75 Increase 10/300 GL. Briefly, the cell pellet was resuspended in lysis buffer (22 mM Tris-HCl, 5 mM EDTA, 1 mM PMSF, and 1 mM DTT at pH 8). Later, lysis by sonication on ice with 60% amplitude, 10 repetitions of 30 s, and 59 s of rest between each pulse. In order to clear up the sample ultracentrifugation at 35,000 rpm for 1 h at 4 ºC was performed. Lactose-Agarose resin was loaded with the soluble fraction pre equilibrated in buffer (50 mM TRIS pH 7.2, 150 mM NaCl). Protein elution was achieved by addition of 150 mM lactose containing PBS buffer. Protein purity was checked by 4–12% SDS-PAGE. Fluorine incorporation levels by following this protocol have been reported to occur in more than 95%.(409) Galectins were thoroughly dialyzed against PBS, pH 7.4 until no lactose was present, before use.

All spectra were performed at 298 K on a Bruker AVANCE 2 600 MHz spectrometer equipped with cryo probe. The ^{19}F-NMR spectra of proteins were recorded using a selective SEF probe with ^{1}H decoupling. Acquisition parameters varied depending on the protein concentration (usually between 40 μM and 100 μM). As an example, for 60 μM of fluorinated protein ^{19}F-NMR spectra were recorded with SW = 60 Hz, ns = 80, TD = 8 K and processed with exponential apodization (lb between 15 and 30 depending on the desired result). All the protein samples (500 μL total in 5 mm standard NMR tubes) were prepared at a concentration between 100 – 40 μM. The buffer used was 90% phosphate-buffered saline (50 mM sodium phosphate, 150 mM NaCl, pH 7.4) and 10% deuterated water (D_2O). Ligands were titrated to the protein sample, and a ^{1}H-decoupled ^{19}F spectra were recorded at each point.

For the experiment with cells and fluorinated galectins the culture of HEK293F cells was grown in suspension using FreeStyle medium and then harvested. The cells were counted and the precise volume required to have the desired concentration into the NMR tube was picked up from the flask. The cells were centrifuged for 5 min at 800 rpm and room temperature. The pellet was re-suspended in 1 mL of PBS 1x pH 7.4 and washed again. The final sample was re-suspended in 500 μL of PBS 1x pH 7.4 containing the fluorinated galectin under analysis and then transferred into the NMR tube. The NMR experiments were acquired immediately after the sample preparation.

References

1. Boeuf G. Marine biodiversity characteristics. Vol. 334, C. R. Biol.; 2011. p. 435–440.

2. Bowler C, Karl DM, Colwell RR. Microbial oceanography in a sea of opportunity. Vol. 459, Nature; 2009. p. 180–184.

3. Santos JD, Vitorino I, Reyes F, Vicente F, Lage OM. From ocean to medicine: Pharmaceutical applications of metabolites from marine bacteria. Vol. 9, Antibiotics; 2020. p. 1–30.

4. Kanase HR, Singh KNM. Marine pharmacology: Potential, challenges, and future in India. Vol. 38, J. Med. Sci. (Taiwan); 2018. p. 49–53.

5. Datta D, Nath Talapatra S, Swarnakar S. Bioactive compounds from marine invertebrates for potential medicines-An overview. Vol. 7, Int. Lett. Nat. Sci.; 2015. p. 42–61.

6. Blunt JW, Carroll AR, Copp BR, Davis RA, Keyzers RA, Prinsep MR. Marine natural products. Vol. 35, Nat. Prod. Rep.; 2018. p. 8–53.

7. Gerwick WH, Moore BS. Lessons from the past and charting the future of marine natural products drug discovery and chemical biology. Vol. 19, Chem. Biol.; 2012. p. 85–98.

8. Lindequist U. Marine-derived pharmaceuticals - challenges and opportunities. Vol. 24, Biomol. Ther. (Seoul); 2016. p. 561–571.

9. Beesoo R, Neergheen-Bhujun V, Bhagooli R, Bahorun T. Apoptosis inducing lead compounds isolated from marine organisms of potential relevance in cancer treatment. Vol. 768, Mutat. Res-Fund. Mol. M.; 2014. p. 84–97.

10. Castro ME, González-Iriarte M, Barrero AF, Salvador-Tormo N, Muñoz-Chápuli R, Medina MÁ, et al. Study of puupehenone and related compounds as inhibitors of angiogenesis. Vol. 110, Int. J. Cancer; 2004. p. 31–38.

11. Yamada T, Iritani M, Minoura K, Numata A, Kobayashi Y, Wang YG. Absolute stereostructures of cell adhesion inhibitors, macrosphelides H and L, from Periconia byssoides OUPS-N133. Vol. 55, J. Antibiot.; 2002. p. 147-154.

12. Ciftci HI, Can M, Ellakwa DE, Suner SC, Ibrahim MA, Oral A, et al. Anticancer activity of Turkish marine extracts: a purple sponge extract induces apoptosis with multitarget kinase inhibition activity. Vol. 38, Invest. New Drugs; 2020. p. 1326-1333.

13. Correia-da-Silva M, Sousa E, Pinto MMM, Kijjoa A. Anticancer and cancer preventive compounds from edible marine organisms. Vol. 46, Semin. Cancer Biol.; 2017. p. 55–64.

14. Arya V, Gupta VK, Shaheed Baba A, Singh A, Singh J. A review on marine immunomodulators. Vol. 2, Int. J. Pharm. Life Sci.; 2011. p. 751-758.

15. Mayer AMS, Rodríguez AD, Berlinck RGS, Hamann MT. Marine pharmacology in 2005-6: Marine compounds with anthelmintic, antibacterial, anticoagulant, antifungal, anti-inflammatory, antimalarial, antiprotozoal, antituberculosis, and antiviral activities; affecting the cardiovascular, immune and nervous systems, and other miscellaneous mechanisms of action. Vol. 1790, Biochim. Biophys. Acta Gen. Subj.; 2009. p. 283–308.

16. Munro MHG, Blunt JW, Dumdei EJ, Hickford SJH, Lill RE, Li S, et al. Biotechnology The discovery and development of marine compounds with pharmaceutical potential. Vol. 35, Dev. Ind. Microbiol.; 1999. p. 15-25.

17. Hu Y, Chen J, Hu G, Yu J, Zhu X, Lin Y, et al. Statistical research on the bioactivity of new marine natural products discovered during the 28 years from 1985 to 2012. Vol. 13, Mar. Drugs; 2015. p. 202–221.

18. Khan MT, Ali A, Wang Q, Irfan M, Khan A, Zeb MT, et al. Marine natural compounds as potents inhibitors against the main protease of SARS-CoV-2—a molecular dynamic study. Vol. 39, J. Biomol. Struct. Dyn.; 2020. p. 3627-3637.

19. Ugwu CU, Aoyagi H, Uchiyama H. Photobioreactors for mass cultivation of algae. Vol. 99, Bioresour. Technol.; 2008. p. 4021–4028.

20. Borowitzka MA. Microalgae as sources of pharmaceuticals and other biologically active compounds. Vol. 7, J. Appl. Phycol.; 1995. p. 3-15.

21. Hussen Bule M, Ahmed I, Maqbool F, Bilal M, Iqbal HMN. Microalgae as a source of high-value bioactive compounds. Vol. 10, Front. Biosci.; 2018. p. 197-216.

22. Vinayak V, Manoylov KM, Gateau H, Blanckaert V, Hérault J, Pencréac'H G, et al. Diatom milking? A review and new approaches. Vol. 13, Mar. Drugs.; 2015. p. 2629–2665.

23. Sahu A, Pancha I, Jain D, Paliwal C, Ghosh T, Patidar S, et al. Fatty acids as biomarkers of microalgae. Vol. 89, Phytochem.; 2013. p. 53–58.

24. Lee JC, Hou MF, Huang HW, Chang FR, Yeh CC, Tang JY, et al. Marine algal natural products with anti-oxidative, anti-inflammatory, and anti-cancer properties. Vol. 13, Cancer. Cell. Int.; 2013. p. 1-7.

25. Besednova NN, Zaporozhets TS, Somova LM, Kuznetsova TA. Review: Prospects for the use of extracts and polysaccharides from marine algae to prevent and treat the diseases caused by Helicobacter pylori. Vol. 20, Helicobacter; 2015. p. 89–97.

26. Cutignano A, Nuzzo G, Ianora A, Luongo E, Romano G, Gallo C, et al. Development and application of a novel SPE-method for bioassay-guided fractionation of marine extracts. Vol. 13, Mar. Drugs; 2015. p. 5736–5749.

27. Ahmad B, Shah M, Choi S. Oceans as a source of immunotherapy. Vol. 17, Mar. Drugs.; 2019. p. 282.

28. McGettigan SE, Debes GF. Immunoregulation by antibody secreting cells in inflammation, infection, and cancer. Vol. 303, Immunol. Rev., JWS; 2021. p. 103–118.

29. Montuori E, de Pascale D, Lauritano C. Recent discoveries on marine organism immunomodulatory activities. Vol. 20, Mar. Drugs; 2022. p. 422.

30. Antonella P, Luca G. The quantitative real-time PCR applications in the monitoring of marine harmful algal bloom (HAB) species. Vol. 20, Environ. Sci. Pollut. Res.; 2013. p. 6851–6862.

31. Marsili L, Casini S, Bucalossi D, Porcelloni S, Maltese S, Fossi MC. Use of immunofluorescence technique in cultured fibroblasts from Mediterranean cetaceans as new ‘in vitro’ tool to investigate effects of environmental contaminants. Vol. 66, Mar. Environ. Res.; 2008. p. 151–153.

32. Campos A, Souza CB, Lhullier C, Falkenberg M, Schenkel EP, Ribeiro-Do-Valle RM, et al. Anti-tumour effects of elatol, a marine derivative compound obtained from red algae Laurencia microcladia. Vol. 64, J. Pharm. Pharmacol.; 2012. p. 1146–1154.

33. Goey AKL, Chau CH, Sissung TM, Cook KM, Venzon DJ, Castro A, et al. Screening and biological effects of marine pyrroloiminoquinone alkaloids: Potential inhibitors of the HIF-1α/p300 interaction. Vol. 79, J. Nat. Prod.; 2016. p. 1267–1275.

34. Xu J, Yi M, Ding L, He S. A review of anti-inflammatory compounds from marine fungi, 2000-2018. Vol. 17, Mar. Drugs.; 2019. p. 636.

35. Liu W, Tang S, Zhao Q, Zhang W, Li K, Yao W, et al. The α-D-glucan from marine fungus Phoma herbarum YS4108 ameliorated mice colitis by repairing mucosal barrier and maintaining intestinal homeostasis. Vol. 149, Int. J. Biol. Macromol.; 2020. p. 1180–1188.

36. Gunathilake V, Bertolino M, Bavestrello G, Udagama P. immunomodulatory activity of the marine sponge, Haliclona (Soestella) sp. (Haplosclerida: Chalinidae), from Sri Lanka in Wistar albino rats: immunosuppression and Th1-skewed cytokine response. J. Immunol. Res. 2020; 2020. p. 1-11.

37. Montuori E, de Pascale D, Lauritano C. Recent discoveries on marine organism immunomodulatory activities. Vol. 20, Mar. Drugs.; 2022. p. 422.

38. Song SK, Beck BR, Kim D, Park J, Kim J, Kim HD, et al. Prebiotics as immunostimulants in aquaculture: A review. Vol. 40, Fish Shellfish Immunol.; 2014. p. 40–48.

39. Klenk E. Neuraminsäure, das Spaltprodukt eines neuen Gehirnlipoids, J. Biol. Chem.; 1941. p. 50-58.

40. Yamashita T, Wada R, Sasaki T, Deng C, Bierfreund U, Sandhoff K, et al. A vital role for glycosphingolipid synthesis during development and differentiation. Vol. 96, PNAS; 1999. p. 9142-9147.

41. Stoffel W, Bosio A. Myelin glycolipids and their functions. Vol. 7, Curr. Opin. Neurobiol.; 1997. p. 654-661.

42. Merrill AH. Sphingolipid and glycosphingolipid metabolic pathways in the era of sphingolipidomics. Vol. 111, Chem. Rev.; 2011. p. 6387–6422.

43. Morimoto T, Nagatsu A, Murakami N, Sakakibara J, Tokuda H. Anti-tumour-promoting glyceroglycolipids from the green alga, chlorella vulgaris. Vol. 40, Phytochem.; 1995. p. 1433-1437.

44. Reshef V, Mizrachi E, Maretzki T, Silberstein C, Loya S, Hizi A, et al. new acylated sulfoglycolipids and digalactolipids and related known glycolipids from

cyanobacteria with a potential to inhibit the reverse transcriptase of HIV-1. Vol. 60, J. Nat. Prod.; 1997. p. 1251-1260.

45. Plouguerné E, da Gama BAP, Pereira RC, Barreto-Bergter E. Glycolipids from seaweeds and their potential biotechnological applications. Vol. 4, Front. Cell. Infect.; 2014. p. 174.

46. Noda H, Amano H, Arashima K, Nisizawa' K. Antitumor activity of marine algae. Vol. 204, Hydrobiologia; 1990. p. 577-584.

47. Naumann I, Darsow KH, Walter C, Lange HA, Buchholz R. Identification of sulfoglycolipids from the alga Porphyridium purpureum by matrix-assisted laser desorption/ionisation quadrupole ion trap time-of-flight mass spectrometry. Vol. 21, Rapid Commun. Mass Spectrom.; 2007. p. 3185–3192.

48. Natori T, Morita M, Akimoto K, Koezuka Y. Agelasphins, novel antitumor and immunostimulatory cerebrosides from the marine sponge agelas mauritianus. Vol. 50, Tetrahedron; 1994. p. 2771-2784.

49. Motoki K, Kobayashi E, Uchida T, Fukushima H, Koezuka Y. antitumor activities of α-, β-monogalactosylceramides and four diastereomers of an α-galactosylceramide. Vol. 5, Bioorganic Med. Chem. Lett.; 1995. p. 705-710.

50. Costantino V, Fattorusso E, Mangoni A, Di Rosa M, Ianaro A. Glycolipids from sponges. 6.1 Plakoside a and b, two unique prenylated glycosphingolipids with immunosuppressive activity from the marine sponge plakortis simplex. Vol. 119, J. Am. Chem. Soc.; 1997. p. 12465-12470.

51. Zhang J, Li C, Yu G, Guan H. Total synthesis and structure-activity relationship of glycoglycerolipids from marine organisms. Vol. 12, Mar. Drugs.; 2014. p. 3634–3659.

52. Aoki S, Ohta K, Yamazaki T, Sugawara F, Sakaguchi K. Mammalian mitotic centromere-associated kinesin (MCAK): A new molecular target of sulfoquinovosylacylglycerols novel antitumor and immunosuppressive agents. Vol. 272, FEBS J.; 2005. p. 2132–2140.

53. Naumann I, Darsow KH, Walter C, Lange HA, Buchholz R. Identification of sulfoglycolipids from the alga Porphyridium purpureum by matrix-assisted laser

desorption/ionisation quadrupole ion trap time-of-flight mass spectrometry. Vol. 21, Rapid Commun. Mass Spectrom.; 2007. p. 3185–3192.

54. Takahashi Y, Itoh K, Ishii M, Suzuki M, Itabashi Y. Induction of larval settlement and metamorphosis of the sea urchin Strongylocentrotus intermedius by glycoglycerolipids from the green alga Ulvella lens. Vol. 140, Mar. Biol.; 2002. p. 763–771.

55. Shao ZY, Cai JN, Ye QZ, Guo YW. Crassicaulisine, a new sulphonoglycolipid from the red alga Chondria crassicaulis Harv. Vol. 4, J. Asian Nat. Prod. Res.; 2002. p. 205–209.

56. Plouguerné E, De Souza LM, Sassaki GL, Cavalcanti JF, Romanos MTV, Da Gama BAP, et al. Antiviral sulfoquinovosyldiacylglycerols (SQDGs) from the Brazilian brown seaweed Sargassum vulgare. Vol. 11, Mar. Drugs; 2013. p. 4628–4640.

57. Mattos BB, Romanos MT V., de Souza LM, Sassaki G, Barreto-Bergter E. Glycolipids from macroalgae: Potential biomolecules for marine biotechnology? Vol. 21, Rev. Bras. Farmacogn.; 2011. p. 244–247.

58. Vo TS, Ngo DH, Ta Q Van, Kim SK. Marine organisms as a therapeutic source against herpes simplex virus infection. Vol. 44, Eur. J. Pharm. Sci.; 2011. p. 11–20.

59. Manzo E, Cutignano A, Pagano D, Gallo C, Barra G, Nuzzo G, et al. A new marine-derived sulfoglycolipid triggers dendritic cell activation and immune adjuvant response. Vol. 7, Sci. Rep.; 2017. p. 6286.

60. Matsumoto Y, Sahara H, Fujita T, Shimozawa K, Takenouchi M, Torigoe T, et al. An immunosuppressive effect by synthetic sulfonolipids deduced from sulfonoquinovosyl diacylglycerols of sea urchin. Vol. 74, Transplantation; 2002. p. 261-267.

61. Osmond DG. Population Dynamics of Bone Marrow B Lymphocytes. Vol. 93, Immunol. Rev.; 1986. p. 103-124.

62. Mosier D, Cantor H. Functional maturation of mouse thymic lymphocytes. Vol. 1, Eur. J. Immunol.; 1971. p. 459-461.

63. Duijvestijn AM, Hoefsmit ECM. cell and tissue research ultrastructure of the rat thymus: the micro-environment of T-lymphocyte maturation. Vol. 218, Cell Tissue Res.; 1981. p. 279-292.

64. Reinherz EL, Schlossman SF. The differentiation and function of human T lymphocytes review, Cell; 1980. p. 7.

65. Bobosha K, Wilson L, van Meijgaarden KE, Bekele Y, Zewdie M, van der Ploeg-van Schip JJ, et al. T-cell regulation in lepromatous leprosy. Vol. 8, PLOS Negl. Trop. Dis.; 2014. e2773.

66. Modlin RL, Robert L. Thl-Th2 paradigm: Insights from leprosy. Vol. 102, J. Invest. Dermatol.; 1993. p. 828-832.

67. Steinhardt PJ, Jeong HC, Saitoh K, Tanaka M, Abe E, Tsai AP. Experimental verification of the quasi-unit-cell model of quasicrystal structure. Vol. 399, Nature; 1999. p. 84.

68. Licona-Limón P, Kim LK, Palm NW, Flavell RA. TH2, allergy and group 2 innate lymphoid cells. Vol. 14, Nat. Immunol.; 2013. p. 536–542.

69. Arellano G, Acuña E, Reyes LI, Ottum PA, Sarno P De, Villarroel L, et al. Th1 and Th17 cells and associated cytokines discriminate among clinically isolated syndrome and multiple sclerosis phenotypes. Vol. 8, Front. Immunol.; 2017. p. 753.

70. Corry DB, Kheradmand F. Induction and regulation of the IgE response. Vol. 402, Nature; 1999. p. 18-23.

71. Li B, Huang L, Lv P, Li X, Liu G, Chen Y, et al. The role of Th17 cells in psoriasis Th17 cells. Vol. 68, Immunol. res.; 2020. p. 296-309.

72. Paulissen SMJ, van Hamburg JP, Dankers W, Lubberts E. The role and modulation of CCR6+ Th17 cell populations in rheumatoid arthritis. Vol. 74, Cytokine.; 2015. p. 43–53.

73. Paul WE, William E, Seder WE. Lymphocyte responses and cytokines. Vol. 76, Cell; 1994. p. 241-251.

74. Hardy RR, Carmack CE, Shinton SA, Kemp JD, Hayakawa K. Resolution and characterization of pro-b and pre-pro-b cell stages in normal mouse bone marrow. Vol. 173, J. Exp. Med.; 1991. p. 1213-1225.

75. Küppers R. B cells under influence: Transformation of B cells by Epstein-Barr virus. Vol. 3, Nat. Rev. Immunol.; 2003. p. 801–812.

76. Gao B, Radaeva S, Park O. Liver natural killer and natural killer T cells: immunobiology and emerging roles in liver diseases. Vol. 86, J. Leukoc. Biol.; 2009. p. 513–528.

77. Beck S, Trowsdale J. The human major histocompatibility complex: Lessons from the DNA sequence. Vol. 1, Annu. Rev. Genomics Hum. Genet.; 2000. p. 117-137.

78. Hewitt EW. The MHC class I antigen presentation pathway: Strategies for viral immune evasion. Vol. 110, Immunology; 2003. p. 163–169.

79. Hansen TH, Bouvier M. MHC class i antigen presentation: Learning from viral evasion strategies. Vol. 9, Nat. Rev. Immunol.; 2009. p. 503–513.

80. Roche PA, Furuta K. The ins and outs of MHC class II-mediated antigen processing and presentation. Vol. 15, Nat. Rev. Immunol.; 2015. p. 203–216.

81. Liu K, Nussenzweig MC. Origin and development of dendritic cells. Vol. 234, Immunol. Rev.; 2010. p. 45-54.

82. Kang S, Keener AB, Jones SZ, Benschop RJ, Caro-Maldonado A, Rathmell JC, et al. IgG-immune complexes promote B cell memory by inducing BAFF. Vol. 196, J. Immunol.; 2016. p. 196–206.

83. Yona S, Jung S. Monocytes: Subsets, origins, fates and functions. Vol. 17, Curr. Opin. Hematol.; 2010. p. 53–59.

84. Calandra T, Roger T. Macrophage migration inhibitory factor: A regulator of innate immunity. Vol. 3, Nat. Rev. Immunol.; 2003. p. 791–800.

85. Epelman S, Lavine KJ, Randolph GJ. Origin and functions of tissue macrophages. Vol. 41, Immunity.; 2014. p. 21–35.

86. Burn GL, Foti A, Marsman G, Patel DF, Zychlinsky A. The neutrophil. Vol. 54, Immunity.; 2021. p. 1377–1391.

87. Zhang JM, An J. Cytokines, inflammation, and pain. Vol. 45, Int. Anesthesiol. Clin.; 2007. p. 27–37.

88. Dinarello CA. Historical insights into cytokines. Vol. 37, Eur. J. Immunol.; 2007. p. S34-S45.

89. Parkin J, Cohen B. An overview of the immune system. Vol. 357, Lancet.; 2001. p. 1777–1789.

90. Schroeder HW, Cavacini L. Structure and function of immunoglobulins. Vol. 125, J. Allergy Clin. Immunol.; 2010. p.S41-S52.

91. Lewis SM, Williams A, Eisenbarth SC. Structure and function of the immune system in the spleen. Vol. 4, Sci. Immunol.; 2019. eaau6085.

92. Sarma JV, Ward PA. The complement system. Vol. 343, Cell Tissue Res.; 2011. p. 227–235.

93. Cueni LN, Detmar M. The lymphatic system in health and disease. Vol. 6, Lymphat. Res. Biol.; 2008. p. 109–122.

94. Cifarelli V, Eichmann A. The intestinal lymphatic system: functions and metabolic implications. Vol. 7, Cell. Mol. Gastroenterol. Hepatol.; 2019. p. 503–513.

95. Delves PJ, Roitt IM. The immune system. Vol. 343, N. Engl. J. Med.; 2000. p. 37-49.

96. Dempsey PW, Vaidya SA, Cheng G. The Art of War: Innate and adaptive immune responses. Vol. 60, Cell. Mol. Life Sci.; 2003. p. 2604–2621.

97. Janeway CA, Medzhitov R. Innate immune recognition. Vol. 20, Annu. Rev. Immunol.; 2002. p. 197–216.

98. Medzhitov R et al. Innate immunity: impact on the adaptive immune response. Vol. 9, Curr. Opin. Immunol.; 1997. p. 4-9.

99. Janeway CA, Medzhitov R. Innate immune recognition. Vol. 20, Annu. Rev. Immunol.; 2002. p. 197–216.

100. Fearon DT, Locksley RM. The instructive role of lnnate lmmunity in the acquired immune response. Vol. 272, Science; 1996. p. 50-54.

101. Banchereau J, Steinman RM. Dendritic cells and the control of immunity. Vol. 392, Nature; 1998. p. 245-252.

102. Janeway CA. How the immune system works to protect the host from infection: A personal view. Vol. 98, Proc. Natl. Acad. Sci.; 2001. p. 7461-7468.

103. Bonilla FA, Oettgen HC. Adaptive immunity. Vol. 125, J. Allergy Clin. Immunol.; 2010. p. S33-S40.

104. Steinman RM, Cohn ZA. Identification of a novel cell type in peripheral lymphoid organs of mice: I. Morphology, quantitation, tissue distribution. Vol. 137, J. Exp. Med.; 1973. p. 1142-1162.

105. Heath WR, Carbone FR. Dendritic cell subsets in primary and secondary T cell responses at body surfaces. Vol. 10, Nat. Immunol.; 2009. p. 1237–1244.

106. Merad M, Sathe P, Helft J, Miller J, Mortha A. The dendritic cell lineage: Ontogeny and function of dendritic cells and their subsets in the steady state and the inflamed setting. Vol. 31, Annu. Rev. Immunol.; 2013. p. 563–604.

107. Steinman RM, Idoyaga J. Features of the dendritic cell lineage. Vol. 234, Immunol. Rev.; 2010. p. 5–17.

108. Paul WE. Bridging innate and adaptive immunity. Vol. 147, Cell.; 2011. p. 1212–1215.

109. Banchereau J, Steinman RM. Dendritic cells and the control of immunity. Vol. 392, Nature; 1998. p. 245-252.

110. Goubier A, Dubois B, Gheit H, Joubert G, Villard-Truc F, Asselin-Paturel C, et al. Plasmacytoid dendritic cells mediate oral tolerance. Vol. 29(3), Immunity; 2008. p. 464–475.

111. Ochando JC, Homma C, Yang Y, Hidalgo A, Garin A, Tacke F, et al. Alloantigen-presenting plasmacytoid dendritic cells mediate tolerance to vascularized grafts. Vol. 7, Nat. Immunol.; 2006. p. 652–662.

112. Mbongue JC, Nieves HA, Torrez TW, Langridge WHR. The role of dendritic cell maturation in the induction of insulin-dependent diabetes mellitus. Vol. 8, Front. Immunol.; 2017. p. 327.

113. Dalod M, Chelbi R, Malissen B, Lawrence T. Dendritic cell maturation: Functional specialization through signaling specificity and transcriptional programming. Vol. 33, EMBO J.; 2014. p. 1104–1116.

114. Banchereau J, Briere F, Caux C, Davoust J, Lebecque S, Liu YJ, et al. Immunobiology of dendritic cells. Vol. 18, Annu. Rev. Immunol.; 2000. p. 767-811.

115. Steinman RM, Banchereau J. Taking dendritic cells into medicine. Vol. 449, Nature; 2007. p. 419–426.

116. Reis and Sousa C. Dendritic cells in a mature age. Vol. 6, Nat. Rev. Immunol.; 2006. p. 476-483.

117. Pulendran B. Immunology variegation of the immune response with dendritic cells and pathogen recognition receptors 1. Vol. 174, J. Immunol.; 2005. p. 2457-2465.

118. Piqueras B, Connolly J, Freitas H, Karolina Palucka A, Banchereau J. Upon viral exposure, myeloid and plasmacytoid dendritic cells produce 3 waves of distinct chemokines to recruit immune effectors. Vol. 107, Blood; 2006. p. 2613-2618.

119. Caetano Reis Sousa B, Hieny S, Scharton-Kersten T, Jankovic D, Charest H, Germain RN, et al. In vivo microbial stimulation induces rapid CD40 ligand-independent production of interleukin 12 by dendritic cells and their redistribution to T cell areas. Vol. 186, J. Exp. Med.; 1997. p. 1819-1829.

120. Dalod M, Salazar-Mather TP, Malmgaard L, Lewis C, Asselin-Paturel C, Brière F, et al. Interferon α/β and interleukin 12 responses to viral infections: pathways regulating dendritic cell cytokine expression in vivo. Vol. 195, J. Exp. Med.; 2002. p. 517-528.

121. Sallusto F, Schaerli P, Loetscher P, Schaniel C, Lenig D, Mackay CR, et al. Rapid and coordinated switch in chemokine receptor expression during dendritic cell maturation. Vol. 28, Eur. J. Immunol.; 1998. p. 2760–2769.

122. Winzler C, Rovere P, Rescigno M, Granucci F, Penna G, Adorini L, et al. Maturation stages of mouse dendritic cells in growth factor-dependent long-term cultures. Vol. 185, J. Exp. Med.; 1997. p. 317-328.

123. Vandebriel RJ, Hoefnagel MHN. Dendritic cell-based in vitro assays for vaccine immunogenicity. Vol. 8, Hum. Vaccin. Immunother.; 2012. p. 1323–1325.

124. Mizumoto N, Gao J, Matsushima H, Ogawa Y, Tanaka H, Takashima A. Discovery of novel immunostimulants by dendritic-cell-based functional screening. Vol. 106, Blood; 2005. p. 3082–3089.

125. Brufsky A, Marti JLG, Nasrazadani A, Lotze MT. Boning up: Amino-bisphophonates as immunostimulants and endosomal disruptors of dendritic cell in SARS-CoV-2 infection. Vol. 18, J. Transl. Med.; 2020. p. 1-6.

126. Rey-Ladino J, Ross AG, Cripps AW, McManus DP, Quinn R. Natural products and the search for novel vaccine adjuvants. Vol. 29, Vaccine; 2011. p. 6464–6471.

127. Cabeza-Cabrerizo M, Cardoso A, Minutti CM, Pereira da Costa M, Reis Sousa C. Annual review of immunology dendritic cells revisited. Vol. 39, Annu. Rev. Immunol.; 2021. p. 131-166.

128. Dowds CM, Kornell SC, Blumberg RS, Zeissig S. Lipid antigens in immunity. Vol. 395, Biol. Chem.; 2014. p. 61–81.

129. Vartabedian VF, Savage PB, Teyton L. The processing and presentation of lipids and glycolipids to the immune system. Vol. 272, Immunol. Rev.; 2016. p. 109-119.

130. Chang YJ, Huang JR, Tsai YC, Hung JT, Wu D, Fujio M, et al. Potent immune-modulating and anticancer effects of NKT cell stimulatory glycolipids. Vol. 104, PNAS; 2007. p. 10299-10304.

131. Cochet F, Peri F. The role of carbohydrates in the lipopolysaccharide (LPS)/toll-like receptor 4 (TLR4) Signalling. Vol. 18, Int. J. Mol. Sci.; 2017. p. 2318.

132. Saitoh SI, Akashi S, Yamada T, Tanimura N, Kobayashi M, Konno K, et al. Lipid A antagonist, lipid IVa, is distinct from lipid A in interaction with Toll-like receptor 4 (TLR4)-MD-2 and ligand-induced TLR4 oligomerization. Vol. 16, Int. Immunol.; 2004. p. 961–969.

133. Grant EP, Degano M, Rosat JP, Stenger S, Modlin RL, Wilson IA, et al. Molecular recognition of lipid antigens by t cell receptors. Vol. 189, J. Exp. Med.; 1999. p. 195-205.

134. Lang GA, Maltsev SD, Besra GS, Lang ML. Presentation of α-galactosylceramide by murine CD1d to natural killer T cells is facilitated by plasma membrane glycolipid rafts. Vol. 112, Immunol.; 2004. p. 386-396.

135. Chang YJ, Huang JR, Tsai YC, Hung JT, Wu D, Fujio M, et al. Potent immune-modulating and anticancer effects of NKT cell stimulatory glycolipids. Vol. 104, Proc. Natl. Acad. Sci.; 2007. p. 10299-10304.

136. Mattner J, DeBord KL, Ismail N, Goff RD, Cantu C, Zhou D, et al. Exogenous and endogenous glycolipid antigens activate NKT cells during microbial infections. Vol. 434, Nature; 2005. p. 525–529.

137. Exley M, Garcia J, Balk SP, Porcelli S. Requirements for CD1d recognition by human invariant V 24 CD4 CD8 T cells. Vol. 186, J. Exp. Med.; 1997. p. 109-120.

138. Gallo C, Manzo E, Barra G, Fioretto L, Ziaco M, Nuzzo G, et al. Sulfavant A as the first synthetic TREM2 ligand discloses a homeostatic response of dendritic cells after receptor engagement. Vol. 79, Cell. Mol. Life Sci.; 2022. p. 369.

139. Kawai T, Akira S. The roles of TLRs, RLRs and NLRs in pathogen recognition. Vol. 21, Int. Immunol.; 2009. p. 317–337.

140. Matzinger P. Tolerance, danger, and the extended family. Vol. 12, Annu. Rev. Immunol.;1994. p. 991-1045.

141. Janeway C A, Medzhitov R. Innate immune recognition. Vol. 20, Annu. Rev. Immunol.; 2002. p. 197–216.

142. Palm NW, Medzhitov R. Pattern recognition receptors and control of adaptive immunity. Vol. 227, Immunol. Rev.; 2009. p. 221–233.

143. Suresh R, Mosser DM. Pattern recognition receptors in innate immunity, host defense, and immunopathology. Vol. 37, Adv. Physiol. Educ.; 2013. p. 284-291.

144. Gordon S. Pattern recognition receptors: doubling up for the innate immune response. Vol. 111, Cell; 2002. p. 927-930.

145. Medzhitov R. Approaching the asymptote: 20 years later. Vol. 30, Immunity; 2009. p. 766–775.

146. Li D, Wu M. Pattern recognition receptors in health and diseases. Vol. 6, Signal Transduct. Target.; 2021. p. 291.

147. Hutcheon C, Paulvannan P, Subramanian N. Cytoplasmic sensing in innate immunity. Vol. 3, Encycl. of Cell Biol.; 2016. p. 710–726.

148. Akira S. Toll-like receptor signaling. Vol. 278, J. Biol. Chem.; 2003. p. 38105–38108.

149. Seya T, Akazawa T, Tsujita T, Matsumoto M. Role of toll-like receptors in adjuvant-augmented immune therapies. Vol. 3, Evid. Based Complementary Altern. Med.; 2006. p. 31–38.

150. Hise AG, Tomalka J, Ganesan S, Patel K, Hall BA, Brown GD, et al. An essential role for the NLRP3 inflammasome in host defense against the human fungal pathogen Candida albicans. Vol. 5, Cell Host Microbe; 2009. p. 487–497.

151. Inohara N, Nuñez G. NODS: Intracellular proteins involved in inflammation and apoptosis. Vol. 3, Nat. Rev. Immunol.; 2003. p. 371–382.

152. Fritz JH, Ferrero RL, Philpott DJ, Girardin SE. Nod-like proteins in immunity, inflammation and disease. Vol. 7, Nat. Immunol.; 2006. p. 1250–1257.

153. Meunier E, Broz P. Evolutionary convergence and divergence in NLR function and structure. Vol. 38, Trends Immunol.; 2017. p. 744–757.

154. Yoneyama M, Onomoto K, Jogi M, Akaboshi T, Fujita T. Viral RNA detection by RIG-I-like receptors. Vol. 32, Curr. Opin. Immunol.; 2015. p. 48–53.

155. Rehwinkel J, Gack MU. RIG-I-like receptors: Their regulation and roles in RNA sensing. Vol. 20, Nat. Rev. Immunol.; 2020. p. 537–551.

156. Fortman JL, Mukhopadhyay A. The future of antibiotics: Emerging technologies and stewardship. Vol. 24, Trends Microbiol.; 2016. p. 515–517.

157. Saito T, Hirai R, Loo YM, Owen D, Johnson CL, Sinha SC, et al. Regulation of innate antiviral defenses through a shared repressor domain in RIG-I and LGP2. Vol. 104, Proc. Natl. Acad. Sci.; 2006. p. 582-587.

158. Vajjhala PR, Ve T, Bentham A, Stacey KJ, Kobe B. The molecular mechanisms of signaling by cooperative assembly formation in innate immunity pathways. Vol. 86, Mol. Immunol.; 2017. p. 23–37.

159. Man SM, Kanneganti TD. Regulation of inflammasome activation. Vol. 265, Immunol. Rev.; 2015. p. 6–21.

160. Chen PA, Shrivastava G, Balcom EF, McKenzie BA, Fernandes J, Branton WG, et al. Absent in melanoma 2 regulates tumor cell proliferation in glioblastoma multiforme. Vol. 144, J. Neurooncol.; 2019. p. 265–273.

161. Gray EE, Winship D, Snyder JM, Child SJ, Geballe AP, Stetson DB. The AIM2-like receptors are dispensable for the interferon response to intracellular DNA. Vol. 45, Immunity; 2016. p. 255–266.

162. Plato A, Hardison SE, Brown GD. Pattern recognition receptors in antifungal immunity. Vol. 37, Semin. Immunopathol.; 2015. p. 97–106.

163. Ebner S, Sharon N, Ben-Tal N. Evolutionary analysis reveals collective properties and specificity in the C-type lectin and lectin-like domain superfamily. Vol. 53, Proteins; 2003. p. 44–55.

164. Freeman SA, Grinstein S. Phagocytosis: Receptors, signal integration, and the cytoskeleton. Vol. 262, Immunol. Rev.; 2014. p. 193–215.

165. Dam TK, Fred Brewer C. Lectins as pattern recognition molecules: The effects of epitope density in innate immunity. Vol. 20, Glycobiol.; 2009. p. 270–279.

166. Lepenies B, Lee J, Sonkaria S. Targeting C-type lectin receptors with multivalent carbohydrate ligands. Vol. 65, Adv. Drug Deliv. Rev.; 2013. p. 1271–1281.

167. Lan T, Li Z, Peng M, Niu D, Li Y, Li J. A four-CRD C-type lectin from razor clam Sinonovacula constricta mediates agglutination and phagocytosis. Vol. 728, Gene; 2020. p. 144287.

168. Gordon S. Myeloid cells in health and disease: a synthesis. John Wiley & Sons, 2020.

169. Sancho D, Reis e Sousa C. Signaling by myeloid C-Type lectin receptors in immunity and homeostasis. Vol. 30, Annu. Rev. Immunol.; 2012. p. 491–529.

170. Zelensky AN, Gready JE. Comparative analysis of structural properties of the C-type-lectin-like domain (CTLD). Vol. 52, Proteins; 2003. p. 466–477.

171. Crusio WE, Dong H, Radeke HH et al. Volume 1204 Series Editors. Advances in experimental medicine and biology. Available from: https://www.springer.com/series/5584

172. Mnich ME, van Dalen R, van Sorge NM. C-type lectin receptors in host defense against bacterial pathogens. Vol. 10, Front. Cell. Infect.; 2020. p. 309.

173. Taylor PR, Tsoni SV, Willment JA, Dennehy KM, Rosas M, Findon H, et al. Dectin-1 is required for β-glucan recognition and control of fungal infection. Vol. 8, Nat. Immunol.; 2007. p. 31–38.

174. Yamaguchi K, Kanno E, Tanno H, Sasaki A, Kitai Y, Miura T, et al. Distinct roles for Dectin-1 and Dectin-2 in skin wound healing and neutrophilic inflammatory responses. Vol. 141, J. Invest. Dermatol.; 2021. p. 164-176.

175. Kaisar MMM, Ritter M, del Fresno C, Jónasdóttir HS, van der Ham AJ, Pelgrom LR, et al. Dectin-1/2–induced autocrine PGE 2 signaling licenses dendritic cells to prime Th2 responses. Vol. 16, PLoS Biol.; 2018. e2005504.

176. Feinberg H, Jégouzo SAF, Rex MJ, Drickamer K, Weis WI, Taylor ME. Mechanism of pathogen recognition by human dectin-2. Vol. 292, J. Biol. Chem.; 2017. p. 13402–13414.

177. Ambati S, Ellis EC, Lin J, Lin X, Lewis ZA, Meagher RB. Dectin-2-targeted antifungal liposomes exhibit enhanced efficacy. Vol. 4, mSphere; 2019. e00715-19.

178. Wittmann A, Lamprinaki D, Bowles KM, Katzenellenbogen E, Knirel YA, Whitfield C, et al. Dectin-2 recognizes mannosylated O-antigens of human opportunistic pathogens and augments lipopolysaccharide activation of myeloid cells. Vol. 291, J. Biol. Chem.; 2016. p. 17629–17638.

179. Ritter M, Gross O, Kays S, Ruland J, Nimmerjahn F, Saijo S, et al. Schistosoma mansoni triggers Dectin-2, which activates the Nlrp3 inflammasome and alters

adaptive immune responses. Vol. 107, Proc. Natl. Acad. Sci. USA; 2010. p. 20459–20464.

180. Pyz E, Marshall ASJ, Gordon S, Brown GD. C-type lectin-like receptors on myeloid cells. Vol. 38, Ann. Med.; 2006. p. 242–251.

181. Figdor CG, Van Kooyk Y, Adema GJ. C-type lectin receptors on dendritic cells and Langerhans cells. Vol. 2, Nat. Rev. Immunol.; 2002. p. 77-84.

182. Sonck E. Immunomodulation of porcine leukocytes and dendritic cells by-(1,3) glucans. PhD Thesis. Ghent University; 2011.

183. Kimberg M, Brown GD. Dectin-1 and its role in antifungal immunity. Vol. 46, Med. Mycol. J.; 2008. p. 631–636.

184. Rogers NC, Slack EC, Edwards AD, Nolte MA, Schulz O, Schweighoffer E, et al. Syk-dependent cytokine induction by dectin-1 reveals a novel pattern recognition pathway for C type lectins. Vol. 22, Immunity; 2005. p. 507–517.

185. Kalia N, Singh J, Kaur M. The role of dectin-1 in health and disease. Vol. 226, Immunobiol.; 2021. p. 152071.

186. Mereiter S, Balmaña M, Campos D, Gomes J, Reis CA. Glycosylation in the era of cancer-targeted therapy: Where are we heading? Vol. 36, Cancer Cell.; 2019. p. 6–16.

187. Cadena AP, Cushman TR, Welsh JW. Glycosylation and antitumor immunity. Vol. 343, Int. Rev. Cell. Mol. Biol.; 2019. p. 111–127.

188. Ostrop J, Lang R. Contact, collaboration, and conflict: Signal integration of Syk-coupled C-type lectin receptors. Vol. 198, J. Immunol.; 2017. p. 1403–1414.

189. Brown GD, Gordon S. A new receptor for β-glucans. Vol. 413, Nature; 2001. p. 36-37.

190. Ambati S, Ferarro AR, Kang SE, Lin J, Lin X, Momany M, et al. Dectin-1-targeted antifungal liposomes exhibit enhanced efficacy. Vol. 4, mSphere; 2019. e00025-19.

191. Fan Y, Li C, Peng X, Jiang N, Hu L, Gu L, et al. Perillaldehyde ameliorates aspergillus fumigatus keratitis by activating the Nrf2/HO-1 signaling pathway and inhibiting dectin-1-mediated inflammation. Vol. 61, IOVS; 2020. p. 51.

192. Walsh NM, Wuthrich M, Wang H, Klein B, Hull CM. Characterization of C-type lectins reveals an unexpectedly limited interaction between Cryptococcus neoformans spores and Dectin-1. Vol. 12, PLoS One; 2017. e0173866.

193. Cao M, Wu Z, Lou Q, Lu W, Zhang J, Li Q, et al. Dectin-1-induced RIPK1 and RIPK3 activation protects host against Candida albicans infection. Vol. 26, Cell Death Differ.; 2019. p. 2622–2636.

194. Kashem SW, Igyártó BZ, Gerami-Nejad M, Kumamoto Y, Mohammed J, Jarrett E, et al. Candida albicans morphology and dendritic cell subsets determine T helper cell differentiation. Vol. 42, Immunity; 2015. p. 356–366.

195. Yuan K, Zhao G, Che C, Li C, Lin J, Zhu G, et al. Dectin-1 is essential for IL-1β production through JNK activation and apoptosis in Aspergillus fumigatus keratitis. Vol. 52, Int. Immunopharmacol.; 2017. p. 168–175.

196. Gow NAR, Netea MG, Munro CA, Ferwerda G, Bates S, Mora-Montes HM, et al. Immune recognition of Candida albicans β-glucan by dectin-1. Vol. 196, J. Infect. Dis.; 2007. p. 1565–1571.

197. Saijo S, Fujikado N, Furuta T, Chung SH, Kotaki H, Seki K, et al. Dectin-1 is required for host defense against Pneumocystis carinii but not against Candida albicans. Vol. 8, Nat. Immunol.; 2007. p. 39–46.

198. Steele C, Marrero L, Swain S, Harmsen AG, Zheng M, Brown GD, et al. Alveolar macrophage-mediated killing of Pneumocystis carinii f. sp. muris involves molecular recognition by the Dectin-1 β-glucan receptor. Vol. 198, J. Exp. Med.; 2003. p. 1677–1688.

199. Deerhake ME, Shinohara ML. Emerging roles of Dectin-1 in noninfectious settings and in the CNS. Vol. 42, Trends Immunol.; 2021. p. 891–903.

200. Chiba S, Ikushima H, Ueki H, Yanai H, Kimura Y, Hangai S, et al. Recognition of tumor cells by Dectin-1 orchestrates innate immune cells for anti-tumor responses. Vol. 3, Elife; 2014. p. 1–20.

201. Thaiss CA, Levy M, Itav S, Elinav E. Integration of innate immune signaling. Vol. 37, Trends Immunol.; 2016. p. 84–101.

202. Gantner BN, Simmons RM, Canavera SJ, Akira S, Underhill DM. Collaborative induction of inflammatory responses by dectin-1 and toll-like receptor 2. Vol. 197, J. Exp. Med.; 2003. p. 1107–1117.

203. Lilly LM, Gessner MA, Dunaway CW, Metz AE, Schwiebert L, Weaver CT, et al. The β-glucan receptor Dectin-1 promotes lung immunopathology during fungal allergy via IL-22. Vol. 189, J. Immunol.; 2012. p. 3653–3660.

204. Reymann AC, Boujemaa-Paterski R, Martiel JL, Guérin C, Cao W, Chin HF, et al. Actin network architecture can determine myosin motor activity. Vol. 336, Science; 2012. p. 1310–1314.

205. LeibundGut-Landmann S, Groß O, Robinson MJ, Osorio F, Slack EC, Tsoni SV, et al. Syk- and CARD9-dependent coupling of innate immunity to the induction of T helper cells that produce interleukin 17. Vol. 8, Nat. Immunol.; 2007. p. 630–638.

206. Underhill DM, Goodridge HS. The many faces of ITAMs. Vol. 28, Trends Immunol.; 2007. p. 66–73.

207. Goodridge HS, Simmons RM, Underhill DM. Dectin-1 stimulation by Candida albicans yeast or zymosan triggers NFAT activation in macrophages and dendritic cells 1. Vol. 178, J. Immunol.; 2007. p. 3107-3115.

208. Gross O, Gewies A, Finger K, Schäfer M, Sparwasser T, Peschel C, et al. Card9 controls a non-TLR signalling pathway for innate anti-fungal immunity. Vol. 442, Nature; 2006. p. 651–656.

209. Slack EC, Robinson MJ, Hernanz-Falcón P, Brown GD, Williams DL, Schweighoffer E, et al. Syk-dependent ERK activation regulates IL-2 and IL-10 production by DC stimulated with zymosan. Vol. 37, Eur. J. Immunol.; 2007. p. 1600–1612.

210. Herre J, Marshall ASJ, Caron E, Edwards AD, Williams DL, Schweighoffer E, et al. Dectin-1 uses novel mechanisms for yeast phagocytosis in macrophages. Vol. 104, Blood; 2004. p. 4038–4045.

211. Geijtenbeek TBH, Gringhuis SI. Signalling through C-type lectin receptors: Shaping immune responses. Vol. 9, Nat. Rev. Immunol.; 2009. p. 465–479.

212. Colonna M, Wang Y. TREM2 variants: New keys to decipher Alzheimer disease pathogenesis. Vol. 17, Nat. Rev. Neurosci.; 2016. p. 201–207.

213. Wunderlich P, Glebov K, Kemmerling N, Tien NT, Neumann H, Walter J. Sequential proteolytic processing of the triggering receptor expressed on myeloid cells-2 (TREM2) protein by ectodomain shedding and γ-secretase- dependent intramembranous cleavage. Vol. 288, J. Biol. Chem.; 2013. p. 33027–33306.

214. Jin SC, Benitez BA, Karch CM, Cooper B, Skorupa T, Carrell D, et al. Coding variants in TREM2 increase risk for Alzheimer's disease. Vol. 23, Hum. Mol. Genet.; 2014. p. 5838–5846.

215. Colonna M. The biology of TREM receptors. Nat. Rev. Immunol.; 2023. p. 1-15.

216. Bouchon A, Dietrich J, Colonna M. Cutting edge: Inflammatory responses can be triggered by TREM-1, a novel receptor expressed on neutrophils and monocytes. Vol. 164, J. Immunol.; 2000. p. 4991–4995.

217. Bouchon A, Facchetti F, Weigand MA, Colonna M. TREM-1 amplifies inflammation and is a crucial mediator of septic shock. Vol. 410, Nature; 2001. p. 1103-1107.

218. Bleharski JR, Kiessler V, Buonsanti C, Sieling PA, Stenger S, Colonna M, et al. A role for triggering receptor expressed on myeloid cells-1 in host defense during the early-induced and adaptive phases of the immune response. Vol. 170, J. Immunol.; 2003. p. 3812–3818.

219. Bouchon A, Hernández-Munain C, Cella M, Colonna M. A DAP12-mediated pathway regulates expression of CC chemokine receptor 7 and maturation of human dendritic cells. Vol. 194, J. Exp. Med.;2001. p. 1111-1122.

220. Daws MR, Lanier LL, Seaman WE, Ryan JC. Cloning and characterization of a novel mouse myeloid DAP12-associated receptor family. Vol. 31, Eur. J. Immunol.;2001. p. 783–791.

221. Sudom A, Talreja S, Danao J, Bragg E, Kegel R, Min X, et al. Molecular basis for the loss-of-function effects of the Alzheimer's disease–associated R47H variant of the immune receptor TREM2. Vol. 293, J. Biol. Chem.; 2018. p. 12634–12646.

222. Lanier LL. DAP10- and DAP12-associated receptors in innate immunity. Vol. 227, Immunol. Rev.; 2009. p. 150–160.

223. Ulland TK, Song WM, Huang SCC, Ulrich JD, Sergushichev A, Beatty WL, et al. TREM2 maintains microglial metabolic fitness in Alzheimer's disease. Vol. 170, Cell; 2017. p. 649-663.e13.

224. Kober DL, Brett TJ. TREM2-ligand interactions in health and disease. Vol. 429, J. Mol. Biol.; 2017. p. 1607–1629.

225. Turnbull IR, Gilfillan S, Cella M, Aoshi T, Miller M, Piccio L, et al. Cutting edge: TREM-2 attenuates macrophage activation. Vol. 177, J. Immunol.; 2006. p. 3520–3524.

226. Hamerman JA, Tchao NK, Lowell CA, Lanier LL. Enhanced Toll-like receptor responses in the absence of signaling adaptor DAP12. Vol. 6, Nat. Immunol.; 2005. p. 579–586.

227. Gratuze M, Leyns CEG, Holtzman DM. New insights into the role of TREM2 in Alzheimer's disease. Vol. 13, Mol. Neurodegener.; 2018. p. 1-16.

228. Wang Y, Cella M, Mallinson K, Ulrich JD, Young KL, Robinette ML, et al. TREM2 lipid sensing sustains the microglial response in an Alzheimer's disease model. Vol. 160, Cell; 2015. p. 1061–1071.

229. Bailey CC, Devaux LB, Farzan M. The triggering receptor expressed on myeloid cells 2 binds apolipoprotein E. Vol. 290, J. Biol. Chem.; 2015. p. 26033–26042.

230. Atagi Y, Liu CC, Painter MM, Chen XF, Verbeeck C, Zheng H, et al. Apolipoprotein E is a ligand for triggering receptor expressed on myeloid cells 2 (TREM2). Vol. 290, J. Biol. Chem.; 2015. p. 26043–26050.

231. Song W, Hooli B, Mullin K, Jin SC, Cella M, Ulland TK, et al. Alzheimer's disease-associated TREM2 variants exhibit either decreased or increased ligand-dependent activation. Vol. 13, Alzheimers. Dement.; 2017. p. 381–387.

232. Ito H, Hamerman JA. TREM-2, triggering receptor expressed on myeloid cell-2, negatively regulates TLR responses in dendritic cells. Vol. 42, Eur. J. Immunol.; 2012. p. 176–185.

233. Daws MR, Sullam PM, Niemi EC, Chen TT, Tchao NK, Seaman WE. Pattern Recognition by TREM-2: Binding of anionic ligands. Vol. 171, J. Immunol.; 2003. p. 594–599.

234. Paloneva J, Autti T, Raininko R, Partanen J, Salonen O, Puranen M et al. CNS manifestations of Nasu-Hakola disease A frontal dementia with bone cysts. Vol 56, Neurology; 2001. p. 1552-1558.

235. Paloneva J, Kestilä M, Wu J, Salminen A, Böhling T, Ruotsalainen V, et al. Loss-of-function mutations in TYROBP (DAP12) result in a presenile dementia with bone cysts. Vol. 25, Nat. Genet.; 2000. p. 357-361.

236. Paloneva J, Manninen T, Christman G, Hovanes K, Mandelin J, Adolfsson R, et al. Report mutations in two genes encoding different subunits of a receptor signaling complex result in an identical disease phenotype. Vol. 71, Am. J. Hum. Genet.; 2002. p. 656-662.

237. Takahashi K, Rochford CDP, Neumann H. Clearance of apoptotic neurons without inflammation by microglial triggering receptor expressed on myeloid cells-2. Vol. 201, J. Exp. Med.; 2005. p. 647–657.

238. Cheng X, Wang X, Nie K, Cheng L, Zhang Z, Hu Y, et al. Systematic pan-cancer analysis identifies TREM2 as an immunological and prognostic biomarker. Vol. 12, Front. Immunol.; 2021. p. 646523.

239. Molgora M, Esaulova E, Vermi W, Hou J, Chen Y, Luo J, et al. TREM2 modulation remodels the tumor myeloid landscape enhancing anti-PD-1 immunotherapy. Vol. 182, Cell; 2020. p. 886-900.e17.

240. Nalio Ramos R, Missolo-Koussou Y, Gerber-Ferder Y, Bromley CP, Bugatti M, Núñez NG, et al. Tissue-resident FOLR2+ macrophages associate with CD8+ T cell infiltration in human breast cancer. Vol. 185, Cell; 2022. p. 1189-1207.e25.

241. Wu SZ, Al-Eryani G, Roden DL, Junankar S, Harvey K, Andersson A, et al. A single-cell and spatially resolved atlas of human breast cancers. Vol. 53, Nat. Genet.; 2021. p. 1334–1347.

242. Obradovic A, Chowdhury N, Haake SM, Ager C, Wang V, Vlahos L, et al. Single-cell protein activity analysis identifies recurrence-associated renal tumor macrophages. Vol. 184, Cell; 2021. p. 2988-3005.e16.

243. Azizi E, Carr AJ, Plitas G, Cornish AE, Konopacki C, Prabhakaran S, et al. Single-cell map of diverse immune phenotypes in the breast tumor microenvironment. Vol 174, Cell; 2018. p. 1293-1308.e36.

244. Xiong D, Wang Y, You M. A gene expression signature of TREM2^{hi} macrophages and γδ T cells predicts immunotherapy response. Vol. 11, Nat. Commun.; 2020. p. 5084.

245. Kemp SB, Steele NG, Carpenter ES, Donahue KL, Bushnell GG, Morris AH, et al. Pancreatic cancer is marked by complement-high blood monocytes and tumor-associated macrophages. Vol. 4, Life Sci. Alliance; 2021. p. 1–17.

246. Poliani PL, Wang Y, Fontana E, Robinette ML, Yamanishi Y, Gilfillan S, et al. TREM2 sustains microglial expansion during aging and response to demyelination. Vol. 125, J. Clin. Investig.; 2015. p. 2161–2170.

247. Cantoni C, Bollman B, Licastro D, Xie M, Mikesell R, Schmidt R, et al. TREM2 regulates microglial cell activation in response to demyelination in vivo. Vol. 129, Acta Neuropathol.; 2015. p. 429–447.

248. Rayaprolu S, Mullen B, Baker M, Lynch T, Finger E, Seeley WW, et al. TREM2 in neurodegeneration: Evidence for association of the p.R47H variant with frontotemporal dementia and Parkinson's disease. Vol. 8, Mol. Neurodegener.; 2013. p. 1-5.

249. Liu G, Liu Y, Jiang Q, Jiang Y, Feng R, Zhang L, et al. Convergent genetic and expression datasets highlight TREM2 in Parkinson's disease susceptibility. Vol. 53, Mol. Neurobiol.; 2016. p. 4931–4938.

250. Borroni B, Ferrari F, Galimberti D, Nacmias B, Barone C, Bagnoli S, et al. Heterozygous TREM2 mutations in frontotemporal dementia. Vol. 35, Neurobiol. Aging; 2014. p. 934.e7-934.e10.

251. Cuyvers E, Bettens K, Philtjens S, Van Langenhove T, Gijselinck I, van der Zee J, et al. Investigating the role of rare heterozygous TREM2 variants in Alzheimer's disease and frontotemporal dementia. Vol. 35, Neurobiol. Aging; 2014. p. 726.e11-726.e19.

252. Cady J, Koval ED, Benitez BA, Zaidman C, Jockel-Balsarotti J, Allred P, et al. TREM2 variant p.R47H as a risk factor for sporadic amyotrophic lateral sclerosis. Vol. 71, JAMA Neurol.; 2014. p. 449–453.

253. Jiang T, Yu JT, Zhu XC, Tan L. TREM2 in Alzheimer's disease. Vol. 48, Mol. Neurobiol.; 2013. p. 180–185.

254. Guerreiro R, Wojtas A, Bras J, Carrasquillo M, Rogaeva E, Majounie E, et al. TREM2 variants in Alzheimer's disease. Vol. 368, N. Engl. J. Med.; 2013. p. 117–27.

255. Jonsson T, Stefansson H, Steinberg S, Jonsdottir I, Jonsson P V., Snaedal J, et al. Variant of TREM2 associated with the risk of Alzheimer's disease. Vol. 368, N. Engl. J. Med.; 2013. p. 107–116.

256. Long JM, Holtzman DM. Alzheimer disease: An update on pathobiology and treatment strategies. Vol. 179, Cell; 2019. p. 312–339.

257. Lessard CB, Malnik SL, Zhou Y, Ladd TB, Cruz PE, Ran Y, et al. High-affinity interactions and signal transduction between Aβ oligomers and TREM 2. Vol. 10, EMBO Mol. Med.; 2018. p. e9027.

258. Zhong L, Wang Z, Wang D, Wang Z, Martens YA, Wu L, et al. Amyloid-beta modulates microglial responses by binding to the triggering receptor expressed on myeloid cells 2 (TREM2). Vol. 13, Mol. Neurodegener.; 2018. p. 1-12.

259. Zhao Y, Wu X, Li X, Jiang LL, Gui X, Liu Y, et al. TREM2 is a receptor for β-amyloid that mediates microglial function. Vol. 97, Neuron; 2018. p. 1023-1031.e7.

260. Zhou Y, Song WM, Andhey PS, Swain A, Levy T, Miller KR, et al. Human and mouse single-nucleus transcriptomics reveal TREM2-dependent and TREM2-independent cellular responses in Alzheimer's disease. Vol. 26, Nat. Med.; 2020. p. 131–142.

261. Song WM, Joshita S, Zhou Y, Ulland TK, Gilfillan S, Colonna M. Humanized TREM2 mice reveal microglia-intrinsic and -extrinsic effects of R47H polymorphism. Vol. 215, J. Exp. Med.; 2018. p. 745–760.

262. Zhou Y, Song WM, Andhey PS, Swain A, Levy T, Miller KR, et al. Human and mouse single-nucleus transcriptomics reveal TREM2-dependent and TREM2-independent cellular responses in Alzheimer's disease. Vol. 26, Nat. Med.; 2020. p. 131–142.

263. Song W, Hooli B, Mullin K, Jin SC, Cella M, Ulland TK, et al. Alzheimer's disease-associated TREM2 variants exhibit either decreased or increased ligand-dependent activation. Vol. 13, Alzheimers. Dement.; 2017. p. 381–387.

264. Kober DL, Alexander-Brett JM, Karch CM, Cruchaga C, Colonna M, Holtzman MJ, et al. Neurodegenerative disease mutations in TREM2 reveal a functional surface and distinct loss-of-function mechanisms. Vol. 5, Elife; 2016. e20391.

265. Menzies GE, Sims R, Williams J. Molecular Dynamics simulations of TREM2 variants R47H and R62H show structural alterations at key binding regions leading to possible implications for mechanisms in Alzheimer's disease. 2019.

266. Wang S, Sudan R, Peng V, Zhou Y, Du S, Yuede CM, et al. TREM2 drives microglia response to amyloid-β via SYK-dependent and -independent pathways. Vol. 185, Cell; 2022. p. 4153-4169.e19.

267. Wang S, Mustafa M, Yuede CM, Salazar SV, Kong P, Long H, et al. Anti-human TREM2 induces microglia proliferation and reduces pathology in an Alzheimer's disease model. Vol. 217, J. Exp. Med.; 2020. e20200785.

268. Ellwanger DC et al. Prior activation state shapes the microglia response to antihuman TREM2 in a mouse model of Alzheimer's disease. Vol. 118, PNAS; 2021. e2017742118.

269. Schlepckow K, Monroe KM, Kleinberger G, Cantuti-Castelvetri L, Parhizkar S, Xia D, et al. Enhancing protective microglial activities with a dual function TREM 2 antibody to the stalk region. Vol. 12, EMBO Mol. Med.; 2020. e11227.

270. Pham AQ, Dore K. Novel approaches to increase synaptic resilience as potential treatments for Alzheimer's disease. Vol. 139, Semin. Cell Dev. Biol.; 2023. p. 84–92.

271. Gallo C, Barra G, Saponaro M, Manzo E, Fioretto L, Ziaco M, et al. A new bioassay platform design for the discovery of small molecules with anticancer immunotherapeutic activity. Vol. 18, Mar. Drugs; 2020. p. 604.

272. Manzo E, Gallo C, Sartorius R, Nuzzo G, Sardo A, De Berardinis P, et al. Immunostimulatory Phosphatidylmonogalactosyldiacylglycerols (PGDG) from the marine diatom Thalassiosira weissflogii: Inspiration for a novel synthetic toll-like receptor 4 agonist. Vol. 17, Mar. Drugs; 2019. p. 103.

273. Lauritano C, Andersen JH, Hansen E, Albrigtsen M, Escalera L, Esposito F, et al. Bioactivity screening of microalgae for antioxidant, anti-inflammatory, anticancer, anti-diabetes, and antibacterial activities. Vol. 3, Front. Mar. Sci.; 2016. p. 68.

274. Gallo C, D'Ippolito G, Nuzzo G, Sardo A, Fontana A. Autoinhibitory sterol sulfates mediate programmed cell death in a bloom-forming marine diatom. Vol. 8, Nat. Commun.; 2017. p. 1292.

275. Goodridge HS, Simmons RM, Underhill DM. Dectin-1 stimulation by Candida albicans yeast or zymosan triggers NFAT activation in macrophages and dendritic cells 1. Vol. 178, J. Immunol.; 2007. p. 3107-3115.

276. Gallo C, Nuzzo G, d'Ippolito G, Manzo E, Sardo A, Fontana A. Sterol sulfates and sulfotransferases in marine diatoms. Vol. 605, Meth. Enzymol.; 2018. p. 101–138.

277. Kostarnoy A V., Gancheva PG, Lepenies B, Tukhvatulin AI, Dzharullaeva AS, Polyakov NB, et al. Receptor Mincle promotes skin allergies and is capable of recognizing cholesterol sulfate. Vol. 114, Proc. Natl. Acad. Sci. USA; 2017. p. E2758–2765.

278. Kiyotake R, Oh-Hora M, Ishikawa E, Miyamoto T, Ishibashi T, Yamasaki S. Human mincle binds to cholesterol crystals and triggers innate immune responses. Vol. 290, J. Biol. Chem.; 2015. p. 25322–25332.

279. Huang Y, Cui J, Li Y, Fan L, Jiao Y, Su S. Syntheses and antiproliferative activity of some sulfated hydroximinosterols. Vol. 22, Med. Chem. Res.; 2013. p. 409–414.

280. Correia-da-Silva M, Sousa E, Pinto MMM. Emerging sulfated flavonoids and other polyphenols as drugs: Nature as an inspiration. Vol. 34, Med. Res. Rev.; 2014. p. 223–279.

281. Sun Q, Cai S, Peterson BR. Practical synthesis of 3β-amino-5-cholestene and related 3β-halides involving i-steroid and retro-i-steroid rearrangements. Vol. 11, Org. Lett.; 2009. p. 567–570.

282. Oza VB, Corcoran RC. A mild preparation of protected phosphate esters from alcohols. Vol. 60, J. Org. Chem.; 1995. p. 3680-3684.

283. Chrobak E, Kadela-Tomanek M, Bębenek E, Marciniec K, Wietrzyk J, Trynda J, et al. New phosphate derivatives of betulin as anticancer agents: Synthesis, crystal structure, and molecular docking study. Vol. 87, Bioorg. Chem.; 2019. p. 613–628.

284. Zemplén G, Kunz A. Studien über Amygdalin, IV: Synthese des natürlichen l-Amygdalins. Vol. 57, Ber. Dtsch. Chem.; 1924. p. 1357-1359.

285. Wahlstrom JL, Ronald RC, Roh M. Organic chemistry of nucleic acids. Vol. 84, J. Chem. Soc., Chem. Commun. Wiley; 1969.

286. Coffman RL, Sher A, Seder RA. Vaccine adjuvants: Putting innate immunity to work. Vol. 33, Immunity; 2010. p. 492–503.

287. Tze LE, Horikawa K, Domaschenz H, Howard DR, Roots CM, Rigby RJ, et al. CD83 increases MHC II and CD86 on dendritic cells by opposing IL-10 - Driven MARCH1-mediated ubiquitination and degradation. Vol. 208, J. Exp. Med.; 2011. p. 149–165.

288. Heufler C, Koch F, Stanzl U, Topar G, Wysocka M, Trinchieri G, et al. Interleukin-12 is produced by dendritic cells and mediates T helper 1 development as well as

interferon-γ production by T helper 1 cells. Vol. 26, Eur. J. Immunol.; 1996. p. 659–668.

289. Humphrey MB, Xing J, Titus A. The TREM2-DAP12 signaling pathway in Nasu-Hakola disease: a molecular genetics perspective. Vol. 89, Res. Rep. Biochem.; 2015. p. 89-100.

290. Deczkowska A, Weiner A, Amit I. The physiology, pathology, and potential therapeutic applications of the TREM2 signaling pathway. Vol. 181, Cell.; 2020. p. 1207–1217.

291. Ulland TK, Colonna M. TREM2 - a key player in microglial biology and Alzheimer disease. Vol. 14, Nat. Rev. Neurol.; 2018. p. 667–675.

292. Appel R. Tertiary phosphane/tetrachloromethane, a versatile reagent for chlorination, dehydration, and P-N linkage. Vol. 14, Angew. Chem. Int. Ed. Engl.; 1975. p. 801-811.

293. Wang Hg. Comprehensive organic name reactions. Vol. 2, Germany: Wiley; 2010. p. 2498-2502.

294. Traboni S, Bedini E, Iadonisi A. Solvent-free conversion of alcohols to alkyl iodides and one-pot elaborations thereof. Vol. 3, ChemistrySelect; 2018. p. 1616–1622.

295. Wang Y, Cella M, Mallinson K, Ulrich JD, Young KL, Robinette ML, et al. TREM2 lipid sensing sustains the microglial response in an Alzheimer's disease model. Vol. 160, Cell; 2015. p. 1061–1071.

296. Li X, Zhao X, Fang Y, Jiang X, Duong T, Fan C, et al. Generation of destabilized green fluorescent protein as a transcription reporter. Vol. 273, J. Biol. Chem.; 1998. p. 34970-34975.

297. Soboleski MR, Oaks J, Halford WP. Green fluorescent protein is a quantitative reporter of gene expression in individual eukaryotic cells. Vol. 19, FASEB J.; 2005. p. 1–20.

298. Staudinger von H, Meyer J. Uber neue organische Phosphorverbindungen 111. Phosphinmethylenderivate und Phosphinimine. Vol. 2, Helv. Chim. Acta; 1919. p. 635-646.

299. Hou A, Hou A, Chen H, Chen H, Zheng C, Xie K, et al. Assembly of a fluorescent chiral photonic crystal membrane and its sensitive responses to multiple signals induced by small molecules. Vol. 14, ACS Nano; 2020. p. 7380–7388.

300. Zhou E, Gong S, Xia Q, Feng G. In vivo imaging and tracking carbon monoxide-releasing molecule-3 with an NIR fluorescent probe. Vol. 6, ACS Sens; 2021. p. 1312–1320.

301. Zhao J, Liu Y, Park HJ, Boggs JM, Basu A. Carbohydrate-coated fluorescent silica nanoparticles as probes for the galactose/3-sulfogalactose carbohydrate-carbohydrate interaction using model systems and cellular binding studies. Vol. 23, Bioconjug. Chem.; 2012. p. 1166–1173.

302. Quah BJC, Parish CR. New and improved methods for measuring lymphocyte proliferation in vitro and in vivo using CFSE-like fluorescent dyes. Vol. 379, J. Immunol. Methods; 2012. p. 1–14.

303. Liu X, Dong T, Zhou Y, Huang N, Lei X. Exploring the binding proteins of glycolipids with bifunctional chemical probes. Vol. 128, Angew. Chem.; 2016. p. 14542–14546.

304. Gutzeit HO, Henker Y, Kind B, Franz A. Specific interactions of quercetin and other flavonoids with target proteins are revealed by elicited fluorescence. Vol. 318, Biochem. Biophys. Res. Commun.; 2004. p. 490–495.

305. Drummen GPC. Fluorescent probes and fluorescence (microscopy) techniques-illuminating biological and biomedical research. Vol. 17, Mol.; 2012. p. 14067–14090.

306. Yan H, Yalagala RS, Yan F. Fluorescently labelled glycans and their applications. Vol. 32, Glycoconj. J.; 2015. p. 559–579.

307. Liu Y, Bittman R. Synthesis of fluorescent lactosylceramide stereoisomers. Vol. 142, Chem. Phys. Lipids; 2006. p. 58–69.

308. Daikoku S, Ono Y, Ohtake A, Hasegawa Y, Fukusaki E, Suzuki K, et al. Fluorescence-monitored zero dead-volume nanoLC-microESI-QIT-TOF MS for analysis of fluorescently tagged glycosphingolipids. Vol. 136, Analyst.; 2011. p. 1046–1050.

309. Pagano RE, Puri V, Dominguez M, Marks DL. Membrane traffic in sphingolipid storage diseases. Vol. 1, Traffic; 2000. p. 807–815.

310. Arai K, Kanie Y, Kanie O, Fukase K, Kabayama K. Temporal analysis of localization and trafficking of glycolipids. Vol. 532, Biochem. Biophys. Res. Commun.; 2020. p. 19–24.

311. Boens N, Leen V, Dehaen W. Fluorescent indicators based on BODIPY. Vol. 41, Chem. Soc. Rev.; 2012. p. 1130–1172.

312. Ni Y, Wu J. Far-red and near infrared BODIPY dyes: Synthesis and applications for fluorescent pH probes and bio-imaging. Vol. 12, Org. Biomol. Chem.; 2014. p. 3774–3791.

313. Pagano RE, Martin OC, Kang HC, Haugland RP. A novel fluorescent ceramide analogue for studying membrane traffic in animal cells: Accumulation at the Golgi apparatus results in altered spectral properties of the sphingolipid precursor. Vol. 113, J. Cell Biol.; 1991. p. 1267-1279.

314. Rasmussen JAM, Hermetter A. Chemical synthesis of fluorescent glycero- and sphingolipids. Vol. 47, Prog. Lipid Res.; 2008. p. 436–460.

315. Karolin J, Lennart B-AJ, Strandberg L, Ny T. Fluorescence and absorption spectroscopic properties of dipyrrometheneboron difluoride (BODIPY) derivatives in liquids, lipid membranes, and proteins. Vol. 116, J. Am. Chem. Soc.; 1994. p. 7801-7806.

316. Johnson ID, Kang HC, Haugland RP. Fluorescent membrane probes incorporating dipyrrometheneboron difluoride fluorophores. Vol. 198, Anal. Biochem.; 1991. p. 228-237.

317. Boldyrev IA, Zhai X, Momsen MM, Brockman HL, Brown RE, Molotkovsky JG. New BODIPY lipid probes for fluorescence studies of membranes. Vol. 48, J. Lipid Res.; 2007. p. 1518–1532.

318. Bittman R. The 2003 ASBMB-Avanti Award in Lipids Address: Applications of novel synthetic lipids to biological problems. Vol. 129, Chem. Phys. Lipids.; 2004. p. 111–131.

319. Yeum KJ, Aldini G, Chung HY, Krinsky NI, Russell RM. The activities of antioxidant nutrients in human plasma depend on the localization of attacking radical species. Vol. 133, J. Nutr.; 2003. p. 2688-2691.

320. Drummen GPC, Van Liebergen LCM, Op Den Kamp JAF, Post JA. C11-BODIPY 581/591. An oxidation-sensitive fluorescent lipid peroxidation probe: (micro)spectroscopic characterization and validation of methodology. Vol. 33, Free Radic. Biol. Med.; 2002. p. 473-490.

321. Guseva GB, Antina E V., Berezin MB, Pavelyev RS, Kayumov AR, Sharafutdinov IS, et al. Meso-substituted-BODIPY based fluorescent biomarker: Spectral characteristics, photostability and possibilities for practical application. Vol. 401, J. Photochem. Photobiol. A Chem.; 2020. p. 112783.

322. Boldyrev IA, Molotkovsky JG. A synthesis and properties of new 4,4-difluoro-3a,4a-diaza-s-indacene (BODIPY)-labeled lipids. Vol. 32, Russ. J. Bioorg. Chem.; 2006. p. 78–83.

323. Loudet A, Burgess K. BODIPY dyes and their derivatives: Syntheses and spectroscopic properties. Vol. 107, Chem. Rev.; 2007. p. 4891–4932.

324. Berendsen MGE, Billiet MHA, Vos De Wael E, Pardoen JA, Van Koeveringe JA, Lugtenburg J. Pyrromethene-BF, complexes (4,4'-difluoro-4-bora-3a,4adiaza-s-indacenes). Synthesis and luminescence properties. Vol. 96, Recl. Trav. Chim. Pays-Bas; 1977. p. 306-309.

325. Ziaco M, Fioretto L, Nuzzo G, Fontana A, Manzo E. Short gram-scale synthesis of sulfavant A. Vol. 24, Org. Process Res. Dev.; 2020. p. 2728–2733.

326. Fioretto L, Ziaco M, Gallo C, Nuzzo G, d'Ippolito G, Lupetti P, et al. Direct evidence of the impact of aqueous self-assembly on biological behavior of amphiphilic molecules: The case study of molecular immunomodulators Sulfavants. Vol. 611, J. Colloid Interface Sci.; 2022. p. 129–136.

327. Manzo E, Fioretto L, Pagano D, Nuzzo G, Gallo C, De Palma R, et al. Chemical synthesis of marine-derived sulfoglycolipids, a new class of molecular adjuvants. Vol. 15, Mar. Drugs; 2017. p. 288.

328. Manzo E, Ciavatta ML, Pagano D, Fontana A. An efficient and versatile chemical synthesis of bioactive glyco-glycerolipids. Vol. 53, Tetrahedron Lett.; 2012. p. 879–881.

329 Pagano D, Cutignano A, Manzo E, Tinto F, Fontana A. Glycolipids synthesis: improved hydrazinolysis conditions for preparation of 1,2-polyunsaturated fatty acyl-β-monogalactosyl-glycerols. Vol. 424, Carbohydr. Res.; 2016. p. 21–23.

330. Taraska JW, Zagotta WN. Fluorescence applications in molecular neurobiology. Vol. 66, Neuron; 2010. p. 170–189.

331. Leblond F, Davis SC, Valdés PA, Pogue BW. Pre-clinical whole-body fluorescence imaging: Review of instruments, methods and applications. Vol. 98, J. Photochem. Photobiol. B Biol.; 2010. p. 77–94.

332. Coste A, Oktay MH, Condeelis JS, Entenberg D. Intravital imaging techniques for biomedical and clinical research. Vol. 97, Cytometry A.; 2020. p. 448–457.

333. Refaat A, Yap ML, Pietersz G, Walsh APG, Zeller J, del Rosal B, et al. In vivo fluorescence imaging: success in preclinical imaging paves the way for clinical applications. Vol. 20, J. Nanobiotechnology; 2022. p. 1-22.

334. Weissleder R, Nahrendorf M, Pittet MJ. Imaging macrophages with nanoparticles. Vol. 13, Nat. Mater.; 2014. p. 125–138.

335. Yang J, Fu Z, Zhang X, Xiong M, Meng L, Zhang Z. TREM2 ectodomain and its soluble form in Alzheimer's disease. Vol. 17, J. Neuroinflammation; 2020. p. 1-12.

336. Kleinberger G, Yamanishi Y, Suárez-Calvet M, Czirr E, Lohmann E, Cuyvers E, et al. TREM2 mutations implicated in neurodegeneration impair cell surface transport and phagocytosis. Vol. 6, Sci. Transl. Med.; 2014. p. 243ra86.

337. Wolf EM, Fingleton B, Hasty AH. The therapeutic potential of TREM2 in cancer. Vol. 12, Front. Oncol.; 2022. p. 984193.

338. Lu JW, Ho YJ, Ciou SC, Gong Z. Innovative disease model: Zebrafish as an in vivo platform for intestinal disorder and tumors. Vol. 5, Biomedicines; 2017. p. 58.

339. Hason M, Bartůněk P. Zebrafish models of cancer-new insights on modeling human cancer in a non-mammalian vertebrate. Vol. 10, Genes; 2019. p. 935.

340. Quan DN, Cooper MD, Potter JL, Roberts MH, Cheng H, Jarvis GA. TREM-2 binds to lipooligosaccharides of Neisseria gonorrhoeae and is expressed on reproductive tract epithelial cells. Vol. 1, Mucosal. Immunol.; 2008. p. 229–238.

341. Dabla A, Liang YC, Rajabalee N, Irwin C, Moonen CGJ, Willis J V., et al. TREM2 promotes immune evasion by mycobacterium tuberculosis in human macrophages. Vol. 13, MBio; 2022. e01456-22.

342. Colonna M. Trems in the immune system and beyond. Vol. 3, Nat. Rev. Immunol.; 2003. p. 445–453.

343. Dean HB, Roberson ED, Song Y. Neurodegenerative disease–associated variants in TREM2 destabilize the apical ligand-binding region of the immunoglobulin domain. Vol. 10, Front. Neurol.; 2019. p. 1252.

344. Yuan P, Condello C, Keene CD, Wang Y, Bird TD, Paul SM, et al. TREM2 haplodeficiency in mice and humans impairs the microglia barrier function leading to decreased amyloid compaction and severe axonal dystrophy. Vol. 90, Neuron; 2016. p. 724–739.

345. Kober DL, Stuchell-Brereton MD, Kluender CE, Dean HB, Strickland MR, Steinberg DF, et al. Functional insights from biophysical study of TREM2 interactions with apoE and Aβ1-42. Vol. 17, Alzheimers. Dement.; 2021. p. 475–488.

346. Xue T, Ji J, Sun Y, Huang X, Cai Z, Yang J, et al. Sphingosine-1-phosphate, a novel TREM2 ligand, promotes microglial phagocytosis to protect against ischemic brain injury. Vol. 12, Acta Pharm. Sin. B; 2022. p. 1885–1898.

347. Genheden S, Ryde U. The MM/PBSA and MM/GBSA methods to estimate ligand-binding affinities. Vol. 10, Expert Opin. Drug Discov.; 2015. p. 449–461.

348. Iizasa E, Chuma Y, Uematsu T, Kubota M, Kawaguchi H, Umemura M, et al. TREM2 is a receptor for non-glycosylated mycolic acids of mycobacteria that limits anti-mycobacterial macrophage activation. Vol. 12, Nat. Commun.; 2021. p. 2299.

349. Shirotani K, Hori Y, Yoshizaki R, Higuchi E, Colonna M, Saito T, et al. Aminophospholipids are signal-transducing TREM2 ligands on apoptotic cells. Vol. 9, Sci. Rep.; 2019. p. 7508.

350. Saravanan C, Liu FT, Gipson IK, Panjwani N. Galectin-3 promotes lamellipodia formation in epithelial cells by interacting with complex N-glycans on α3β1 integrin. Vol. 122, J. Cell Sci.; 2009. p. 3684–3693.

351. Thode C, Woetmann A, Wandall HH, Carlsson MC, Qvortrup K, Kauczok CS, et al. Malignant T cells secrete galectins and induce epidermal hyperproliferation and disorganized stratification in a skin model of cutaneous T-cell lymphoma. Vol. 135, J. Dermatol.; 2015. p. 238–246.

352. Adria Â N Rabinovich G. Galectins: an evolutionarily conserved family of animal lectins with multifunctional properties; a trip from the gene to clinical therapy. Vol. 6, Cell Death Differ.; 1999. p. 711-721.

353. Cooper DNW, Barondes SH. God must love galectins; he made so many of them. Vol. 9-10, Glycobiol.; 1999. p. 979-984.

354. Liu FT. Galectins: A new family of regulators of inflammation. Vol. 97, Clin. Immunol.; 2000. p. 79–88.

355. Corfield AP. The interaction of the gut microbiota with the mucus barrier in health and disease in human. Vol. 6, Microorganisms; 2018. p. 78.

356. Salomonsson E, Carlsson MC, Osla V, Hendus-Altenburger R, Kahl-Knutson B, Öberg CT, et al. Mutational tuning of galectin-3 specificity and biological function. Vol. 285, J. Biol. Chem.; 2010. p. 35079–35091.

357. Yang RY, Rabinovich GA, Liu FT. Galectins: Structure, function and therapeutic potential. Vol. 10, Expert Rev. Mol. Med.; 2008. e17.

358. Leffler H, Carlsson S, Hedlund M, Qian Y, Poirier F. Introduction to galectins. Vol. 19, Glycoconj. J.; 2002. p. 433-440.

359. Cooper DN. Galectin-1: secretion and modulation of cell interactions with laminin. Vol. 9, Trends Glycosci. Glycotechnol.; 1997. p. 57-67.

360. Mehul B, Hughes RC. Plasma membrane targetting, vesicular budding and release of galectin 3 from the cytoplasm of mammalian cells during secretion. Vol. 110, J. Cell Sci.; 1997. p. 1169-1178.

361. Gorski JP, Liu FT, Artigues A, Castagna LF, Osdoby P. New alternatively spliced form of galectin-3, a member of the β-galactoside-binding animal lectin family, contains a predicted transmembrane-spanning domain and a leucine zipper motif. Vol. 277, J. Biol. Chem.; 2002. p. 18840–18848.

362. Pereira MS, Alves I, Vicente M, Campar A, Silva MC, Padrão NA, et al. Glycans as key checkpoints of T cell activity and function. Vol. 9, Front. immunol.; 2018. p. 2754.

363. Gilson RC, Gunasinghe SD, Johannes L, Gaus K. Galectin-3 modulation of T-cell activation: mechanisms of membrane remodelling. Vol. 76, Prog. Lipid Res.; 2019. p. 101010.

364. Thiemann S, Baum LG. Galectins and Immune Responses-Just How Do They Do Those Things They Do? Vol. 34, Annu. Rev. Immunol.; 2016. p. 243–264.

365. Murali-Krishna K, Altman JD, Suresh M, Sourdive DJD, Zajac AJ, Miller JD, et al. Counting antigen-specific CD8 T cells: a reevaluation of bystander activation during viral infection. Vol. 8, Immunity; 1998. p. 177-187.

366. Pardo E, Cárcamo C, Martín RUS, Ciampi E, Segovia-Miranda F, Curkovic-Peña C, et al. Galectin-8 as an immunosuppressor in experimental autoimmune encephalomyelitis and a target of human early prognostic antibodies in multiple sclerosis. Vol. 12, PLoS One; 2017. e0177472.

367. Toscano MA, Bianco GA, Ilarregui JM, Croci DO, Correale J, Hernandez JD, et al. Differential glycosylation of TH1, TH2 and TH-17 effector cells selectively regulates susceptibility to cell death. Vol. 8, Nat. Immunol.; 2007. p. 825–834.

368. Zhu C, Anderson AC, Schubart A, Xiong H, Imitola J, Khoury SJ, et al. The Tim-3 ligand galectin-9 negatively regulates T helper type 1 immunity. Vol. 6, Nat. Immunol.; 2005. p. 1245–1452.

369. Sturm A, Lensch M, André S, Kaltner H, Wiedenmann B, Rosewicz S, et al. Human galectin-2: Novel inducer of T cell apoptosis with distinct profile of caspase activation. Vol. 173, J. Immunol.; 2004. p. 3825–3837.

370. Perillo NL, Pace KE, Seilhamer JJ, Baum LG. Apoptosis of T cells mediated by galectin-1. Vol. 378, Nature; 1995. p. 736-739.

371. Oliveira FL, Bernardes ES, Brand C, dos Santos SN, Cabanel MP, Arcanjo KD, et al. Lack of galectin-3 up-regulates IgA expression by peritoneal B1 lymphocytes during B cell differentiation. Vol. 363, Cell Tissue Res.; 2016. p. 411–426.

372. Liang CC, Li CS, Weng IC, Chen HY, Lu HH, Huang CC, et al. Galectin-9 is critical for mucosal adaptive immunity through the T helper 17–IgA axis. Vol. 188, Am. J. Pathol.; 2018. p. 1225–1235.

373. Liu FT, Stowell SR. The role of galectins in immunity and infection. Nat. Rev. Immunol.; 2023. p. 1-16.

374. Fermin Lee A, Chen HY, Wan L, Wu SY, Yu JS, Huang AC, et al. Galectin-3 modulates Th17 responses by regulating dendritic cell cytokines. Vol. 183, Am. J. Pathol.; 2013. p. 1209–1922.

375. Jiang HR, Al Rasebi Z, Mensah-Brown E, Shahin A, Xu D, Goodyear CS, et al. Galectin-3 Deficiency Reduces the Severity of Experimental Autoimmune Encephalomyelitis. Vol. 182, J. Immunol.; 2009. p. 1167-1173.

376. Reichert F, Rotshenker S. Galectin-3 (MAC-2) controls microglia phenotype whether amoeboid and phagocytic or branched and non-phagocytic by regulating the cytoskeleton. Vol. 13, Front. Cell Neurosci.; 2019. p. 90.

377. Querol Cano L, Tagit O, Dolen Y, van Duffelen A, Dieltjes S, Buschow SI, et al. Intracellular galectin-9 controls dendritic cell function by maintaining plasma membrane rigidity. Vol. 22, iScience; 2019. p. 240–255.

378. Siew JJ, Chen HM, Chen HY, Chen HL, Chen CM, Soong BW, et al. Galectin-3 is required for the microglia-mediated brain inflammation in a model of Huntington's disease. Vol. 10, Nat. Commun.; 2019. p. 3473.

379. Burbidge K, Rademacher DJ, Mattick J, Zack S, Grillini A, Bousset L, et al. LGALS3 (galectin 3) mediates an unconventional secretion of SNCA/α-synuclein in response to lysosomal membrane damage by the autophagic-lysosomal pathway in human midbrain dopamine neurons. Vol. 18, Autophagy; 2022. p. 1020–1048.

380. Jiang P, Gan M, Yen SH, McLean PJ, Dickson DW. Impaired endo-lysosomal membrane integrity accelerates the seeding progression of α-synuclein aggregates. Vol. 7, Sci. Rep.; 2017. p. 1-13.

381. Schjoldager KT, Narimatsu Y, Joshi HJ, Clausen H. Global view of human protein glycosylation pathways and functions. Vol. 21, Nat. Rev. Mol. Cell Biol.; 2020. p. 729–749.

382. Krautter F, Iqbal AJ. Glycans and glycan-binding proteins as regulators and potential targets in leukocyte recruitment. Vol. 9, Front. Cell Dev. Biol.; 2021. p. 624082.

383. Varki A, Cummings RD, Esko JD, Freeze HH, Stanley P, Marth JD, et al. Symbol nomenclature for glycan representation. Vol. 9, Proteomics; 2009. p. 5398–5399.

384. Varki A. Biological roles of glycans. Vol. 27, Glycobiol.; 2017. p. 3–49.

385. Fontana C, Widmalm G. Primary structure of glycans by NMR spectroscopy. Vol. 123, Chem. Rev.; 2023. p. 1040–1102.

386. Gabius HJ, André S, Jiménez-Barbero J, Romero A, Solís D. From lectin structure to functional glycomics: Principles of the sugar code. Vol. 36, Trends Biochem. Sci.; 2011. p. 298–313.

387. Gordon S. Pattern recognition receptors: doubling up for the innate immune response. Vol. 111, Cell; 2002. p. 927-930.

388. Johannes L, Jacob R, Leffler H. Galectins at a glance. Vol. 131, J. Cell Sci.; 2018. jcs208884.

389. Laaf D, Bojarová P, Elling L, Křen V. Galectin–carbohydrate interactions in biomedicine and biotechnology. Vol. 37, Trends Biotechnol.; 2019. p. 402–415.

390. Bertuzzi S, Quintana JI, Ardá A, Gimeno A, Jiménez-Barbero J. Targeting galectins with glycomimetics. Vol. 8, Front. Chem.; 2020. p. 8593.

391. Spiwok V. CH/π interactions in carbohydrate recognition. Vol. 22, Mol.; 2017. p. 1038.

392. Di Lella S, Sundblad V, Cerliani JP, Guardia CM, Estrin DA, Vasta GR, et al. When galectins recognize glycans: From biochemistry to physiology and back again. Vol. 50, Biochem.; 2011. p. 7842–7857.

393. Hsieh SL. Lectin in host defense against microbial infections. Vol. 1204, Singapore: Springer; 2020.

394. Asensio JL, Ardá A, Cañada FJ, Jiménez-Barbero J. Carbohydrate-aromatic interactions. Vol. 46, Acc. Chem. Res.; 2013. p. 946–954.

395. Valverde P, Quintana JI, Santos JI, Ardá A, Jiménez-Barbero J. Novel NMR avenues to explore the conformation and interactions of glycans. Vol. 4, ACS Omega; 2019. p. 13618–13630.

396. Ardá A, Jiménez-Barbero J. The recognition of glycans by protein receptors. Insights from NMR spectroscopy. Vol. 54, Chem. Comm.; 2018. p. 4761–4769.

397. Shishmarev D, Fontenelle CQ, Kuprov I, Linclau B, Kuchel PW. Transmembrane exchange of fluorosugars: characterization of Red Cell GLUT1 kinetics using 19F NMR. Vol. 115, Biophys. J.; 2018. p. 1906–1919.

398. Lete MG, Franconetti A, Bertuzzi S, Delgado S, Azkargorta M, Elortza F, et al. NMR Investigation of protein-carbohydrate interactions: the recognition of glycans by galectins engineered with fluorotryptophan residues. Vol. 29, Chem. - Eur. J.; 2023. e202202208.

399. Diercks T, Infantino AS, Unione L, Jiménez-Barbero J, Oscarson S, Gabius HJ. Fluorinated Carbohydrates as Lectin Ligands: Synthesis of OH/F-substituted N-glycan core trimannoside and epitope mapping by 2D STD-TOCSYreF NMR spectroscopy. Vol. 24, Chem. - Eur. J.; 2018. p. 15761–15765.

400. Wamhoff EC, Hanske J, Schnirch L, Aretz J, Grube M, Varón Silva D, et al. 19F NMR-guided design of glycomimetic langerin ligands. Vol. 11, ACS Chem. Biol.; 2016. p. 2407–2413.

401. Nielsen MI, Stegmayr J, Grant OC, Yang Z, Nilsson UJ, Boos I, et al. Galectin binding to cells and glycoproteins with genetically modified glycosylation reveals galectin–glycan specificities in a natural context. Vol. 293, J. Biol. Chem.; 2018. p. 20249–20262.

402. Nason R, Büll C, Konstantinidi A, Sun L, Ye Z, Halim A, et al. Display of the human mucinome with defined O-glycans by gene engineered cells. Vol. 12, Nat. Commun.; 2021. p. 4070.

403. Crowley PB, Kyne C, Monteith WB. Simple and inexpensive incorporation of 19F-tryptophan for protein NMR spectroscopy. Vol. 48, Chem. Comm.; 2012. p. 10681–10683.

404. Kitevski-Leblanc J. Development and spplication of 19F NMR of proteins. 2010. PhD Thesis.

405. Kim HW, Perez JA, Ferguson SJ, Campbell ID. The specific incorporation of labelled aromatic amino acids into proteins through growth of bacteria in the presence of glyphosate Application to fluorotryptophan labelling to the H^+-ATPase of Escherichia coli and NMR studies. Vol. 272, FEBS Lett.; 1990. p. 34-36.

406. Gómez-Redondo M, Delgado S, Núñez-Franco R, Jiménez-Osés G, Ardá A, Jiménez-Barbero J, et al. The two domains of human galectin-8 bind sialyl-and fucose-containing oligosaccharides in an independent manner. A 3D view by using NMR. Vol. 2, RSC Chem. Biol.; 2021. p. 932–941.

407. Bertuzzi S, Gimeno A, Núñez-Franco R, Bernardo-Seisdedos G, Delgado S, Jiménez-Osés G, et al. Unravelling the time scale of conformational plasticity and allostery in glycan recognition by human galectin-1. Vol. 26, Chem. - Eur. J.; 2020. p. 15643–15653.

408. Gimeno A, Delgado S, Valverde P, Bertuzzi S, Berbís MA, Echavarren J, et al. Minimizing the entropy penalty for ligand binding: Lessons from the molecular recognition of the histo blood-group antigens by human galectin-3. Vol. 131, Angew. Chem.; 2019. p. 7346–7350.

409. Moure MJ, Gimeno A, Delgado S, Diercks T, Boons GJ, Jiménez-Barbero J, et al. Selective 13C-labels on repeating glycan oligomers to reveal protein binding epitopes through NMR: Polylactosamine binding to galectins. Vol. 60, Angew. Chem. Int. Ed.; 2021. p. 18777–18782.

410. Biannic B, Bozell JJ, Elder T. Steric effects in the design of Co-Schiff base complexes for the catalytic oxidation of lignin models to para-benzoquinones. Vol. 16, Green Chem.; 2014. p. 3635-3642.

Appendix

The ^{1}H-NMR and HSQC-NMR spectra of the following compounds are given below: Compound **17**, Sulf-Eterate, Sulf-BODIPY, Sulf-A-C6.

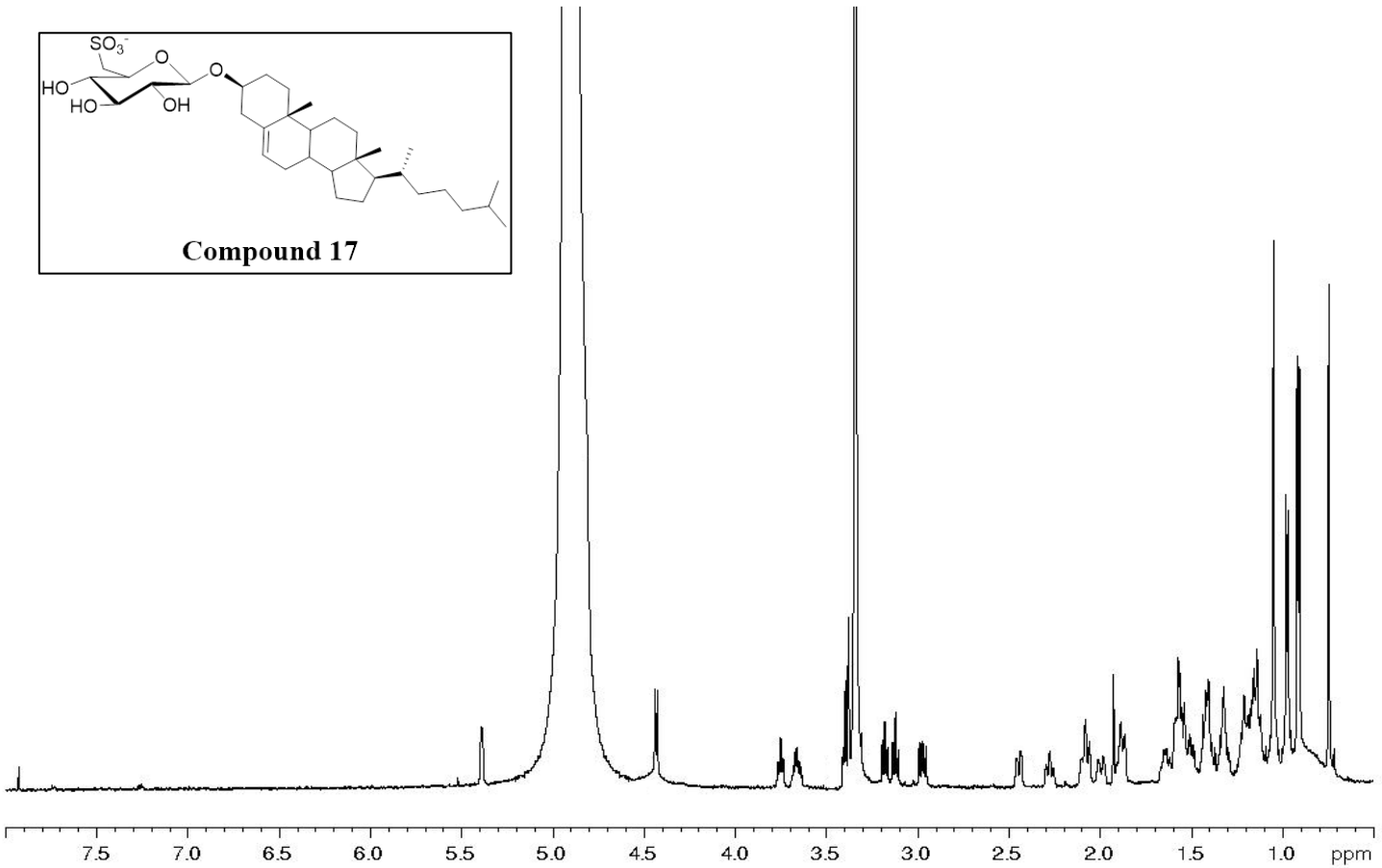
SO3-
O
O
HO
HO
OH
Compound 17
7.5
7.0
6.5
6.0
5.5
5.0
4.5
4.0
3.5
3.0
2.5
2.0
1.5
1.0
ppm

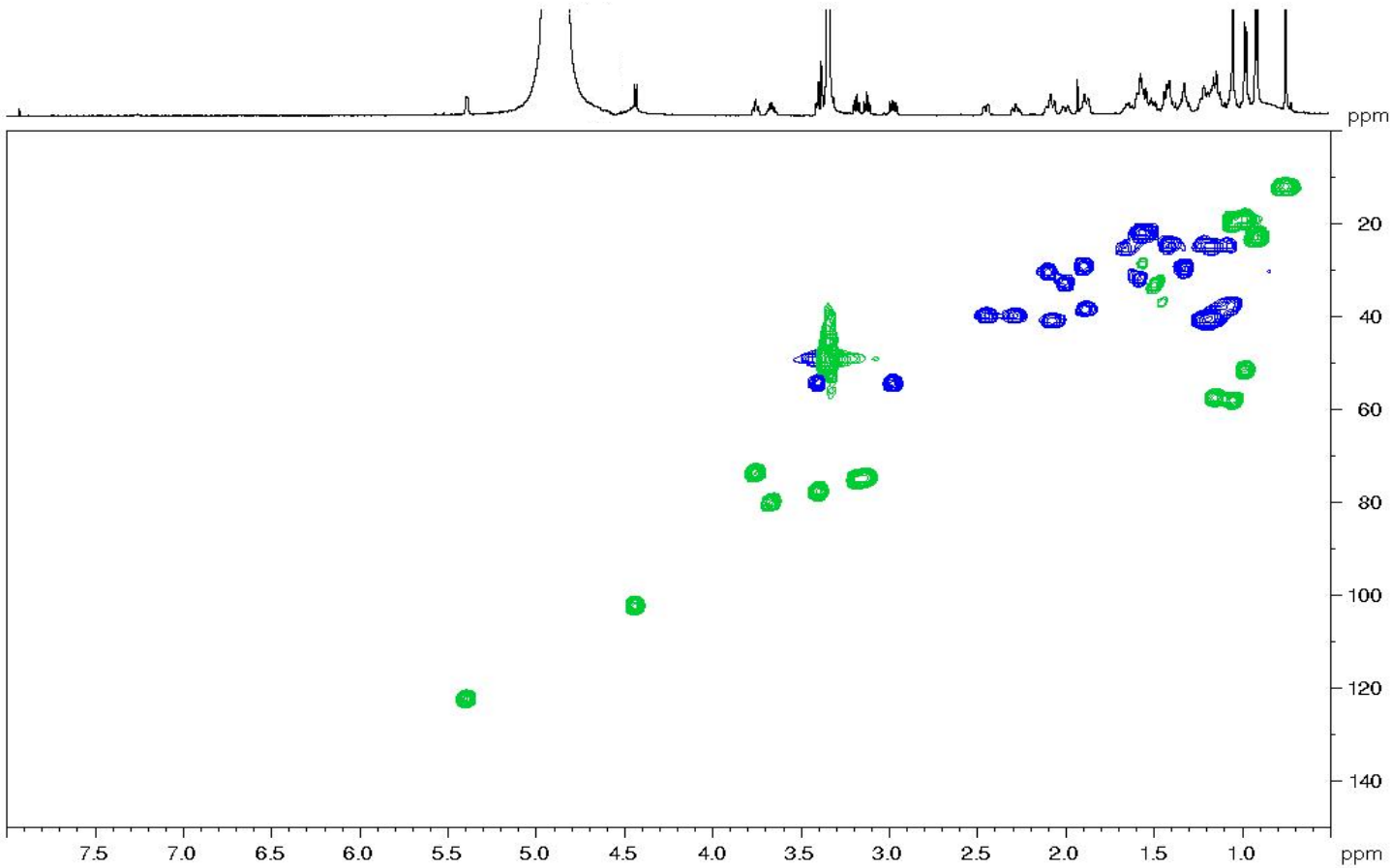
ppm
20
40
60
80
100
120
140
7.5
7.0
6.5
6.0
5.5
5.0
4.5
4.0
3.5
3.0
2.5
2.0
1.5
1.0
ppm

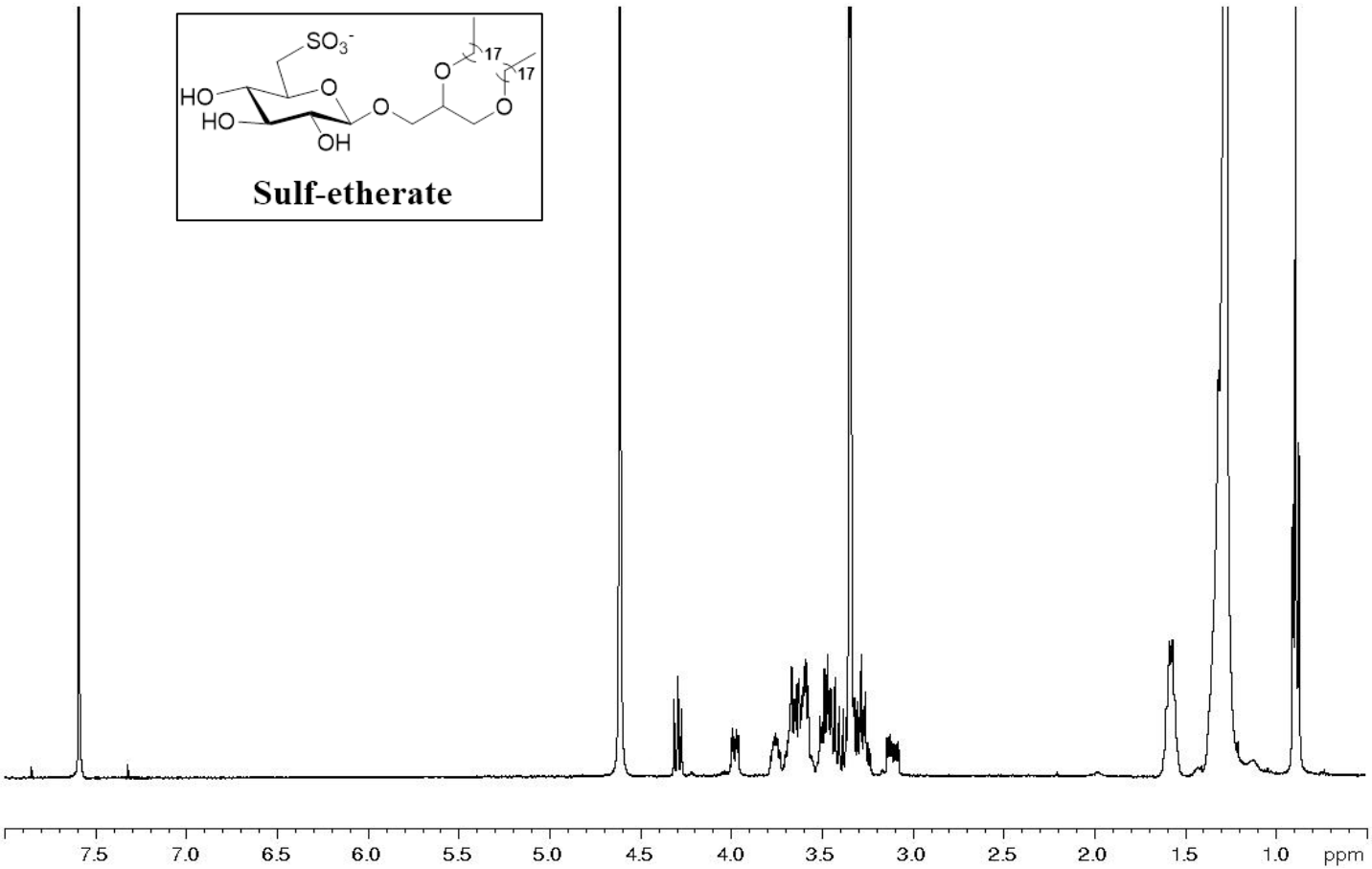
SO3-
HO
HO
OH
O
O
O
O
17
17
Sulf-etherate
7.5
7.0
6.5
6.0
5.5
5.0
4.5
4.0
3.5
3.0
2.5
2.0
1.5
1.0
ppm

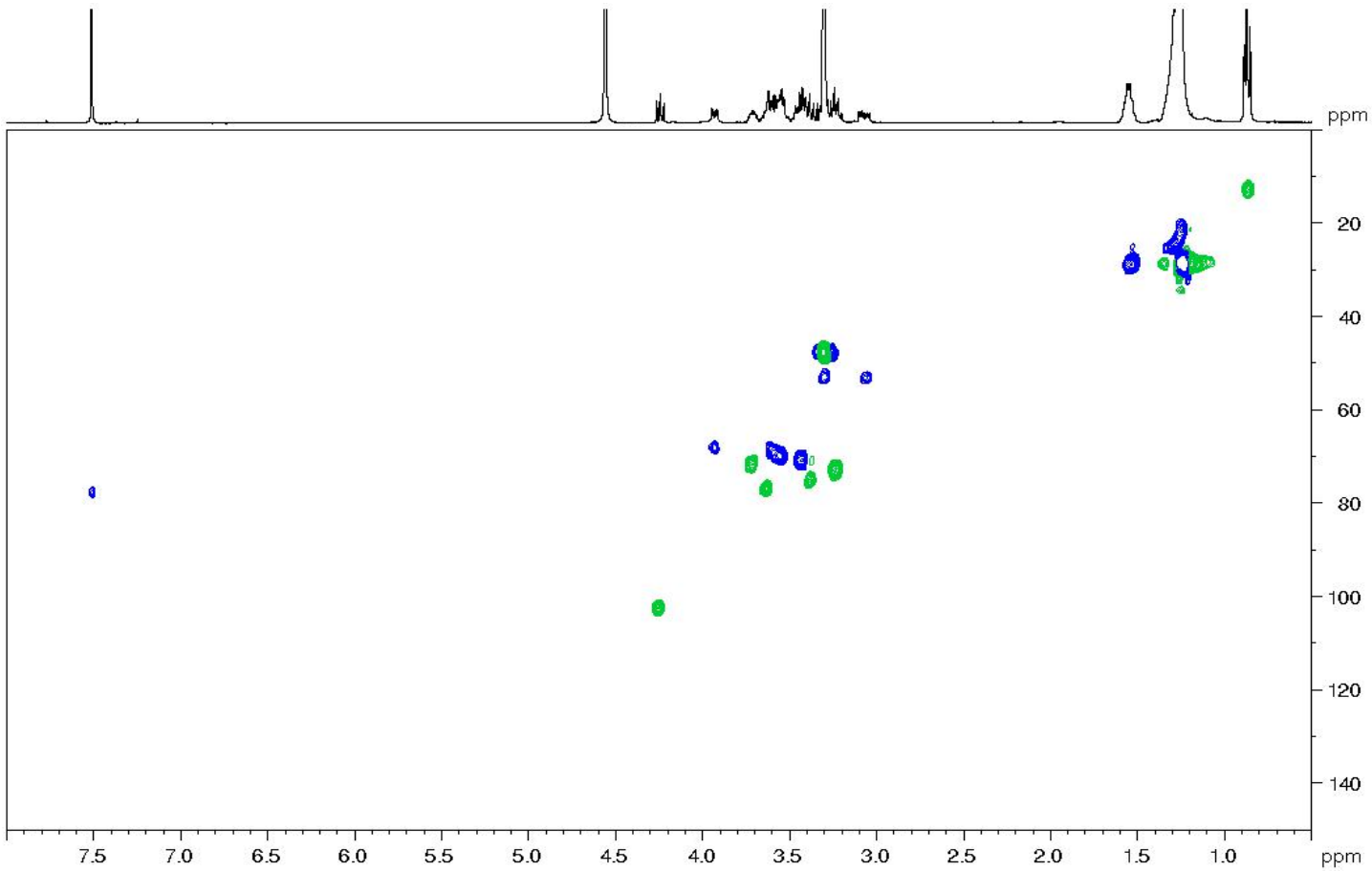
ppm
20
40
60
80
100
120
140
7.5
7.0
6.5
6.0
5.5
5.0
4.5
4.0
3.5
3.0
2.5
2.0
1.5
1.0
ppm

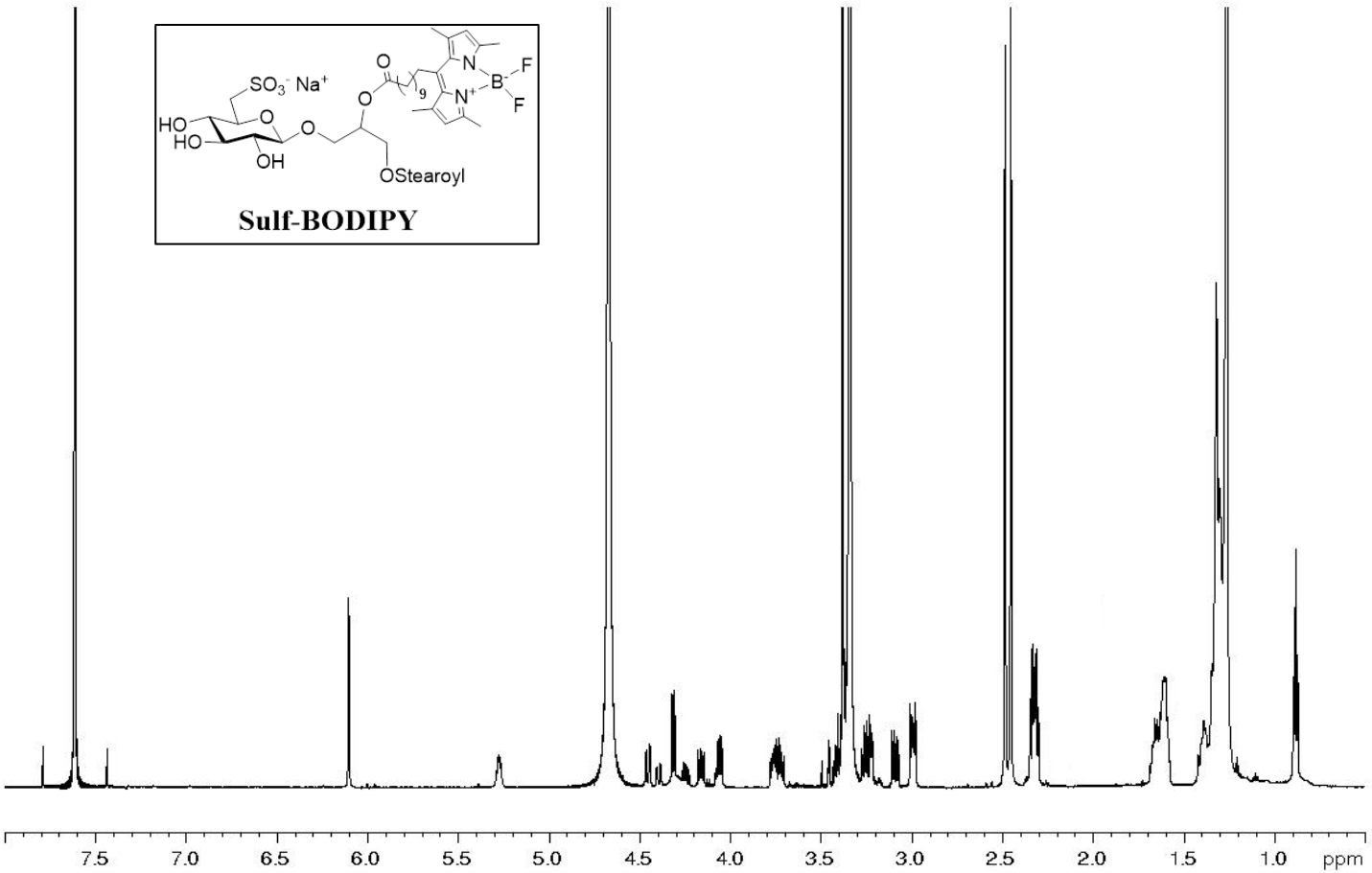
SO3- Na+
HO
HO
OH
O
O
O
O
9
N
B
F
F
N+
OStearoyl
Sulf-BODIPY
7.5
7.0
6.5
6.0
5.5
5.0
4.5
4.0
3.5
3.0
2.5
2.0
1.5
1.0
ppm

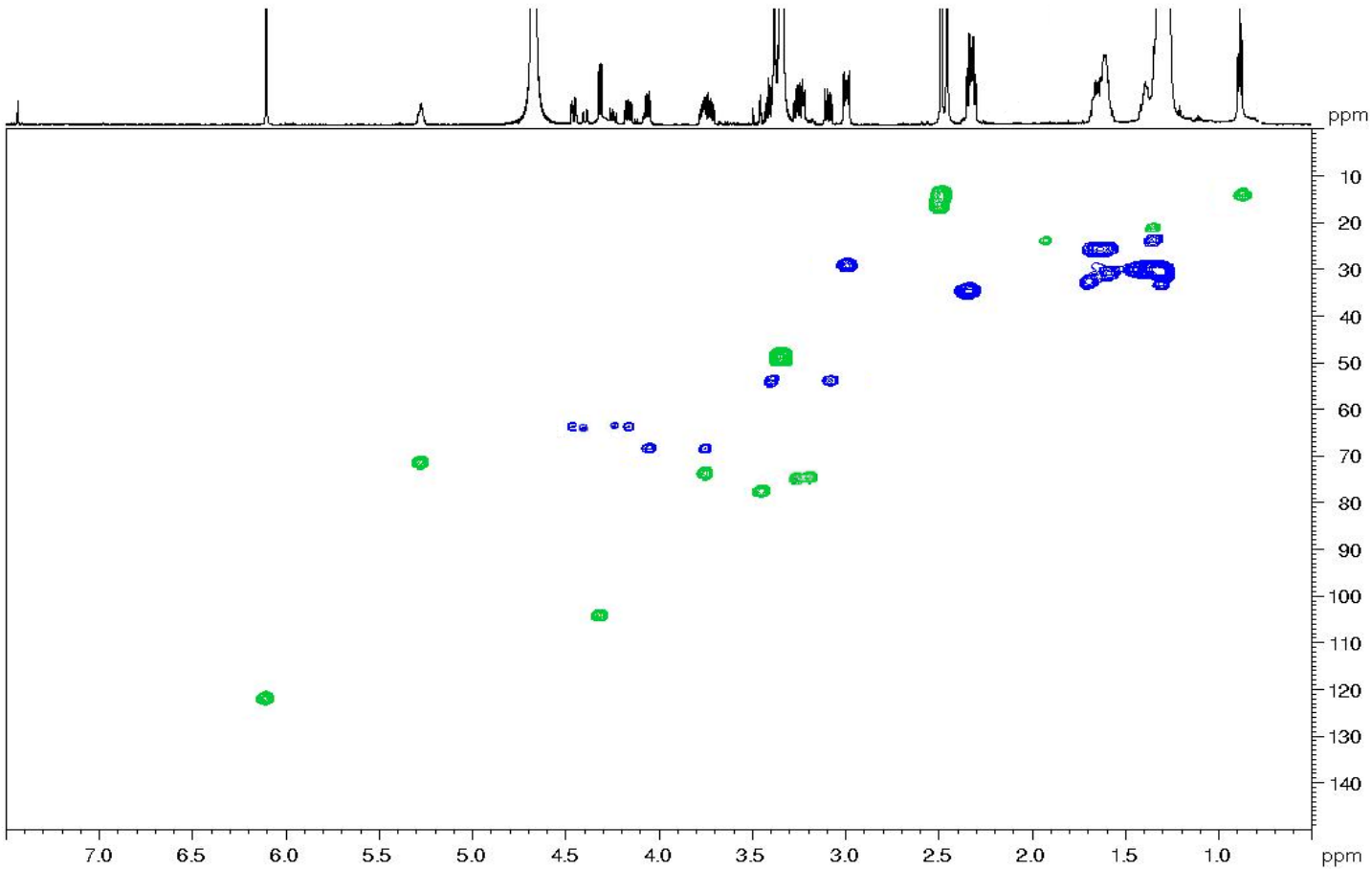
ppm
10
20
30
40
50
60
70
80
90
100
110
120
130
140
7.0
6.5
6.0
5.5
5.0
4.5
4.0
3.5
3.0
2.5
2.0
1.5
1.0
ppm

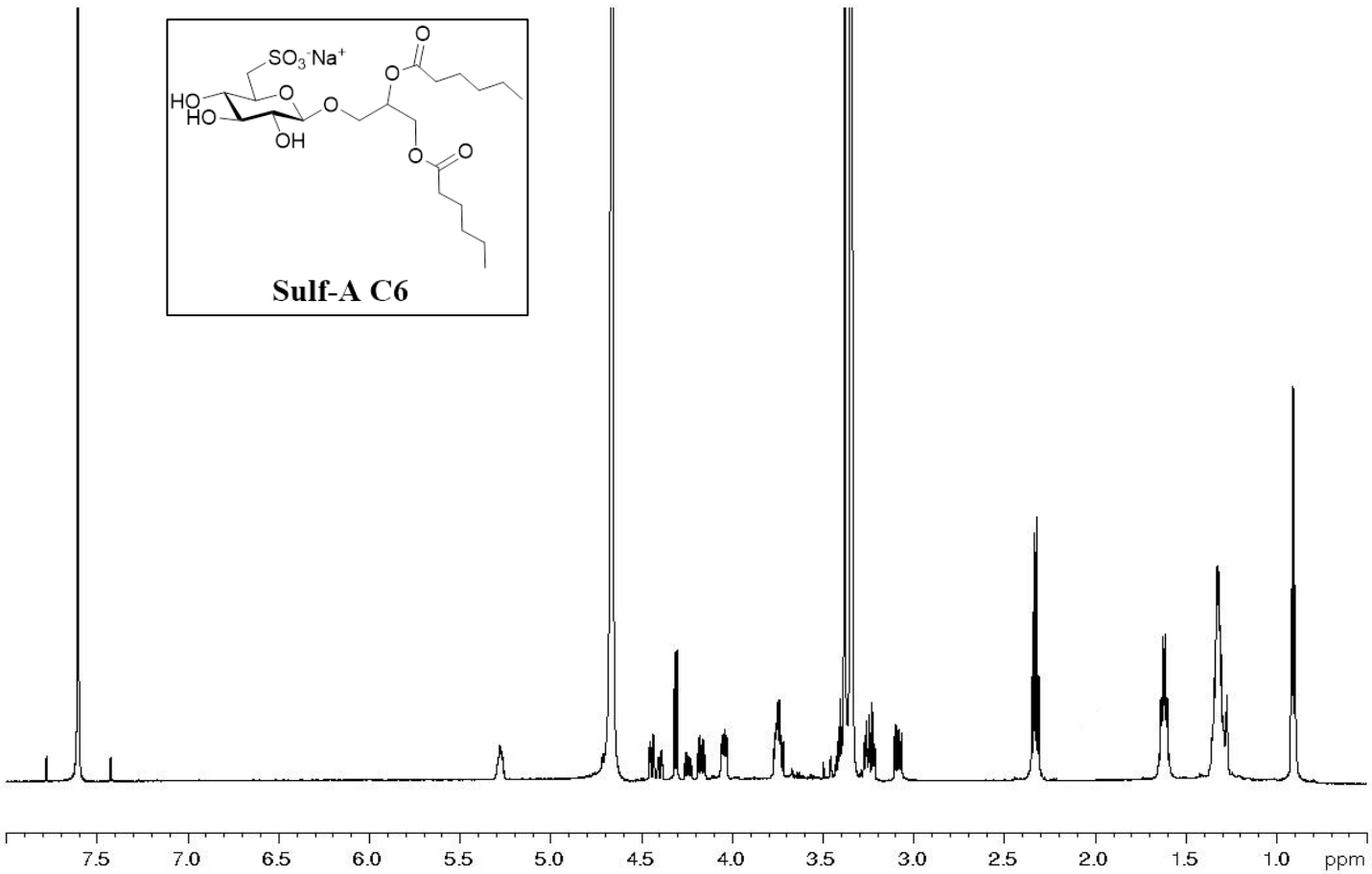
SO3-Na+
HO
HO
OH
O
O
O
O
O
O
Sulf-A C6
7.5
7.0
6.5
6.0
5.5
5.0
4.5
4.0
3.5
3.0
2.5
2.0
1.5
1.0
ppm

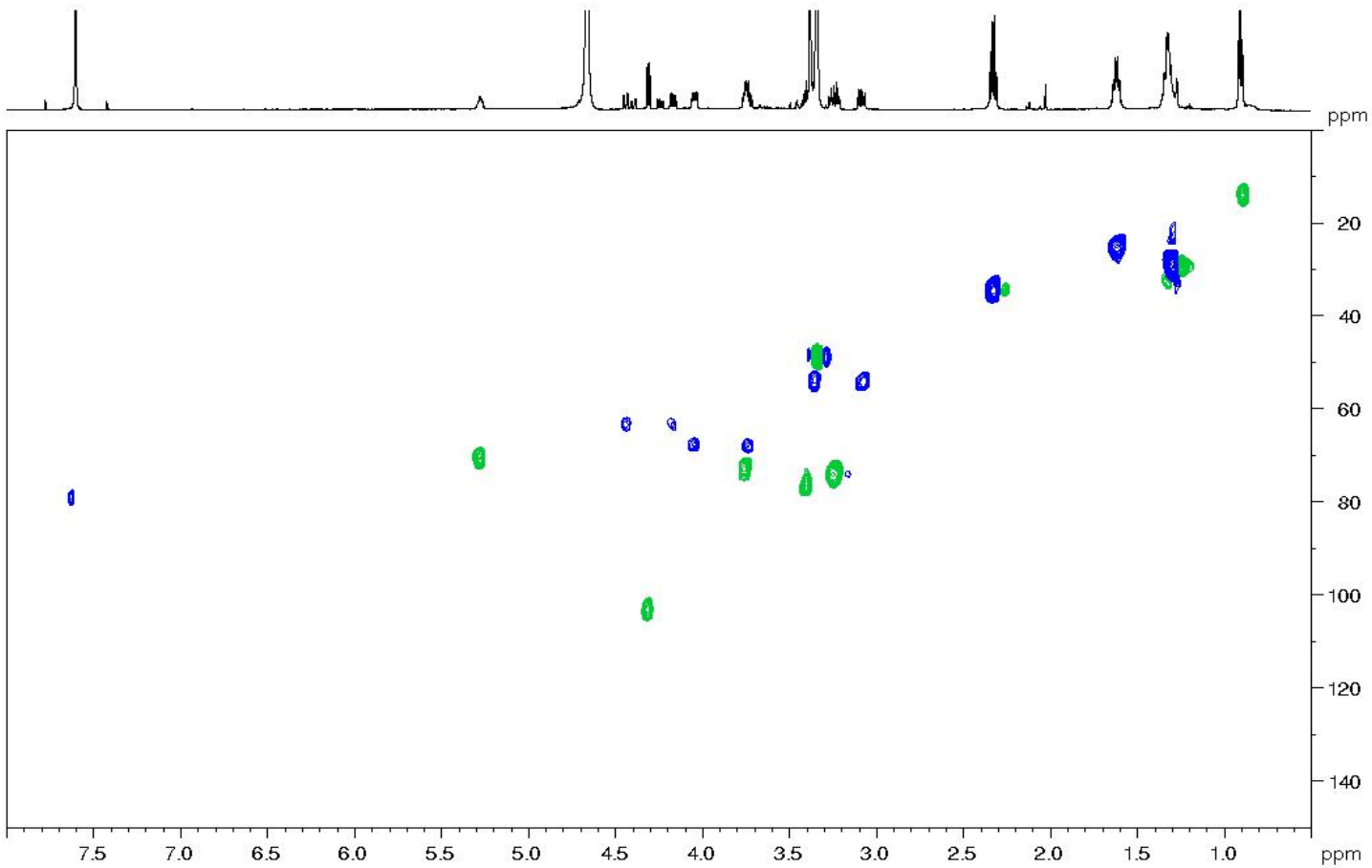
ppm
20
40
60
80
100
120
140
7.5
7.0
6.5
6.0
5.5
5.0
4.5
4.0
3.5
3.0
2.5
2.0
1.5
1.0
ppm

Acknowledgements

All the research work in this thesis has been carried out thanks to the support and guidance of my supervisors: Prof. Marina della Greca, an always helpful and kind person, who gave me useful and smart advice throughout this journey and Dr. Emiliano Manzo, who guided, taught and supported me in my scientific work but also morally, showing knowledge, patience and empathy. I would also like to thank my examiner Prof. Antonio Molinaro for supervising the work during these years, providing innovative ideas and sharing resources, contacts and opportunities. I would also like to thank Prof. Jesus-Jimenez Barbero for his warm hospitality during my time abroad at the CIC-BioGUNE centre in Bilbao and all my colleagues I met there. My sincere thanks go to the people at the ICB-CNR institute in Pozzuoli who were involved in my project, in particular Dr. Marcello Ziaco, Dr. Laura Fioretto, Dr. Giuliana d'Ippolito, Dr. Carmen Gallo, Dr. Jenny Nuzzo, Dr. Daniela Castiglia and Prof. Angelo Fontana, who allowed me to join his research team and his laboratories and provided me with invaluable advice and scientific support. I am honoured to have worked with them, without whom this thesis would not have been possible.

Thanks to my colleagues of the '3-4-5' labs, who have experienced with me all the results I have achieved and all the messes I have caused by always remaining united and close to me as a real team. Special thanks are due to Dr. Laura Fioretto and Dr. Marcello Ziaco. Laura, who has a great passion for science and is the true soul of the lab, helped me a lot with my thesis and my path, allowing me to overcome any obstacle and transmitting confidence and conviction. Marcello has followed my work from the beginning with passion, dedication and commitment, believing in me first of all as a person and then as a colleague. The patience, affection and professionality with which he has dedicated to me are unique and always made me feel at home.

Thanks to all my friends who are my daily support and my rock. Thanks to Benna who, since being by my side, has encouraged me in every moment, given me the love and strength to carry on and believed in me more than I could. You are my safe shelter and my beacon in the night.

Without my family, I would not have taken a single step out of my house. It is thanks to them that I have been able to follow this path and pursue my passion. Mari is always ready to help me with kindness and empathy and has always been a role model for me to follow and be inspired by. Dad, you are my pillar and I admire you more than anyone else. Thank you for always being there, for sharing the joys and the tears, and for being my hero. Thanks to who is able to love me and put up with me without saying a word, thank you Hope. And finally, thank you, Mum. You are my light, my breath, my guide. It is because of you that I have come this far and it is because of you that I have had the strength to carry on and be who I am today. I dedicate this thesis to you because you taught me, with a smile on your face, to fight until the end for what you love.